Pattern formation in the wake of external mechanisms

A DISSERTATION
SUBMITTED TO THE FACULTY OF THE GRADUATE SCHOOL
OF THE UNIVERSITY OF MINNESOTA
BY

Ryan Nolan Goh

IN PARTIAL FULFILLMENT OF THE REQUIREMENTS
FOR THE DEGREE OF
Doctor of Philosophy

Advisor: Professor Arnd Scheel

June, 2016

Acknowledgements

There are many people who have helped me on my mathematical journey and I would like to thank a few here. To my parents, who taught me the value of hard work and humility, and encouraged me to think deeply about the mysteries of the natural world. To my sister, whose kindness and love is always a source of inspiration and comfort.

Thank you to the many educators who helped me take all of my mathematical steps. In particular, to Nancy Casserley and Lynn Pittner, who gave me a chance. To Kevin Harrington, who showed me how to do math with joy and inspiration. To Keith Promislow, for the patience and generosity to take the time late on Friday afternoons to meet with an eager, naive, and young undergraduate student. To my advisor Arnd Scheel. Your insight, patience, and enthusiasm were essential to my development as a mathematician. I am forever grateful for all the advice and guidance you provided me with, and for the countless hours spent in your office working on problems and talking about mathematics. Thank you.

To all my friends and colleagues at Michigan State University and the University of Minnesota, thank you for the camaraderie and support throughout out all these years. The numerous caffeine filled and sleepless nights talking about math and doing problem sets were all the better having you with me.

I would also like to thank Professors Hans Othmer, Peter Polacik, and Daniel Spirn for taking the time to serve on my committee. I would like to acknowledge the support of the National Science Foundation through the grants NSF- DMS-0806614 and NSF-DMS- 1311740, an NSF graduate fellowship NSF-GFRP-00006595, as well as a UMN Doctoral Dissertation Fellowship.

Dedication

For my wife Madeline. You are my best friend and have been there for me throughout all of the journey through graduate school. You have keept me grounded, balanced, and (mostly :P) sane. We have become a wonderful team and this work is a testament to us.

Abstract

Pattern formation in nature has intrigued humans for centuries, if not millennia. In the past few decades researchers have become interested in harnessing these processes to engineer and manufacture self-organized and self-regulated devices at various length scales. Since many natural pattern forming processes nucleate or grow from a homogeneous unstable state, they typically create defects, caused by thermal and other inherent sources of noise, which can hamper effectiveness in applications. One successful experimental method for controlling the pattern forming process is to use an external mechanism which moves through a system, transforming it from a stable state to an unstable state from which the pattern forming dynamics can take hold.

In this thesis, we rigorously study partial differential equations which model how such triggering mechanisms can select and control patterns. We first use dynamical systems techniques to study the case where a spatial trigger perturbs a pattern forming freely invading front in a scalar partial differential equation. We study such perturbations for the two generic types of scalar invasion fronts, known as pulled and pushed fronts, which roughly correspond to fronts which invade either through a linear or nonlinear mechanism. Our results give the existence of perturbed fronts and provide expansions in the speed of the triggering mechanism for the wavenumber perturbation of the pattern formed.

With the hope of moving towards the more complicated geometries which can arise in two spatial dimensions, where many dynamical systems methods cannot be readily applied, we also develop a functional analytic method for the study of Hopf bifurcation in the presence of continuous spectrum. Our method, while still giving computable information about the bifurcating solution, is more direct than previously proposed methods. We develop this method in the context of a triggered Cahn-Hilliard equation, in one spatial dimension, which has been used to study many triggered pattern forming systems. Furthermore, we use these abstract results to characterize an explicit example and also use our method to give a simplified proof of the bifurcation of oscillatory shock solutions in viscous conservation laws.

Contents

List of Figures

Chapter 1

Introduction

1.1 Introduction

Nature has a vast array of tools and processes by which it forms its many beautiful coherent structures. Such processes have intrigued researchers in many fields of natural science across the ages, from the study of nature's "forms" by Plato and Pythagoras, the artistic drawings of Ernst Haeckel showing the beauty and variety of marine life [71], the investigations of D'arcy Wentworth Thompson describing natural forms with simple mathematical equations [161], the chemical experiments of Raphael Liesegang [95], to the mathematical investigations of biological morphogenesis by Alan Turing [154]. In the past half century or so, the application of mathematical models and analysis has lead to a deeper understanding of these processes in many different areas such as polymer network formation [119, 118, 109], plant phylotaxis [113, 112] , chemical deposition [140, 63, 62], fluid dynamics [31], animal coats [29, 159], and vegetation and population patterns [143].[1]

With the recent advent of micro- and nano-meter scale devices in diverse areas such as optics, thin-film solar cells, micro-fluid medical devices, and nano-electronics, much interest has arisen from engineering communities to harness the natural pattern-forming processes of nature to fabricate structures which are functionalized, self-organized, and

[1]This introductory chapter is a reformulation and unification of the introductions contained in the works [65, 66, 64] which comprise this thesis.

self-mediated; see for example [104, 145, 160]. The utilization of such processes could lead to significant simplification of fabrication processes, cost reduction, and increased structure complexity compared to existing techniques, such as lithography where one typically has to use tools at the same length-scale of the desired structure. In short, the main question is:

Can the pattern forming processes of nature be used to create complicated and functional structures in a more cost effective and efficient manner?

Many of the pattern forming processes mentioned above form via the nucleation, growth, and invasion of a localized instability into a homogeneous unstable state. This growth leads to the formation of a traveling front which typically moves at a constant speed c and leaves behind some sort of periodic pattern in its wake; see for example Fig. 1.2.1. The wavenumber of this periodic pattern is typically independent of the type of perturbation and is selected by the nonlinear front propagation. There has been much experimental, numerical, and theoretical work done in the past few decades to study such pattern forming invasion fronts (see [156, 33, 11]) and front propagation remains an active area of study today; see for example [43, 113, 52, 72, 166].

In practice and experiment, these fronts are typically difficult to control as the preparation of a homogeneous unstable state requires uniform suppression of random fluctuations. Otherwise, such fluctuations will cause patches of spatial patterns to fill the medium and collide with each other forming various types of defects; see Figure 1.1.1 for an example of this. Furthermore, even if such suppression is achieved, one must have control of the internal system parameters to tune the type of pattern formed by the invasion front. For these reasons, freely invading fronts are most likely of little use in the engineering applications mentioned above.

One successful experimental method for controlling these pattern forming processes is to use an external mechanism which moves through a *stable* system and spatially progressively excites it into an unstable state. Once the latter state is established, the pattern forming mechanisms inherent in the system can take hold. In this way, the mechanism can be thought of as "triggering", and subsequently mediating, a pattern forming process. This is the primary type of trigger which we consider in this thesis and the mantra which underlies the study at hand could be posed as follows:

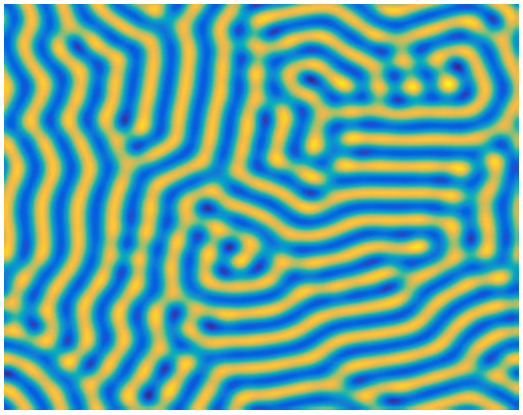

Figure 1.1.1: Evolution of the cubic Swift-Hohenberg equation in two spatial dimensions from small random perturbations of the state $u \equiv 0$. Patches of coherent stripes form which interact along various slowly evolving defects.

By controlling the spatially progressive way one excites a stable system into an unstable state, one can control the pattern which is selected by the system.

A recent example of this method comes from the field of ion-milling. Here, a broad beam of ions bombards a flat surface of metallic alloy and, instead of homogeneously eroding it as might be expected, excites a secondary "sputtering" instability which creates a variety of coherent structures; see [14, 165, 15, 59, 148, 75]) and Figure 1.1.2 for a few examples. If the entire plate is bombarded at once, the whole surface becomes unstable, leading to the formation of patches of patterns with defects at their domain boundaries. If instead, the beam is masked and progressively moved across the surface, exciting only a portion of the metal at a time, a sizeable reduction in the amount of defects is observed [59].

Another example arises in the field of evaporative chemical deposition [151]. Here particles (on the micron to nanometer length scale depending on the situation) are deposited on a surface via the progressive evaporation of a solvent. A household example of this phenomenon is the formation of ring like stains formed when spilled coffee evaporates on a tabletop. By controlling the evaporation process - typically by drawing the surface out of the solvent in a controlled manner - a vast array of uniform spatial patterns can

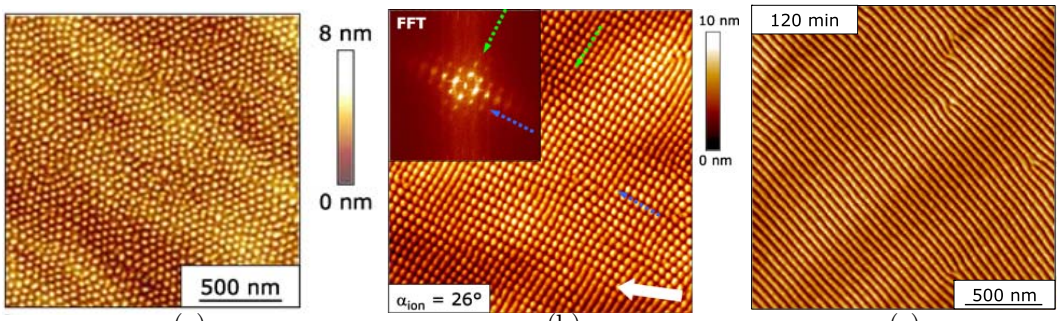

(a) (b) (c)

Figure 1.1.2: Examples of patterns formed by bombardment of surfaces (Germanium and Silicon) with noble gas ions, Reprinted from [55], with permission of Springer.

be achieved such as stripes, dots, chevrons, and hexagons; see [151] and Figure 1.1.3.

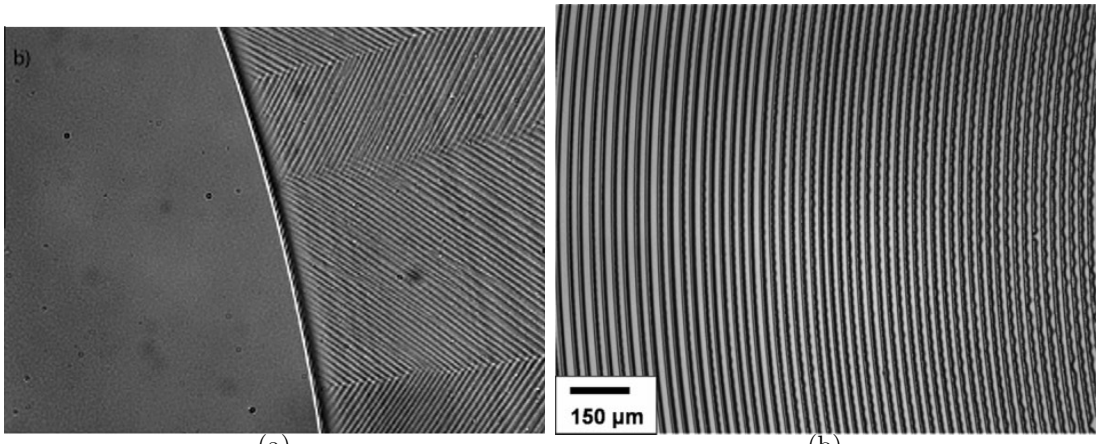

(a) (b)

Figure 1.1.3: Various examples of pattern formation via evaporated deposition. (a) Reprinted from [13] (2012), with permission from Elsevier, (b) Reproduced from [82], (2007) with permission from WILEY-VCH Verlag GmbH & Co. KGaA, Weinheim.

Here the evaporation line acts as a spatial trigger, inducing phase separative instabilities as solvent evaporates from the particles. These evaporative processes have wide application, and have been shown to deposit many different types of materials such as polymers, nanoparticles, and biomaterials; see [73] for an especially interesting review.

Furthermore, such deposition processes are similar to recurrent precipitation patterns that arise in the wake of a diffusion front to form banded ring-like patterns, as originally

observed by Liesegang [95]. Models of these processes often include a simple bimolecular reaction whose product feeds as a diffusive source term into a model for the precipitation kinetics; see for instance [40, 87]. Lastly, we mention patterns produced through growth and chemotaxis in bacterial colonies; see for instance [100]. In a first approximation, one can envision patterns formed by chemotactic motion in the wake of a spatially spreading growth process [2], with phenomena reminiscent of patterns in the wake of trigger fronts in two-dimensional Cahn-Hilliard equations [54].

While the area of triggered pattern formation has been the focus of much experimental, and numerical work, where evolutionary partial differential equations have been proposed to model these phenomenon, little mathematically rigorous study has been performed. Thus it is the goal of this thesis to rigorously investigate how spatial triggers, which typically arise as some sort of spatial inhomogeneity in the equations modeling the system, affect the patterns formed in a system. In particular, we wish to use techniques from dynamical systems, partial differential equations, and functional analysis to more deeply understand the known phenomena and predict new and interesting structures, with the hope that the deeper knowledge leads to the creation of new fabrication techniques.

In its first two parts, this thesis mathematically contributes another drop to the ever growing spring of research showing how dynamical systems techniques, such as spatial dynamics, heteroclinic bifurcation theory, and geometric desingularization, can be used to study evolutionary partial differential equations. In its third part, this work shows how functional analytic methods could be used to "cut to the heart of the matter" and study systems which have in the past resisted dynamical systems treatments. In particular, we develop a novel and direct approach for studying bifurcation in the presence of essential spectrum. These methods, in addition to being somewhat more efficient than the spatial dynamics approach, have the added benefit that they should allow for the study of higher-dimensional spatial patterns (discussed briefly in Section 1.5 below).

In the rest of this introduction we will review the main results of this thesis, putting them in context of the existing field of research, and briefly discussing the ingredients of proof. Before doing these things, I will discuss and review the two generic types of free invasion fronts, as the concepts permeate the rest of our work.

1.2 Invasion and pattern formation into an unstable state

Since the external mechanisms discussed above often create patterns by mediating some sort of invasion process, we must take some time to discuss front propagation into a homogeneous unstable state. Invasion fronts of this type were first studied in the pioneering works of Kolmorgorov, Petrovsky, and Piscunov [90], and Fisher [53] in the first part of the 20-th century in the context of population models. In the mathematical community, work continued along this vein (in the context of nonlinear diffusion equations) culminating in the outstanding work of Aronson and Weinberger [7] where a certain type of monotonicity was taken advantage of to employ comparison principle arguments and prove the existence and stability/robustness of nonlinear invasion fronts. Recent studies of fronts have focused on such phenomenon in more complicated settings such as nonlocal equations [72] as well as inhomogeneous, random, and stochastic media [167, 12, 89, 164].

In the physics community, invasion processes have been studied in many different areas over the past half-century. The first such studies arose in plasma physics [18] where the propagation of electron streamers was considered. Later, studies were also done in the context of the formation and selection of patterns in various physical systems such as dendritic growth [33, 17], fluid flows [27, 26, 25], and in general nonlinear systems [157, 155]. At present, significant amount of work is focused on studying pattern forming invasion fronts in higher-dimensional spatial configurations where the leading edge of the front interface forms a co-dimension one subspace in the spatial domain [54, 113, 37, 4].

As an explanatory example for this introduction consider the one-dimensional cubic-quintic complex Ginzburg-Landau (cGL) equation,

$$A_t = (1+\mathrm{i}\alpha)A_{xx} + A + (\rho+\mathrm{i}\gamma)A|A|^2 - (\beta_1+\mathrm{i}\beta)A|A|^4, \qquad x,t\in\mathbb{R},\ \ A\in\mathbb{C}, \quad (1.2.1)$$

with $\beta_1 > 0$. This equation is a prototypical model for the emergence of self-organized, regular spatio-temporal patterns in spatially extend systems and has been used as a modulation equation to study the onset of coherent structures in many physical systems ([102, 3, 141]). Due to the gauge invariance $A \mapsto \mathrm{e}^{\mathrm{i}\theta}A$, this equation possesses explicit periodic wave-trains of the form $A_{\mathrm{p}}(x,t) = r\mathrm{e}^{\mathrm{i}(\omega t - kx)}$, where $k,\omega\in\mathbb{R}, r\in\mathbb{R}_+$ satisfy

the nonlinear dispersion relation

$$\begin{aligned} 1 &= k^2 - \rho r^2 + \beta_1 r^4, \\ \omega &= \alpha k^2 - \gamma r^2 + \beta r^4, \end{aligned} \tag{1.2.2}$$

so that wave-trains can be parameterized by their temporal frequency ω. Pattern forming free invasion fronts, $A_{\rm ff}(x,t)$, arise as modulated traveling waves which satisfy $A_{\rm ff}(x,t) \to A_{\rm p}(x,t)$ as $x \to -\infty$ and $A_{\rm ff}(x,t) \to 0$ as $x \to +\infty$, with an interface which invades with some constant non-zero speed c.

Thus, we view (1.2.1) in the co-moving frame $\xi := x - ct$,

$$A_t = (1+\mathrm{i}\alpha)A_{\xi\xi} + cA_\xi + A + (\rho+\mathrm{i}\gamma)A|A|^2 - (\beta_1+\mathrm{i}\beta)A|A|^4, \qquad \xi, t \in \mathbb{R}, \;\; A \in \mathbb{C}. \tag{1.2.3}$$

In this frame of reference, the dispersion relation is shifted

$$\begin{aligned} 1 &= k^2 - \rho r^2 + \beta_1 r^4, \\ \omega - ck &= \alpha k^2 - \gamma r^2 + \beta r^4. \end{aligned} \tag{1.2.4}$$

Pattern forming invasion fronts come in two generic types known as *pulled* and *pushed*. These names, coined in the physics literature, correspond to whether the linear dynamics of the homogeneous state ahead of the front determine the invasion speed, and hence "pull" the front forward, or the nonlinearities in the system amplify perturbations faster than the linear growth, "pushing" the front forward faster than the linear prediction for the speed. Both of these types of fronts exist in (1.2.3) above for different parameter ranges. We shall now briefly discuss their defining characteristics. For an excellent, and much more detailed, review of these types of invasion fronts with a catalog of different and interesting physical examples see [156].

1.2.1 Pulled fronts

Pulled fronts can be described to very good approximation by a linear analysis based on branch points of a complex dispersion relation. The speed of such a front, known as the *linear spreading speed* and which we denote as $c_{\rm lin}$, is determined by a marginal stability

criterion [33] which requires that the trivial state is point-wise marginally stable with respect to localized perturbations in a frame moving with this speed. In other words, when decreasing the speed c of the frame of observation, compactly supported initial conditions grow exponentially point-wise. Such a stability criterion is best understood by looking for singularities of the resolvent $(L-\lambda)^{-1}$ of the linearization L of the system about the unstable state in a co-moving frame of speed c. After using Fourier-Laplace, the resolvent can be represented as a convolution with a point-wise Green's function $G_\lambda(x,s)$. Since we only study local perturbations, bounded-invertibility of the resolvent only requires the point-wise analyticity of $G_\lambda(x,s)$ in λ. This last condition is equivalent to being able to perturb the Laplace integration contour off of the imaginary axis. Hence, instabilities will arise as singularities of G_λ which lie in the right half-plane. Hence, the linear spreading speed is found as the speed at which such singularities cross the imaginary axis. Moreover these singularities in many cases arise as double-roots of the complex dispersion relation $d_c(\lambda,\nu)$, found by inserting the ansatz $e^{\lambda t+\nu x}$ into the system linearized about the homogeneous state; see (1.2.5) and subsequent discussion for an example in cGL. For a systematic study of front propagation from this viewpoint see [80].

In the physics literature, as the frame of reference speed c decreases below c_{lin}, the instability of the trivial state is said to change from convective to absolute. Furthermore, the invasion of such fronts is governed by linear growth in the leading edge which then saturates in the wake due to the nonlinearities of the system. Such nonlinear pulled fronts are known to be very sensitive to disturbances in the leading edge. Convergence towards, as well as relaxation of small perturbations to, pulled fronts is typically slow, in fact algebraic in time. In a co-moving frame, this type of invasion can be either stationary or oscillatory with frequency ω_{fr}. This frequency is typically a fraction of the frequency derived by the marginal stability criterion, $\omega_{\text{fr}} = \omega_{\text{lin}}/\ell$. The case of strong resonance, $\ell = 1$, is often referred to as node conservation in the leading edge. Pulled fronts are named as such because the linearized dynamics of the unstable state ahead of the front determine its propagation speed and, in a sense, "pull" it forward. In (1.2.3), such fronts exist in the supercritical regime with ρ negative; see [157] for specific parameter ranges.

In cGL, pulled fronts can be found in the supercritical regime with $\rho < 0$; see Fig. 1.2.1.

The linear complex dispersion relation can be obtained by inserting the ansatz $\mathrm{e}^{\lambda t+\nu x}$ into the linearization of (1.2.3) about the trivial state $A \equiv 0$ to obtain

$$d_c(\lambda, \nu) = (1 + \mathrm{i}\alpha)\nu^2 + 1 - \lambda + c\nu. \tag{1.2.5}$$

The branch points can then be found by solving for double roots of d_c,

$$d_c(\lambda, \nu) = 0, \quad \frac{d}{d\nu} d_c(\lambda, \nu) = 0, \tag{1.2.6}$$

These roots, which we denote as $(\lambda_*(c), \nu_*(c))$, mediate the transition between absolute and convective stability. The linear spreading speed, c_{lin}, is then determined as

$$c_{\mathrm{lin}} = \inf\{c : \mathrm{Re}\{\lambda_*(c)\} \geq 0\}$$

We denote the frequency where the branch point crosses as $\mathrm{i}\omega_{\mathrm{lin}} = \lambda_*(c_{\mathrm{lin}})$. In this specific case we have

$$c_{\mathrm{lin}} = 2\sqrt{1+\alpha^2}, \qquad \omega_{\mathrm{lin}} = \alpha, \qquad \nu_{\mathrm{lin}} = -\frac{1-\mathrm{i}\alpha}{\sqrt{1+\alpha^2}}. \tag{1.2.7}$$

and in the generic case where there are no quintic terms, $\beta = \beta_1 = 0$, and $\rho = 1$, studied in Chapter 2 below, the spatial pattern $A(x,t) = \sqrt{1-k_{\mathrm{lin}}^2}\mathrm{e}^{\mathrm{i}(\omega_{\mathrm{lin}}t+k_{\mathrm{lin}}x)}$ in the wake of the free front A_{ff} has wavenumber

$$k_{\mathrm{lin}} = \begin{cases} -\frac{\sqrt{1+\gamma^2}-\sqrt{1+\alpha^2}}{\gamma-\alpha}, & \text{for } \gamma \neq \alpha \\ -\frac{\alpha}{\sqrt{1+\alpha^2}}, & \text{for } \gamma = \alpha. \end{cases} \tag{1.2.8}$$

We also note that the group velocity of wave trains in the wake of the invasion front points away from the front interface,

$$c_{\mathrm{g}} := \frac{\mathrm{d}\Omega(k; c_{\mathrm{lin}})}{\mathrm{d}k}\Big|_{k=k_{\mathrm{lin}}} = -2\sqrt{1+\gamma^2} < 0. \tag{1.2.9}$$

In other words, the invasion front acts as a wave source in its co-moving frame; see [132].

We remark that in general such double roots must also satisfy certain genericity conditions and a so-called "pinching condition" which requires that the spatial eigenvalues ν, which split off from ν_{lin} as λ moves from $i\omega_{\text{lin}}$, diverge to $\pm\infty$ respectively as λ is taken to $+\infty$ along some smooth curve. These conditions are trivially satisfied in this case and we refer to [80] and [156] for more detail.

As it will be important in Chapter 2, we also remark that in many cases, including cGL above, these branch points consist of the rightmost points in $\mathbb{C}$ of what is known as the absolute spectrum. This is the limiting set for the eigenvalues of the linearization about the background state (in this case $A \equiv 0$) when posed on a large, bounded domain with separated boundary conditions [126]. Heuristically, this set corresponds to when the projectivized linear dynamics about the background state in a spatial dynamics formulation are relatively neutral; see Chapter 2 and also Section 4.4 for more discussion, [124] for another schematic overview, and [126] for precise results. One could also see [80, §8.3] for more discussion on the connection between absolute spectrum and spreading speeds.

1.2.2 Pushed fronts

Pushed fronts arise when nonlinearities amplify linear growth sufficiently so that the speed of propagation of disturbances exceeds the linear spreading speed c_{lin}. Their leading edge decay is generally steeper and convergence towards them is fast, being exponential in time. In fact, the Green's function for the linearization at pushed fronts exhibits simple poles associated with the neutral Goldstone modes, while the linearization near pulled fronts exhibits a singularity with structure similar to the 3-dimensional heat kernel [56]. In the language of spatial dynamical systems, such a pushed front consists of a heteroclinic orbit which converges to an equilibrium along a strong-stable invariant manifold. In general, much less in known about pushed fronts in comparison to their pulled counterparts. Rigorous theoretical study has been limited to a small number of mathematical models including the Nagumo equation [155], coupled-KPP equations [79], Lotka-Volterra systems [78], and the Complex Ginzburg Landau equation (1.2.3) where pushed free fronts have been shown to exist in the weakly subcritical regime with ρ sufficiently large.

Furthermore, existence of pattern-forming pushed fronts has, to the authors' knowledge, only been proven in the last of the aforementioned systems. In this last equation, the work of [157, Fig. 7+8, §4.2] uses phase-wavenumber variables, a spatial dynamics framework, and dimension counting (of invariant manifolds) arguments to study these fronts. When written as a four-dimensional real system, the equilibrium $A \equiv 0$ has a two complex conjugate pairs of eigenvalues, $\nu_{\mathrm{ss}}, \overline{\nu_{\mathrm{ss}}}$ and $\nu_{\mathrm{su}}, \overline{\nu_{\mathrm{ss}}}$ with

$$\mathrm{Re}\{\nu_{\mathrm{ss}}\} < \mathrm{Re}\{\nu_{\mathrm{su}}\} < 0,$$

while A_{p} has one neutral and one unstable Floquet multiplier. The existence of invading fronts is then obtained by finding intersections of the strong stable manifold of $A \equiv 0$ corresponding to $\nu_{\mathrm{ss}}, \overline{\nu_{\mathrm{ss}}}$ and the center-unstable manifold emanating from a wave-train A_{p}. This gives existence for specific parameter ranges. See Figure 1.2.1 for a space-time diagram of such a front where the front invades much quicker than the pulled speed with a steeper leading edge and significantly different wavenumber.

Despite the relatively small amount of analytical results available, there has been an abundance of numerical results exhibiting such fronts. One such interesting example arises in the modeling of plant phyllotaxis where [113] used a Swift-Hohenberg model to study the formation of Fibonacci spirals in seed growth on flowers. Such growth was found to behave as a pushed front which invaded a circular domain with hexagons spiraling in towards the center. Another example is given in Chapter 3 below, where a modified Cahn-Hilliard equation is shown to exhibit pushed pattern forming fronts. More examples can be found in [156]. We also remark that for systems of equations (i.e. non-scalar equations), the pushed speed c_{p} is not necessarily greater than the linear speed c_{lin}; see for example [78].

1.3 Patterns in the wake of triggers in one spatial dimension

Many different mechanisms have been proposed and studied to spatially progressively excite pattern forming systems. In this thesis, we consider mechanisms which travel through a stable medium and locally excite it into an unstable state. We shall call such

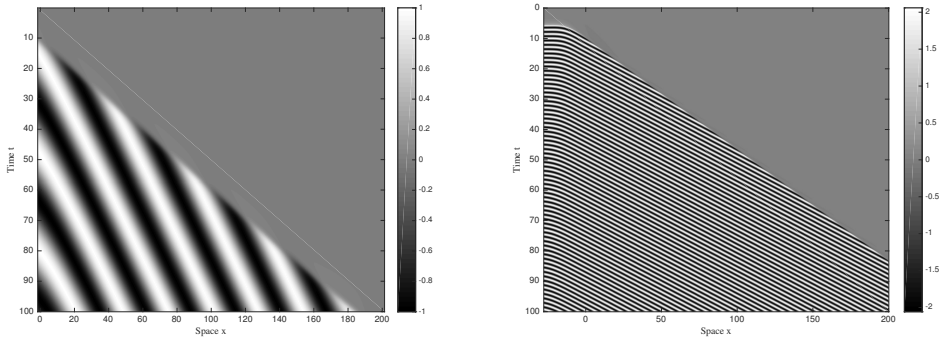

Figure 1.2.1: Pulled front on the left with $\rho = -1$ and invasion speed $c_{\text{lin}} \approx 2.09$, pushed front the right with $\rho = 4$ and invasion speed $c_{\text{p}} \approx 2.66$; both with $\alpha = 0.3, \gamma = -0.2, \beta = 0.2, \beta_1 = 1$. Note the increased wavenumber, increased invasion speed, and sharper decay in the pushed case.

a mechanism a *trigger* and the resulting front, which connects the unstable and stable states, a *preparation front*. Once the unstable state is established, the mechanism which governs the free front causes a uniformly patterned state to nucleate in the wake of the trigger. We shall call the resulting pattern-forming front a *trigger front*; see Figure 1.3.1 for a schematic of this process. The two most common, and in some sense simplest when formulated mathematically, types of spatial triggers take the form of traveling source terms and parameter ramps. These can both be exemplified in the Cahn-Hilliard equation,

$$u_t = -(u_{xx} + u - u^3)_{xx}, \quad x, t, u \in \mathbb{R}, \tag{1.3.1}$$

a phenomenological model first used to study phase-separation in a bi-metallic alloy which undergoes under rapid quenching [20, 50, 107] and which has recently been used to study many other pattern forming systems [152, 91].

Traveling source triggers In this context, a uniformly propagating source term $\chi(x - ct)$ could be used to deposit mass into a stable homogeneous system, progressively moving it into a unstable state with some speed $c > 0$,

$$u_t = -(u_{xx} + u - u^3)_{xx} + c\chi(x - ct). \tag{1.3.2}$$

For example, the gaussian source term

$$\chi(\xi) = (\pi\delta)^{-1/2}\mathrm{e}^{-\delta^{-1}(\xi)^2}, \quad 0 < \delta \ll 1,$$

leads to the creation of a traveling front solution $u_{\mathrm{pr}}(x-ct)$ connecting the stable state $u \equiv -1$ as $x \to \infty$ with the unstable $u \equiv 0$ as $x \to -\infty$. This front is a preparation front in our nomenclature. It is readily seen that u_{pr} is unstable and hence is a precursor to the formation of a patterned state. By controlling the evolution of u_{pr}, the source term χ mediates the pattern in the wake. The resulting front which connects the patterned state as $x \to -\infty$ with the stable state $u \equiv -1$ is an example of a trigger front; see Figure 4.1.3 for an example.

Such source terms arise in chemical deposition and precipitation systems where mass is deposited, moving a stable medium into an unstable state. Specific examples include the controlled evaporation, or "de-wetting" processes discussed above [151], and precipitation systems like the Liesegang reaction [152, 40, 87, 146] where a bi-molecular reaction front travels through a gel suspension creating a diffusive source term which deposits precipitate into the system. Source term triggers also appear in combustive systems where two combustive gases react [150], or in chemotactic aggregation of bacteria where the creation of chemical gradient causes organisms to form interesting spatial patterns [19, 2, 77].

Parameter ramp triggers Parameter ramps can also be studied in this setting by introducing a inhomogeneous coefficient,

$$u_t = -(u_{xx} + \chi(x-ct)u - u^3)_{xx}, \quad \chi(\xi) = -\tanh(\epsilon\xi),\ 0 < \epsilon \ll 1. \tag{1.3.3}$$

Here the preparation front is $u_*(x) \equiv 0$, as χ makes the homogeneous state u_* stable for $\xi > 0$ and unstable for $\xi < 0$. Since Cahn-Hilliard can be derived as an H^{-1}-gradient flow (see [50]) which minimizes the energy

$$\mathcal{E}[u] = \int W(u) + \frac{1}{2}|u_x|^2 dx, \tag{1.3.4}$$

with $W(u)$ a double-well potential, χ be seen as changing or tilting the potential and hence altering the phase separative dynamics. One of the main examples where this is most evident, is in dip-coating experiments where a surfactant lying on top of a liquid solvent is deposited onto a surface by the emersion and controlled withdrawal of the surface [91, 92, 163]. In particular, a modified Cahn-Hilliard equation in the form of (1.3.3) arises as a reduced model for thin film equations which govern these processes. We also remark such experiments have many similarities to the patterned deposition of chemical particles on surfaces via the controlled evaporation of a solvent [151, 73] mentioned above.

These parameter ramps could also be used to study triggered patterns in the Ginzburg-Landau example discussed above where the linear term is modified,

$$A_t = (1+\mathrm{i}\alpha)A_{xx} + \chi(x-ct)A + (\rho+\mathrm{i}\gamma)A|A|^2 - (\beta_1+\mathrm{i}\beta)A|A|^4, \qquad x,t\in\mathbb{R},\ \ A\in\mathbb{C}, \tag{1.3.5}$$

and the homogeneous state $A_* \equiv 0$ is excited. Since cGL is a universal modulation equation for oscillatory instabilities at onset, the model (1.3.5) should be a prototypical description for many typical triggered patterns. One example of such a system is the formation of periodic vortices in open shear flows in fluids [22, 10]. Other examples of such "triggered" systems arise in light-sensitive reaction-diffusion systems [99, 103], phase-field systems [51, 60, 63], directional quenching experiments [54, 93], and the ion-milling experiments mentioned above [59].

In these two types of triggers, the excitation speed c is the main parameter of control. If c is much larger than the speed of the free invasion speed (i.e. c_{lin} or c_{p}), then any perturbation will grow and invade the unstable state in the wake of the preparation front but at a slower rate than the preparation front. Hence the pattern will be selected by the free invasion process. If c is lowered just below the free invasion speed then any pattern forming instability will "catch up" with the trigger interface at $\xi = 0$ and lock with it; see for example Figure 2.1.2 below. Heuristically, one can view this locking as the trigger interface exerting a pressure on the patterned state which causes a perturbation in the selected wavenumber. It is in this regime, $c \sim c_{\mathrm{lin}}$ or $c \sim c_{\mathrm{p}}$, that much of our studies are focused on. Here the pattern forming front in the wake of the trigger forms as a perturbation, or bifurcation, from the free invasion front; see Fig 1.3.1. Other

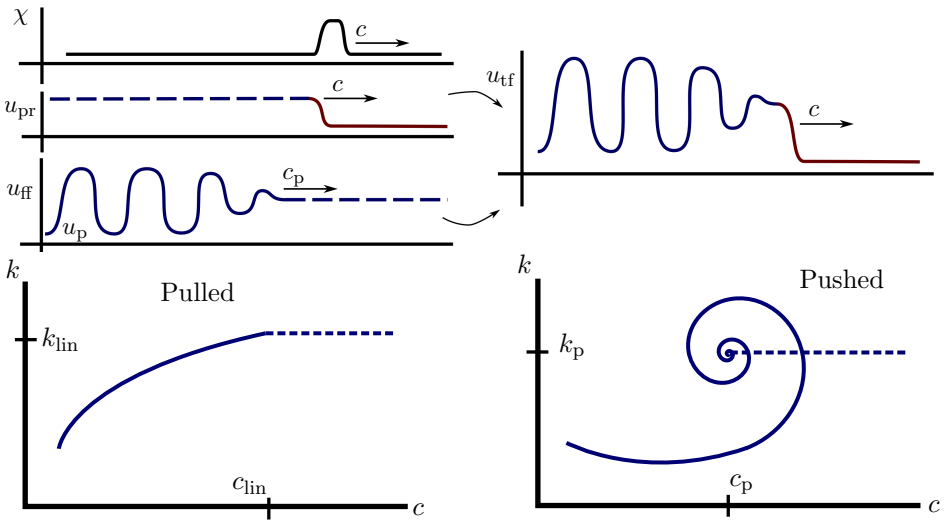

Figure 1.3.1: Top: schematic of the ingredients of a trigger front, the trigger χ, preparation front $u_{\rm pr}$, and the free front $u_{\rm ff}$. Bottom: Behavior of selected wavenumber of pattern when pulled (left) and pushed (right) patterns are triggered, the dotted lines depict where the pattern "unlocks" from the trigger and the free front is selected. Appeared originally in [66]

speed regimes, such as $c \sim 0$, are very interesting and are the subject of current and future research. We shall briefly discuss this regime, as well as other types of triggering mechanisms, in Section 1.3.3 below.

In the next two sections we shall overview our results for c near the free invasion speed in both the case where a trigger perturbs a pulled free invasion front, and the case where it perturbs a pushed free invasion front. To reiterate, the basic mathematical ingredients for control which we study are the following. Take a system in which there exists pattern forming invasion fronts which invade a homogeneous unstable state and in which a spatially progressive triggering mechanism exists which creates a front that connects a stable homogeneous state to the unstable state. Then by mediating the triggering mechanism, one can control the pattern in the wake. For a schematic description of this approach see the top of Figure 1.3.1. Not only do our results give rigorous existence, they also give expansions for how the wavenumber of the pattern changes as the speed c is moved from $c_{\rm lin}$ or $c_{\rm p}$. Such expansions should hopefully give experimentalists more information on how to design and fabricate a specific structure.

1.3.1 Pulled trigger fronts

In Chapter 2 we study the case where a trigger perturbs a pulled free invasion front. Our rigorous results there concern pulled trigger fronts in the complex Ginzburg Landau equation (1.2.3); see Theorem 2.1.1 below. We view these results as prototypical for many pattern forming systems so that many features of our analysis can be immediately transferred to more general pattern-forming systems, such as the examples listed above. The advantage of the Ginzburg-Landau equation is that, due to the gauge symmetry, periodic patterns are explicit and invasion as well as trigger fronts can be found as heteroclinic orbits in a 4-dimensional traveling-wave equation, thus avoiding the (well-understood) complications of infinite-dimensional, ill-posed systems for modulated traveling waves [63, 84, 88, 130, 132]. On the other hand, the complex Ginzburg-Landau equation is of interest since it approximately describes many pattern-forming systems near onset.

After briefly describing our results, we outline how they could possibly be generalized for a given system which possesses pattern forming pulled fronts.

Results in complex Ginzburg-Landau equation In this chapter, we set $\beta_1 = \beta = 0$ for simplicity as the associated quintic terms should only affect the selected wavenumber and amplitude through the nonlinear dispersion relation. We use the gauge invariance $A \mapsto \mathrm{e}^{\mathrm{i}\theta}A$ to factor out temporal oscillations $A \mapsto \mathrm{e}^{\mathrm{i}\omega t}A$, allowing us to study trigger fronts as heteroclinic orbits in the finite-dimensional non-autonomous dynamical system

$$0 = (1+\mathrm{i}\alpha)A_{\xi\xi} + cA_{\xi\xi} + (\chi - \mathrm{i}\omega)A + (\rho+\mathrm{i}\gamma)A|A|^2 - (\beta_1+\mathrm{i}\beta)A|A|^4, \qquad \xi, t \in \mathbb{R},\ \ A \in \mathbb{C}, \tag{1.3.6}$$

which connect the periodic orbit A_p as $\xi \to -\infty$ and the homogeneous state $A_* = 0$ as $\xi \to +\infty$. Since χ is piecewise constant, the dynamical system is autonomous for $\xi > 0$ with $\chi \equiv -1$, and for $\xi < 0$ with $\chi \equiv 1$. Thus, trigger fronts can be found by overlaying the two corresponding phase portraits and finding intersections between the unstable manifold, $W^{\mathrm{cu}}_-(A_p)$, of the periodic orbit in the $\chi \equiv 1$ dynamics and the stable manifold, $W^{\mathrm{s}}_+(0)$, of the origin in the $\chi \equiv -1$ dynamics; see Figure 2.2.1 below. In practice, this

can be viewed as a shooting problem, where trajectories in $W^{\mathrm{cu}}_{-}(A_p)$ are evolved close to the origin and then matched with the effective boundary condition created by $W^{\mathrm{s}}_{+}(0)$ by varying parameters c and ω.

To make the analysis more tractable, we use the gauge invariance of the system to obtain invariant coordinates for the phase space which collapse periodic orbits to points. In these coordinates we use the leading order scaling symmetry to blow-up the origin into a 2-sphere, $\mathcal{S}^2$, so that the phase space becomes $\mathcal{S}^2 \times \mathbb{R}_+$, where $\mathbb{R}_+$ denotes the non-negative real half-line. The dynamics on this sphere, which are governed by a complex Riccatti equation, exactly give the flow on the 2-Grassmannian induced by the linearization about the origin. Since $\mathcal{S}^2 \times \{0\}$ is a normally hyperbolic invariant manifold in these reduced dynamics, we can employ Fenichel's smooth foliation results [46, 47, 48] to straighten fibers and project the dynamics down onto the sphere where we can almost explicitly perform the desired matching for the shooting problem. This matching process gives expansions for the frequency ω, and subsequently the wavenumber k, in the trigger speed c near c_{lin}. These expansions compare quite well with numerics performed in both direct simulations and AUTO computations; see Fig. 2.5.1.

Heuristically, one has the best chance for finding such connections when such Grassmanian dynamics are relatively neutral and consist of rotations. Since the absolute spectrum $\Sigma_{\mathrm{abs}}(c)$ of the state u_* (when viewed in a co-moving frame $\xi = x - ct$) corresponds exactly to such neutral projectivized linear dynamics, one then expects to find intersections on S^2 for frequencies near $\omega = \omega_{\mathrm{abs}}(c)$ where $\{\pm \mathrm{i}\omega_{\mathrm{abs}}(c)\} := \Sigma_{\mathrm{abs}}(c) \cap \mathrm{i}\mathbb{R}$ and c is near c_{lin}.

Indeed, for $(\omega, c) = (\omega_{\mathrm{lin}}, c_{\mathrm{lin}})$, the dynamics on $\mathcal{S}^2$ consist of a family of homoclinic orbits converging to the equilibrium, denoted as z_{b}, which corresponds to the eigenspace of the branch point ν_{lin}; recall here that the equilibria in projectivized dynamics correspond to eigenspaces of the linear dynamics. When c is decreased, and ω is varied along $\omega_{\mathrm{abs}}(c)$, the branch point splits into two eigenvalues with the same real part, so that the equilibrium z_{b} splits into two centers $z_{\pm}$ and the dynamics on S^2 consist of periodic orbits; recall here that eigenvalues of projective equilibria are equal to differences in eigenvalues of the linear system. If ω is perturbed slightly away from $\omega_{\mathrm{abs}}(c)$ then the periodic orbits will break and slowly spiral into the two equilibria z_+ and z_- in forwards

and backwards time. For a pictorial description of these dynamics see Figure 2.3.1.

General result We believe that these results are prototypical and have should have broad application. A schematic framework of such a general result should go as follows.

Schematic result for pulled trigger fronts

In a scalar evolutionary pattern-forming PDE posed on $x \in \mathbb{R}$ assume the following,

- *There exists a pulled invasion front u_{ff} which invades with the linear spreading speed c_{lin} and connects a periodic wave-train u_{per} as $x \to -\infty$ to a homogeneous unstable state u_* as $x \to +\infty$.*

- *The free front u_{ff} satisfies the following decay condition, for some $a_\infty, b_\infty \in \mathbb{R}$ with $a_\infty \neq 0$, in a co-moving frame $\xi = x - c_{\text{lin}}t$,*

$$u_{\text{ff}}(\xi) = a_\infty \xi \mathrm{e}^{\nu_{\text{lin}}\xi} + b_\infty \mathrm{e}^{\nu_{\text{lin}}\xi}\left(1 + o_\xi(1)\right), \quad \xi \to +\infty, \ ,$$

  where ν_{lin} is the spatial eigenvalue at the branch point $\lambda_*(c_{\text{lin}})$ discussed in Section 1.2.1 above.

- *In the wake of a spatial trigger moving at any speed $c \sim c_{\text{lin}}$, there exists a preparation front u_{pr} connecting a stable homogeneous state $\tilde{u}_*$ as $x \to \infty$ and u_* as $x \to +\infty$.*

Then for trigger speeds c with $0 < c_{\text{lin}} - c << 1$ there exists a trigger front solution which connects a spatially periodic pattern to the state $\tilde{u}_*$. Moreover, the temporal frequency ω of the periodic pattern has the following leading order expansion for $c < c_{\text{lin}}$:

$$\omega - \omega_{\text{lin}} \sim K_1(c - c_{\text{lin}}) + K_2(c - c_{\text{lin}})^{3/2}.$$

Here $\mathrm{i}\omega_{\text{lin}}$ is the crossing location of the branch point $\lambda_*(c_{\text{lin}})$ defined above, K_1 is determined by the curvature of the absolute spectrum Σ_{abs} near the branch point, and K_2 is determined by a projectivized distance between the unstable invariant manifold of u_* and the stable manifold of $\tilde{u}_*$ when considered near the origin in a spatial dynamics framework.

From the temporal frequency ω, one can then determine the asymptotic wavenumber through some sort of dispersion relation. In the case of Cahn-Hilliard, periodic patterns are stationary in a stationary frame so that the temporal frequency, when considered in a moving frame with speed c, is $\omega = ck$. In the CGL example in (1.2.3) above, k is determined by solving the nonlinear dispersion relation (1.2.4). The genericity condition on the free front is most readily understood when viewed in a spatial dynamics formulation. In particular, since u_{ff} is a heteroclinic orbit connecting a stable sink equilibrium with a periodic orbit, this condition requires that the configuration of the stable and unstable manifolds of these respective states are generic. That is, the unstable manifold of the periodic orbit does not converge to u_* along the strong stable manifold. This theorem states that the wavenumber selection imposed by the trigger is monotonic in the speed c to leading order; see Figure 1.3.1 for a schematic and Figure 2.4.1 for numerical results. Furthermore, not only would such a result give rigorous existence of these fronts, the information obtained from such a dynamical systems framework could give experimentalists and engineers a prediction for how to select specific patterns in their system.

Such a result should be able to be proved by employing a spatial dynamics formulation in the co-moving frame variable $\xi = x - ct$ to view the problem as a heteroclinic bifurcation. As the periodic pattern left behind in the wake becomes time-periodic in a co-moving frame, this formulation will yield an infinite-dimensional dynamical system; unless one can factor out, or "de-tune" the temporal oscillations as in CGL. In this system the fronts u_{ff} and u_{pr} will form a heteroclinic chain $u_{\text{per}} \to u_* \to \tilde{u}_*$. For $c \sim c_{\text{lin}}$, by varying the parameter ω one would then attempt find intersections of the unstable manifold coming from a periodic orbit close to u_{per} with the stable manifold of the equilibrium arising from $\tilde{u}_*$. Existence of such manifolds in this infinite dimensional system could be obtained in a tubular neighborhood of the heteroclinic chain using exponential dichotomies arising from the linear variational equation along the heteroclinics.

In order to exploit the linear information coming from u_{ff} one would look for such intersections in a neighborhood of u_*, studying how these invariant manifolds and their tangent spaces vary near the intermediate equilibrium u_*. As was done nearly explicitly in the example of cGL discussed above, this corresponds to studying the projectivized

linear dynamics, or in other words, the dynamics on the Grassmannian induced by linearized flow near u_*. One would either have to isolate relevant finite dimensional subspaces to evolve on the Grassmannian or use the recent results [34] to study the evolution of infinite dimensional subspaces. Just as in the example above, one would need to look for connections in the Grassmannian dynamics for parameters near the frequencies $\omega_{\text{abs}}(c)$ for speed c near c_{lin}.

1.3.2 Pushed trigger fronts

In Chapter 3 of this thesis we study trigger fronts perturbed from a pattern forming *pushed* free front. Due to the sharp oscillatory decay of such fronts, many interesting phenomenon can be induced when they are perturbed by a spatial triggering mechanism. In this chapter, we construct an abstract framework and sufficient hypotheses for the existence of a pushed trigger front in a pattern forming system in one spatial dimension. We also obtain expansions for temporal frequencies, and thus wave-numbers, in terms of the trigger speed with coefficients dependent on the properties of the free front and preparation front. We then use these results to study to specific examples, the first being the cubic-quintic CGL equation (1.3.5) discussed above, and the second a modified Cahn-Hilliard equation. Conceptually, our schematic result goes as follows.

Sketch of Theorem 3.3.2

Assume that a one-dimensional, evolutionary pattern forming system has the following properties:

- *There exists a spatially oscillating pushed free front u_{ff} invading an unstable homogeneous equilibrium u_* with speed $c_{\text{p}} > 0$.*
- *For speed c_{p}, there exists a preparation front $u_{\text{pr}}(x - c_{\text{p}}t)$ formed in the wake of a spatial trigger which connects u_* to a stable homogeneous state $\tilde{u}_*$ as $\xi := x - c_{\text{p}}t$ increases from $-\infty$ to $+\infty$.*
- *The fronts u_{ff} and u_{pr} are generic. In other words, when viewed as heteroclinic orbits in a spatial dynamics formulation using the co-moving frame variable ξ, u_{pr} is transverse while u_{ff} is transversely unfolded in parameters ω and c, where ω is*

the temporal frequency of the periodic pattern associated with u_{ff} and c is the speed of the trigger.

- *The inclination properties of the relevant invariant manifolds about u_{pr} are generic.*

Then for trigger speeds close to the free invasion speed c_{p}, there exists a family of pushed trigger fronts connecting a spatially periodic orbit to the stable state $\tilde{u}_*$. Moreover, this family has a bifurcation curve in the parameter space $\mu := (c - c_{\mathrm{p}}, \omega - \omega_{\mathrm{p}}) \in \mathbb{R}^2$, with the asymptotic form

$$\mu(L) = K\mathrm{e}^{\Delta\nu L}(1 + \mathcal{O}\left(\mathrm{e}^{-\delta L}\right)), \quad L \gg 1, \tag{1.3.7}$$

where K is a linear mapping from $\mathbb{C}$ to $\mathbb{R}^2$ (see Fig. 1.3.2), and $\Delta\nu$ denotes the difference of strong stable eigenvalues associated with the decay of the free pushed front, and other weakly stable eigenvalues (see Fig. 1.3.1 and 1.3.3).

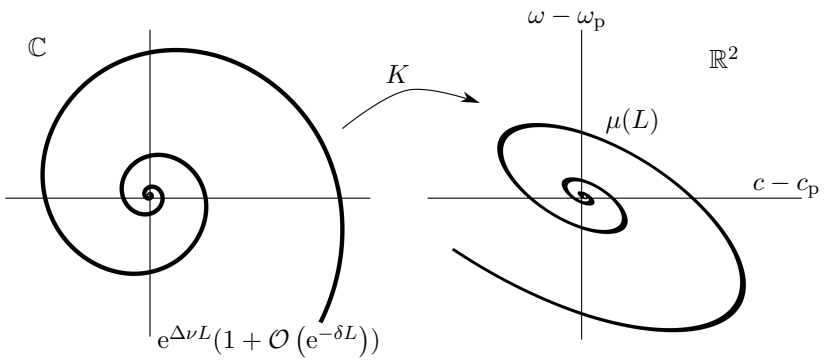

Figure 1.3.2: Leading order bifurcation curve of pushed trigger fronts in μ-parameter space.

If a pushed free front is oscillatory, the bifurcation curve, and hence the selected wave-number, of pushed trigger fronts is non-monotonic and takes on a logarithmic spiral shape; see Figures 1.3.1 and 1.3.2 for a schematic, and Figure 3.2.1 below for numerical results in (1.3.5). This leads to a variety of interesting phenomena which do not occur in the pulled case discussed above. Namely, such trigger fronts will exhibit snaking behavior. This leads to the possibility of multi-stability of fronts, locking behavior for trigger speeds higher than the free invasion speed c_{p}, and finally hysteretic switching between different wave-numbers. This last effect is particularly interesting as it could potentially

be exploited in the design and control of self-organized patterning processes. Heuristically, these non-monotonic behaviors are caused by the interaction of the oscillatory exponentially small tail of the free front u_{ff} with the effective boundary condition created by the trigger interface. Moreover, if this tail were not oscillatory, the bifurcation curve would not exhibit the leading order spiraling behavior shown above.

The genericity assumptions above can also be formulated in terms of spectral information. For u_{ff}, such hypotheses are equivalent to assuming that the Evans function [85] associated with the linearization about the front has a zero of algebraic multiplicity two at the origin, corresponding to the temporal and spatial translation symmetries of the front. For u_{pr}, the associated Evans function has no zeros at the origin. We remark that there is no spatial translation symmetry because of the spatial inhomogeneity introduced by the triggering mechanism. We also note that the linear transformation K above is determined by a matrix of Melnikov integrals corresponding to parameter derivatives of the dynamical system evaluated along the front u_{ff}.

Outline of proof Technically, we use an abstract formulation motivated by the spatial dynamics approach and employ heteroclinic matching techniques in the spirit of [120] which used an alteration of Lin's method [96] to study homoclinic orbits near a heteroclinic cycle consisting of a periodic orbit and equilibrium point in finite-dimensional dynamical systems; see also [81] for an excellent review of such techniques. In particular, we use exponential dichotomies to glue solutions near the equilibrium u_* and then subsequently match them, in transverse sections to the heteroclinic orbits, with the center-unstable manifold of the periodic orbit and the stable manifold of the equilibrium $\tilde{u}_*$; see Figure 3.4.1 for a schematic of this process. We prove existence of pushed trigger fronts and give universal asymptotics for their frequency and wave-numbers. We shall show that the front dynamics are, to leading order, governed by the spectral gap $\Delta\nu = \nu_{\mathrm{ss}} - \nu_{\mathrm{su}}$, between a leading strong-stable spatial eigenvalue ν_{ss}, which governs the asymptotic decay of the free pushed front, and the nearest weakly stable eigenvalue ν_{su}. As seen in Figure 1.3.3, the simplest form of such a gap may come in several varieties, each of which may lead to different phenomena. We shall focus on the case depicted on the left where the gap is determined by two complex conjugate pairs. The other cases in this figure may also lead to many interesting phenomena and are briefly discussed in

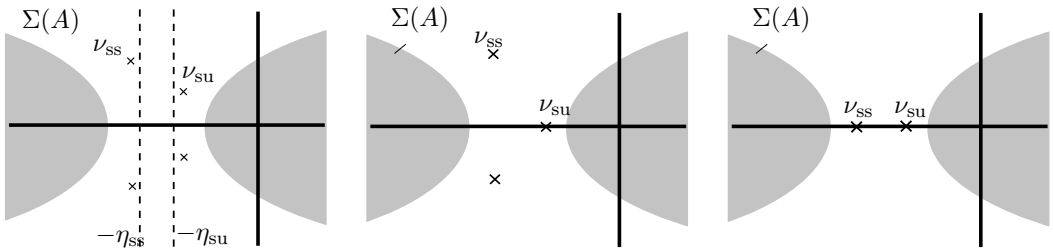

Figure 1.3.3: Depiction of different cases for splitting of spatial eigenvalues corresponding to a free pushed front. The grey areas denote the rest of the spectrum of the linearization of the spatial dynamics formulation. We study the case depicted in the left plot, here the dotted lines denote the exponential weights we use to select relevant solutions near the origin. Appeared originally in [66].

Section 3.5.2.

Application of results To elucidate our abstract results in this case, we consider two prototypical examples. The first of these is the cubic-quintic complex Ginzburg-Landau equation (cGL) already described above. We choose this relatively simple example to demonstrate our results and motivate their application to more complicated systems. In the same ways as in the pulled case, finding pushed trigger fronts in the cGL equation can be reduced to a finite dimensional traveling-wave ODE in which all of the required hypotheses for our result have been proven in previous studies, or can be obtained by straightforward arguments; see Section 3.2.1 and Section 3.5.1.

The second example we consider is a modified Cahn-Hilliard (CH) equation. This equation will serve as an illustration for how our results apply in the case where the existence problem is inherently infinite-dimensional. While in this setting, it is not straightforward to verify the required hypotheses (see Section 3.2.2 and Section 3.5.1), we provide numerical evidence showing the predicted phenomenon, and also evidence for one of our most important hypotheses: the existence of an oscilliatory pushed free front; see Section 3.2.2 and Section 3.5.1.

1.3.3 Slow triggers

In addition to the speed regimes $c \sim c_{\text{lin}}$ and $c \sim c_{\text{p}}$ for pushed and pulled trigger fronts respectively, the other interesting speed regime where a perturbative approach could be used is the slow speed limit $0 < c \ll 1$. While such results are not considered in this thesis, we have recently found that in this regime it is advantageous to view the trigger interface, which connects the patterned state with the stable homogeneous state, as an effective boundary condition. This becomes more clear from a spatial dynamics framework where the stable manifold of the homogeneous equilibrium for the dynamics ahead of the trigger, $\xi > 0$, plays the role of the boundary subspace.

From this view point, the recent results of [106], which characterize how boundary conditions affect the selection of phase and wavenumber of a stable periodic pattern in both semi-infinite, $x \in [-\infty, 0]$, and bounded domains, $x \in [-L, L]$, should give information on how a slow trigger would perturb a pattern. The regime $0 < c \ll 1$ can be viewed as a perturbation of this setting, where the spatial domain is now time dependent, say $[-\infty, ct]$ or $[-L - ct, L + ct]$. Such non-adiabatic movements of the boundary cause a periodic motion in the phase, composed of a slow drift where the phase is locked to the boundary and the wavenumber slowly stretches, and followed by a fast snapping where the phase jumps a half or full period. The recent work [61], uses a Cross-Newell phase-diffusion approximation [30] and formal multi-scale asymptotic expansions to obtain a "universal" leading order expansion for the wavenumber perturbation

$$\Delta k \sim \tilde{K}_1 c^{1/2} + \tilde{K}_2 c^{3/4},$$

where the coefficients $\tilde{K}_1, \tilde{K}_2$ are determined by the behavior of the system at $c = 0$, the effective diffusivity of the periodic pattern, and, somewhat amazingly, the evaluations of the Riemann zeta function $\zeta(1/2), \zeta(-1/2)$; see [61] for more detail.

In the context of slow spatial triggers, one would need to understand how the effective boundary condition of the trigger interface affects the phase/wavenumber relationship in the speed $c = 0$ case. This would then allow for the application of the aforementioned results to obtain expansions for the perturbed wavenumber. One such example of this was explored numerically in [61] where a reaction-diffusion system with a small

amplitude spatial trigger was found to behave as described above.

1.4 Stability and other types of triggers

1.4.1 Stability of triggered solutions

We expect many of the solutions discussed above to be stable. For example, in the pushed and pulled cGL examples above, continuous spectrum, as well as point spectrum coming from the absolute spectrum, would arise from the asymptotic linearizations at $\xi = \pm\infty$. For speeds $c \sim c_{\mathrm{p}}$ or $c \sim c_{\mathrm{lin}}$, and parameters α, γ not too large, these linearizations are stable. Hence instabilities would only arise from the interface of the trigger. If this interface is sufficiently steep, or localized, we expect there to be no such instabilities. In the Cahn-Hilliard equation, the asymptotic wave-trains are typically unstable, and are typically invaded by a period-doubling coarsening front [139]

1.4.2 Other types of triggers

There are many types of triggers other than the parameter ramps and source terms with discontinuous or steep interfaces which we have considered above. One such example are triggers which slowly vary, so that $|\chi'| \ll 1$, but are still asymptotically constant. In this case, in addition to the instabilities studied above, we expect resonance poles to arise corresponding to localized instabilities in the large interfacial region. Another example, would be for a non-monotone trigger where, in (1.3.5) for example, $\chi \equiv a > 0$ with $a \neq 1$ for ξ in some compact region. This would once again lead to resonance poles and could significantly alter the front selection dynamics. Moreover, along the lines of the types of trigger front used in Section 1.5, one could study a trigger of the form

$$\chi(\xi) = \begin{cases} \chi & \equiv 1, \quad \xi \in [-\ell, \ell] \\ \chi & \equiv -1, \quad \xi \notin [-\ell, \ell]. \end{cases}$$

Here we expect the analysis used above to still be applicable, especially in the $\ell \gg 1$ limit. More examples include triggers which are temporally dependent, $\chi(\xi, t)$, creating a triggered system which is forced. Such a regime is potentially an interesting line of

inquiry and we expect studies such as [57, 58, 101] to be relevant and help in the analysis. Other examples arise in various types of "pre-patterning" where $\chi(\xi)$ is periodic, representing an experimentalist preparing the medium before triggering the system; see for example [162, 163, 111]. For more discussion on these types of triggers see Sections 2.5 and 3.5.3.

In these two chapters, we mostly focused on scalar partial differential equations (except for the abstract formulation used in Chapter 3 in which a system of equations could still be studied). We believe that our other results could be extended for systems in some circumstances, but also remark that many other scenarios could be studied, possibly leading to the observation of new and interesting phenomena. One interesting avenue would be to study how a triggered instability could affect the "anomalous" spreading in certain types of reaction-diffusion systems [79, 78] where various types of two-stage invasion, and slow fronts (which invade slower than the linear spreading speed) have been shown to exist.

1.5 Towards a general study of patterns in higher spatial dimensions: an alternative approach

In spatial dimensions greater than one, triggering mechanisms are able to create a plethora in interesting patterns in addition to the planar stripes studied in the one-dimensional systems discussed above; see examples in Figures 1.1.2 and 1.1.3 above. The symmetry of some of these structures allows for their study in a channel shaped domain $(x, y) \in \mathbb{R} \times [0, 2\pi/\omega]$ where the spatial dynamics approach can still be applied to construct the desired solutions. For example, in the Cahn-Hilliard equation mentioned above

$$u_t = -\Delta(\Delta u + u - u^3) \quad x, y \in \mathbb{R}, \tag{1.5.1}$$

"slanted" stripe patterns arise as solutions $u_{\text{st}}(x, y) = v(k(x\cos\phi - y\sin\phi))$ for some 2π-periodic function $v(\cdot)$ with an angle $\phi \in [0, 2\pi)$ and wavenumber k. Triggered solutions could then be studied in a system of the form

$$u_t = -\Delta(\Delta u + u - u^3) + c\chi(x - ct) \quad x, y \in \mathbb{R}, \tag{1.5.2}$$

where χ is a y-independent source term which creates a y-independent preparation front $u_{\rm pr}$. Triggered solutions, connecting the stable state ahead of the trigger with a slanted stripe $u_{\rm st}$ behind it, then arise as stationary solutions of the following system, obtained by making the coordinate changes $\xi = x - ct$, $\tilde{y} = k_y y - \omega t$ with $k_y = k \sin\phi$ and $\omega = ck_y$,

$$0 = -\omega\partial_y u - \Delta_{k_y}(\Delta_{k_y} u + u - u^3) + c\partial_\xi u + c\chi(\xi), \quad \Delta_{k_y} = \partial_\xi^2 + k_y^2\partial_{\tilde{y}}^2, \quad \tilde{y} \in [0, 2\pi], \xi \in \mathbb{R}. \tag{1.5.3}$$

This equation can then be written as a dynamical system with time-like variable ξ in the phase space of periodic functions in y. Since the y-domain is compact the resulting linearization of the dynamical system has compact resolvent and thus has spectrum composed of eigenvalues with finite algebraic multiplicity. This allows for the construction of invariant manifolds which can be used to find specific desired solutions.

In other cases one cannot compactify one of the spatial dimensions so that any spatial dynamics formulation will still have continuous spectrum. If this spectrum is bounded away from the origin, a center manifold reduction may still be applied [74]. If not, as in many interesting problems, it becomes difficult to yield meaning information out of the formulation. Some examples of such problems include the existence of fully localized hexagon patches in the Swift-Hohenberg equation [97] and the formation of corner interfaces between two pattern forming fronts. Another interesting example arises in (1.5.2) where

$$\chi = \chi(\xi, y) = \frac{u_0 - u_m}{\sqrt{\delta\pi}} \mathrm{e}^{-(\xi^2 + \delta_y y^2)/\delta}, \tag{1.5.4}$$

is a fully localized source term depositing mass in a strip of $\mathbb{R}^2$ with an initial condition of $u \equiv u_m \in [-1, 1]$ a constant. As seen in Figure 1.5.1 many interesting patterns arise which are not periodic in y hence requiring study on all of $\mathbb{R}^2$. If one looks in a fixed x-cross-section, different transverse and planar modes appear to be locally selected as one moves farther away from $y = 0$ (depending on the steepness of the source), leading to the interaction of stripes, fingers, and dot patterns at the leading edge and in the wake. Indeed after proving the existence of a transverse, weakly sub-critical bifurcation from a preparation front, one could try to study the interfacial dynamics (i.e. analyze the cross-section $\xi = 0$) in y by deriving a modulation equation for these complicated

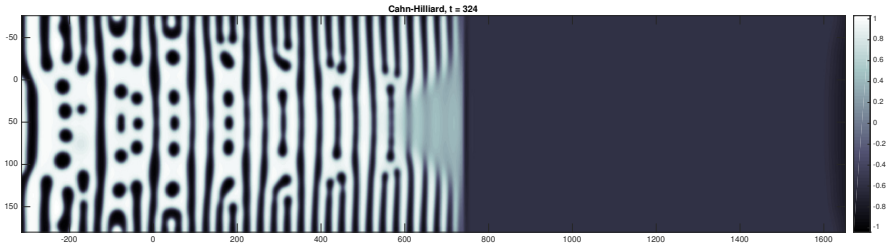

(a) $(1, 10^{-4}, 0.4, -0.58)$

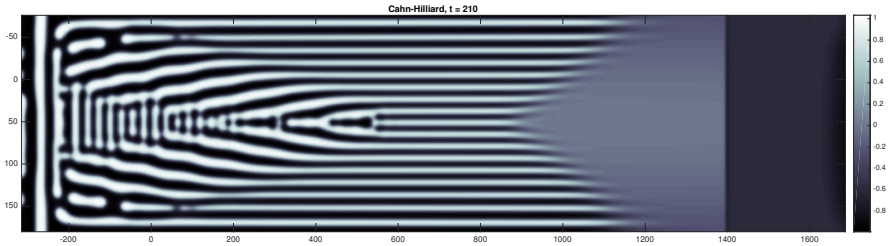

(b) $(2.5, 10^{-4}, 0.0, -0.6)$

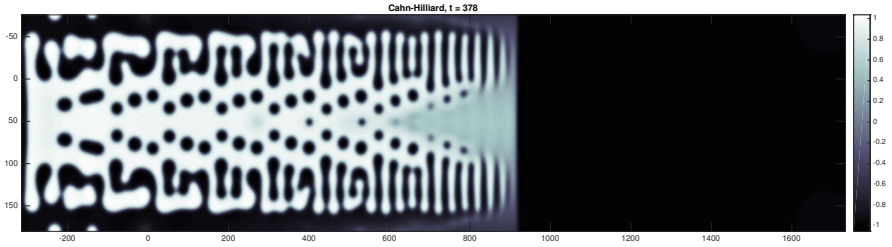

(c) $(1, 2 * 10^{-4}, 0.5, -0.6)$

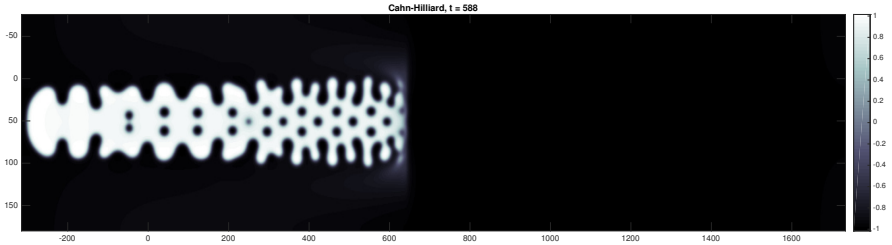

(d) $(0.5, 10^{-3}, 0.5, -1)$,

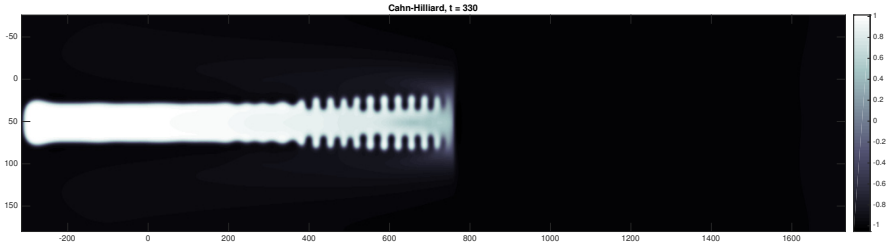

(e) $(1, 2 \times 10^{-3}, 0.5, -0.6)$

Figure 1.5.1: Various patterns in (1.5.2) in the wake of traveling gaussian (1.5.4). Gaussian and initial condition parameters (c, δ_y, u_0, u_m) are listed.

dynamics.

Other examples where spatial dynamics may not apply, include the study of traveling waves whose interfaces are perpendicular to the direction of motion; see [54]. Furthermore, in the broad field of non-local evolution equations, many systems cannot be studied with spatial dynamics due to the absence of a flow [45].

Thus, in the last part of this thesis, we wish to study a more abstract approach which uses functional analysis in the place of spatial dynamics to rigorously obtain solutions. The natural starting point for this abstract approach is to study a problem in which the existing methods can still be applied so that one can learn about the benefits and pitfalls of this new approach.

1.5.1 Hopf bifurcation from fronts in Cahn-Hilliard in 1-D

In Chapter 4 of this work we study modified Cahn-Hilliard models of the form,

$$u_t = -\left(u_{xx} + f(x - ct, u)\right)_{xx} + c\chi(x - ct; c), \quad x, t \in \mathbb{R} \tag{1.5.5}$$

which combine both types of triggers described in (1.3.2) and (1.3.3) above. Recall $u(x,t)$ is an order parameter which denotes the concentration of precipitate at a certain space-time point (x,t) and $\chi(x-ct)$ is a source term which travels through the domain with a constant speed c, leaving behind a monotone, uniformly translating front $u_*(x,t) = u_*(x-ct)$. The spatially dependent nonlinearity f encodes any changes of the medium itself, in the wake of the moving source.

We study the behavior of the system near fronts $u_*(x-ct)$ which connect two homogenous equilibria lying outside or barely inside the spinodally unstable regime, where $f' > 0$; see [50]. As this front travels, there must be a moving spatial domain $[-\ell - ct, \ell - ct]$ where the front takes values inside this unstable regime. In the moving frame coordinate $\xi := x - ct$, for large trigger speeds c, instabilities which may arise in this domain are convective ([126], [153]), and get absorbed into the homogeneous equilibrium in the wake. As c decreases through a certain threshold, an absolute instability may arise, causing the formation of a periodic pattern which saturates the moving domain. In the physical literature, such a "self-sustaining" pattern is referred to as a nonlinear global

mode; see [25]. See Figure 1.5.2 for a schematic plot of these two types of instabilities.

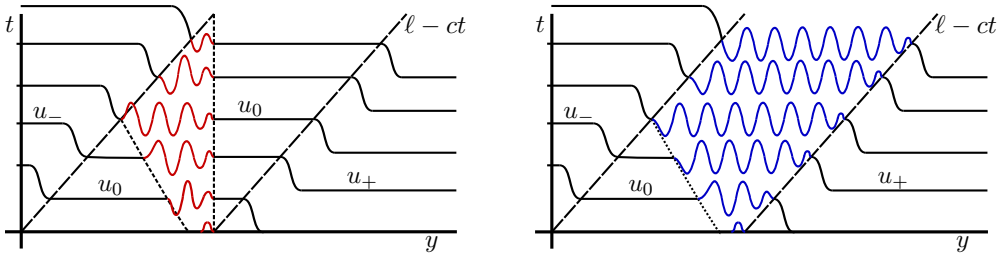

Figure 1.5.2: Development of an instability in spinodal regime of the traveling front u_*. (Left): Instability is stationary (convective in the moving frame), and is "eaten" by the trailing homogeneous state. (Right): Instability is absolute and is sustained as the front propagates through the medium. Originally appeared in [65]

Since these patterns are stationary in a stationary frame, they become time-periodic in a co-moving frame $\xi = x - ct$. Allowing for variations in the temporal frequency ω, we scale $\tau = \omega t$ to obtain

$$\omega u_\tau = -\left(u_{\xi\xi} + f(\xi, u)\right)_{\xi\xi} + c\chi(\xi; c) + cu_\xi, \quad \tau \in [0, 2\pi), \ \xi \in \mathbb{R} \tag{1.5.6}$$

Hence, in this frame of reference, this convective-to-absolute instability transition can be viewed as a Hopf-bifurcation where for some speed c_*, the linearization

$$Lv := -(u_{\xi\xi} + f(\xi, u_*))_{\xi\xi} + c\chi(\xi; c) + cu_\xi$$

has a complex-conjugate pair of eigenvalues $\lambda(c) = \mu(c) \pm \mathrm{i}\kappa(c)$ which cross the imaginary axis with non-zero speed, $\mu'(c_*) > 0$, leading to a localized instability arising in the plateau region $[-\ell, \ell]$. Since far field fluctuations are neutrally unstable due to the mass conserving properties of the Cahn-Hilliard equation, the continuous spectrum of L intersects the origin. Furthermore, since we allow for asymptotic states $u_*(\pm\infty)$ which are weakly unstable in our approach, the continuous spectrum can also marginally reside in the unstable half-plane. For our specific construction, we also require that the continuous spectrum is not resonant with the Hopf frequency. That is, the bifurcating eigenvalues (and their integer multiples) do not lie in the essential spectrum. Two examples of this spectral configuration are given in Figure 1.5.3.

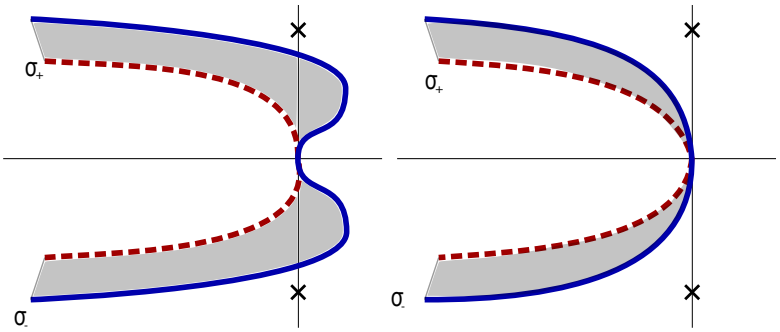

Figure 1.5.3: Allowed spectral configurations in our abstract framework, here the crosses denote Hopf eigenvalues, grey regions denote the essential spectrum, and blue and red lines denote the Fredholm borders.

Our main contributions are threefold: a technically simple proof for Hopf bifurcation in the presence of essential spectrum, a rigorous existence proof of patterned fronts in the Cahn-Hilliard equation, and the analysis of an explicit, prototypical example. The rigorous result roughly goes as follows:

Sketch of Theorem 4.1.3

In the system (1.5.6) *above, assume the following:*

- *The inhomogeneities f and χ are smooth and converge exponentially fast as $\xi \to \pm\infty$.*
- *There exists a travelling wave solution u_* which travels with speed c_* and is robust, monotone, and asymptotically constant in space with exponentially fast convergence.*
- *The linearization L about u_*, posed on $L^2(\mathbb{R})$, has a simple Hopf eigenvalue crossing for some $\lambda = \pm i\omega_*$ and speed $c_* > 0$ with eigenfunctions $p \in L^2(\mathbb{R})$.*
- *For all $\lambda \in i\omega_*\mathbb{Z} \setminus \{0, \pm 1\}$, the operator $L - \lambda$ is invertible when considered on $L^2(\mathbb{R})$.*

Then there exists a one-parameter family of $2\pi/\omega_*$-periodic solutions which bifurcate

from u_* which can be parameterized by a real amplitude $r > 0$ such that

$$c = c_* + \frac{\mathrm{Re}\{\theta_+\}}{\mu'(c_*)} r^2 + \mathcal{O}(r^4), \quad \omega = \omega_* + \mathrm{Im}\{\theta_+\}|r|^2 + \mathcal{O}(|r|^4),$$
$$u = u_* + rp(\xi)\cos(\omega t) + \mathcal{O}(r^2),$$

where θ_+ is determined by the spectral information and the nonlinearity f.

Existence of pattern forming fronts. This result shows the existence of pattern forming fronts in the Cahn-Hilliard equation (1.5.6). As evidenced above, such fronts have been widely studied experimentally and numerically. Furthermore, we obtain computable bifurcation coefficients allowing for the characterization of bifurcations and hopefully a deeper understanding of the patterns being formed. In terms of understanding triggered pattern formation, this result gives predictions for how the wavenumber can be controlled, using the relation $k = \omega/c$. We also remark that our results compare well to the numerical investigations of [92, 91], where numerical continuation was used to find modulated and un-modulated traveling wave solutions, revealing a rich snaking structure of saddle-node and Hopf-bifurcations as the speed of the trigger is varied.

Bifurcation in the presence of essential spectrum. We wish to study the bifurcation of eigenvalues when essential spectrum is present on the imaginary axis. This absence of a spectral gap precludes any center manifold reduction and hence does not allow the immediate use of standard finite-dimensional bifurcation techniques. Several methods have been developed to get around this difficulty. In the context of Hopf bifurcation in viscous shocks and combustion waves, Texier and Zumbrun [149, 150] use subtle point-wise estimates for the temporal semi-group of the linearization to obtain solutions via a Poincare return map. Alternatively, a more geometric approach via spatial dynamics (described in the sections above) can be used to study the spatial evolution of time-periodic functions. Bifurcating solutions then are constructed via a point-wise matching of infinite dimensional invariant manifolds. Such techniques have been applied in the study of viscous shocks by Sandstede and Scheel [135], extending their previous work on Hopf bifurcations due to essential spectrum crossing the imaginary axis [125, 128, 129], and also in the propagation of water waves by Barrandon,

Dias, and Iooss [9], [36]. Interaction between Hopf bifurcation and essential spectra was also studied in a spirit similar to [149, 150], yet without the assumption of a conservation law, in [94, 16], exploiting the sufficiently strong diffusive decay of modes associated with essential spectra in higher space dimensions. Hopf bifurcation in the presence of essential spectra is also responsible for the meandering transition of spiral waves [8, 137, 138, 67]. While rigorous Hopf bifurcation results are not available for Archimedean spirals, the essential spectrum has striking consequences for the shape of bifurcating patterns, creating an intricate rotating super-spiral structure [131].

A direct functional analytic approach Our main contribution is a much more direct functional analytic approach to this problem. While we develop our approach in the context of the Cahn-Hilliard equation, it could also be used in the context of [150, 135] to significantly simplify proofs. In particular see Section 4.7 where we give a simplified proof of the existence result in [135] for bifurcation in of oscillatory viscous shocks. Our approach is simpler as it restricts the linear analysis to Fredholm properties on time-periodic functions, avoiding the subtle diffusive decay properties for infinite times used in [150] or the point-wise reduction based on exponential dichotomies in [135].

In the Cahn-Hilliard setting we described above, we study bifurcating solutions of (1.5.6) as solutions of a nonlinear operator

$$0 = \mathcal{F}(u, \omega, c) = \omega u_\tau + (u_{\xi\xi} + f(\xi, u))_{\xi\xi} - c\chi(\xi; c) - cu_\xi. \tag{1.5.7}$$

Our approach then exploits the techniques in [123] to determine that the linearization of $\mathcal{F}$ about u_*

$$\mathcal{L}v := \omega_* v_\tau + \big(v_{\xi\xi} + f'(\xi, u_*)v\big)_{\xi\xi} - c_* v_\xi,$$

is Fredholm with index -1 when considered on an exponentially weighted function space $L^2_\eta(\mathbb{R}, L^2(\mathbb{T}))$, with norm

$$\int_{\mathbb{R}} \mathrm{e}^{\eta\sqrt{1+x^2}} ||v(x,\cdot)||^2_{L^2(\mathbb{T})} dx, \quad 0 < \eta \ll 1,$$

where we have imposed temporal periodicity. This norm shifts the Fredholm boundaries

of the essential spectrum and in effect suppresses the neutrally unstable far field caused by mass conservation. Furthermore, this mass conservation then allows us to restrict the codomain of the nonlinear operator to the subspace of functions perpendicular to the constants, where $\mathcal{L}$ has index 0. Eigenfunctions, $p(\xi)$, of L corresponding to the Hopf mode then span the kernel of $\mathcal{L}$

$$\ker \mathcal{L} = \operatorname{span}\{\mathrm{e}^{\mathrm{i}\tau} p(\xi), \mathrm{e}^{-\mathrm{i}\tau}\overline{p(\xi)}\},$$

while adjoint eigenfunctions span the cokernel. We then apply a Lyapunov-Schmidt reduction to the restriction of $\mathcal{L}$ to obtain existence of bifurcating solutions and expansions of bifurcation parameters. We also add that our method gives computable expressions for bifurcation coefficients. In previous studies, such coefficients appear difficult to obtain; see for example Eqn. 3.35 of [135, §3.2].

Explicit characterization of a prototypical example. In Section 4.4, we apply our results to an idealization of the motivating examples discussed above which exhibits many interesting phenomena. In particular, we study a nonlinearity of the form

$$f(x - ct, u) = \chi(x - ct)u + \gamma u^3 - \beta u^5,$$

and solutions which bifurcate from a trivial front $u_* \equiv 0$. Here $\beta > 0$, $\chi \equiv 1$ for all $\xi = x - ct \in [-l, l]$, and $\chi \equiv -1$ elsewhere. As it travels through the domain, the parameter ramp triggering mechanism χ does not add mass to the system but instead alters the stability of the homogeneous solution u_*. Indeed $\partial_u f(\xi, 0) > 0$ (spinodally unstable) for all $\xi \in [-l, l]$ and $\partial_u f(\xi, u_0) < 0$ (spinodally stable) for all $\xi \notin [-l, l]$. As c decreases through a certain speed c_*, we show that there exists a first-crossing of a pair of eigenvalues with non-zero imaginary part. The piecewise constant dependence of f on ξ allows us to construct an explicit Evans function, and use spatial dynamics to determine the leading order expansions for the accompanying eigenfunctions, for l sufficiently large.

While the piecewise constant linearization of f allows for relatively straight forward study of spectra, its discontinuities cause the linearized operator to not be well-defined

on the previous "nice" function spaces. To overcome this, optimal parabolic regularity and trace estimates are used to adapt the function spaces and obtain the necessary Fredholm properties; see Section 4.2.2. We then apply our main result to conclude the existence of bifurcating solutions and furthermore that the bifurcation is subcritical for $\gamma > 0$ and supercritical for $\gamma < 0$.

1.5.2 Higher dimensional patterns

We believe that the analytic method outlined above, and discussed in detail in Chapter 4 below, should be able to be lifted to the more complicated settings discussed at the beginning of this section.

For example in the Cahn-Hilliard equation (1.5.3) posed on an infinite cylinder $(x, y) \in \mathbb{R} \times [0, 2\pi)$,

$$0 = -\omega u_y - \Delta_{k_y}(\Delta_{k_y} u + f(\xi, u)) + c\partial_\xi u + c\chi(\xi), \quad \Delta_{k_y} = \partial_\xi^2 + k_y^2 \partial_y^2, \quad \ell \in \mathbb{Z}, \xi \in \mathbb{R}, \tag{1.5.8}$$

one could hope to prove a result similar to the $O(2)$-Hopf bifurcation result in [117] (because of the reflection and translation symmetries in y) or the transverse steady bifurcation in [105]. That is assuming the existence of bifurcating transverse eigenfunctions, one would hope to obtain a Fredholm linearization using an abstract closed range lemma with suitably defined function spaces and then determine the index by decomposing the linearized operator into its Fourier components in y,

$$\mathcal{L}_\ell v := \omega \mathrm{i}\ell v - \hat{\Delta}_{k_y}(\hat{\Delta}_{k_y} v + f'(\xi, u_*)v) + c\partial_\xi v, \quad \hat{\Delta}_{k_y} = \partial_\xi^2 - k_y^2 \ell^2, \quad \ell \in \mathbb{Z}, \xi \in \mathbb{R}, \tag{1.5.9}$$

and determining the index of each separately. Through a suitably arranged Lyapunov-Schmidt argument one could then prove the existence of transversely modulated patterns such as the slanted stripe pattern shown in Figure 1.5.4.

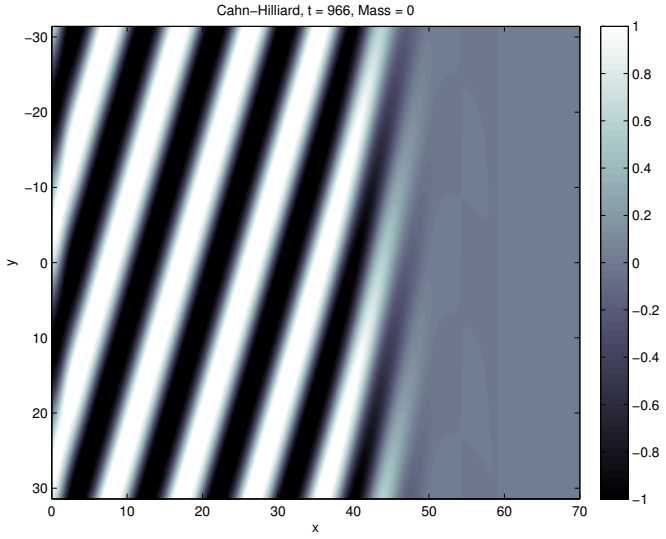

Figure 1.5.4: Transverse pattern in triggered Cahn-Hilliard equation.

Chapter 2

Pattern formation in the wake of pulled trigger fronts

The contents of this chapter originally appeared in [64]; with permission of Springer.

2.1 Introduction and main results

In this chapter we study how spatial triggers can perturbed pulled free invasion fronts in the prototypical complex Ginzburg-Landau equation (CGL),

$$A_t = (1 + \mathrm{i}\alpha)\Delta A + A - (1 + \mathrm{i}\gamma)A|A|^2, \tag{2.1.1}$$

As is typical for pattern-forming systems, CGL supports a variety of coherent and complex patterns. Even in parameter regimes $\alpha \sim \gamma$, when the equation is close to a gradient-like flow, there exist continua of stable periodic patterns, $A \sim \mathrm{e}^{\mathrm{i}(\omega(k)t - k\cdot x)}$, and coherent defects, most prominently Nozaki-Bekki holes in one space dimension and spiral waves in two space-dimension, both having vanishing amplitude $A = 0$ at $x = 0$. As described in Section 1.2.1, when starting with spatially localized initial conditions, one observes a spatial invasion process that leaves distinct wavetrains in its wake, whose wavenumber does not depend on the initial condition but only on system parameters; see [11, 33, 156].

We shall study how a parameter-ramp type trigger can select wavenumbers in one spatial dimension with the modified equation

$$A_t = (1 + \mathrm{i}\alpha)A_{xx} + \chi A - (1 + \mathrm{i}\gamma)A|A|^2, \tag{2.1.2}$$

where $\chi = \chi(x - ct)$, $c > 0$, and, setting $\xi = x - ct$, $\chi(\xi) \to \chi_\pm$ for $x \to \pm\infty$, with $\chi_- > 0 > \chi_+$.

We now describe the basic scenario that we will analyze quantitatively in this article. In the following work we fix

$$\chi(\xi) = \begin{cases} \chi_- = +1, & \text{for } \xi \leq 0 \\ \chi_+ = -1, & \text{for } \xi > 0 \end{cases} \tag{2.1.3}$$

and consider (2.1.2) with fixed α, γ, while varying the speed c of the trigger χ as our primary bifurcation parameter. Our results can be easily adapted to different values of $\chi_\pm$. Smooth triggers χ with derivative χ' sufficiently localized would also be immediately amenable to the following analysis.

Phenomenologically, one observes roughly two different regimes. For large speeds c, one observes patterns in the wake of a front that propagates with a speed $c_{\mathrm{lin}} < c$. The patterns created in the wake of that front are roughly independent of the speed c. When the trigger speed is decreased below c_{lin}, patterns nucleate roughly at the location of transition from stability to instability. The wavenumber of patterns in the wake now depends smoothly on the speed c. At the transition, $c \sim c_{\mathrm{lin}}$, the wavenumber in the wake depends continuously on c, constant for $c > c_{\mathrm{lin}}$, and, to leading order, linear for $c \lesssim c_{\mathrm{lin}}$. This scenario is illustrated in space-time plots of direct numerical simulations in Figure 2.1.1 and Figure 2.1.2. There, the trigger moves into the medium from the left, sending out a periodic wave-train in it's wake. The right-hand figure shows the same system in a moving frame of speed c. The trigger is placed near the right boundary of the domain and sends out waves to the left. Since $A \equiv 0$ is unstable for $\xi < 0$, without any local perturbations, the system oscillates homogeneously. As time evolves, a periodic wave train emitted from the trigger invades these homogeneous oscillations along a sink [132, 157].

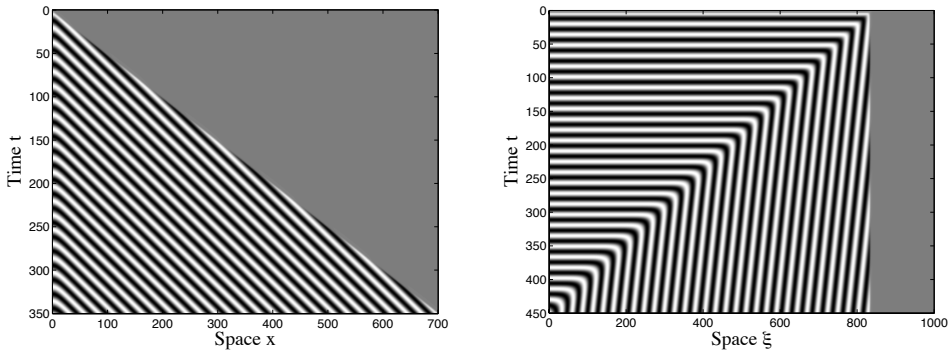

Figure 2.1.1: Simulations of trigger fronts in both stationary (left) and moving (right) frames; $\alpha = -0.1, \gamma = -0.4, c = 1.8 < c_{\text{lin}} = 2\sqrt{1+\alpha^2} \approx 2.01$.

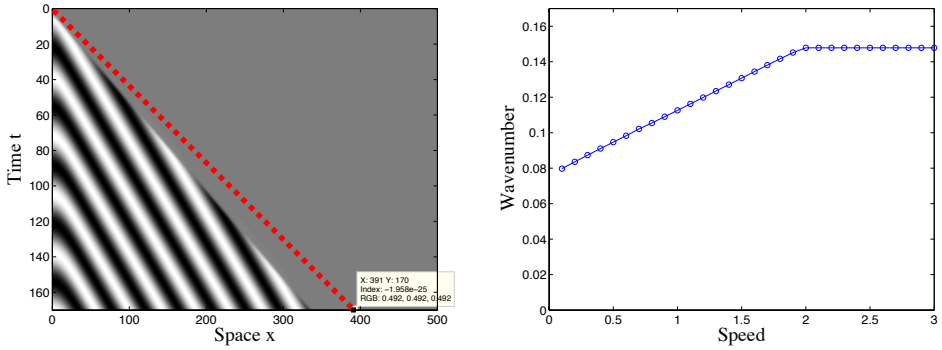

Figure 2.1.2: The figure on the right gives the selected wavenumber for a range of trigger speeds; $\alpha = -0.1, \gamma = -0.2$. The figure on the left shows the space-time plot in the case $c = 2.3 > c_{\text{lin}}$, when the constant wavenumber k_{lin} is selected. The dotted red line denotes the path of the trigger $x = ct$.

Before continuing, we recall the properties of the pulled free front stated in Section 1.2.1. Namely, the linear spreading speed can be obtained from inserting the ansatz $A \sim \mathrm{e}^{\lambda t + \nu x}$ into (2.1.1). In our case this relation takes the form $d(\lambda, \nu) = (1 + \mathrm{i}\alpha)\nu^2 + 1 - \lambda$, by solving[1]

$$d(\mathrm{i}\omega - c\nu, \nu) = 0, \qquad \frac{\mathrm{d}}{\mathrm{d}\nu} d(\mathrm{i}\omega - c\nu, \nu) = 0$$

[1]In general, one also needs to verify a pinching condition, which however in our case is automatically satisfied.

where $\frac{d}{d\nu}$ is evaluated as a total derivative. One finds

$$c_{\rm lin} = 2\sqrt{1+\alpha^2}, \qquad \omega_{\rm lin} = \alpha, \qquad \nu_{\rm lin} = -\frac{1-{\rm i}\alpha}{\sqrt{1+\alpha^2}}. \tag{2.1.4}$$

One derives a *linear prediction for the nonlinear pattern* in the wake of the front from this linear information as follows. Nonlinear spatio-temporally periodic patterns are, in the simplest form, solutions of the form

$$A(t,x) = {\rm e}^{{\rm i}\Omega_{\rm nl}(k)t}A^{\rm p}(x;k), \qquad A^{\rm p}(x;k) = \sqrt{1-k^2}{\rm e}^{-{\rm i}kx}, \quad \text{where } \Omega_{\rm nl}(k) = -\alpha k^2 - \gamma(1-k^2).$$

In the comoving frame of speed c, the frequency of these patterns is determined by the nonlinear dispersion relation in the comoving frame,

$$\Omega(k;c) = -\alpha k^2 - \gamma(1-k^2) - ck. \tag{2.1.5}$$

One can solve $\Omega(k, c_{\rm lin}) = \omega_{\rm lin}$ for $k =: k_{\rm lin}$, using that $|k| < 1$, and thereby derive a linear prediction for a nonlinear selected wavenumber,

$$k_{\rm lin} = \begin{cases} -\dfrac{\sqrt{1+\gamma^2}-\sqrt{1+\alpha^2}}{\gamma-\alpha}, & \text{for } \gamma \neq \alpha \\ -\dfrac{\alpha}{\sqrt{1+\alpha^2}}, & \text{for } \gamma = \alpha. \end{cases} \tag{2.1.6}$$

We also recall that the group velocity of wave trains in the wake of the invasion front points away from the front interface so that the front acts as a source in a co-moving frame of speed $c_{\rm lin}$,

$$c_{\rm g} := \frac{{\rm d}\Omega(k;c_{\rm lin})}{{\rm d}k}\Big|_{k=k_{\rm lin}} = -2\sqrt{1+\gamma^2} < 0. \tag{2.1.7}$$

In order to state our main assumption, we first give a precise characterization of invasion fronts in the form needed later.

Definition 2.1.1 (Generic free fronts)**.** *A free front is a solution to CGL, (2.1.2) with $\chi \equiv 1$, of the form $A(t,x) = {\rm e}^{{\rm i}\omega_{\rm lin}t}A^{\rm f}(x - c_{\rm lin}t)$, that satisfies*

$$A^{\rm f}(\xi) \to 0 \text{ for } \xi \to \infty, \qquad |A^{\rm f}(\xi) - A^{\rm p}(\xi; k_{\rm lin})| \to 0 \text{ for } \xi \to -\infty.$$

We say a free front is generic if there exist $\mathcal{A}_\infty, \mathcal{B}_\infty \in \mathbb{C}$ *with* $\mathcal{A}_\infty \neq 0$ *such that*

$$A^{\mathrm{f}}(\xi) = \Big(\mathcal{A}_\infty \xi \mathrm{e}^{\nu_{\mathrm{lin}}\xi} + \mathcal{B}_\infty \mathrm{e}^{\nu_{\mathrm{lin}}\xi}\Big)\Big(1 + \mathcal{O}_\xi(1)\Big), \text{ for } \xi \to \infty.$$

Trigger fronts and main result. Our goal is to find solutions to (2.1.2) that describe the triggered invasion process when the speed of the trigger is less than, but close to, the speed of the invasion front. In a completely analogous fashion to free fronts, we define trigger fronts as spatial connections between $A = 0$ at $\xi = +\infty$ and a periodic wave train at $\xi = -\infty$.

Definition 2.1.2 (Trigger fronts)**.** *A trigger front with frequency* ω_{tf} *is a solution to CGL, (2.1.2), with trigger speed* c*, of the form* $A(t,x) = \mathrm{e}^{\mathrm{i}\omega_{\mathrm{tf}}t}A^{\mathrm{tf}}(x-ct)$*, that satisfies*

$$A^{\mathrm{tf}}(\xi) \to 0 \text{ for } \xi \to \infty, \qquad |A^{\mathrm{tf}}(\xi) - A^{\mathrm{p}}(\xi; k_{\mathrm{tf}})| \to 0 \text{ for } \xi \to -\infty,$$

where k_{tf} *is such that* $\omega_{\mathrm{tf}} = \Omega(k_{\mathrm{tf}}; c)$ *and the group velocity*

$$c_{\mathrm{g}}(k_{\mathrm{tf}}) := \frac{\mathrm{d}\Omega(k;c)}{\mathrm{d}k}\Big|_{k=k_{\mathrm{tf}}} < 0.$$

In other words, trigger fronts are time-periodic with frequency ω_{tf} *and emit wave trains with wavenumber* k_{tf}*. Furthermore, for a fixed* $\delta > 0$ *sufficiently small, we define the front interface distance as*

$$\xi_* := \inf\left\{\xi; \sup_{\xi' > \xi} |A(\xi')| < \delta\right\}$$

.

We are now ready to state our main result.

Theorem 2.1.1. *Fix* $\alpha, \gamma \in \mathbb{R}$ *and assume that there exists a generic free front. Then there exist trigger fronts for* $c < c_{\mathrm{lin}}$*,* $|c - c_{\mathrm{lin}}|$ *sufficiently small. The frequency of the trigger front possesses the expansion*

$$\omega_{\mathrm{tf}}(c) = \omega_{\mathrm{abs}}(c) + \frac{2}{\pi}(1+\alpha^2)^{3/4}|\Delta Z_{\mathrm{i}}|(c_{\mathrm{lin}} - c)^{3/2} + \mathcal{O}((c_{\mathrm{lin}} - c)^2). \tag{2.1.8}$$

Here,

$$\omega_{\mathrm{abs}}(c) = -\alpha + \frac{\alpha c^2}{2(1+\alpha^2)},$$

and ΔZ_{i} *is defined in (2.3.22), below. Furthermore, for* $\alpha \neq \gamma$ *the selected wavenumber has the expansion*

$$k_{\mathrm{tf}} = k_{\mathrm{lin}} - g_1(\alpha,\gamma)(c_{\mathrm{lin}} - c) - \frac{2(1+\alpha^2)^{3/4}|\Delta Z_{\mathrm{i}}|}{\pi(1+\gamma^2)^{1/2}}(c_{\mathrm{lin}} - c)^{3/2} + \mathcal{O}((c_{\mathrm{lin}} - c)^2)$$

where $g_1(\alpha,\gamma) = \frac{1}{2(\gamma-\alpha)}\left(1 - \frac{1+2\alpha\gamma-\alpha^2}{\sqrt{(1+\alpha^2)(1+\gamma^2)}}\right)$*. The distance between the trigger and the front interface is given by*

$$\xi_* = \pi(1+\alpha^2)^{1/4}(c_{\mathrm{lin}} - c)^{-1/2} + (1+\alpha^2)^{1/2}\,\Delta Z_{\mathrm{r}} + \mathcal{O}((c_{\mathrm{lin}} - c)^{1/2}),$$

where ΔZ_{r} *is defined in (2.3.22) as well.*

In the following, we elaborate on assumptions and conclusions in this result.

Interpreting the expansion. The frequency ω_{abs} is determined by the intersection of the absolute spectrum [126] of the linearization at the origin in a frame moving with speed c and the imaginary axis. Roughly speaking, the absolute spectrum denotes curves in the complex plane that emanate from double roots of the dispersion relation such that finitely truncated boundary-value-problems possess dense clusters of eigenvalues at these curves as the size of the domain goes to infinity [126]. The absolute spectrum is a natural first-order prediction for frequencies of trigger fronts as we shall explain in Section 2.2. Intersection points with the imaginary axis arise when the edge of the absolute spectrum crosses the imaginary axis. This happens precisely when c is decreased below c_{lin}, so that quite generally there will be a unique intersection point, smoothly depending on c; see Figure 2.1.3.

The term ΔZ_{i} that describes corrections to the leading-order prediction can be interpreted as a distance in projective space between tangent spaces of stable manifold and unstable manifold. Roughly speaking, decay at $\xi = +\infty$ creates an effective boundary condition of Robin type at $\xi = 0$, while the leading edge of the invasion front approximately satisfies a different Robin boundary condition. The distance between those

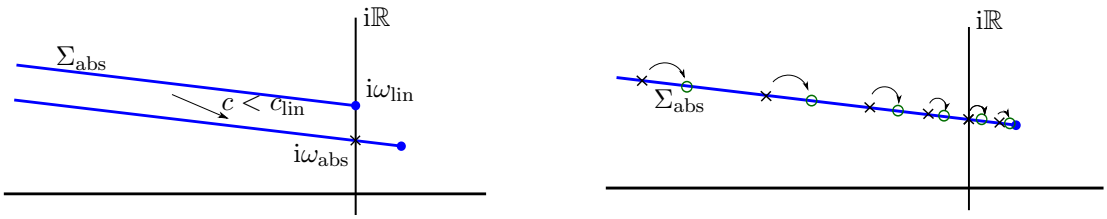

Figure 2.1.3: Left: Plot of the absolute spectrum $\Sigma_{\rm abs}$ in the complex plane. The blue dots denote double roots. The curve moves into the right half plane for $c < c_{\rm lin}$, intersecting $i\mathbb{R}$ at $i\omega_{\rm abs}$. Right: As the domain size L increases to $+\infty$ the spectrum of the linear operator accumulates on $\Sigma_{\rm abs}$.

two boundary conditions, measured in an appropriate coordinate system, is denoted by $\Delta Z_{\rm i}$. Using a simple shooting algorithm, one can evaluate $\Delta Z_{\rm i}$ quite accurately; see our numerical studies in Section 2.4.

The assumption on existence, non-uniqueness, and more fronts. We will see in our proof that the expansion of invasion fronts at $\xi \to \infty$ holds for any invasion front with $|\mathcal{A}_\infty| + |\mathcal{B}_\infty| > 0$, so that genericity refers to the (open) condition $\mathcal{A}_\infty \neq 0$, only. Existence can be cast as the problem of existence of a heteroclinic connection between an unstable equilibrium and a sink. Genericity refers to unstable and stable manifolds being in general position.

We are not aware of results guaranteeing the existence of generic invasion fronts, or any evidence pointing towards non-existence. We show in Proposition 2.3.3 that generic invasion fronts exist for $|\alpha - \gamma|$ sufficiently small.

In a different interpretation, vanishing of $\mathcal{A}_\infty$ characterizes fronts at the boundary between pushed and pulled invasion in parameter space. In the case of cubic CGL, considered here, such a transition has not been observed. On the other hand, the transition is usually accompanied by an increase in the (nonlinear) invasion speed, so that one expects trigger fronts to exist for speeds larger than $c_{\rm lin}$ beyond this transition; see the discussion in Section 2.5.

The fronts we find are *not unique*. In fact, our proof gives the existence of a countable

family of invasion fronts, indexed by $j = 1, 2, \ldots$, with frequencies

$$\omega_{\mathrm{tf}}(c; j) = \omega_{\mathrm{abs}}(c) + \frac{2|\Delta Z_{\mathrm{i}}|}{\pi j (1+\alpha^2)^{3/4}} (c_{\mathrm{lin}} - c)^{3/2} + \mathcal{O}((c_{\mathrm{lin}} - c)^{5/2}). \tag{2.1.9}$$

Roughly speaking, the distance between front interface (measured by, say, the location of $|A| = \delta > 0$, fixed) and the trigger location $\xi = 0$ increases linearly with the index j. We expect these fronts to be unstable with Morse index increasing linearly in j.

Stability and secondary instabilities. We did not attempt to prove stability but we suspect that the fronts we find are stable in a suitable sense. In fact, stability of the free front is known for $\alpha = \gamma = 0$ [42] and one can show that fronts with $\alpha \sim \gamma$ are at least linearly stable. It would be interesting to conclude stability of the trigger fronts that we find from spectral stability of the free front. On the other hand, free fronts can be unstable. In particular, the wave train selected by the invasion (or trigger) front is in fact unstable for many values of α and γ. Most dramatically, for $\alpha\gamma < -1$, *all* wave trains are unstable. The instability may propagate slower than the primary invasion front, leading to a wedge in space-time plots where the (unstable) selected wave train can be observed. For large α, γ, the secondary instability invades at a fixed distance behind the primary front; see [156, §2.11.5], [144] and Figure 2.1.4 for an illustration.

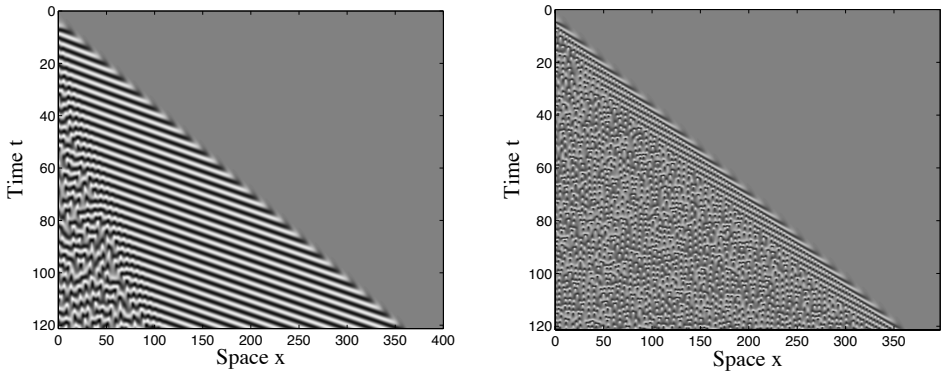

Figure 2.1.4: Invasion of spatio-temporal chaos after formation of periodic pattern in wake of a trigger; parameters in the Benjamin Feir instability range: $\alpha = -1.2, c = 0.95 \cdot c_{\mathrm{lin}} = 1.90 \cdot \sqrt{1+\alpha^2}$ and $\gamma = 2$ (left), and $\gamma = 8$ (right).

Spatial dynamics. We prove our main result by rewriting the existence problem for a trigger front as a non-autonomous ODE for $A^{\mathrm{tf}}(\xi)$,

$$A_{\xi\xi} = -\frac{1}{(1+\mathrm{i}\alpha)}\left[(\chi(\xi) - i\omega)A + cA_\xi - (1+\gamma\mathrm{i})A|A|^2\right]. \tag{2.1.10}$$

Here, c is the (externally prescribed) bifurcation parameter and ω is a matching parameter that will be used to achieve appropriate intersections of stable and unstable manifolds. In fact, one can most easily understand this ODE by separately considering dynamics with $\chi \equiv \chi_+$ and $\chi = \chi_-$, thus obtaining two separate 4-dimensional phase portraits. For $\chi = \chi_+$, we will find the equilibrium $A = A_\xi = 0$ with a two-dimensional stable manifold. For $\chi = \chi_-$, we find that $A = A_\xi = 0$ is stable with an open basin of attraction. On the other hand, we also have a periodic orbit A^{p}, depending on c and ω, with a two-dimensional unstable manifold. Existence of a free front implies that there exists a heteroclinic orbit between A^{p} and the origin. The strategy of the proof is to find intersections between the unstable manifold of A^{p} in the χ_--phase-space and the stable manifold of the origin in the χ_+-phase space. We will find these intersections bifurcating from the origin upon decreasing c below c_{lin} and adjusting ω appropriately. A key technical ingredient to our result is a geometric blowup of the origin which both factors the S^1-action on $(A, A_\xi) \in \mathbb{C}^2$ induced by the gauge symmetry, and desingularizes the vector field by effectively separating eigenspaces near an algebraically double complex eigenvalue. Intersections can then be found almost explicitly on a singular sphere, and lifted using Fenichel's invariant foliation methods [46, 47, 48].

Outline. The remainder of this paper is organized as follows. Section 2.2 gives heuristics and a conceptual outline of the proof of Theorem 2.1.1, describing the role of the absolute spectrum in finding the desired heteroclinic intersection. Section 2.3 contains the proof of our main theorem. Section 2.4 gives comparisons between our expansions, direct simulations, and direct computations of heteroclinic orbits. Finally, Section 2.5 gives a discussion of our results and directions for future research.

2.2 Heuristics — formal asymptotics and the role of the absolute spectrum.

We present several concepts that help understand the result. We first explain the role of absolute spectra and then present a formal *exponential matching* argument that mimicks the main strategy of proof. Last, we give a brief outline of *geometric desingularization*, the center piece of our approach and connect it with these two other points of view.

Absolute spectra. Taking the perspective of a numerical simulation in a comoving frame, we could attempt to understand trigger fronts as steady states (up to the gauge symmetry) bifurcating from the trivial state $A \equiv 0$ when the latter looses stability. One would then linearize the system at $A \equiv 0$ in a bounded domain, in a comoving frame, equipped with separated boundary conditions. In order to realistically capture the phenomena, we would assume that the size of the domain L is large. One can even simplify further and substitute "effective" boundary conditions at $\xi = 0$ and restrict to $\xi \in [-L, 0]$. The linearized operator $(1 + \mathrm{i}\alpha)\partial_{\xi\xi} + c\partial_\xi + 1 - \mathrm{i}\omega$ then possesses constant coefficients but is not self-adjoint and spectra in large domains are not approximated by spectra in unbounded domains. In fact, eigenvalues of the linearized operator in the bounded interval accumulate, as $L \to \infty$, at curves referred to as the *absolute spectrum*, Σ_{abs} [126]; see Fig. 2.1.3. Those curves can be computed from the dispersion relation $d(\lambda, \nu) = 0$ as follows. One varies λ as a parameter, solves for all roots $\nu = \nu_j(\lambda)$, and orders those roots by real part $\operatorname{Re}\nu_1 \leq \operatorname{Re}\nu_2 \leq \ldots \leq \operatorname{Re}\nu_N$ for each fixed λ. For $\operatorname{Re}\lambda \to \infty$, one always finds $\operatorname{Re}\nu_j < 0 < \operatorname{Re}\nu_{j'}$, for $j \leq M < j'$, with some fixed M. The absolute spectrum then is the set of λ so that $\operatorname{Re}\nu_M(\lambda) = \operatorname{Re}\nu_{M+1}(\lambda)$.

In our case, $d_c(\lambda, \nu) = (1 + \mathrm{i}\alpha)\nu^2 + c\nu + 1 - \lambda$, with roots

$$\nu_\pm = -\frac{c}{2(1+\mathrm{i}\alpha)} \pm \sqrt{\frac{c^2}{4(1+\mathrm{i}\alpha)^2} - \frac{1-\lambda}{1+\mathrm{i}\alpha}}.$$

At the absolute spectrum, we must have $\operatorname{Re}\nu_+ = \operatorname{Re}\nu_-$, so

$$\frac{c^2}{4(1+\mathrm{i}\alpha)^2} - \frac{1-\lambda}{1+\mathrm{i}\alpha} < 0. \tag{2.2.1}$$

Bifurcations in a bounded domain occur when eigenvalues cross the imaginary axis, $\lambda = \mathrm{i}\omega$, leading to periodic orbits with frequency close to ω. We are therefore interested in the intersection of the absolute spectrum with the imaginary axis, which, starting with (2.2.1), is readily found at

$$\omega_{\mathrm{abs}}(c) = -\alpha + \frac{\alpha c^2}{2(1+\alpha^2)}, \tag{2.2.2}$$

for $c < c_{\mathrm{lin}}$. We caution the reader that ω_{abs} is not constant, due to two effects: the curve of absolute spectrum is not horizontal and the imaginary part of the leading edge will depend on c. As the domain size increases, eigenvalues will move along the curve of absolute spectrum towards the edge [126, Lemma 5.5], which is located in $\{\mathrm{Re}\lambda > 0\}$, thus leading to a sequence of Hopf bifurcations. The periodic solutions with frequency ω emerging from these Hopf bifurcations converge to the trigger fronts described in our main result; see also the subsequent discussion, pointing to a countable family of trigger fronts.

While this view point gives a rather simple and universal prediction, it is generally not clear how the bifurcating solutions evolve as $L \to \infty$. One can easily envision pushed fronts leading to a faster propagation mechanism, thus inducing turning points in the branch of periodic solutions. We refer to [25, 153, 134] for more detailed analyses in this direction.

Inspecting the proofs in [126], eigenvalues are generated by oscillatory dynamics in the Grassmannian: one evolves the boundary condition at $\xi = -L$ as an element of the Grassmannian and seeks intersections with the boundary condition at $\xi = L$. Since eigenvalues in the Grassmannian are differences of eigenvalues in the linear system, oscillatory dynamics occur when $\mathrm{Re}\nu_- = \mathrm{Re}\nu_+$, in our simple case. In the following, we explain how these oscillatory dynamics can be found in a more local analysis.

Exponential matching. Starting with the assumption that the amplitude of the trigger front would be small at $\xi = 0$ when $c \lesssim c_{\mathrm{lin}}$, we try to glue the free front, shifted appropriately, at $\xi = 0$ with an exponentially decaying tail in $\xi > 0$.

To leading order, the free front decays like $\mathcal{A}_\infty \zeta \mathrm{e}^{\nu(\xi+\zeta)} + \mathcal{B}_\infty \mathrm{e}^{\nu(\xi+\zeta)}$, with shifted variable

ζ. We next vary ω and c and neglect the dependence of the coefficients $\mathcal{A}_\infty$ and $\mathcal{B}_\infty$ on c, ω. In order to track the dependence of the exponential rate ν on ω, c, we inspect the linear dispersion relation $(1 + \mathrm{i}\alpha)\nu^2 + c\nu + 1 - \mathrm{i}\omega = 0$. Near $\omega = \omega_{\mathrm{lin}}$ and $c = c_{\mathrm{lin}}$, we have two roots $\nu_1 \sim \nu_2$, so that one expects decay in the front profile $\mathcal{A}\mathrm{e}^{\nu_2(\xi+\zeta)}$, when $\mathrm{Re}\,\nu_1 < \mathrm{Re}\,\nu_2 < 0$.

On the other side, small solutions in $\xi > 0$ decay like $\mathcal{A}_+\mathrm{e}^{\nu_+\xi}$, where ν_+ solves $(1 + \mathrm{i}\alpha)\nu^2 + c\nu - 1 - \mathrm{i}\omega = 0$.

Trying to match A and A_ξ at $\xi = 0$, we find that due to leading order scaling invariance (keeping only linear terms) and gauge invariance, it is enough to match A_ξ/A. This however gives $\nu_+ = \nu_1$ in our leading order expansion, an equation that cannot be solved varying ω and c locally. In fact, our expansion for the invasion front $\mathcal{A}\mathrm{e}^{\nu_1(\xi+\zeta)}$ is not valid uniformly when varying ω and c. In order to get smooth and uniform expansions, one needs to use a smooth expansion in terms of exponentials near the double root, using either smooth normal forms near a Jordan block [6] or, more along the lines of our strategy, normal forms for the induced flow on A_ξ/A. Without going into details, one readily finds that the expansion in $\mathrm{e}^{\nu_2\xi}$ alone will fail near $\mathrm{Re}\,\nu_1 = \mathrm{Re}\,\nu_2$, where one would keep both terms $\mathcal{A}\mathrm{e}^{\nu_1\zeta} + \mathcal{B}\mathrm{e}^{\nu_2\zeta}$. Varying ζ and the difference $\nu_1 - \nu_2$ as a function of ω, one can then solve the matching problem with $\xi > 0$.

Note that here the absolute spectrum appears in a natural way as parameter values ω where $\mathrm{Re}\nu_1 = \mathrm{Re}\nu_2$.

Geometric desingularization. The global aspect of the matching procedure is illustrated in Figure 2.2.1. The dynamics with $\chi \equiv \chi_-$ show a periodic orbit A^{p} with a two-dimensional unstable manifold that converges to the stable equilibrium $A \equiv 0$. In this phase portrait, the linearization at the origin is a complex Jordan block. Overlayed is the phase portrait for $\chi \equiv \chi_+$, where $A \equiv 0$ possesses a two-dimensional stable manifold. Factoring the S^1-symmetry, both manifolds are 1-dimensional in a 3-dimensional ambient space. We are looking for intersections close to the origin. Our main control parameter is ω, which, together with the bifurcation parameter c unfolds the complex Jordan block and leads to possible flips in the position of the unstable manifold of A^{p} near $A \equiv 0$.

From the above discussion, it is apparent that a description of a neighborhood of $A = A_\xi = 0$ is crucial to the understanding of the matching procedure. There are several dynamical systems techniques for such a description. First, one can try to use smooth linearization for the ODE (2.1.10). Since $\nu = \nu_{\text{lin}}$ has negative real part, the double eigenvalue is in fact non-resonant, and smooth linearization results are available; see for instance [86, §6.6]. In our context, we would however also require smooth parameter-dependence and S^1-equivariance. While such results may well be true, our approach appears more robust and elementary. Roughly speaking, we introduce polar coordinates for $(A, A_\xi) \in \mathbb{C}^2 \sim \mathbb{R}_+ \times S^3$, and factor the gauge symmetry, $\mathbb{C}^2/S^1 \sim \mathbb{R}_+ \times (S^3/S^1) \sim \mathbb{R}^+ \times S^2$, where the last equivalence collapses the Hopf fibration. Identifying S^2 with the Riemann sphere $\overline{\mathbb{C}}$, we end up with coordinates $|A|^2$ and A_ξ/A, that we identified above. In these coordinates, the sphere $|A|^2 = 0$ is normally hyperbolic and carries an explicit linear projective flow that allows us to compute expansions at leading order. Matching outside of the sphere, which corresponds to taking higher-order terms in the exponential matching procedure into account, can be readily achieved after straightening out smooth foliations. We refer to the next sections for details of this procedure.

2.3 Heteroclinic bifurcation analysis

In this section we prove our main result. We start in Section 2.3.1 by several simple rescaling transformations and calculate dimensions of stable and unstable manifolds using information from the dispersion relation. Section 2.3.2 introduces the coordinate system near the origin that we use to factor the gauge symmetry and desingularize the linear dynamics. Section 2.3.3 examines the asymptotics of the free invasion front and shows that our assumptions are verified in the regime $\alpha \sim \gamma$. Section 2.3.4 contains the matching analysis in the desingularized coordinates.

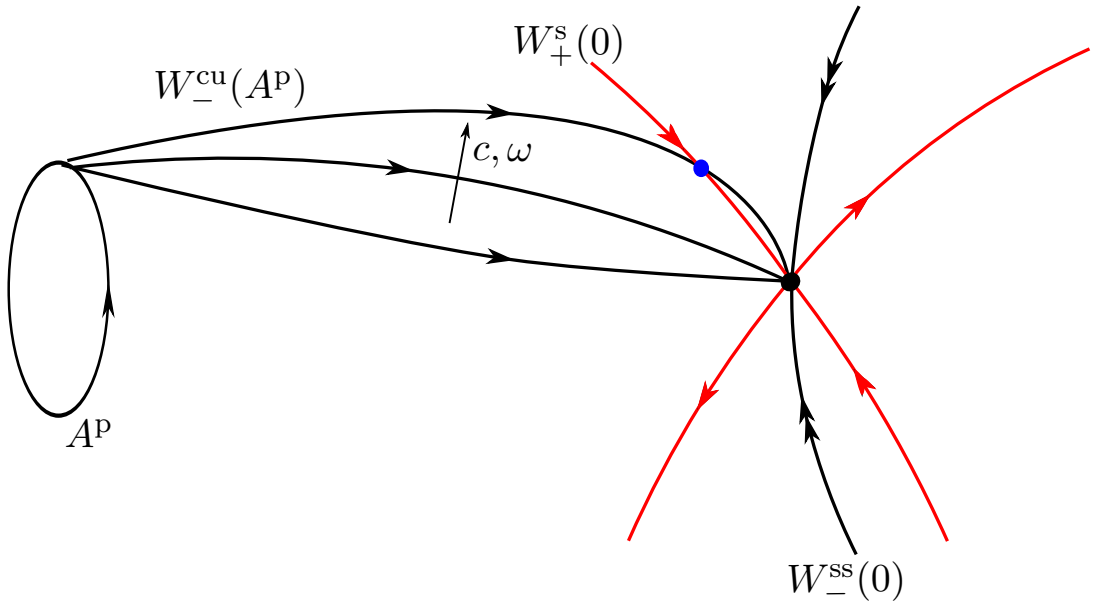

Figure 2.2.1: Schematic diagram of intersection between $W^{\rm cu}_-(A^{\rm p})$ and $W^{\rm s}_+(0)$. The red lines denote the invariant manifolds of the origin in the $\xi > 0$ dynamics. These act as boundary conditions for a shooting from $W^{\rm cu}_-(A^{\rm p})$. Unfolding c and ω from $c_{\rm lin}$ and $\omega_{\rm lin}$, we obtain a non-trivial intersection at $(\xi, \omega) = (\xi_*, \omega_{\rm tf}(c))$ (blue dot) .

2.3.1 Scalings and dimension counting

The following change of variables will slightly simplify the remainder of our analysis, essentially eliminating α as a parameter. Suppose first that $1 + \alpha\gamma > 0$. Setting

$$S = \frac{c\alpha}{2(1+\alpha^2)}, \quad m^2 = 1 + \frac{(c\alpha)^2}{4(1+\alpha^2)} - \alpha\omega, \quad l^2 = \frac{1+\alpha\gamma}{m^2}, \tag{2.3.1}$$

we scale and parameterize

$$a = l\mathrm{e}^{-\mathrm{i}S\xi}A, \quad \hat{c} = \frac{c}{m\sqrt{1+\alpha^2}}, \quad \hat{\omega} = \frac{\omega - \omega_{\rm abs}(\alpha, c)}{m^2}, \quad \zeta = \frac{m}{\sqrt{1+\alpha^2}}\xi, \quad \hat{\gamma} = \frac{\gamma - \alpha}{1+\gamma\alpha}, \tag{2.3.2}$$

so that (2.1.10) simplifies to

$$a_{\zeta\zeta} = -(1 - \mathrm{i}\hat{\omega})a - \hat{c}a_\zeta + (1 + \mathrm{i}\hat{\gamma})a|a|^2 + \frac{(1-\chi)}{m^2}(1 + \mathrm{i}\alpha)a. \tag{2.3.3}$$

If we restrict to $\zeta < 0$ we have $\chi = 1$ and obtain

$$a_{\zeta\zeta} = -(1 - \mathrm{i}\hat{\omega})a - \hat{c}a_{\zeta} + (1 + \mathrm{i}\hat{\gamma})a|a|^2, \tag{2.3.4}$$

whereas for $\zeta \geq 0$ we obtain

$$a_{\zeta\zeta} = -(1 - \mathrm{i}\hat{\omega})a - \hat{c}a_{\zeta} + (1 + \mathrm{i}\hat{\gamma})a|a|^2 + \frac{2}{m^2}(1 + \mathrm{i}\alpha)a. \tag{2.3.5}$$

The cases $1+\alpha\gamma < 0$ and $1+\alpha\gamma = 0$ can be treated in a similar fashion. For $1+\alpha\gamma < 0$ one finds

$$a_{\zeta\zeta} = -(1 - \mathrm{i}\hat{\omega})a - \hat{c}a_{\zeta} + (-1 + \mathrm{i}\hat{\gamma})a|a|^2 + \frac{(1-\chi)}{m^2}(1 + \mathrm{i}\alpha)a, \tag{2.3.6}$$

and for $1 + \alpha\gamma = 0$ we find

$$a_{\zeta\zeta} = -(1 - \mathrm{i}\hat{\omega})a - \hat{c}a_{\zeta} + \mathrm{i}\hat{\gamma}a|a|^2 + \frac{(1-\chi)}{m^2}(1 + \mathrm{i}\alpha)a. \tag{2.3.7}$$

Since those cases do not alter the subsequent discussion, we omit the straightforward details and focus on the case $1 + \alpha\gamma > 0$ in the sequel.

Remark 2.3.1. *The fact that the scaled equation changes type when $1 + \alpha\gamma$ changes sign reflects the Benjamin-Feir instability: for $1 + \alpha\gamma < 0$, all wave trains are unstable. One observes secondary invasion fronts, Figure 2.1.4, which for moderate values of $|\alpha\gamma|$ propagate slower than the primary invasion front, leaving a long plateau of unstable wave trains. For large values of $|\alpha\gamma|$, the instability catches up with the primary front and one observes chaotic dynamics in the immediate wake of the primary front. In this case, our results, while correct, do not describe actually observed wavenumbers due to the strong, absolute instability in the wake; we refer to [156, §2.11.5] and [108] for a discussion of this behavior for free invasion fronts.*

For the remainder of the proof, we will consider the first order form of (2.3.3), writing

ζ as our spatial variable, A once again as the amplitude, and $B := A_\zeta$.

$$\begin{aligned} A_\zeta &= B \\ B_\zeta &= -(1-\mathrm{i}\hat{\omega})A - \hat{c}A_\zeta + (1+\mathrm{i}\hat{\gamma})A|A|^2 + \frac{(1-\chi)}{m^2}(1+\mathrm{i}\alpha)A. \end{aligned} \tag{2.3.8}$$

The following proposition shows that free fronts are unique up to spatial translation and gauge symmetry.

Proposition 2.3.2. *Let $c = c_{\mathrm{lin}}$ and $\omega = \omega_{\mathrm{lin}}$. Then the CGL traveling wave equation* (2.1.10) *possesses a unique relative equilibrium A^{p} with wavenumber k_{lin}. In other words, there exists a unique wave train with frequency ω_{lin} in a frame moving with speed c_{lin}. In* (2.1.10)*, this relative equilibrium possesses a smooth two-dimensional center-unstable manifold $W^{\mathrm{cu}}_-(A^{\mathrm{p}})$.*

Proof. The proof of the proposition is a direct calculation of eigenvalues of the linearization at A^{p}. We refer to [157, §2.2.3], where explicit conditions are given so that this linearization possesses precisely one unstable eigenvalue but caution the reader that the convention in this chapter is to define frequency and wavenumber of wavetrains via $A = r\mathrm{e}^{-\mathrm{i}\omega t + kx}$ (i.e. with the opposite sign as ours). Substituting $c = c_{\mathrm{lin}}$ and $\omega = \omega_{\mathrm{lin}}$ into the formulas there, we obtain the desired result for all α, γ. ■

2.3.2 Symmetry reduction and geometric blowup

In order to carry out the matching procedure near the origin, we would like to quotient the S^1-action and exhibit the leading-order scaling symmetry from the linearized equation. It turns out that this can be achieved in a very simple fashion, introducing $|A|^2 \geq 0$ and $A_\zeta/A \in \mathbb{C}$ as new variables. While very effective, this choice appears somewhat arbitrary and we will show how to obtain these coordinates in a systematic fashion.

Since the S^1-action is not free near the origin, the quotient $\mathbb{C}^2/S^1$ is not a manifold. A canonical parameterization of the orbit space is given by the Hilbert map and canonical coordinates are given by the generators of the ring of invariants of the action; see [24,

Thm 5.2.9]. In our case, the ring of invariants is generated by

$$R = |A|^2, \qquad S = |B|^2, \qquad N = A\bar{B} \tag{2.3.9}$$

where, once again, we have set $B = A_\zeta$, with a relation

$$H(R, S, N) := RS - N\bar{N} = 0, \quad R \geq 0, \quad S \geq 0, \tag{2.3.10}$$

hold. The generators of the ring of invariants can be found either through a direct computation or using the general theory of invariants as outlined in [24, §5]. Explicitly, one checks that a monomial $A^{\ell_1}\bar{A}^{\ell_2}B^{\ell_3}\bar{B}^{\ell_4}$ is invariant if $\ell_1 + \ell_3 = \ell_2 + \ell_4$, which defines a submodule $\mathcal{M}$ of $\mathbb{N}^4$. One then readily verifies that this submodule is generated by the vectors

$$e_1 = (1, 1, 0, 0), \quad e_2 = (0, 0, 1, 1), \quad e_3 = (1, 0, 0, 1)$$

which correspond to the monomials in (2.3.9) above. In other words, any invariant monomial can be written as a product of R, S, N, and $\bar{N}$ in an obvious fashion. More generally, one can compute the Molien series [24, Thm 5.4.1] of this specific representation of the group S^1 as $\frac{1+z^2}{(1-z^2)^3}$. The denominator indicates three algebraically independent quadratic monomials, say $R, S, \mathrm{Re}(N)$, and the numerator suggests another, algebraically dependent, quadratic invariant, $\mathrm{Im}(N)$; see [24, Rem 5.4.2].

The orbit space $\mathbb{C}^2/S^1$ is then homeomorphic to the subset of $R, S, N \in \mathbb{R}^2 \times \mathbb{C}$ where the relations (2.3.10) hold. One can now express (2.3.8) in invariants, only, and derive equations for R, S, N [24, §6].

We next would like to eliminate the leading-order scaling symmetry, which, since all invariants are quadratic, acts equally on R, S, N. Directional blowup [41], allows us to exploit the leading-order scaling symmetry in an explicit fashion. We therefore use an equivariant, R, and associated invariants S/R, N/R, with respect to the scaling symmetry as new variables. The idea is that the invariants represent the quotient space and the equivariant, which commutes with the action of the scaling group rather than being invariant, tracks the scaling action. One finds that the relations simplify and the orbit space is given as a graph, $S/R = N/R \cdot \overline{N}/R$, so that we may consider the invariant

$z = \bar{N}/R = B/A \in \mathbb{C}$, only[2]. We find the system

$$\begin{aligned} z' &= -z^2 - \hat{c}z - (1 - \mathrm{i}\hat{\omega}) + (1 + \mathrm{i}\hat{\gamma})R \\ R' &= 2\mathrm{Re}(zR) = R(z + \overline{z}) \end{aligned} \tag{2.3.11}$$

in the phase space $\mathbb{R}^+ \times \overline{\mathbb{C}}$. In order to obtain a complete set of charts in a neighborhood of the origin, one also uses the directional blowup in the S-direction, with variables $\tilde{z} = A/B = 1/z$ and S,

$$\begin{aligned} \tilde{z}' &= 1 + \hat{c}\tilde{z} + \tilde{z}^2 \left[1 + \mathrm{i}\hat{\omega} - (1 + \mathrm{i}\hat{\gamma})|\tilde{z}|S^2\right] \\ S' &= 2S \left[-\mathrm{Re}((1 - \mathrm{i}\hat{\omega})\tilde{z}) - c + \mathrm{Re}((1 + \mathrm{i}\hat{\gamma})\tilde{z})|\tilde{z}|^2 S\right). \end{aligned} \tag{2.3.12}$$

Note that the $\tilde{z}$ equation is precisely the Poincaré inversion of the z-equation in system (2.3.11), and that the singularity $z = \infty$ is non-degenerate, with $\tilde{z}' = 1$.

Also, note that the sphere $z \in \mathbb{C}$, $R = 0$, together with the point $\tilde{z} = 0$, $S = 0$, is flow-invariant, the blown-up origin of the original system. On this *singular sphere* $\mathcal{S}$, we isolated the scaling-invariant, leading-order part of the equation. Of course, the sphere can also be understood as the result of collapsing the Hopf fibration, obtained via $\mathbb{C}^2/S^1 \sim \mathbb{R}^+ \times (S^3/S^1) \sim \mathbb{R}^+ \times S^2$.

Since a direct calculation using (2.1.4) and (2.3.2) shows that $\hat{c}_{\mathrm{lin}} = 2$, it is convenient to introduce the detuning of the trigger speed from the free front speed as a new parameter,

$$\Delta\hat{c} = \hat{c}_{\mathrm{lin}} - \hat{c} = 2 - \hat{c}, \quad 0 < \Delta\hat{c} \ll 1.$$

The system (2.3.11) now reads

$$\begin{aligned} z' &= -(z + 1)^2 + \Delta\hat{c}\, z + \mathrm{i}\hat{\omega} + (1 + \mathrm{i}\hat{\gamma})R \\ R' &= 2\mathrm{Re}(zR) = R(z + \overline{z}). \end{aligned} \tag{2.3.13}$$

To conclude this section, we study the flow on the singular sphere, given by the Riccati

[2]We do not know when to expect such a simplification for more general group actions.

equation

$$z' = -(z+1)^2 + \Delta\hat{c}\, z + \mathrm{i}\hat{\omega}. \tag{2.3.14}$$

Equilibria

$$z^{-}_{1/2} = -\frac{2-\Delta\hat{c}}{2} \pm \sqrt{-\Delta\hat{c} - \mathrm{i}\hat{\omega} + \frac{(\Delta\hat{c})^2}{4}},$$

correspond to eigenspaces of the original linearized equation. The equilibria undergo a complex saddle-node at $z = -1$ when $\Delta\hat{c} = 0$, $\hat{\omega} = 0$, and a Hopf bifurcation at $\Delta\hat{c} > 0$, $\hat{\omega} = 0$. At the Hopf bifurcation, the flow on $\mathcal{S}$ consists of periodic orbits, whereas outside of the Hopf bifurcation, all non-equilibrium trajectories converge to the same equilibrium. At the saddle-node, all trajectories are homoclinic to $z = -1$. Of course, the Riccati equation can be integrated explicitly, and we will exploit this later on.

We also note that for the $\zeta > 0$ dynamics ($\chi(\zeta) = -1$) the equilibria on $\mathcal{S}$ satisfy

$$z^2 + (2-\Delta\hat{c})z + (-1+\mathrm{i}\hat{\omega}) + \frac{2}{m^2}(1+\mathrm{i}\alpha), = 0.$$

The equilibrium with negative real part corresponds to the tangent space of the stable manifold W^s_+ and is explicitly given through

$$z_+ = -\frac{2-\Delta\hat{c}}{2} - \sqrt{2 - \Delta\hat{c} - \mathrm{i}\hat{\omega} + \frac{(\Delta\hat{c})^2}{4} + \frac{2}{m^2}(1+\mathrm{i}\alpha)}. \tag{2.3.15}$$

2.3.3 Existence of generic free invasion fronts and the blowup geometry

We show that generic free fronts exist when $|\alpha - \gamma| \ll 1$ and analyze asymptotics in our blowup coordinates. As we saw in the previous section, the dynamics on the sphere consist of homoclinic orbits converging to a saddle-node equilibrium $z_{\mathrm{b}} = -1$ when $\Delta\hat{c} = \hat{\omega} = 0$, corresponding to the unscaled parameters $c = c_{\mathrm{lin}}$ and $\omega = \omega_{\mathrm{lin}}$. In particular, there exists a unique trajectory in the strong stable manifold of the equilibrium, which corresponds to decay $\mathrm{e}^{-\zeta}$. All other trajetories decay with rate $1/\zeta$ in the tangent space of the sphere, which translates into decay $A(\zeta) \sim \mathcal{A}_\infty \zeta \mathrm{e}^{-\zeta} + \mathcal{B}_\infty \mathrm{e}^{-\zeta}$ with $\mathcal{A}_\infty \neq 0$. In

fact, one readily obtains

$$z^f(\zeta) \sim \nu + \frac{1}{\zeta + \frac{\mathcal{B}_\infty}{\mathcal{A}_\infty}} = -1 + \frac{1}{\zeta + \frac{\mathcal{B}_\infty}{\mathcal{A}_\infty}}, \quad R^f(\zeta) = \mathrm{e}^{2\mathrm{Re}\,\nu\zeta}|\mathcal{A}_\infty\zeta + \mathcal{B}_\infty|. \tag{2.3.16}$$

The following proposition shows that $\mathcal{A}_\infty \neq 0$ for $\alpha \sim \gamma$.

Proposition 2.3.3. *For fixed α, generic free fronts as defined in Definition 2.1.1 exist when $|\alpha - \gamma|$ is sufficiently small.*

Proof. In scaled variables, when $\hat{c} = \hat{c}_{\mathrm{lin}} = 2$ and $\hat{\omega} = \hat{\omega}_{\mathrm{lin}} = 0$, we find

$$A'' = -A - 2A' + (1 + \mathrm{i}\hat{\gamma})A|A|^2, \tag{2.3.17}$$

where, from (2.3.2), $\hat{\gamma} = \mathcal{O}(|\gamma - \alpha|)$. For $\hat{\gamma} = 0$, this equation posseses a real heteroclinic solution connecting $A = 1$ to $A = 0$, with the desired asymptotics $A(\zeta) \sim \mathcal{A}_\infty\zeta\mathrm{e}^{-\zeta} + \mathcal{B}_\infty\mathrm{e}^{-\zeta}$, $\mathcal{A}_\infty > 0$. Since the heteroclinic is a saddle-sink connection between the circle of relative equilibria $|A| = 1$ and the origin, it persists for small values of $\hat{\gamma}$ as a heteroclinic orbit between a nearby relative equilibrium and the origin. Moreover, the heteroclinic is not contained in the strong stable manifold of the saddle-node equilibrium at $\alpha = \gamma$ and therefore does not lie in the strong stable manifold for $|\alpha - \gamma| \ll 1$. This proves the proposition. ■

These genericity assumptions can be visualized in the blowup coordinates coordinates of Section 2.3.2. Since the gauge symmetry is eliminated in such coordinates, the neutral direction of the periodic orbit is removed so that $\dim W^{\mathrm{cu}}_-(A^{\mathrm{p}}) = 1$; see Figure 2.3.1 for a schematic drawing of dynamics in blowup coordinates near the origin.

We also tested our hypotheses on existence and genericity of free fronts numerically for $\alpha - \gamma$ not necessarily small. Using a shooting method for (2.3.13), we calculate the unstable manifold of

$$z_p = \mathrm{i}\tilde{k}_{\mathrm{lin}}, \qquad R = \sqrt{1 - \tilde{k}^2_{\mathrm{lin}}},$$

where $\tilde{k}_{\mathrm{lin}}$ is the linearly selected wavenumber calculated using (2.3.4). We then track the base point z_* of the fiber in which this trajectory lies when $R = \delta$ small. For parameters at the branch point, if z_* is far away from $z_{\mathrm{b}} = -1$, we observe that $W^{\mathrm{cu}}_-(A^{\mathrm{p}})$ does not

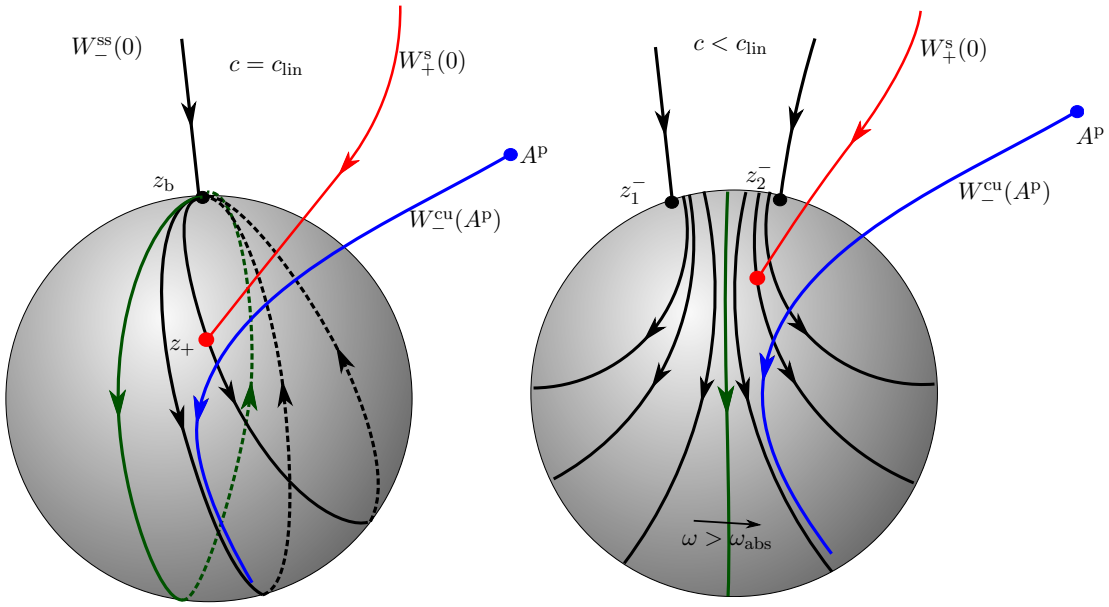

Figure 2.3.1: Dynamics near the singular sphere: free front heteroclinic (blue) and stable manifold $W^{s}_{+}(0)$ (red). Left: Unscaled parameters set $c = c_{lin}$, $\omega = \omega_{lin}$. On the sphere, homoclinic trajectories are tangent to the real circle (green) at the branch point z_b. Right: Perturb in $c < c_{lin}$ at $\omega = \omega_{abs}(c)$. The branch point z_b bifurcates into two equilibria which are encircled by periodic orbits. For ω perturbed away from ω_{abs} equilibria become unstable and stable respectively causing drift along the family of periodics.

approach the sphere along the strong stable manifold of the branch point. Thus if the quantity $|z_* + 1|$ is non-zero we obtain that the free front is generic and thus $\mathcal{A}_\infty \neq 0$. This quantity is plotted for a range of γ-values in Figure 2.3.2. Recall that $\alpha = \gamma$ implies that in our scaled coordinates $\hat{\gamma} = 0$. Using z_* we can also calculate ΔZ_i defined in (2.3.22). We then use this in calculating our $\mathcal{O}((\Delta c)^{3/2})$-prediction in Figure 2.4.1. The righthand side shows the coefficient ΔZ_i over a range of $\hat{\gamma}$-values.

2.3.4 Matching stable and unstable manifolds at $\zeta = 0$

We now prove our main result. The road map is as follows. We shall see that the singular sphere $\mathcal{S}$ is normally hyperbolic. This will give that the flow is locally foliated by smooth one dimensional fibers with base points in $\mathcal{S}$. Then, well-known results of

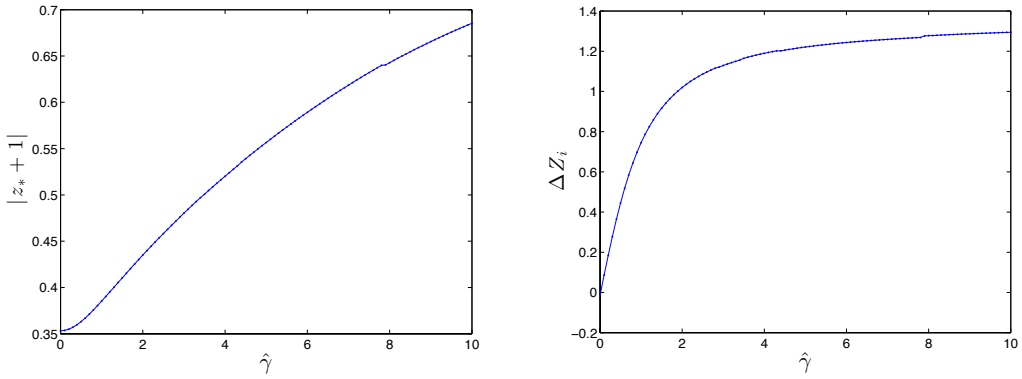

Figure 2.3.2: Left: Plot of $|z_* + 1|$ for $\hat{\gamma}$ ranging from zero to ten. Right: Plot of ΔZ_{i} over the same range of $\hat{\gamma}$.

Fenichel and an inclination lemma will essentially reduce the connection problem to the singular sphere $\mathcal{S}$. On the sphere, we give a series of coordinate changes which allow us to explicitly integrate the dynamics on $\mathcal{S}$ in a robust fashion, dependent on the scaled parameters $\Delta\hat{c}$ and $\hat{\omega}$. We find a connecting orbit using time and $\hat{\omega}$ as matching parameters. A local analysis yields a leading order expansion for the angular frequency $\hat{\omega}_{\mathrm{sel}}(\Delta\hat{c})$ in $\Delta\hat{c}$ near zero. We finally unwind our scaling transformations to obtain an expansion of ω_{tf} in the unscaled $\Delta c := c_{\mathrm{lin}} - c$. This expansion can then be inserted into the dispersion relation (2.1.5) to obtain a wavenumber prediction for the pattern left in the wake of a trigger front.

Normal hyperbolicity and smooth foliations near $\mathcal{S}$. In what follows, consider all manifolds in the reduced phase space $\mathbb{R}_+ \times S^2$. Let Φ_ζ be the flow of the full system (2.3.13) and ϕ_ζ the flow on $\mathcal{S}$. Now, note for $\Delta\hat{c} = \hat{\omega} = 0$, all trajectories on the sphere $\mathcal{S}$ converge to the branch point z_{b} with algebraic decay $\mathcal{O}(1/\zeta)$. Since the the linearization at z_{b} is normally hyperbolic, this implies that the invariant singular sphere $\mathcal{S}$ is normally hyperbolic and Fenichel's results [46, 48] imply that the phase space $\mathbb{R}^+ \times S^2$ is locally smoothly foliated by smooth one-dimensional strong-stable invariant fibers $\Phi_\zeta \mathcal{F}_z \subset \mathcal{F}_{\phi_\zeta(z)}$. More precisely, all leaves are C^k manifolds, with C^k-dependence on base point and parameters, for any finite fixed $k < \infty$.

As a consequence, there exists a smooth change of coordinates that straightens out the

local stable foliation, so that (2.3.13) can be written as

$$\begin{aligned} z' &= -(z+1)^2 + \Delta\hat{c}\, z + \mathrm{i}\hat{\omega} \\ R' &= R \cdot g(R, z; \hat{\omega}, \Delta\hat{c}\,), \end{aligned} \tag{2.3.18}$$

where $g(0, -1; 0, 0) = -1$.

To prove existence of the desired connection, we need to choose $\Delta\hat{c} > 0$ small and find $\hat{\omega}_*$ and ζ_* such that there exists a point $(R, z) = (\delta, z_-) \in W^{\mathrm{cu}}_-(A^{\mathrm{p}})$ with $\delta > 0$ sufficiently small so that

$$\Phi_{-\zeta_*}\left(W^{\mathrm{s}}_+(0)\right) \cap W^{\mathrm{cu}}_-(A^{\mathrm{p}}) \ni (\delta, z_-).$$

Before we prove the existence of such an intersection, we investigate the structure of $W^{\mathrm{s}}_+(0)$. It is important to remember that $W^{\mathrm{s}}_+(0)$ is not a stable or unstable manifold in the $\zeta < 0$ dynamics, but just the set of initial conditions for the $\zeta < 0$ flow that will give rise to decaying solutions when integrated forward in the $\zeta > 0$ dynamics. In the blowup coordinates (2.3.13), $W^{\mathrm{s}}_+(0)$ is one dimensional and can be written locally as a graph over the fiber $\mathcal{F}_{z_+}$ in the $\zeta < 0$ dynamics. More precisely, there exists an $h : \mathbb{R}^+ \to \mathbb{C}$, with $h(0) = 0$ so that locally

$$W^{\mathrm{s}}_+(0) = \{(R, z_+ + h(R)) \,|\, R \geq 0\}.$$

The normal hyperbolicity of $\mathcal{S}$ then allows us to study how this set evolves under the flow. Heuristically, when flowed in backwards time, a piece $W^{\mathrm{s}}_+(0)_{\mathrm{loc}}$ of the $\zeta > 0$ local stable manifold will be stretched out in the normal direction while expanding comparatively little in the $\mathcal{S}$ directions. Since $W^{\mathrm{s}}_+(0)$ is a graph over the strong stable fiber $\mathcal{F}_{z_+}$, the considerations above imply that $\Phi_{-\zeta}(W^{\mathrm{s}}_+(0))$ will remain a graph over the strong-stable fiber with base point $\phi_\zeta(z_+)$. This graph will converge to the strong stable fibration as ζ increases. This strong inclination result is commonly referred to as a λ-Lemma and is stated precisely in the following lemma; see also Figure 2.3.3 for an illustration.

Lemma 2.3.4 (λ-Lemma)**.** *The image of the local $\zeta > 0$-stable manifold $W^{\mathrm{s}}_+(0)_{\mathrm{loc}}$ under*

the flow $\Phi_{-\zeta}$, with $\zeta > 0$, large, is exponentially close to the strong stable fiber $\mathcal{F}_{\phi_{-\zeta}(,z_+)}$. More precisely, there exist constants $\kappa, C > 0$ and a function $\tilde{h}(\cdot, z_+) : \mathbb{R}^+ \to \mathbb{C}$ such that

$$\Phi_{-\zeta}(W^{\mathrm{s}}_+(0)_{\mathrm{loc}}) = \{\Big(R, \phi_{-\zeta}(z_+) + \tilde{h}(R, -\zeta, z_+)\Big) \mid R \geq 0\}$$

where $\|\tilde{h}(R, -\zeta, z_+)\|_{C^k} \leq C\mathrm{e}^{-\kappa\zeta}$ for any $k < \infty$, $\tilde{h}(0, \zeta, z) = 0$, and $\partial_z \tilde{h} \neq 0$.

Proof. This lemma is a consequence of the existence proof for invariant foliations [48]: one shows that trial foliations over the linear strong stable foliation converge to the invariant foliation when transported with the backward flow. ■

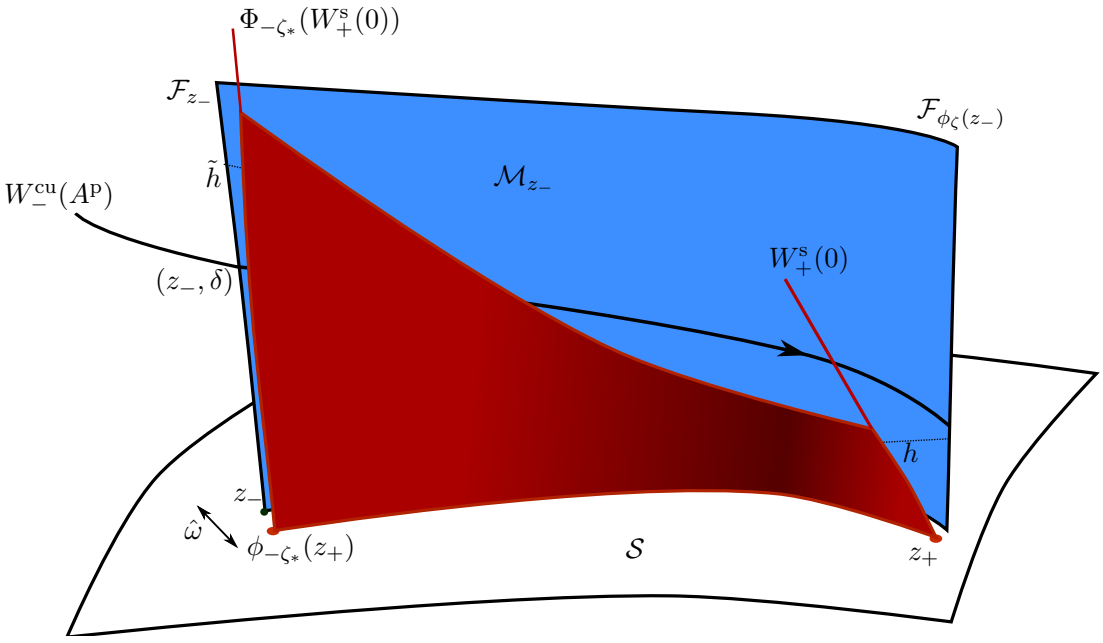

Figure 2.3.3: Depiction of foliations and heteroclinic connection. The strong-stable foliation of the trajectory $\phi_\zeta(z_-)$ is denoted as $\mathcal{M}_{z_-}$ (blue). Here $\tilde{h} = \tilde{h}(\delta, -\zeta_*, z_+)$ and $h = \tilde{h}(\delta, 0, z_+)$. The stable manifold $W^{\mathrm{s}}_+(0)$ (dark red) is stretched in the normal direction under the backwards flow, approaching $\mathcal{M}_{z_-}$. We vary $\hat{\omega}$ and ζ so that $\Phi_{-\xi_*}(W^{\mathrm{s}}_+(0)) \cap \mathcal{F}_{z_-} = (z_-, \delta)$.

Connecting via the singular flow. With these results in hand,we wish to establish a connection by finding a time-of-flight ζ_* and frequency $\hat{\omega}_*$ such that

$$z_- = \phi_{-\zeta_*}(z_+; \hat{\omega}_*) + \tilde{h}(\delta, -\zeta_*, z_+). \tag{2.3.19}$$

Recall that z_+ is the base point of $W^s_+(0)$ and z_- is the base point of the strong stable fiber that contains $W^{\mathrm{cu}}_-(A^{\mathrm{p}})$ with $R = \delta$.

We rewrite (2.3.19) as

$$\phi_{-\zeta}(z_+; \hat{\omega}_*) = z_- - \tilde{h}(\delta, -\zeta^*, z_+), \tag{2.3.20}$$

and change variables in parameter space,

$$\mu(\Delta\hat{c}\,, \hat{\omega}) = -\Delta\hat{c} + \mathrm{i}\hat{\omega} + \frac{(\Delta\hat{c}\,)^2}{4} := M^2 \mathrm{e}^{\mathrm{i}\theta}, \qquad M, \theta \in \mathbb{R}.$$

Next, we shift $z = \hat{z} + \frac{\Delta\hat{c}}{2} - 1$ in (2.3.18) and obtain

$$\hat{z}' = -\hat{z}^2 + \mu(\hat{\omega}, \Delta\hat{c}\,). \tag{2.3.21}$$

In these variables, $W^{\mathrm{s}}_+(0)$ intersects the blowup sphere at the point

$$\hat{z}_+ = \hat{z}_+(\Delta\hat{c}, \hat{\omega}) = z_+ - \frac{\Delta\hat{c}}{2} + 1 = -\sqrt{K - \Delta\hat{c} + \frac{(\Delta\hat{c})^2}{4} - i\hat{\omega}} = -\sqrt{K + M^2 \mathrm{e}^{i\theta}},$$

where $K = 2 + \frac{2}{m^2}(1 + \mathrm{i}\alpha)$, m was defined in (2.3.1), and z_+ was defined in (2.3.15).

We note that $\hat{z}_+(0,0) = 4 + 2\mathrm{i}\alpha$ is non-zero. Also, our assumptions give that $\hat{z}_-$ is non-zero, but needs to be evaluated numerically. This allows us to define,

$$\Delta Z = \left(\frac{1}{\hat{z}_+} - \frac{1}{\hat{z}_-}\right)\Bigg|_{M=0}, \qquad \Delta Z_{\mathrm{r}} = \mathrm{Re}\,\Delta Z, \qquad \Delta Z_{\mathrm{i}} = \mathrm{Im}\,\Delta Z. \tag{2.3.22}$$

Note that $M = 0$ corresponds to $\Delta\hat{c} = \hat{\omega} = 0$.

Next, we scale $\hat{z} = Mw$, $\hat{\zeta} = M\zeta$ and use the Möbius transformation

$$\rho = \frac{w+\eta}{w-\eta}, \qquad \eta = \mathrm{e}^{\mathrm{i}\frac{\theta}{2}}$$

to shift equilibria to the north and south pole of the sphere, respectively.

Last, we set $r = \log(\rho)$ and find the constant vector field

$$\dot{r} = (\log(\rho))_{\hat{\zeta}} = 2\eta. \tag{2.3.23}$$

In our new coordinates, the points $\hat{z}_+$ and $\hat{z}_- - \tilde{h}(\delta, \hat{z}_-, -\hat{\zeta}/M)$, which we wish to connect, have the representations

$$r_+ = \log\left(\frac{1+\frac{M\eta}{\hat{z}_+}}{1-\frac{M\eta}{\hat{z}_+}}\right) + \mathrm{i}(2\pi j_+), \qquad r_- = \log\left(\frac{1+\frac{M\eta-\tilde{h}}{\hat{z}_-}}{1-\frac{M\eta-\tilde{h}}{\hat{z}_-}}\right) + \mathrm{i}(2\pi j_-),$$

where $\tilde{h} = \tilde{h}(\delta, \hat{z}_+, -\hat{\zeta}/M)$, and $j_\pm \in \mathbb{Z}$ take into account that the complex logarithm is multi-valued. By varying μ (i.e. $\hat{\omega}$ and $\Delta\hat{c}$) we wish to find a solution $r(\widehat{\zeta})$ connecting these points in finite time $\widehat{\zeta} = \widehat{T}$.

As we are expanding from $\Delta\hat{c} = \omega = 0$, we have that M is small. Thus we find to first order

$$r_+ = \mathrm{i}(2\pi j_+) + \frac{2M\eta}{\hat{z}_+} + O(M^3), \qquad r_- = \mathrm{i}(2\pi j_-) + 2\frac{M\eta-\tilde{h}}{\hat{z}_-} + \mathcal{O}(M^3).$$

Now integrating (2.3.23), setting $r(0) = r_+$ and $r(-\hat{\zeta}) = r_-$, we obtain

$$-2\eta\,\hat{\zeta} = r_- - r_+ = -\mathrm{i}(2\pi\Delta j) - 2\eta\,M\,\Delta Z - \frac{2\tilde{h}}{\hat{z}_-} + O(M^3), \tag{2.3.24}$$

where $\Delta j = j_+ - j_-$ and we have discarded all but the leading order term, in M, of $\frac{1}{\hat{z}_+} - \frac{1}{\hat{z}_-}$. We then obtain the equation

$$\hat{\zeta} = \mathrm{i}\Delta j\pi\mathrm{e}^{-i\frac{\theta}{2}} + M\cdot\Delta Z + \frac{2\tilde{h}}{\eta\hat{z}_-} + O(M^3). \tag{2.3.25}$$

By Lemma 2.3.4, we have for $\hat{\zeta} > 0$, $\tilde{h} = \tilde{h}(\delta, -\hat{\zeta}/M, \hat{z}_+) = \mathcal{O}(M^k)$ for all $k \geq 1$. Thus, we can smoothly extend $\tilde{h}$ at $M = 0$ to $\tilde{h} = 0$.

Now setting $\hat{\theta} = -\pi + \theta$ we obtain

$$\hat{\zeta} = -\Delta j \pi \mathrm{e}^{-\frac{\hat{\theta}}{2}} + M\Delta Z + O(M^3) \tag{2.3.26}$$

This equation has the solution

$$M = 0, \quad \hat{\theta} = 0, \quad \hat{\zeta} = -\Delta j\, \pi.$$

We choose $\Delta j < 0$ so that $\hat{\zeta} > 0$. We wish to find a solution near this point for M small. Considering the imaginary part of (2.3.26)

$$0 = \Delta j \pi \sin(\hat{\theta}/2) + M\, \Delta Z_{\mathrm{i}} + \mathcal{O}(M^3)$$

and expanding in $\hat{\theta}$, we obtain

$$\hat{\theta} = -2\frac{M\, \Delta Z_{\mathrm{i}}}{\pi \Delta j} + \mathcal{O}(M^3).$$

Inserting this into the real part of (2.3.26) and solving for $\hat{\zeta}$, we obtain

$$\hat{\zeta} = -\pi \Delta j + M\, \Delta Z_{\mathrm{r}} + \mathcal{O}(M^2).$$

Now using the polar change of coordinates $-\Delta\hat{c} + (\Delta\hat{c})^2/4 + \mathrm{i}\hat{\omega} = M^2 \mathrm{e}^{\mathrm{i}\theta}$, the Implicit Function Theorem allows us to obtain the expansion

$$-\Delta\hat{c} + \frac{(\Delta\hat{c})^2}{4} + \mathrm{i}\hat{\omega} = -M^2 \cdot \left(1 + \mathrm{i}\frac{2\Delta Z_{\mathrm{i}}}{\pi\Delta j} M + \mathcal{O}(M^2)\right).$$

Noticing that $M = \sqrt{\Delta\hat{c}} + \mathcal{O}(\Delta\hat{c})$, we solve the imaginary part of this equation for $\hat{\omega}$ and expand

$$\hat{\omega}(\Delta\hat{c}) = -\frac{2\Delta Z_{\mathrm{i}}}{\pi\Delta j}(\Delta\hat{c})^{3/2} + \mathcal{O}((\Delta\hat{c})^2).$$

We summarize the above discussion in the following proposition.

Proposition 2.3.5. *Set* $\Delta Z_{\mathrm{i}} := \mathrm{Im}(\frac{1}{\hat{z}_+} - \frac{1}{\hat{z}_-})$ *where* $z = \hat{z} + \frac{\Delta\hat{c}}{2} - 1$ *and choose* $\Delta j \in \mathbb{Z}_-$, *fixed. Then for* $\Delta\hat{c} > 0$ *small, there exists* ζ_* *and* $\hat{\omega}_*$ *for which* (2.3.19) *is satisfied. Furthermore, we have the following expansions:*

$$\hat{\omega}_*(\Delta\hat{c}) = -\frac{2\Delta Z_{\mathrm{i}}}{\pi\Delta j}(\Delta\hat{c})^{3/2} + O((\Delta\hat{c})^2), \qquad \zeta_* = -\pi(\Delta j)(\Delta\hat{c})^{-1/2} + \Delta Z_{\mathrm{r}} + \mathcal{O}((\Delta\hat{c})^{1/2}). \tag{2.3.27}$$

Remark 2.3.6. *We emphasize that the behavior of* $W^{\mathrm{s}}_+(0)$ *and* $W^{\mathrm{cu}}_-(A^{\mathrm{p}})$ *near the origin determine the coefficient* ΔZ_{i} *of the leading order term in the expansion (2.3.27). As pointed out in the introduction,* ΔZ_{i} *measures a distance between the leading edge of the front and the stable subspace in projective coordinates. This can be made explicit by considering the Poincaré-inverted coordinates* $z_{\mathrm{inv}} = 1/(z+1)$, *in which* $\Delta Z = z^+_{\mathrm{inv}} - z^-_{\mathrm{inv}}$. *Since* z^-_{inv}, *the base point of the stable fiber corresponding to* W^{cu}_-, *is only defined up to flow translates, we can vary* $\mathrm{Re}(z^-_{\mathrm{inv}})$ *arbitrarily by shifting the free front. Therefore, the imaginary part* ΔZ_{i} *merely measures the distance between* z^+_{inv} *and the homoclinic orbit in the base of the fibers corresponding to* W^{cu}_-.

Also notice that, since trajectories approaching $\mathcal{S}$ *have the asymptotic form* (2.3.16), *we have that*

$$\mathrm{Im}\{\frac{1}{z_-}\} = \mathrm{Im}\{\zeta + \mathcal{B}_\infty/\mathcal{A}_\infty\} = \mathrm{Im}\{\mathcal{B}_\infty/\mathcal{A}_\infty\}.$$

2.3.5 Proof of Theorem 2.1.1

Proposition 2.3.5 gives the existence of trigger fronts: Given $(\hat{\omega}_*, \hat{\zeta}_*)$ there are corresponding ω_* and ξ_* such that $W^{\mathrm{s}}_+(0)$ and $W^{\mathrm{cu}}_-(A^{\mathrm{p}})$ intersect non-trivially. By taking points in this intersection as an initial condition at $\xi = 0$, then sending $\xi \to -\infty$, the trajectory (which is in $W^{\mathrm{cu}}_-(A^{\mathrm{p}})$) must converge to A^{p} . In the same way, sending $\xi \to +\infty$ the trajectory (which is in $W^{\mathrm{s}}_+(0)$) must converge to $A \equiv 0$.

In order to prove our main result, it remains to track the scalings from Section 2.3.1. We therefore reintroduce hats, writing for instance $\hat{\omega}$ for the frequency in scaled coordinates as given in Proposition 2.3.5, and ω for the parameter in CGL (2.1.2); see (2.3.1) and (2.3.2).

We use (2.3.2) to write the leading order expansion from the above proposition in terms

of the unscaled variables $\Delta c := (c_{\rm lin} - c)$ and $\Delta\omega := (\omega_{\rm lin} - \omega)$. Near the linear spreading parameters $c_{\rm lin}, \omega_{\rm lin}$ the nonlinear transformation $\Upsilon : (c, \omega) \mapsto (\hat{c}, \hat{\omega})$ is, at leading order, equal to its linear approximation,

$$(\hat{c}, \hat{\omega}) = (2, 0) + D\Upsilon\Big|_{c_{\rm lin}, \omega_{\rm lin}} (\Delta c, \Delta\omega) + \mathcal{O}((\Delta\hat{c})^2, (\hat{\omega})^2).$$

Then by the Inverse Function Theorem the expansions in (2.3.27) yield

$$\Delta\omega = -\left(\partial_c \omega_{\rm abs}(\alpha, c_{\rm lin})\right) \Delta c + \frac{2\Delta Z_{\rm i}}{\pi\Delta j}(1+\alpha^2)^{3/4}(\Delta c)^{3/2} + \mathcal{O}((\Delta c)^2)$$

from which we obtain the expansion as stated in the main theorem by setting $\Delta j = -1$:

$$\omega = \omega_{\rm abs}(\alpha, c) - \frac{2\Delta Z_{\rm i}(1+\alpha^2)^{3/4}}{\pi\Delta j}(c_{\rm lin} - c)^{3/2} + \mathcal{O}((c_{\rm lin} - c)^2).$$

In the same manner we can also obtain the expansions for the unscaled ξ_*, the distance between the trigger and the invasion front, and $k_{\rm tf}$ the selected wavenumber as given in Theorem 2.1.1.

2.4 Comparison with direct simulations and heteroclinic continuation

We now compare our leading order prediction with both direct simulation of (2.1.2) and computation of trigger fronts via continuation. For the direct simulations, we used a first order spectral solver, simulating in a moving frame of speed c. The calculations were performed on a large domain ($L = 2400$) to avoid wavenumber/wavelength measurement error. Since wavelengths converge slowly as expected [156], simulations were run for sufficiently long times ($t \sim 5000$). To corroborate these simulations, we used the continuation software AUTO07P to find the heteroclinic orbit directly as solution to a truncated boundary value problem, and then continue in c with ω as a free parameter. As seen in Figure 2.4.1, both methods are in reasonably good agreement.

We also give comparisons between AUTO07P computations, the prediction based on the absolute spectrum $\omega \sim \omega_{\rm abs}$, and the $\mathcal{O}((\Delta c)^{3/2})$ correction from Theorem 2.1.1 in

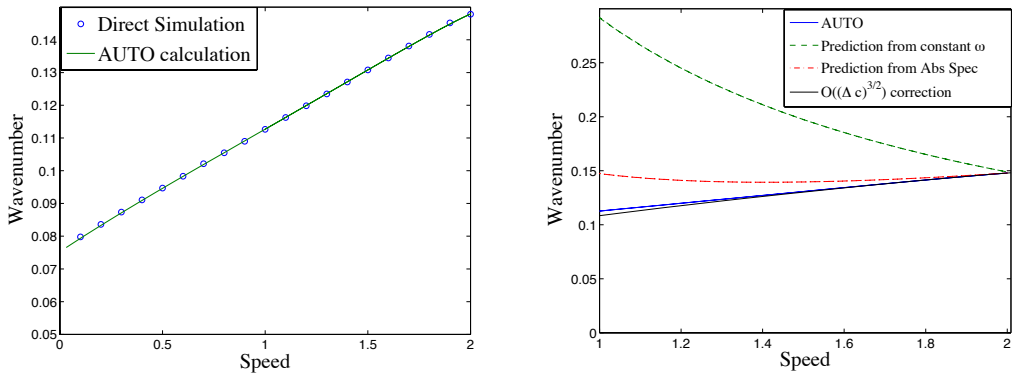

Figure 2.4.1: Left: Comparison of wavenumbers from direct simulations with AUTO07P calculations for a range of c values for fixed $\alpha = -0.1, \gamma = -0.2$. Discrepancy between the two calculations is less than 0.1% for $dt = 0.01$ and $dx = 0.0767$. Right: Comparison of different predictions for the selected wavenumber with AUTO07p calculations. The speed is varied while other parameters are fixed at $\alpha = -0.1, \gamma = -0.2$.

Figure 2.4.1. There we also compare with a somewhat naive prediction, assuming that the frequency ω of the invasion process is constant at leading order. As pointed out in Figure 2.1.3, this neglects frequency detuning based on wavenumber changes (slope of absolute spectrum) and speed (shift of absolute spectrum). Finally, Figure 2.4.2 shows how our predictions fare when c is fixed and γ is varied, as well as a log-log plot of $\omega_{\mathrm{tf}} - \omega_{\mathrm{abs}}$, confirming the exponent 3/2 and the coefficient ΔZ_{i}.

2.5 Discussion and Future Work

In this work, we have proved the existence of a coherent triggered front in the CGL equation for trigger speeds close to, but less than, the linear invasion speed, under mild generic assumptions on free invasion fronts. Furthermore, we have shown how the trigger *selects* the periodic wave-train created in the wake and how its speed affects the wavenumber. Our main tools were a sequence of coordinate changes in a neighborhood of the origin, based on geometric desingularization and invariant foliations. As a byproduct, we establish expansions for the frequency of the trigger front with universal leading order coefficient determined by the absolute spectrum. At higher order, coefficients in the expansion depend on a projective distance between the leading edge of the

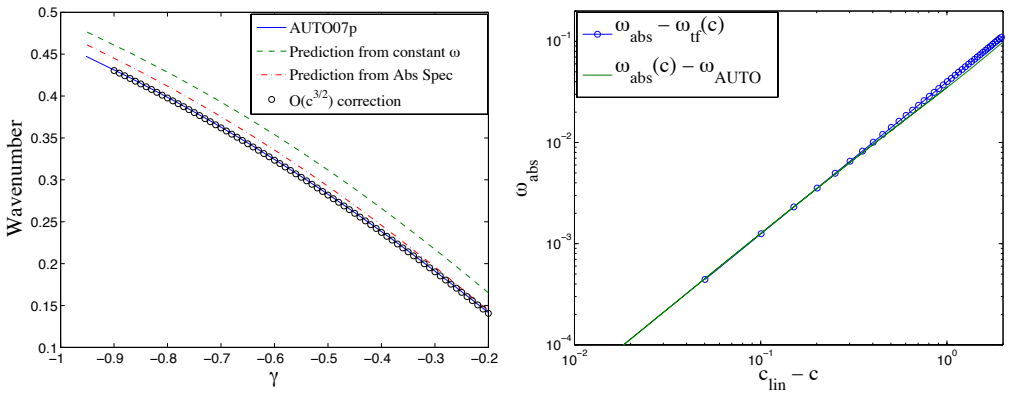

Figure 2.4.2: Left: Comparison of different predictions for the selected wavenumber with AUTO07p calculations for a range of γ with fixed $c = 1.8$ and $\alpha = -0.1$. Right: Logarithmic plot of the difference $\omega_{\text{abs}}(c) - \omega_{\text{tf}}(c)$ using expansion from the Theorem 2.1.1 above, and data from AUTO07p continuation.

front and a stable manifold ahead of the trigger.

While some of the tools used in this chapter may not immediately apply in other situations (such as those mentioned in the introduction), we expect that one could adapt the main concepts from Section 2.2. Namely, for a triggered front in such systems, selected wave numbers should be determined by the intersection of the absolute spectrum with the imaginary axis at leading order. In many of these systems, explicit expressions for the spectra are not known but simple algebraic continuation usually allows one to easily obtain accurate predictions.

The present paper addresses existence and qualitative properties of trigger fronts in the simplest possible (yet interesting) context, leaving many open questions.

First, it would be interesting to study stability of the trigger fronts. Stability is determined, at first approximation, by spectral properties of the linearization at such a front. Essential and absolute stability of this linearized operator are determined by essential and absolute spectra at $\xi = \pm\infty$. Since we have stability at $\xi = +\infty$, the only destabilizing influence in the far field comes from instabilities of wave trains in the wake. For $c \sim c_{\text{lin}}$ these instabilities are known to be convective [108, 157] or absent for α, γ not too large. In addition, it would be interesting to study and possibly exclude instabilities via the extended point spectrum. Based on the geometric construction of coherent

trigger fronts and direct simulations, we do not anticipate such instabilities. We do suspect however that fronts with $\Delta j < -1$ (2.1.9) would pick up unstable eigenvalues near $A = 0$ and hence be unstable. A larger Δj will lead to fronts with larger distance ξ_* to the trigger location $\xi = 0$ (2.3.27) and several small oscillations in this gap. One then expects this unstable plateau to generate unstable eigenvalues in the linearization; see [127] for a similar scenario. From a different perspective, fronts with higher $|\Delta j|$ arise through bifurcations from an already unstable primary state as explained in the discussion of the role of absolute spectra in Section 2.2, when considering large, bounded domains. As a consequence, one expects the bifurcated states to be unstable as well.

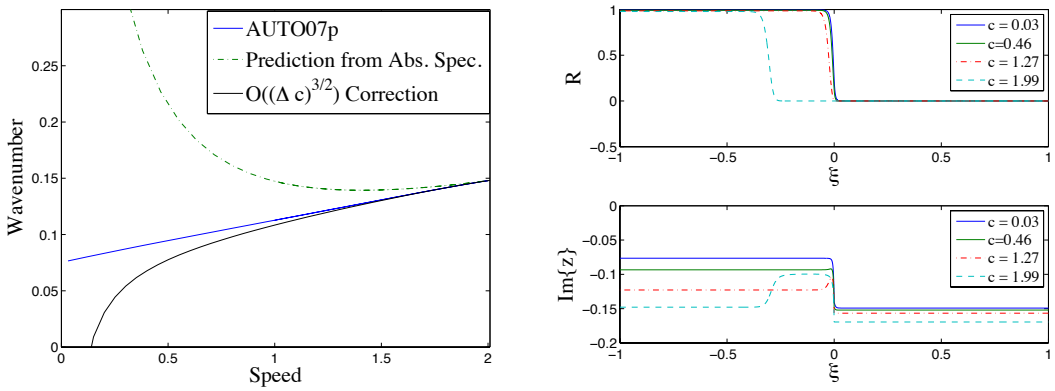

Figure 2.5.1: We fix $\alpha = -0.1, \gamma = -0.2$. Left: Comparison of AUTO07p calculation with the absolute spectrum prediction and the $\mathcal{O}((\Delta c)^{3/2})$ correction for speeds ranging from $c = 0$ to $c = c_{\text{lin}}$. Right: Front profiles calculated in the blow-up coordinates using AUTO07p for various speeds. Here the left boundary condition is given by the periodic orbit $(z, R) = (\mathrm{i}k_{\text{tf}}, 1 - k_{\text{tf}}^2)$ and the right is given by $(z_+, 0)$.

One can also envision many generalizations of our result. Using ill-posed spatial dynamics on time-periodic functions as in [63, 132], one can study similar problems in pattern-forming systems without gauge symmetry. In a different direction, we expect that triggers χ with χ' sufficiently localized would be immediately amenable to our analysis. In particular, monotone triggers with χ' sufficiently localized should yield the same type of expansion, albeit with different, non-explicit, projective distances ΔZ. On the other hand, one can envision how non-monotone triggers with long plateaus where $\chi > \chi_-$, would generate triggered fronts even for speeds $c > c_{\text{lin}}$. In terms of our linear

heuristics, the linearized operator at the origin, $(1+\mathrm{i}\alpha)\partial_{\xi\xi}+c\partial_{\xi}+\chi-\mathrm{i}\omega$ now possesses unstable extended point spectrum [121] in addition to the unstable absolute spectrum. In a different direction, slowly varying triggers $|\chi'|\ll 1$ or triggers that do not simply modify the linear driving coefficient pose a variety of interesting challenges.

Another direction is suggested by Figures 2.4.2 and 2.5.1. For speeds further away from the linear spreading speed, our predictions deviate significantly from the actual selected wavenumber and it is not clear in which context one might be able to establish analytic predictions. Going all the way to trigger speed $c=0$ could however serve as another point in parameter space where analytic expansions can be derived. In fact, thinking of the trigger as an effective Dirichlet-type boundary condition, one expects standing triggers similar to Nozaki-Bekki holes [133]. Such holes are explicitly known coherent structures in CGL that emit wave trains. Selected wavenumbers for c close to zero would be corrections to the wave numbers selected by these coherent structures.

Chapter 3

Pattern formation in the wake of pushed trigger fronts

3.1 Introduction

In this chapter, trigger fronts which are perturbed from pushed free fronts are considered. As discussed in Section 1.3.2, such fronts behave in a strikingly different manner than in the pulled case, exhibiting non-monotonic wavenumber selection, multi-stability, and hysteresis. In contrast to the previous chapter, where we study a prototypical example, here we construct an abstract framework and necessary conditions under which a pushed trigger front exists. Our main hypotheses consist of the existence of a pattern forming pushed free front, u_{ff} and a robust preparation front, u_{pr}, which is created by some spatial trigger. In addition we require certain genericity and inclination conditions on these two fronts which give an appropriate setting when they are viewed in a spatial dynamics framework; see Section 1.3.2 above for a sketch and Section 3.3 for precise statements. We then apply this theory to two examples, the prototypical cubic-quintic

CGL equation

$$A_t = (1+\mathrm{i}\alpha)A_{xx} + \chi(x-ct)A + (\rho+\mathrm{i}\gamma)A|A|^2 - (1+\mathrm{i}\beta)A|A|^4, \qquad x,t\in\mathbb{R},\ \ A\in\mathbb{C}, \tag{3.1.1}$$

where $\chi(\xi) = -\tanh(\epsilon\xi)$ with $0 < \epsilon << 1$ and $\xi := x - ct$. This parameter-ramp trigger travels through the domain with speed c making the homogeneous state $A_* \equiv 0$, which is a preparation front, being stable for $\xi := x - ct > 0$, and unstable for $\xi < 0$. It is in the latter domain where wave-trains can form.

Heuristically, one can think of the trigger χ as an effective boundary condition for the system in $\xi < 0$ when posed in a co-moving frame of speed c. Stationary solutions in this coordinate frame are usually referred to as nonlinear global modes [22]. They mediate the transition from convective to absolute instability in a semi-infinite domain. From this perspective, our problem is somewhat equivalent to problems studied in [26, 23, 115], where oscilliatory solutions in open shear flows was studied. Moreover, our results can be understood as a rephrasing and improvement of expansions in [27]. In particular, we emphasize universality in expansions for wave-number and frequency in terms of only properties of the corresponding free front. We also note that a slightly different but related approach was used in [39] to study the effect of defects on one-dimensional localized structures.

The rest of the chapter is structured as follows. In Section 3.2 we give examples of the relevant phenomena in specific equations. In Section 3.3 we formulate our abstract hypotheses and state our main result. In Section 3.4 we then give the heteroclinic matching proof for the existence of pushed trigger fronts and obtain leading order expansions for the bifurcation curve in terms of the spectral information of the system. We conclude our work in Section 3.5 by discussing future areas of work and how our results could be improved and extended.

3.2 Examples and numerical results

To motivate our results, we briefly describe examples in the cubic-quintic complex Ginzburg-Landau and Cahn-Hilliard equations which illustrate the phenomena mentioned in the introduction.

3.2.1 Complex Ginzburg-Landau equation

The complex Ginzburg-Landau equation has been used as a modulation equation to study the onset of coherent structures in many physical systems; see for example [102, 3, 141]. As mentioned above, pattern-forming free fronts have been extensively studied in this setting. In particular, it has been shown in [157] that the cubic-quintic variant discussed above

$$\tilde{u}_t = (1+\mathrm{i}\alpha)\tilde{u}_{xx} + \tilde{u} + (\rho+\mathrm{i}\gamma)\tilde{u}|\tilde{u}|^2 - (1+\mathrm{i}\beta)\tilde{u}|\tilde{u}|^4, \qquad x,t\in\mathbb{R},\ \ \tilde{u}\in\mathbb{C}, \tag{3.2.1}$$

possesses pushed free invasion front solutions for a range of parameters $\rho, \alpha, \gamma, \beta$. That is, there exist front solutions which asymptotically approach a wave train $u_p(x,t) = r\mathrm{e}^{\mathrm{i}(k_\mathrm{p}x-\omega_\mathrm{p}t)}$ as $x\to-\infty$, and approach the unstable homogeneous equilibrium $u_*\equiv 0$ as $x\to\infty$ with an interface which invades the unstable state u_* with a speed, c_p, faster than the linearized dynamics predict. The parameters of the asymptotic wave train, $r, k, \omega\in\mathbb{R}$, can be found to satisfy the nonlinear dispersion relation

$$\begin{aligned} 1 &= k^2 - \rho r^2 + r^4, \\ \omega - ck &= \alpha k^2 - \gamma r^2 + \beta r^4. \end{aligned} \tag{3.2.2}$$

By shifting into a co-moving frame $\xi = x - c_\mathrm{p}t$ and detuning by $u = \mathrm{e}^{\mathrm{i}\omega_\mathrm{p}t}\tilde{u}$, such a traveling front takes the form of a heteroclinic orbit in the finite-dimensional system

$$0 = (1+\mathrm{i}\alpha)u_{\xi\xi} + c_\mathrm{p}u_\xi + (1-\mathrm{i}\omega)u + (\rho+\mathrm{i}\gamma)u|u|^2 - (1+\mathrm{i}\beta)u|u|^4. \tag{3.2.3}$$

In this setting, we can then study how a spatially progressive triggering mechanism, χ_ϵ,

affects this pattern-forming front using the following system

$$0 = (1 + \mathrm{i}\alpha)u_{\xi\xi} + cu_{\xi} + (\chi_\epsilon(\xi) - \mathrm{i}\omega)u + (\rho + \mathrm{i}\gamma)u|u|^2 - (1 + \mathrm{i}\beta)u|u|^4, \tag{3.2.4}$$

$$\epsilon\frac{d}{d\xi}\chi_\epsilon = \chi_\epsilon^2 - 1, \qquad \chi_\epsilon(0) = 0, \tag{3.2.5}$$

where $0 < \epsilon << 1$ and χ_ϵ takes the role of the trigger, satisfying $\chi_\epsilon(\xi) = -\tanh(\epsilon\xi)$. The initial condition of χ_ϵ fixes the location of the trigger interface. When viewed in the stationary coordinate frame, the inhomogeneity χ_ϵ travels through the spatial domain, altering the PDE-stability of u_*. For $\xi > 0$ the state is stable, while for $\xi < 0$ it is unstable. In the language we defined above, the trivial solution $u_{\mathrm{pr}} = u_*$ is a preparation front in the triggered system (3.2.4). Thus, if u_{pr} is locally perturbed, an oscillatory instability will develop, leading to the formation of a patterned state in the domain $\xi < 0$, or in the wake of χ_ϵ.

Numerical simulations show that such a mechanism creates pattern-forming fronts which behave in a strikingly different manner than in the pulled case. The upper left of Figure 3.2.1 depicts the non-monotonic bifurcation curve (gold line) for pushed trigger fronts near the free front parameters $(c_{\mathrm{p}}, k_{\mathrm{p}})$; compare with the bifurcation curve in [64, §4] briefly discussed in the above section. As can be seen in the upper right plot of Figure 3.2.1, the front exhibits snaking behavior as the trigger speed c is varied near c_{p}. This figure plots the distance of the front to the trigger interface as the trigger speed non-monotonically approaches c_{p}; see also solution profiles (i) - (iii) plotted in the bottom row for various points along the bifurcation curve. Furthermore, observe that trigger fronts lock and persist for speeds larger than the free invasion speed c_{p} (see for example profile (iii)), in contrast to the pulled case. In the top row, blue and orange dotted lines show the results of direct simulations where the trigger speed was varied adiabatically and evidence how the wave-number and front distance varies hysteretically as the speed is decreased (blue) and then increased (orange).

These results were obtained using both numerical continuation and direct simulation of (3.2.4). The yellow curves were found via numerical continuation in AUTO07P. In order to avoid periodic boundary conditions, these computations were done in the blow-up coordinates derived in [63], where periodic orbits in the traveling wave equation collapse

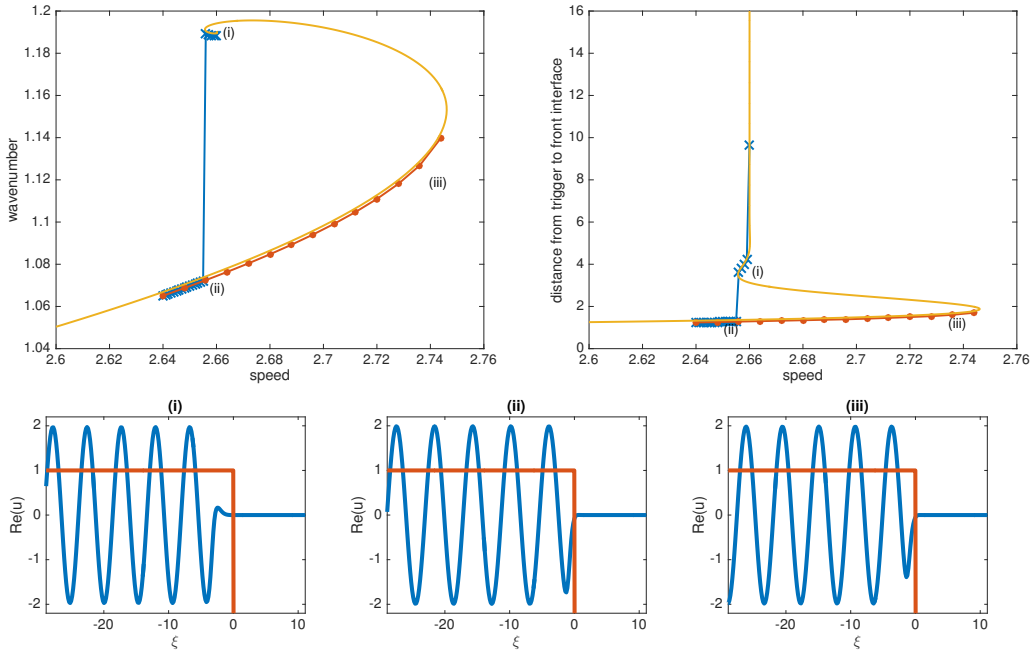

Figure 3.2.1: Numerical bifurcation diagrams comparing computations of triggered qcGL equation (3.2.4) from AUTO07P (yellow) and direct simulation (blue x's and orange dots) with parameter values $\alpha = 0.3, \gamma = -0.2, \beta = 0.2, \rho = 4$ so that $(k_{\rm p}, c_{\rm p}) \approx (2.66, 1.19)$. Bottom three figures depict triggered pushed front profiles for a range of parameter values: (i): $(c, k) = (2.656, 1.1894)$, (ii): $(c, k) = (2.646, 1.0678)$, (iii) $(c, k) = (2.728, 1.1181)$, zoomed in near the trigger χ_ϵ which is overlaid in orange.

to equilibrium points. The dotted lines (blue and orange) come from measurements of direct simulations. In these simulations the homogeneous state u_* was locally perturbed far away from the trigger interface, resulting in a patterned state which locked some distance away from the interface (blue curve). The trigger speed c was then adiabatically decreased and, when c reached the turning point of the bifurcation curve found using AUTO07P, the front detached and re-locked to a solution branch with front interface closer to the trigger and a different wave-number. The trigger speed c was then adiabatically increased, continuing solutions along this different branch (orange curve). The direct simulations used a 2nd-order exponential time differencing scheme (see [28]) with $dt = 0.01$, a spectral spatial discretization with 2^{10} Fourier modes, and were run in the co-moving frame with speed c. Note the trigger was made negative near the left

boundary at $\xi = -70$ (not pictured) to accommodate for the periodic boundary conditions. This was not found to affect the results as the nucleated patterns were unaffected by this interface, having negative group velocity.

3.2.2 Cahn-Hilliard equation

We have also have investigated these types of fronts in a modified Cahn-Hilliard equation

$$u_t = -(u_{xx} + f(u))_{xx}, \quad f(u) := u + \gamma u^3 - u^5, \quad x, t, u \in \mathbb{R}. \tag{3.2.6}$$

Because the linearization about the homogeneous unstable state $u_* \equiv 0$ is the same as the standard Cahn-Hilliard equation with $f(u) = u - u^3$, (3.2.6) will have the same linear spreading speed [156],

$$c_{\text{lin}} = \frac{2}{3\sqrt{6}} \left(2 + \sqrt{7}\right) \sqrt{\sqrt{7} - 1}.$$

Direct numerical simulations using both spectral and finite-difference methods have suggested that, for $\gamma > 0$ sufficiently large, this equation possesses oscillatory pushed invasion fronts which freely invade the homogenous state u_*. Figure 3.2.2 depicts space-time diagrams of two free invasion fronts in (3.2.6), both invading $u_* \equiv 0$, one with $\gamma < 0$ and one with $\gamma > 0$. In the former case the front approximately travels with the linear speed c_{lin}, while in the latter case the front travels with a faster speed, c_{p}, and possesses steeper decay at the leading edge. To the author's knowledge the rigorous existence for such pushed fronts in a Cahn-Hilliard system of this form is still an open and interesting problem.

The Cahn-Hilliard equation possesses periodic solutions $u(kx; k, m)$, where m quantifies an average mass in the system, which are weakly unstable against coarsening processes [70, 69]. Instabilities result in the creation of such periodic patterns as transients. In particular, there exist invasion fronts that create such periodic patterns. Note however, that the periodic patterns are time periodic in a co-moving frame, $u(kx, k, m) = u(k(\xi + ct); k, m)$, with period $2\pi/kc$, so that the invasion front will be time periodic. In the complex Ginzburg-Landau equation, this time periodicity could be eliminated by exploiting the gauge symmetry (see above), but for Cahn-Hilliard one

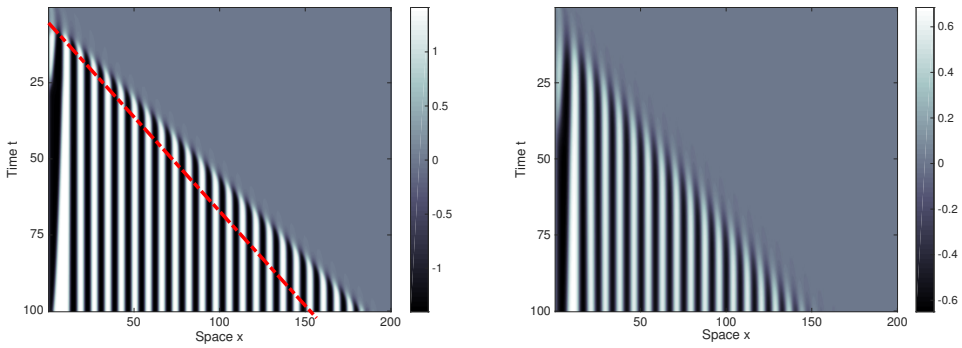

Figure 3.2.2: Free invasion fronts in (3.2.6) for $\gamma = 1.5$ (left) and $\gamma = -1.5$ (right). The invasion speed on the right is the linear speed predicted by the linearization about $u_* \equiv 0$ while the invasion speed on the left is much faster and the corresponding front has a sharp leading edge, indicating a nonlinear front. The dashed red line overlaid on the left indicates the path of the pulled front on the right. Here (3.2.6) was simulated using a semi-implicit time stepping method with second order finite differences in space ($dx = 0.2$) and first order in time ($dt = 0.01$).

must study the modulated traveling wave problem; see [63, §4.2]. That is, pushed free fronts arise in a co-moving frame of speed c_{p} as time-periodic solutions with some temporal frequency ω_{p}. In other words they are time time-periodic solutions of the equation

$$\omega_{\mathrm{p}} u_\tau = -(u_{\xi\xi} + f(u))_{\xi\xi} + c_p u_\xi, \quad \xi \in \mathbb{R},\ \tau \in \mathbb{T} := \mathbb{R}/2\pi\mathbb{Z}. \tag{3.2.7}$$

We can then study pushed trigger fronts by introducing a uniformly-translating spatial trigger as in qcGL above

$$\omega u_\tau = -(u_{\xi\xi} + \tilde{f}(\xi, u))_{\xi\xi} + c u_\xi, \quad \tilde{f}(\xi, u) := \chi(\xi) u + \gamma u^3 - u^5, \quad \epsilon \frac{d}{d\xi} \chi_\epsilon = \chi_\epsilon^2 - 1 \tag{3.2.8}$$

with $\epsilon > 0$ small, so that χ_ϵ is once again a hyperbolic tangent and we fix the trigger interface by setting $\chi_\epsilon(0) = 0$. As in the qcGL case above, the preparation front is trivial, $u_{\mathrm{pr}} \equiv 0$, and is stable for $\xi > 0$, and is unstable for $\xi < 0$. We note that for Cahn-Hilliard a different type of triggered system can also be studied; see (3.5.2) below. There the spatial inhomogeneity is not a linear coefficient but a traveling source term, which leaves behind a preparation front connecting two homogeneous states.

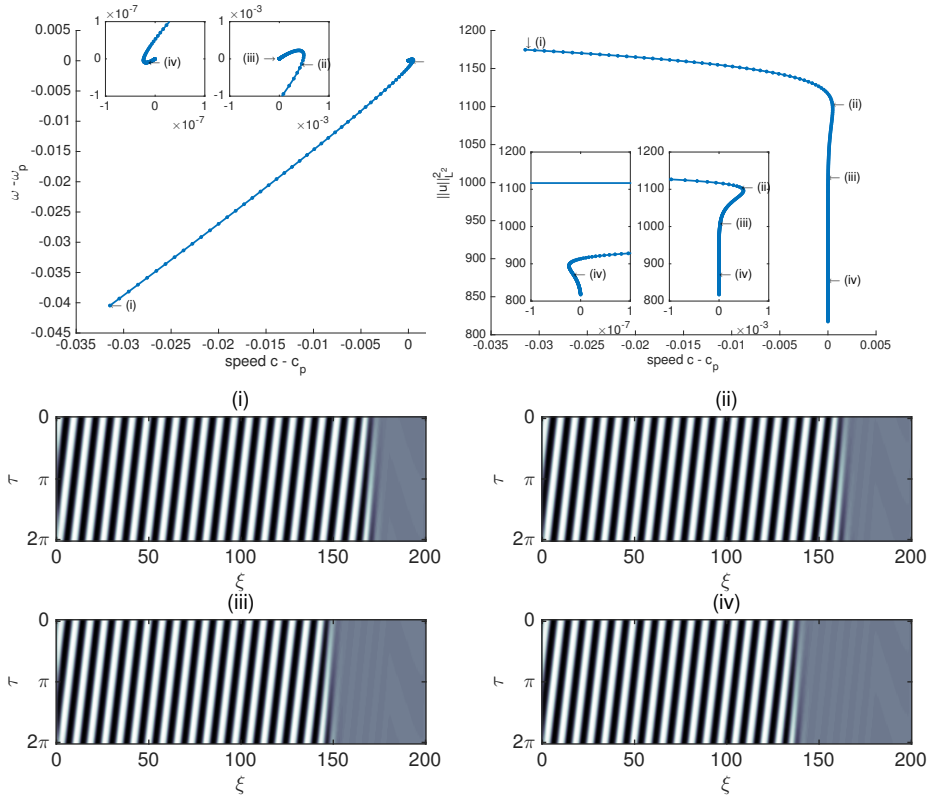

Figure 3.2.3: (upper left): Bifurcation curve for triggered pushed fronts in (3.2.8) with temporal frequency ω and trigger speed c with $\gamma = 1.5$ for which the free pushed parameters are $(c_p, \omega_p) = (2.0324, 1.5115)$. (upper right): Plot of the L^2 norm of solutions against the trigger speed c. Insets are zoomed in near the value $c = c_{\mathrm{p}}$ (lower): Space-time diagrams of solutions for a selection of points (i): $(c, \omega) = (2.001, 1.471)$, (ii): $(c, \omega) = (2.0329, 1.5113)$, (iii): $(c, \omega) = (2.0325, 1.5115)$, (iv): $(c, \omega) = (2.0324, 1.5115)$ along the bifurcation curve. First order forward differences for ∂_t and centered second-order differences for ∂_x were used, with step sizes $dt = 0.2, dx = 0.5$ respectively, and $N = 200$. Note also the trigger interface is located at $\xi = 175$.

Using numerical arc-length continuation we found that, in a narrow parameter regime, pushed trigger fronts in (3.2.8) possess a spiraling bifurcation curve and thus exhibit locking and multi-stability phenomena, as in qcGL; see Figure 3.2.3. Here we used the temporal frequency ω in our bifurcation diagrams and note that the wave-number k can be determined by the relation $c = \frac{\omega}{k}$ since the spatial pattern is stationary in a stationary frame. We also mention that this locking behavior was corroborated in

semi-implicit time-stepping simulations. In these simulations, if the homogeneous state was perturbed near the trigger, then the resulting patterned state would lock close to the trigger (i.e. farther out on the spiral). If the homogeneous state was perturbed far away from the trigger then the pattern would lock far away from the trigger (i.e. closer to (ω_p, c_p) on the spiral).

Our numerical continuation method used finite-differences to discretize both temporal and spatial derivatives and the MATLAB Newton solver "fsolve" to continue solutions on the domain $(\xi, \tau) \in [0, N] \times [0, 2\pi]$ in c and ω for some fixed N large. To accommodate for the second parameter ω we appended the phase condition

$$\int_0^{2\pi} \langle \partial_\tau u(\cdot, s), u(\cdot, s) - u_{\text{old}}(\cdot, s) \rangle_{L^2([0,L])} \, ds = 1,$$

where u_{old} is the solution found at the previous continuation step. This eliminates the non-uniqueness due to the translation symmetry in time and allows the modulated traveling wave equation 3.2.8 to be solved uniquely. The initial guess for the continuation algorithm was one full time-period of a solution obtained from an semi-implicit time-stepping method, with the same spatial discretizations as above. More details of our continuation method can be found in the caption of Figure 3.2.3, and more details on how our theory applies to this equation will be provided in Section 3.3 and Section 3.5.1.

3.3 Abstract formulation

Our theoretical approach is motivated by the spatial dynamics method first formulated by Kirchgässner and subsequently developed by many others over the past few decades [49, 83, 88, 130]. By viewing a pattern-forming system as a continuous-time dynamical system, where the spatial co-moving frame variable ξ is viewed as the "time-like" variable, the existence of a trigger front can be obtained as a heteroclinic bifurcation from a nearby pushed free front.

In particular, we shall study a system of the form

$$\frac{d}{d\xi}u_0 = f_0(u_0;\mu) \tag{3.3.1}$$

$$\frac{d}{d\xi}u_1 = Au_1 + f_1(u_0,u_1;\mu)u_1, \qquad \xi\in\mathbb{R}, \mu\in\mathbb{R}^2, \tag{3.3.2}$$

where μ shall consist of system parameters, $u_0 \in X_0 := \mathbb{R}^n$, and $u_1 \in X_1$, a real Hilbert space. Equation (3.3.1) governs the triggering mechanism as in (3.2.5), while (3.3.2) governs the pattern forming system as in (3.2.4). Here, we chose to provide an ODE for the triggering mechanism for convenience, thus casting the system in a more conventional context for heteroclinic and homoclinic bifurcation theory. Let $A : Y_1 \subset X_1 \to X_1$ be a closed linear operator where $Y_1 := D(A)$ is also a real Hilbert space which is dense and compactly embedded in X_1. Furthermore we shall assume that there exists a projection P such that $A^{\mathrm{s}} := AP$ and $-A^{\mathrm{u}} := -(1-P)A$ are sectorial operators.

Next we assume that the function f_0 satisfies

$$f_0(0,\mu) = f_0(\tilde{u}_0^*(\mu),\mu) = 0,$$

where $\tilde{u}_0^*(\mu) \in X_0$ varies smoothly in μ in an open neighborhood of the origin in $\mathbb{R}^2$. Furthermore we assume

$$f_0 \in \mathcal{C}^k(X_0\times\mathbb{R}^2, X_0), \qquad f_1 \in \mathcal{C}^k(X_0\times X_1\times\mathbb{R}^2, X_1),$$

for some $k \geq 1$. Defining $X := X_0 \times X_1$, it is readily seen that $U_* := (0,0)$, $\tilde{U}_*(\mu) := (\tilde{u}_0^*(\mu),0)$ are equilibria of the system

$$\frac{d}{d\xi}U = F(U;\mu), \qquad F(U;\mu) = \begin{pmatrix} f_0(u_0;\mu) \\ Au_1 + f_1(U;\mu)u_1 \end{pmatrix}, \quad U = \begin{pmatrix} u_0 \\ u_1 \end{pmatrix}, \tag{3.3.3}$$

and

$$D_U F(\tilde{U}_*(\mu);\mu) = \begin{pmatrix} D_{u_0}f_0(\tilde{u}_0^*,\mu) & 0 \\ 0 & A + f_1(\tilde{u}_0^*,0,\mu) \end{pmatrix},$$

$$D_U F(U_*;\mu) = \begin{pmatrix} D_{u_0}f_0(0,\mu) & 0 \\ 0 & A + f_1(0,0,\mu) \end{pmatrix}.$$

In this formulation, the preparation front will be a heteroclinic orbit contained in the $\{u_1 = 0\}$ subspace which connects U_* to $\tilde{U}_*$ as ξ increases, while the pushed free front will be a heteroclinic orbit contained in the $\{u_0 = 0\}$ subspace approaching U_* as $\xi \to \infty$; see Hypothesis 3.3.7. In our formulation, we have fixed $U_* = (0, 0)$ independent of μ, as it is where we perform most of our analysis. Also, we have chosen μ to be two-dimensional to match the examples above, and to accommodate the co-dimension assumptions that we make in Hypothesis 3.3.12 below. In spatial dynamics terms the preparation front will be a transverse heteroclinic and the pushed free front will be co-dimension two, thus requiring a two-dimensional parameter to complete our heteroclinic gluing and matching argument in Section 3.4. In the examples of Section 3.2, μ corresponds to the bifurcation parameters $\omega - \omega_{\mathrm{p}}$ and $c - c_{\mathrm{p}}$. Next, motivated by the time-translation symmetry which occurs in a typical spatial dynamics formulation of a modulated traveling wave problem (see for example [125, §3.1], [129, §5], or the Cahn-Hilliard example below), we assume the following:

Hypothesis 3.3.1. *Let $T_1 : S^1 \times X \to X$ be a strongly continuous group action of the circle, S^1, on X such that $X_0 \times \{0\} \subset \mathrm{Fix}(T_1)$, and A and f_1 are both equivariant under this action.*

Furthermore, we remark that this action arises as a gauge symmetry in qcGL. Such a symmetry arises from averaging out time when deriving cGL as a modulation equation for oscilliatory instabilities in a system with time-translation symmetry. Finally, we assume the existence of a smooth family of periodic orbits.

Hypothesis 3.3.2. *There exists a family of periodic solutions $U_p(\xi; \mu)$ of (3.3.3), smooth in μ, which lie entirely in the subspace $\{0\} \times X_1$ and possess trivial isotropy with respect to T_1 which acts by,*

$$T_1(k\zeta)\, U_p(\xi, \mu) = U_p(\xi + \zeta; \mu)$$

where $k = k(\mu)$ defines the period, $2\pi/k(\mu)$, of U_p.

Hypothesis 3.3.2 encodes the existence of periodic patterns. These are typically of the form $u(k\xi - \omega(k)t; k)$, where $\omega(k)$ is known as a nonlinear dispersion relation [38, 122].

In spatial dynamics, the time t-dependence is encoded in the function space, $u = u(k\xi - \cdot; k) \in L^2(\mathbb{T})$, and the time shift symmetry of Hypothesis 3.3.1 acts as $u(k\xi - \cdot + \zeta)$. In other words, spatially periodic orbits are relative equilibria with respect to the time shift symmetry in spatial dynamics in a co-moving frame.

Remark 3.3.3. *Note that the u_1-components of the equilibria U_* and $\tilde{U}_*$ are the same. We have simplified the setting to reflect those of the examples given above where the trigger is a inhomogeneous coefficient in the linear term which progressively changes the stability of a constant preparation front. We remark that our abstract setting could be readily altered to instead study a system with a source-term trigger, such as* (3.5.2)*, which moves the system from one spatially homogeneous equilibrium to another.*

Next, we show how the two examples of Sections 3.2.1 and 3.2.2 can be put into this abstract formulation.

CGL spatial dynamics In the setting of the complex Ginzburg-Landau equation given in (3.2.4)-(3.2.5), a formulation as above can be obtained by converting (3.2.4) into a first order complex system for u and $v := u_\xi$, and then decomposing into equations for the real and imaginary parts of each $u = s + \mathrm{i}t$, $v = z + \mathrm{i}w$ so that $s_\xi = z$ and $t_\xi = w$. Setting $u_0 = \chi_\epsilon$ and $u_1 = (s, t, z, w)^T$, one obtains the system

$$\epsilon \frac{d}{d\xi} u_0 = u_0^2 - 1, \tag{3.3.4}$$

$$\frac{d}{d\xi} u_1 = A(c, \omega) u_1 + f_1(u_0, u_1; c, \omega) u_1 \tag{3.3.5}$$

with

$$A(\alpha, c, \omega) = -\frac{1}{1+\alpha^2} \begin{pmatrix} 0 & I_2 \\ A_1 & A_2 \end{pmatrix},$$

$$f_1(u_0, u_1; c, \omega) u_1 = B u_1 + c(u_1)^T C u_1 + d(u_1)^T D u_1,$$

$$B = -\frac{1}{1+\alpha^2} \begin{pmatrix} 0 & 0 \\ B_1 & 0 \end{pmatrix}, \quad C = -\frac{1}{1+\alpha^2} \begin{pmatrix} 0 & 0 \\ C_1 & 0 \end{pmatrix}, \quad D = \frac{1}{1+\alpha^2} \begin{pmatrix} 0 & 0 \\ D_1 & 0 \end{pmatrix},$$

where all the zeros are 2×2 zero-matrices, I_2 is the 2×2 identity, and

$$A_1 = \begin{pmatrix} 1-\alpha\omega & \omega+\alpha \\ -(\omega+\alpha) & 1-\alpha\omega \end{pmatrix},\ B_1 = \begin{pmatrix} u_0-1 & \alpha(u_0-1) \\ \alpha(1-u_0) & u_0-1 \end{pmatrix},$$
$$C_1 = \begin{pmatrix} \rho+\alpha\gamma & \alpha\rho-\gamma \\ \gamma-\alpha\rho & \rho+\alpha\gamma \end{pmatrix},\ D_1 = \begin{pmatrix} 1+\alpha\beta & \alpha-\beta \\ \beta-\alpha & 1+\alpha\beta \end{pmatrix},$$
$$c(u_1) = (s^2+t^2)\cdot(0,0,1,1)^T, \quad d(u_1) = (s^2+t^2)^2\cdot(0,0,1,1)^T.$$

Here, the phase space is simply $X = \mathbb{R}^5$ and the preparation front $u_{\rm pr}$ is a heteroclinic orbit contained in the $\{u_1 = 0\}$ subspace connecting $U_* = (u_0, u_1) = (1, 0)$ with $\tilde{U}_* = (u_0, u_1) = (-1, 0)$, while $u_{\rm ff}$ is a heteroclinic orbit contained in the $\{u_0 = 1\}$ subspace. Also the S^1-action arises in the original variables (u, v) as the gauge-symmetry,

$$T_1(\theta) : (u, v) \mapsto \mathrm{e}^{\mathrm{i}\theta}(u, v).$$

We remark that change of coordinates $u_0 \mapsto (u_0 - 1)/2$ is required to obtain the exact formulation of (3.3.1) - (3.3.2).

Cahn-Hilliard spatial dynamics In the context of the modified Cahn-Hilliard equation given in (3.2.8), a formulation as above can be obtained by setting

$$u_0 := \chi, \quad u_1 = (u, v, \theta, w)^T := (u,\, u_\xi,\, u_{\xi\xi} + \tilde{f}(\xi, u),\, (u_{\xi\xi} + \tilde{f}(\xi, u))_\xi)^T$$

from which one finds

$$\epsilon \frac{d}{d\xi} u_0 = u_0^2 - 1, \tag{3.3.6}$$
$$\frac{d}{d\xi} u_1 = A(c, \omega)u_1 + f_1(u_0, u_1; \gamma)u_1, \tag{3.3.7}$$

with

$$A(c,\omega) = \begin{pmatrix} b_1 & I_3 \\ -\omega\partial_\tau & b_2(c) \end{pmatrix}, \quad f_1(u_0,u_1;\mu) = -\begin{pmatrix} 0 & 0 & 0 & 0 \\ 1-u_0+\gamma u^2-u^4 & 0 & 0 & 0 \\ 0 & 0 & 0 & 0 \\ 0 & 0 & 0 & 0 \end{pmatrix}, \tag{3.3.8}$$

where $0 < \epsilon \ll 1$, I_3 is the three dimensional identity matrix, $b_1 = (0,1,0)^T$, and $b_2(c) = (c,0,0)$. This is then an evolution equation on the Banach space $X = \mathbb{R} \times H^3(\mathbb{T}) \times H^2(\mathbb{T}) \times H^1(\mathbb{T}) \times L^2(\mathbb{T})$, so that each element $u_1 \in H^3(\mathbb{T}) \times H^2(\mathbb{T}) \times H^1(\mathbb{T}) \times L^2(\mathbb{T})$ is a time-periodic vector and the linear operator A has domain $Y = \mathbb{R} \times H^4(\mathbb{T}) \times H^3(\mathbb{T}) \times H^2(\mathbb{T}) \times H^1(\mathbb{T})$. Even though the initial-value problem for this equation is ill-posed (this can be seen using an argument similar to [130, §2.2]), exponential dichotomies can be used to construct invariant manifolds and find the solutions of interest; see for example [114, 125, 130]. In this form, u_{pr} corresponds to a heteroclinic orbit contained in the $\{u_1 = 0\}$ subspace, while u_{ff} is a heteroclinic orbit contained in the $\{u_0 = 1\}$ subspace. Here, the S^1-action arises as a time-shift symmetry

$$T_1(\theta) : (u_0, u_1(\cdot)) \mapsto (u_0, u_1(\cdot - \theta)) .$$

By setting $\mu = (c - c_{\mathrm{p}}, \omega - \omega_{\mathrm{p}})$ and making the change of coordinates $u_0 \mapsto (u_0 - 1)/2$ we obtain a system of the form given in (3.3.3) above.

3.3.1 Spectral hypotheses

Next, we state our spectral hypotheses for the equilibria $U_*, \tilde{U}_*$, and the relative equilibrium U_p of (3.3.3). It follows from the compact embedding of $Y_1 \subset X_1$ that the spectra of $D_U F$, evaluated at each of these, consists of isolated eigenvalues of finite multiplicity. We thus assume the following,

Hypothesis 3.3.4. *(i) The linearization of F about U_* at $\mu = 0$ has the following properties:*

- *The operator $D_U F(U_*; 0)$ has algebraically simple eigenvalues $\nu_{\mathrm{ss}} = -r_{\mathrm{ss}} \pm$*

$\mathrm{i}\sigma_{\mathrm{ss}}$, $\nu_{\mathrm{su}} = -r_{\mathrm{su}} \pm \mathrm{i}\sigma_{\mathrm{su}}$ *such that* $r_{\mathrm{ss}} > r_{\mathrm{su}} > 0$, $\sigma_{\mathrm{ss}}, \sigma_{\mathrm{su}} \neq 0$, *and all other* $\nu \in \Sigma\left(D_U F(U_*; \mu)\right)$ *satisfy either* $\mathrm{Re}\{\nu\} > -r_{\mathrm{su}}$ *or* $\mathrm{Re}\{\nu\} < -r_{\mathrm{ss}}$.

- $D_{u_0} f_0(0,0)$ *has a real unstable eigenvalue* $\nu_{\mathrm{u}} = r_{\mathrm{u}} > 0$ *which satisfies* $r_{\mathrm{u}} > 2r_{\mathrm{ss}} - r_{\mathrm{su}}$.

(ii) The periodic orbit U_p *is hyperbolic. That is, the linearization about* U_p *has spectrum bounded away from the imaginary axis except for a simple Floquet exponent, located at* $0 \in \mathbb{C}$.

(iii) The spectrum $\Sigma(D_U F(\tilde{U}_*); 0)$ *is bounded away from the imaginary axis. That is, there exists a* $\gamma > 0$ *such that all eigenvalues satisfy* $|\mathrm{Re}\{\nu\}| > \gamma$.

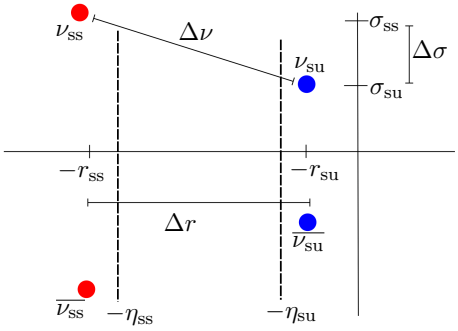

Figure 3.3.1: Schematic diagram of notation for leading eigenvalues and relevant quantities.

The first bullet of Hypothesis 3.3.4(i) encodes the spectral splitting, depicted in Figure 3.3.1, corresponding to the leading order decay of the free pushed front. The second bullet describes the decay of the preparation front in backwards time, requiring that it decays with a fast rate. This will aid in our analysis and is not restrictive in our results since we imagine such a front to be controlled by the experimenter or an outside mechanism. For instance, for the examples given in Section 3.2, one could obtain such a fast decay by tuning $\epsilon > 0$ to be sufficiently small. Hypothesis 3.3.4(ii) readily gives that U_p is not degenerate with respect to perturbations in μ. Such a hypothesis could be checked using the relationship between the PDE-stability of the wave-train and the hyperbolicity of its spatial dynamics formulation; see [132, §3.1] for more detail. Hypotheses 3.3.4(iii) reflects the fact that the state $\tilde{U}_*$, which corresponds to the asymptotic state ahead of

the trigger, is typically PDE-stable. We chose the subscripts "ss/su/u" above as these eigenvalues will give the leading order decay of strong-stable, weak stable-unstable, and unstable invariant manifolds which are constructed in Proposition 3.3.10 and will be important in our work.

Remark 3.3.5. *These spectral hypotheses would need to be adapted if the PDE from which the system originated possessed any conserved quantities or additional symmetries. We briefly discuss how our results would change for these cases (such as in Cahn-Hilliard) in Section 3.5.*

Using the sectoriality of the decomposition of A, we can define spectral projections $P_{1,\infty}^{\mathrm{ss/su}}$ to obtain eigenspaces, $E_{1,\infty}^{\mathrm{ss}}$ and $E_{1,\infty}^{\mathrm{su}}$ of $D_U F(U_*)$ which are associated with the spectral splitting in Hypothesis 3.3.4(i). These spaces have the decomposition

$$E_{1,\infty}^{\mathrm{ss}} = E_{1,\infty}^{\mathrm{ss,l}} + E_{1,\infty}^{\mathrm{ss,s}}, \qquad E_{1,\infty}^{\mathrm{su}} = E_{1,\infty}^{\mathrm{su,l}} + E_{1,\infty}^{\mathrm{su,u}}, \tag{3.3.9}$$

where "l" denotes the 2-dimensional eigenspaces corresponding to the leading eigenvalues $\nu_{\mathrm{ss/su}}$ and "s/u" denote the eigenspaces corresponding to the spectral sets $\{\nu < -r_{\mathrm{ss}}\}$ and $\{\nu > -r_{\mathrm{su}}\}$ respectively. Also, let $e_{1,\infty}^{\mathrm{ss/su}} \in E_{1,\infty}^{\mathrm{ss/su,l}}$ denote the unit-normed complex eigenvectors of $D_U F(U_*)$ associated with the eigenvalues $\nu_{\mathrm{ss/su}}$ respectively, and let $e_{j,\infty}^*$ denote the complex eigenvector of the adjoint linearization $-D_U F(U_*)^*$ with eigenvalue $-\overline{\nu_{\mathrm{su}}}$.

From these spectral hypotheses we have the following result on locally invariant manifolds around U_*.

Lemma 3.3.6. *According to the spectral splitting*

$$\Big(\Sigma\left(D_U F(U_*;0)\right) \cap \{\mathrm{Re}\ \nu \leq -r_{\mathrm{ss}}\}\Big) \bigcup \Big(\Sigma\left(D_U F(U_*;0)\right) \cap \{\mathrm{Re}\ \nu \geq -r_{\mathrm{su}}\}\Big),$$

the system (3.3.3) *possesses locally-invariant manifolds $W_{\mathrm{loc}}^{\mathrm{ss}}(U_*)$ and $W_{\mathrm{loc}}^{\mathrm{su}}(U_*)$ which are C^k- and C^1-smooth respectively. Furthermore, the periodic orbit U_p and equilibrium $\tilde{U}_*$ possess C^k-smooth locally invariant manifolds $W_{\mathrm{loc}}^{\mathrm{cu}}(U_p)$, and $W_{\mathrm{loc}}^{\mathrm{s}}(\tilde{U}_*)$.*

Proof. This follows by standard results on infinite dimensional locally invariant manifolds (see [76] or [158]). We also mention that higher degrees of smoothness of $W^{\mathrm{su}}_{\mathrm{loc}}(U_*)$ can be obtained if the spectral gap $\Delta\eta = r_{\mathrm{ss}} - r_{\mathrm{su}}$ is sufficiently large. □

Next we state our assumptions on the heteroclinic orbits formed by the preparation and pushed free fronts.

Hypothesis 3.3.7. *For $\mu = 0$, there exist C^k-smooth heteroclinic solutions $q_i^0(\xi)$ of (3.3.3) for $i = 1, 2$ such that for some $S > 0$ sufficiently large*

- $q_1^0(\xi) \in \{\{0\} \times X_1\}$ *and* $q_2(\xi) \in \{X_0 \times \{0\}\}$ *for all* $\xi \in \mathbb{R}$,
- $\{q_1^0(\xi)\}_{\xi\in[S,\infty)} \subset W^{\mathrm{ss}}_{\mathrm{loc}}(U_*)$,
- $\{q_1^0(\xi)\}_{\xi\in(-\infty,-S]} \subset W^{\mathrm{cu}}_{\mathrm{loc}}(U_p)$,
- $\{q_2^0(\xi)\}_{\xi\in(-\infty,-S]} \subset W^{\mathrm{su}}_{\mathrm{loc}}(U_*)$,
- $\{q_2^0(\xi)\}_{\xi\in[S,\infty)} \subset W^{\mathrm{s}}_{\mathrm{loc}}(\tilde{U}_*)$.

Furthermore, for some $\epsilon > 0$ small, there exist $a, b \in \mathbb{C}$ such that q_i^0 has the following asymptotics,

$$q_1^0(\xi) = a\mathrm{e}^{\nu_{\mathrm{ss}}\xi} e^{\mathrm{ss,l}}_{1,\infty} + \text{c.c.} + \mathcal{O}(\mathrm{e}^{-(r_{\mathrm{ss}}+\epsilon)\xi}), \quad \textit{as} \quad \xi \to +\infty, \tag{3.3.10}$$

$$q_2^0(\xi) = b\mathrm{e}^{\nu_{\mathrm{u}}\xi} e^{\mathrm{u}}_{1,\infty} + \mathcal{O}(\mathrm{e}^{(r_{\mathrm{u}}+\epsilon)\xi}), \quad \textit{as} \quad \xi \to -\infty, \tag{3.3.11}$$

where c.c. *stands for complex-conjugate and the vectors $e^{\mathrm{ss,l}}_{1,\infty} \in E^{\mathrm{ss,l}}_{1,\infty}$, and $e^{\mathrm{u}}_{1,\infty} \in E^{\mathrm{u}}_{1,\infty}$ have unit-norm and are complex eigenvectors of the linearization $D_U F(U_*)$ associated with the leading eigenvalues ν_{ss} and ν_{u} respectively.*

Finally, the orbit q_2^0 is robust to perturbations in μ. That is there exists a smooth family of heteroclinic orbits $q_2(\xi, \mu)$ satisfying the above properties for all $|\mu| \ll 1$ and $q_2(\xi; 0) = q_2^0(\xi)$.

The second part of this hypothesis states that, to leading order, q_1^0 and q_2^0 approach U_* along the leading eigenspaces $E^{\mathrm{ss,l}}_{1,\infty}$ and $E^{\mathrm{u,l}}_{1,\infty}$ as $\xi \to \pm\infty$ respectively. In this notation, q_1^0 denotes the pushed free front, while q_2 denotes the preparation front. See Figure 3.4.1 for a depiction of these heteroclinic orbits.

3.3.2 Invariant manifolds and variational set-up

We now construct global invariant manifolds in neighborhoods of the heteroclinic orbits q_1^0 and q_2^0. To do so we define variations, $w_i^0(\xi) = U(\xi) - q_i^0(\xi)$, about such orbits with $i = 1, 2$, and study the variational equations

$$\frac{d}{d\xi} w_i^0 = A_i(\xi) w_i^0 + g_i^0(\xi, w_i^0), \qquad \xi \in \mathbb{R}, \tag{3.3.12}$$

with

$$A_i(\xi) := D_U F(q_i^0(\xi); 0), \quad g_i^0(\xi, w_i^0) := F(q_i^0(\xi) + w_i^0; \mu) - F(q_i^0(\xi); 0) - A_i(\xi) w_i^0.$$

In order to study these variations we shall use exponential dichotomies of the linear variational equations and their adjoints

$$\frac{d}{d\xi} w = A_i(\xi) w, \tag{3.3.13}$$

$$\frac{d}{d\xi} \psi = -A_i(\xi)^* \psi, \qquad i = 1, 2. \tag{3.3.14}$$

Before doing so, we require the following well-posedness assumption.

Hypothesis 3.3.8. *For both $i = 1, 2$, if $w_0(\xi)$ is a bounded solution of either of the linear variational equations* (3.3.13) *or* (3.3.14) *for all $\xi \in \mathbb{R}$ and $w_0(\xi_0) = 0$ for some $\xi_0 \in \mathbb{R}$, then $w_0 \equiv 0$.*

We remark that for finite-dimensional systems and many parabolic equations this hypothesis holds via parabolic regularity results; see [21, 130]. For more discussion and some examples of when this hypothesis is satisfied see [114, §6]. For an example where this hypothesis is not satisfied see [32, Ch. 4].

Proposition 3.3.9. *(Existence of Exponential Dichotomies) Assuming the above hypotheses,* (3.3.13) *has exponential dichotomies on $J_1 = \mathbb{R}^+ = [0, \infty)$, $J_2 = \mathbb{R}^- = (-\infty, 0]$ with a splitting according to the eigenspaces $E_{1,\infty}^{\mathrm{ss/su}}$ given above. That is there exist projections $P_i^{\mathrm{ss/su}}(\xi) : X \to X$ for $\xi \in J_i$ such that the following holds for some $K > 0$:*

- *For any $\zeta \in J_i$ and $u \in X$, there exists a solution $\Phi_i^{\mathrm{ss}}(\xi, \zeta)u$ of* (3.3.13) *defined for $\xi \geq \zeta$, continuous in (ξ, ζ) for $\xi \geq \zeta$, and differentiable in (ξ, ζ) for $\xi > \zeta$,*

such that $\Phi_i^{\rm ss}(\zeta,\zeta)u = P_i^{\rm ss}(\zeta)u$ *and*

$$|\Phi_i^{\rm ss}(\xi,\zeta)u| \leq K\,{\rm e}^{-r_{\rm ss}(\xi-\zeta)}|u|, \quad \xi \geq \zeta \tag{3.3.15}$$

- *For any* $\zeta \in J_i$ *and* $u \in X$*, there exists a solution* $\Phi_i^{\rm su}(\xi,\zeta)u$ *of* (3.3.13) *defined for* $\xi \leq \zeta$*, continuous in* (ξ,ζ) *for* $\xi \leq \zeta$*, and differentiable in* (ξ,ζ) *for* $\xi < \zeta$*, such that* $\Phi_i^{\rm su}(\zeta,\zeta)u = P_i^{\rm su}(\zeta)u$ *and*

$$|\Phi_i^{\rm su}(\xi,\zeta)u| \leq K\,{\rm e}^{-r_{\rm su}(\xi-\zeta)}|u|, \quad \xi \leq \zeta. \tag{3.3.16}$$

- *The solutions* $\Phi_i^{\rm ss}(\xi,\zeta)u$ *and* $\Phi_i^{\rm su}(\xi,\zeta)u$ *satisfy*

$$\begin{aligned} &\Phi_i^{\rm ss}(\xi,\zeta)u \in {\rm Rg}(P_i^{\rm ss}(\xi)) \quad \textit{for all} \qquad \xi \geq \zeta, \qquad \xi,\zeta \in J_i,\\ &\Phi_i^{\rm su}(\xi,\zeta)u \in {\rm Rg}(P_i^{\rm su}(\xi)) \quad \textit{for all} \qquad \xi \leq \zeta, \qquad \xi,\zeta \in J_i, \end{aligned}$$

where $|\cdot|$*, unless otherwise stated, denotes the norm on* X*.*

Proof. See [114] or [130]. □

We remark that the first two bullets of this proposition correspond to the usual stable-unstable dichotomy when considered in an weighted norm $||u||_\eta := \sup_{\xi\in J_i} {\rm e}^{\eta\xi}|u(\xi)|$ with $0 < r_{\rm su} < \eta < r_{\rm ss}$. The third bullet gives the usual invariance of the dichotomies under the linear evolution.

Let us denote $E_i^j(\xi) = P_i^j(\xi)X$, for $i = 1,2$ and $j = {\rm ss}, {\rm su}$. Also, as they will be necessary to the subsequent analysis, we isolate the leading components of these ξ-dependent subspaces as follows

$$E_i^{\rm ss}(\xi) = E_i^{\rm ss,l}(\xi) + E_i^{\rm ss,s}(\xi), \qquad E_i^{\rm su}(\xi) = E_i^{\rm su,l}(\xi) + E_i^{\rm su,u}(\xi), \quad i = 1,2, \tag{3.3.17}$$

such that the spaces $E_i^{\rm ss/su,l}(\xi)$ are unique and satisfy

$$\begin{aligned} E_1^{\rm ss/su,l}(\xi) &\to E_{1,\infty}^{\rm ss/su,l} \qquad \xi \to \infty,\\ E_2^{\rm ss/su,s/u}(\xi) &\to E_{1,\infty}^{\rm ss/su,s/u} \qquad \xi \to -\infty. \end{aligned} \tag{3.3.18}$$

Such a decomposition of, say for example $E_2^{\rm ss}(\xi)$, can be achieved by first obtaining exponential dichotomies associated with the spectral sets $\{\nu : \mathrm{Re}\{\nu\} \leq -r_{\rm ss}\}$, $\{\nu : \mathrm{Re}\{\nu\} \geq -r_{\rm ss}\}$ and then taking the intersection of their associated ξ-dependent subspaces. Denote the resulting dichotomies of these restricted subspaces as $\Phi_i^{\rm ss/su,l}$ for $i = 1, 2$.

From Proposition 3.3.9, we are then able to obtain the existence of globally invariant manifolds in a neighborhood of $q_i^0(\xi)$ for all $\xi \in J_i$, and μ sufficiently small.

Proposition 3.3.10. *For all μ sufficiently small, the equilibrium U_* in* (3.3.3) *possesses strong stable and weak-stable/unstable invariant manifolds $W^{\rm ss}(U_*)$ and $W^{\rm su}(U_*)$ which exist in a neighborhood of the orbits q_1^0 and q_2^0 respectively. Furthermore, $W^{\rm ss}(U_*)$ is C^k-smooth while $W^{\rm su}(U_*)$ is in general only C^1-smooth. In an exponentially weighted space with weight $\eta \in (r_{\rm su}, r_{\rm ss})$ and for μ sufficiently small, $W^{\rm ss}(U_*)$ contains all solutions which stay close to $q_1^0(\xi)$ for all $\xi \geq 0$ while $W^{\rm su}(U_*)$ contains all solutions which stay close to $q_2^0(\xi)$ for all $\xi \leq 0$. Finally, these manifolds are smooth in the parameter μ and have tangent spaces which satisfy, for $\mu = 0$,*

$$T_{q_i^0(\xi)} W^j(U_*) = E_i^j(\xi), \qquad j = \mathrm{ss}, \mathrm{su},\ i = 1, 2.$$

Proof. This proof follows in the same way as those in [125, Sec. 3.5] which use the existence of exponential dichotomies from [114, Thm. 3.3.3] and infinite-dimensional center manifold results of [158]; see also [130, 132]. □

In an analogous fashion, one may use the spectral properties of the linearization about U_p and $\tilde{U}$ to obtain the following proposition,

Proposition 3.3.11. *For all μ sufficiently small, the equilibria U_p and $\tilde{U}_*$ of* (3.3.3) *possess C^k-smooth center-unstable and stable manifolds, denoted as $W^{\rm cu}(U_p)$ and $W^{\rm s}(\tilde{U}_*)$, which exist in a neighborhood of the orbits q_1^0 and q_2^0, and are smooth in the parameter μ. Here, $W^{\rm cu}(U_p)$ contains all solutions which stay close to $q_1^0(\xi)$ for all $\xi \leq 0$ and $W^{\rm s}(\tilde{U}_*)$ contains those which stay close to $q_2^0(\xi)$ for all $\xi \geq 0$.*

Proof. The hypothesis on the linearizations at U_p and $\tilde{U}_*$ give the existence of center-unstable and stable dichotomies $\Phi_{-1}^{\rm s/cu}$ along $q_1^0(\xi)$ for $\xi \leq 0$, and stable and unstable

dichotomies $\Phi^{\mathrm{s/u}}_{+2}$ along $q^0_2(\xi)$ for $\xi \geq 0$. As in Proposition 3.3.10, one can then use these dichotomies and variation of constants formulas to prove the above proposition. □

See Figure 3.4.1 for a depiction of these invariant manifolds and how they relate to our heteroclinic gluing construction.

3.3.3 Intersection hypotheses

We wish to construct pushed trigger fronts as intersections between $W^{\mathrm{cu}}(U_p)$ and $W^{\mathrm{s}}(\tilde{U}_*)$ near the equilibrium U_* under certain conditions on the heteroclinic chain composed of q^0_1 and q^0_2. We first assume the tangent spaces of the invariant manifolds along $q^0_i(\xi)$ generically behave as a codimension-two heteroclinic bifurcation problem:

Hypothesis 3.3.12. *(i) The tangent spaces $T_{q^0_1(0)}W^{\mathrm{cu}}(U_p)$, and $T_{q^0_1(0)}W^{\mathrm{ss}}(U_*)$ form a Fredholm pair with index 0, and satisfy*

$$\dim\Big(T_{q^0_1(0)}W^{\mathrm{cu}}(U_p) + T_{q^0_1(0)}W^{\mathrm{ss}}(U_*)\Big)^{\perp} = \dim\Big(T_{q^0_1(0)}W^{\mathrm{cu}}(U_p) \cap T_{q^0_1(0)}W^{\mathrm{ss}}(U_*)\Big) = 2. \tag{3.3.19}$$

(ii) The tangent spaces $T_{q^0_2(0)}W^{\mathrm{su}}(U_*)$, and $T_{q^0_2(0)}W^{\mathrm{s}}(\tilde{U}_*)$ intersect transversely, form a Fredholm pair of index 1, and satisfy

$$\dim\Big(T_{q_2(0)}W^{\mathrm{su}}(U_*) \cap T_{q_2(0)}W^{\mathrm{s}}(\tilde{U}_*)\Big) = 1. \tag{3.3.20}$$

These hypotheses enforce genericity on the heteroclinic orbits in the sense that q^0_1, while not persisting for all μ sufficiently small, can be transversely unfolded in the parameter μ. In the setting of an evolutionary PDE with both time- and space-translational symmetries (like the Cahn-Hilliard equation mentioned above), q^0_1 is a modulated traveling wave with both τ- and ξ-derivative lying in the intersection $T_{q^0_1(0)}W^{\mathrm{cu}}(U_p) \cap T_{q^0_1(0)}W^{\mathrm{ss}}(U_*)$, while q^0_2 lies in the subspace of time-independent functions and thus has only ξ-derivative lying in the intersection $T_{q_2(0)}W^{\mathrm{su}}(U_*) \cap T_{q_2(0)}W^{\mathrm{s}}(\tilde{U}_*)$. See [63, Sec. 4.3] for more discussion on this topic.

We must also make an assumption on the inclination properties of the invariant manifolds between U_* and $\tilde{U}_*$. Let $P^{\mathrm{su}}_{2,+}(\xi)$ denote the projection in X onto $E^{\mathrm{su}}_2(\xi) =$

$T_{q_2^0(\xi)}W^{\mathrm{su}}(U_*)$ along $\tilde{E}^{\mathrm{s}}_{+2}(\xi)$, the orthogonal complement of $\frac{dq_2^0}{d\xi}(\xi)$ in $T_{q_2^0(\xi)}W^{\mathrm{s}}(\tilde{U}_*)$. Such a projection can be constructed in the same manner as in [114, Eqn. 3.20].

Hypothesis 3.3.13. *(Inclination property) The restricted projection*

$$\mathcal{P}^{\mathrm{l}} := P^{\mathrm{su}}_{2,+}(0)\Big|_{E_2^{\mathrm{ss,l}}(0)}$$

is an isomorphism from $E_2^{\mathrm{ss,l}}(0)$ *onto* $E_2^{\mathrm{su,l}}(0)$.

We note that the equivariance of F with respect to the S^1-action implies that $\mathcal{P}^{\mathrm{l}}$ commutes with T_1. This equivariance makes $\mathcal{P}^{\mathrm{l}}$ complex linear when considered on the complexification of the subspaces $E_2^{\mathrm{ss/su,l}}(0)$ and will enforce certain conditions on the coefficients of the bifurcation equation, see Section 3.4.6 below. Additionally, this hypothesis can be given a geometric interpretation when the invariant manifold $W^{\mathrm{s}}(\tilde{U}_*)$ about $q_2(\xi)$ can be extended for all $\xi \in \mathbb{R}$, as is the case when X is finite dimensional. In such a situation, this hypothesis says that $W^{\mathrm{s}}(\tilde{U}_*)$ converges towards the non-leading strong-stable eigenspace $E^{\mathrm{ss,s}}_{1,\infty}$ in backwards time and hence does not lie in an inclination-flip configuration [81].

Remark 3.3.14. *Since X is a Hilbert space, it can be decomposed as a sum of complex one-dimensional irreducible representations. In the spatial-dynamics formulation for the Cahn-Hilliard equation for $u_0 \equiv 1$, this decomposition is simply the Fourier series*

$$U(t) = \sum_{\ell\in\mathbb{Z}} U_\ell \mathrm{e}^{\mathrm{i}\ell\tau}, \quad U_\ell \in \mathbb{R}^4,$$

and can be used to determine the spatial eigenvalues of the linearization of (3.3.7) *about the equilibrium $u_1 = 0$. Replacing ∂_τ by $\mathrm{i}\ell$, and setting $(c,\omega) = (c_{\mathrm{p}}, \omega_{\mathrm{p}})$, the linearization can be broken down into a set of infinitely many finite-dimensional linear systems, whose eigenvalues ν_ℓ satisfy*

$$0 = \nu_\ell^4 + f'(u_*)\nu_\ell^2 - c_{\mathrm{p}}\nu_\ell + \mathrm{i}\omega_{\mathrm{p}}\ell, \quad \ell \in \mathbb{Z}, \tag{3.3.21}$$

with corresponding eigenspaces lying in the subspaces

$$Y_\ell = \mathrm{span}_{U_\ell, U_{-\ell}\in\mathbb{R}^4}\{U_\ell \mathrm{e}^{\mathrm{i}\ell\tau}, U_{-\ell}\mathrm{e}^{-\mathrm{i}\ell\tau}\}.$$

Hypothesis 3.3.13 then requires that each of the leading eigenspaces, $E^{\mathrm{ss/su,l}}_{1,\infty}$, must lie in the same subspace Y_ℓ for some ℓ. If this was not true, we would obtain that the two irreducible representations $\theta \mapsto \mathrm{e}^{\mathrm{i}\ell_1\theta}$, and $\theta \mapsto \mathrm{e}^{\mathrm{i}\ell_2\theta}$ for distinct ℓ_1 and ℓ_2 are isomorphic, a contradiction.

As in other heteroclinic bifurcation problems, we must require the invertibility of a certain mapping constructed using Melnikov integrals. Hence for $j = 1, 2$ we let $e^*_j(\xi)$ be bounded solutions of the adjoint variational equation (3.3.14) such that $e^*_j(0) = e^*_{j,0}$ for vectors $e^*_{j,0} \in X$ with unit-norm which satisfy

$$\mathrm{span}_{j=1,2}\{e^*_{j,0}\} = \left(T_{q_1(0)}W^{\mathrm{cu}}(U_p) + T_{q_1(0)}W^{\mathrm{ss}}(U_*)\right)^\perp.$$

We then assume the following

Hypothesis 3.3.15. *The following mapping is invertible,*

$$\begin{aligned}\mathcal{M} :&\mathbb{R}^2 \to (E^{\mathrm{ss}}_1(0) + E^{\mathrm{cu}}_{-1}(0))^\perp,\\ &\mu \mapsto \sum_{i=1,2}\int_{-\infty}^{\infty} \langle D_\mu F(q^0_1(\zeta);0)\mu, e^*_j(\zeta)\rangle d\zeta\ e^*_{j,0}.\end{aligned}$$

3.3.4 Statement of main result

With all of these hypotheses in hand, we define the desired solution as follows,

Definition 3.3.16. *A* pushed trigger front *is a heteroclinic orbit $U_{\mathrm{tf}}(\xi;\mu)$ of* (3.3.3) *which satisfies the following properties:*

(i) $|U_{\mathrm{tf}}(\xi;\mu) - U_p(\xi;\mu)| \to 0$ *and U_{tf} converges along the invariant manifold $W^{\mathrm{cu}}(U_p)$ as $\xi \to -\infty$ with asymptotic phase.*

(ii) $U_{\mathrm{tf}}(\xi;\mu) \to \tilde{U}_*(\mu)$ *along the invariant manifold $W^{\mathrm{s}}(U_*)$ as $\xi \to \infty$.*

Since we only discuss pushed trigger fronts in the rest of this work, we shall henceforth refer to such solutions as just trigger fronts.

Theorem 3.3.2. *Assume Hypotheses 3.3.1–3.3.15 and recall the definition of the eigenvectors $e^{\mathrm{su,l}}_{1,\infty}$, and $e^*_{j,\infty}$ from Section 3.3.1. Then, there are constants $\rho, L_* > 0$ so that*

for all $L > L_*$ there exists a triggered pushed front $U_{\mathrm{tf}}(\xi;\mu_*(L))$, with bifurcation curve $\mu_*(L)$ that has the leading order expansion,

$$\mu_*(L) = -\sum_{j=1,2} \left[\mathrm{e}^{2\Delta\nu L} d_j + \mathrm{c.c.}\right] \mathcal{M}^{-1} e^*_{j,0} + \mathcal{O}(\mathrm{e}^{-(2\Delta r+\rho)L})).$$

Here,

$$d_j = a c_1 \overline{\tilde{c}_j} \left\langle e^{\mathrm{su,l}}_{1,\infty}, e^*_{j,\infty} \right\rangle_{\mathbb{C}}, \quad \Delta\nu = \nu_{\mathrm{ss}} - \nu_{\mathrm{su}}, \quad \Delta r = \mathrm{Re}\,\Delta\nu,$$

the Melnikov mapping $\mathcal{M}$ is defined in Hypothesis 3.3.15, the constants $a, c_1, \tilde{c}_j \in \mathbb{C}$ are defined in Hypothesis 3.3.7, Lemma 3.4.9, and Lemma 3.4.10 respectively, and $\langle\cdot,\cdot\rangle_{\mathbb{C}}$ is the complexified inner product induced by the real inner product on X. Moreover, for each L, the elements of the group orbit $\{T_1(\theta)U_{\mathrm{tf}}(\xi,\mu_*(L)) : \theta \in [0,2\pi)\}$ are also pushed triggered fronts. Compare this expansion with Figure 3.3.1 for a schematic of $\nu_{\mathrm{ss/su}}$ and $\Delta\nu$.

Remark 3.3.17. *In a typical spatial dynamics formulation, temporal translations form the group orbit of each trigger front, U_{tf}.*

3.4 Proof of Main Theorem

3.4.1 Variational set-up

Our approach to proving Theorem 3.3.2 will follow that of Rademacher in [120]. There, a gluing-matching procedure akin to Lin's method [96] was used to construct solutions near a heteroclinic cycle between a periodic orbit and an equilibrium. Our case is simpler as we glue near a fixed equilibrium, not a periodic orbit.

We wish to construct the desired solution, which connects U_p to $\tilde{U}_*$, by studying variational equations about the heteroclinic orbits corresponding to the preparation front and the pushed front. For the former, since the heteroclinic $q_2(\xi;\mu)$ is robust in μ, we study variations $w_2(\xi) = U(\xi) - q_2(\xi;\mu)$ and define the system

$$\frac{d}{d\xi} w_2 = A_2(\xi) w_2 + g_2(\xi, w_2; \mu), \qquad \xi \in \mathbb{R}, \tag{3.4.1}$$

with

$$A_2(\xi) := D_U F(q_2(\xi;0)), \quad g_2(\xi, w_i) := F(q_2(\xi;\mu) + w_2;\mu) - F(q_2(\xi;\mu);\mu) - A_2(\xi)w_2.$$

For the variations about the pushed front more care must be taken due to the fact that, because the subspace pair in Hypothesis 3.3.12(i) has non-zero co-dimension, $q_1^0(\xi)$ does not generically persist for all μ in a neighborhood of the origin. To deal with this we select a trajectory, $q_1(\xi;\mu)$, defined for $\xi \geq 0$, which is contained in the strong-stable manifold $W^{\mathrm{ss}}(U_*)$, and approaches q_1^0 uniformly as $\mu \to 0$. This can be done by realizing that trajectories which are near q_1^0 and lie in the strong stable manifold are described using the following variation of constants formula

$$\begin{aligned} v^{\mathrm{ss}}(\xi;\mu,v_0) &= \Phi_1^{\mathrm{ss}}(\xi,0)v_0 + \\ &\qquad \int_0^\xi \Phi_1^{\mathrm{ss}}(\xi,\zeta)G_1(\zeta,v^{\mathrm{ss}}(\zeta);\mu)d\zeta + \int_\infty^\xi \Phi_1^{\mathrm{su}}(\xi,\zeta)G_1(\zeta,v^{\mathrm{ss}}(\zeta);\mu)d\zeta, \qquad (3.4.2)\\ G_1(\xi,v;\mu) &= F(q_1^0(\xi)+v;\mu) - F(q_1^0(\xi);\mu) - D_U F(q_1^0(\xi);0)v, \end{aligned}$$

where $v_0 \in E_1^{\mathrm{ss}}(0)$. In a similar manner we may also define for $\xi \leq 0$,

$$\begin{aligned} v^{\mathrm{cu}}(\xi;\mu,v_0) = \Phi_{-1}^{\mathrm{cu}}(\xi,0)v_0 &+ \int_0^\xi \Phi_{-1}^{\mathrm{cu}}(\xi,\zeta)G_1(\zeta,v^{\mathrm{cu}}(\zeta);\mu)d\zeta \\ &+ \int_{-\infty}^\xi \Phi_{-1}^{\mathrm{s}}(\xi,\zeta)G_1(\zeta,v^{\mathrm{cu}}(\zeta);\mu)d\zeta, \qquad (3.4.3) \end{aligned}$$

where $v_0 \in E_{-1}^{\mathrm{cu}}(0)$, and $\Phi_{-1}^{\mathrm{cu/s}}$ is the dichotomy associated with the periodic orbit U_p along q_1^0 for $\xi \leq 0$.

It then follows for μ sufficiently small (see [81, Lem 2.1]) that there exists vectors $v_0^{\mathrm{ss}}(\mu) \in E_1^{\mathrm{ss}}(0)$ and $v_0^{\mathrm{cu}}(\mu) \in E_{-1}^{\mathrm{cu}}(0)$, smooth in μ, such that $v_0^{\mathrm{ss}}(0) = v_0^{\mathrm{su}}(0) = 0$ and

$$v^{\mathrm{ss}}(0;\mu,v_0^{\mathrm{ss}}) - v^{\mathrm{cu}}(0;\mu,v_0^{\mathrm{cu}}) \in \left(T_{q_1^0(0)}W^{\mathrm{ss}}(U_*) + T_{q_1^0(0)}W^{\mathrm{cu}}(U_*)\right)^\perp. \qquad (3.4.4)$$

Indeed, this can be obtained by using the Implicit Function theorem to solve the projected equation

$$\begin{aligned} 0 &= \mathcal{Q}\left[v^{\mathrm{ss}}(0;\mu,v_0^{\mathrm{ss}}) - v^{\mathrm{cu}}(0;\mu,v_0^{\mathrm{cu}})\right], \\ &= v_0^{\mathrm{ss}} - v_0^{\mathrm{cu}} + \mathcal{Q}\left(\int_\infty^0 \Phi_1^{\mathrm{su}}(\xi,\zeta)G_1(\zeta,v^{\mathrm{ss}}(\zeta);\mu)d\zeta - \int_{-\infty}^0 \Phi_{-1}^{\mathrm{s}}(\xi,\zeta)G_1(\zeta,v^{\mathrm{cu}}(\zeta);\mu)d\zeta\right), \end{aligned}$$

for v_0^{ss} and v_0^{cu} in terms of μ, where $\mathcal{Q}$ is the orthogonal projection of X onto the subspace

$$\left(T_{q_1^0(0)}W^{\mathrm{ss}}(U_*) + T_{q_1^0(0)}W^{\mathrm{cu}}(U_*)\right).$$

We shall denote such unique trajectories as

$$\begin{aligned} q_1(\xi;\mu) &:= v^{\mathrm{ss}}(\xi;\mu,v_0^{\mathrm{ss}}(\mu)), \quad \xi \geq 0, \\ q_1^-(\xi;\mu) &:= v^{\mathrm{su}}(\xi;\mu,v_0^{\mathrm{su}}(\mu)), \quad \xi \leq 0, \end{aligned}$$

so that q_1 approaches U_* along the strong-stable manifold $W^{\mathrm{ss}}(U_*)$ as $\xi \to +\infty$ and satisfies $q_1(\xi;0) = q_1^0(\xi)$ for $\xi \geq 0$, while q_1^- approaches U_p along the center-unstable manifold $W^{\mathrm{cu}}(U_p)$ as $\xi \to -\infty$ and satisfies $q_1(\xi;0) = q_1^0(\xi)$ for $\xi \leq 0$.

We can then define the variation $w_1(\xi) = U(\xi) - q_1(\xi;\mu)$ for $\xi \geq 0$ and the variational equation

$$\frac{d}{d\xi}w_1 = A_1(\xi)w_1 + g_1(\xi,w_1;\mu), \qquad \xi \in \mathbb{R}^+, \tag{3.4.5}$$

with

$$A_1(\xi) := D_U F(q_1(\xi;0);0), \quad g_1(\xi,w_i) := F(q_1(\xi;\mu)+w_1;\mu) - F(q_1(\xi;\mu);\mu) - A_1(\xi)w_1.$$

Next, let

$$\Sigma_i = \left(\frac{dq_i^0}{d\xi}(0)\right)^\perp, \quad i = 1,2$$

be fixed transverse sections to q_i, with ξ chosen so that each Σ_i lies in a small neighborhood of U_* and the orthogonal complement is taken in X. In order to construct the trigger front we wish to find solutions $w_1(\xi)$ and $w_2(\xi)$ of the variational equations in (3.4.1) and (3.4.5) which lie in $W^{\mathrm{cu}}(U_p)$ and $W^{\mathrm{s}}(\tilde{U}_*)$ respectively and satisfy the

following "gluing" condition for some $L > 0$:

$$w_2(-L) - w_1(L) = q_1(L;\mu) - q_2(-L;\mu). \tag{3.4.6}$$

If these conditions hold then the corresponding solutions U_i of (3.3.3) satisfy

$$U_1(L) = U_2(-L), \qquad |U_1(-\xi) \to U_p(\xi)| + |U_2(\xi) - \tilde{U}_*| \to 0, \quad \xi \to \infty,$$

so that the solution composed of the concatenation of U_1 and U_2 is the desired heteroclinic. Also, the smoothness of F gives the following pointwise estimates on the variational nonlinearities

Lemma 3.4.1. *There exists constants $C_i > 0$ such that g_i and its derivative $D_{w_i} g_i$ satisfy the following estimates for all ξ and sufficiently small $w_i \in X$ and $\mu \in \mathbb{R}^2$,*

$$|g_i(\xi_i, w_i; \mu)| \leq C\left(|w_i|^2 + |\mu||w_i|\right), \tag{3.4.7}$$

$$|D_{w_i} g_i(\xi_i, w_i; \mu)| \leq C(|w_i| + |\mu|). \tag{3.4.8}$$

Proof. This follows from the assumptions on F and the heteroclinic solutions q_i above. ∎

We construct solutions $w_i(\xi)$ to (3.4.5) and (3.4.1) separately, with each satisfying Silnikov boundary conditions for sufficiently large $L > 0$:

$$P_1^{\mathrm{ss}}(0)w_1(0) = \mathfrak{s}_1, \quad P_1^{\mathrm{su}}(L)w_1(L) = \mathfrak{u}_1, \tag{3.4.9}$$

$$P_2^{\mathrm{ss}}(-L)w_2(-L) = \mathfrak{s}_2, \quad P_2^{\mathrm{su}}(0)w_2(0) = \mathfrak{u}_2, \tag{3.4.10}$$

where $\mathfrak{u}_i, \mathfrak{s}_i \in X$ are free variables satisfying

$$\mathfrak{s}_1 \in E_1^{\mathrm{ss}}(0), \qquad \mathfrak{u}_1 \in E_1^{\mathrm{su}}(L), \tag{3.4.11}$$

$$\mathfrak{s}_2 \in E_2^{\mathrm{ss}}(-L), \qquad \mathfrak{u}_2 \in E_2^{\mathrm{su}}(0). \tag{3.4.12}$$

Also, we require that $w_i(0) \in \Sigma_i$. To simplify notation, let $\mathfrak{W}_i := (\mathfrak{s}_i, \mathfrak{u}_i)$ for $i = 1, 2$.

With these solutions we follow the gluing-matching procedure used in [120], which is

outlined below and depicted in Figure 3.4.1.

- **Section 3.4.2 (Silnikov Solutions)**: Use variation of constants formulas to prove existence of variational solutions $w_i(\mathfrak{W}_i;\mu,L)$, lying near q_1 and q_2, which lie in certain exponentially weighted function spaces and satisfy the boundary conditions (3.4.11)-(3.4.12).

- **Section 3.4.3 (Gluing)**: Use the gluing condition (3.4.6) to solve for the "outer" boundary variables $\mathfrak{W}^0 := (\mathfrak{s}_1, \mathfrak{u}_2)$ in terms of the "inner" boundary variables $\mathfrak{W}^L := (\mathfrak{s}_2, \mathfrak{u}_1), L$, and μ.

- **Section 3.4.4 (Transverse intersection)**: Match the solution $w_2(\mathfrak{W}^0;\mu,L)$ with $W^{\mathrm{s}}(\tilde{U}_*(\mu))$ in the transverse section Σ_2 of $q_2(0)$.

- **Section 3.4.5 (Non-transverse intersection)**: Match the the solution $w_1(\mathfrak{W}^0;\mu,L)$ with $W^{\mathrm{cu}}(U_p)$ in the transverse section Σ_1 of $q_1(0)$ by first solving the matching condition in $E_1 := E_1^{\mathrm{ss}}(0) + E_{-1}^{\mathrm{cu}}(0)$ where $E_{-1}^{\mathrm{cu}}(0) := T_{q_1(0)}W^{\mathrm{cu}}(U_p)$. Then solve the condition in the complement $E_1^{\perp}$ using Melnikov integrals.

In Section 3.4.6 we then derive asymptotics which allow us to obtain the bifurcation curve discussed in Theorem 3.3.2.

3.4.2 Silnikov Solutions

In order to find solutions with the desired decay, we use exponentially weighted norms. Let $\eta_{\mathrm{ss}}, \eta_{\mathrm{su}} > 0$ be fixed constants such that $\delta_{\mathrm{ss}} := r_{\mathrm{ss}} - \eta_{\mathrm{ss}}$ and $\delta_{\mathrm{su}} := \eta_{\mathrm{su}} - r_{\mathrm{su}}$ are positive and arbitrarily small. Also define the quantity $m := \eta_{\mathrm{ss}} - 2\eta_{\mathrm{su}}$, which quantifies the size of the spectral gap $\Delta\eta := \eta_{\mathrm{ss}} - \eta_{\mathrm{su}}$, so that $m < 0$ if and only if $\eta_{\mathrm{ss}}/\eta_{\mathrm{su}} < 2$.

To begin we define the L-dependent norms

$$||w_1||_{1,L} := \sup_{\xi\in I_1} \mathrm{e}^{\eta_{\mathrm{ss}}\xi+\gamma_{\mathrm{ss}}L}|w_1^{\mathrm{ss}}(\xi)| + \sup_{\xi\in I_1} \mathrm{e}^{\eta_{\mathrm{su}}\xi+\gamma_{\mathrm{su}}L}|w_1^{\mathrm{su}}(\xi)| \tag{3.4.13}$$

$$||w_2||_{2,L} := \sup_{\xi\in I_2} \mathrm{e}^{\eta_{\mathrm{ss}}(\xi+L)+\kappa_{\mathrm{ss}}L}|w_2^{\mathrm{ss}}(\xi)| + \sup_{\xi\in I_2} \mathrm{e}^{\eta_{\mathrm{su}}(\xi+L)+\kappa_{\mathrm{su}}L}|w_2^{\mathrm{su}}(\xi)| \tag{3.4.14}$$

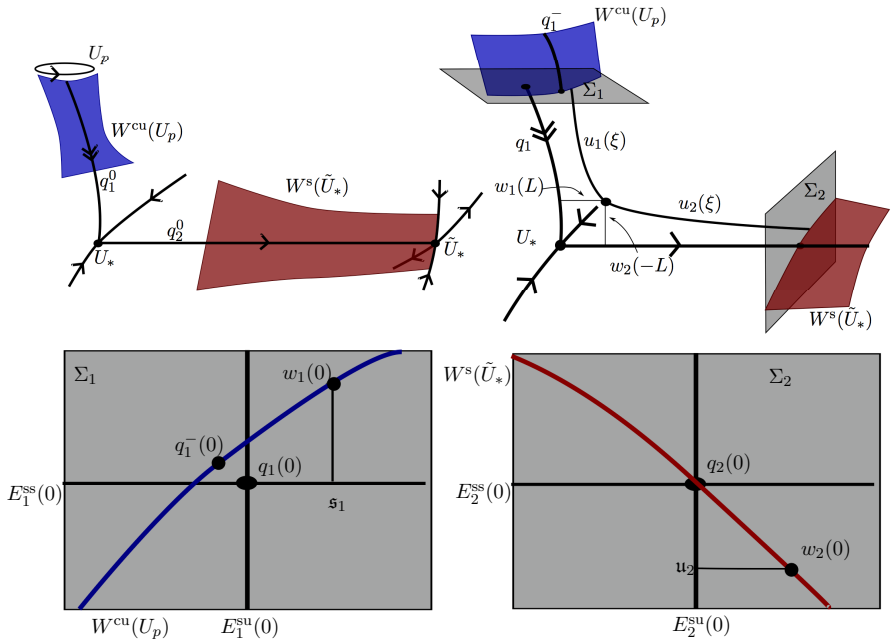

Figure 3.4.1: Schematic diagram of gluing construction. The top left figure depicts the global phase portrait in X for $\mu = 0$, showing the two manifolds we wish to connect. The top right figure depicts the gluing construction near the equilibrium U_* for μ close to 0, where initial data are taken in transverse sections Σ_1, Σ_2. These sections are depicted in the bottom figure with the corresponding Silnikov data $\mathfrak{s}_1, \mathfrak{u}_2$ prescribed in each.

where $I_1 = [0, L]$, $I_2 = [-L, 0]$, $w_i^j(\xi) := P_i^j(\xi) w_i(\xi)$ for $i = 1, 2$, $j = \mathrm{ss}, \mathrm{su}$ and

$$\gamma_{\mathrm{ss}} = \Delta\eta + |m| - \eta_{\mathrm{su}}, \quad \gamma_{\mathrm{su}} = \Delta\eta + |m| - \eta_{\mathrm{su}}, \quad \kappa_{\mathrm{ss}} = \Delta\eta + |m|, \quad \kappa_{\mathrm{su}} = \Delta\eta + |m| + \rho,$$

with $\rho > 0$ arbitrarily small. Note by the definition of m, these quantities are all positive.

Remark 3.4.2. *These norms were determined in order to make the upcoming fixed point operators uniform contractions in a sufficiently small neighborhood of the origin, and accommodate for all sizes of the spectral gap $\Delta\eta$ in the gluing-matching procedure. We remark that more general conditions on $\gamma_{\mathrm{ss/su}}$ and $\kappa_{\mathrm{ss/su}}$ can be determined, but we have omitted them for the sake of presentation.*

We denote

$$\Gamma^{\epsilon}_{1,L} := \{w_1 \in C^k([0,L],X) \,:\, ||w_1||_{1,L} < \epsilon\,\},$$
$$\Gamma^{\epsilon}_{2,L} := \{w_2 \in C^k([-L,0],X) \,:\, ||w_2||_{2,L} < \epsilon\},$$

and define the variation-of-constants operators

$$\Psi_i(w_i, \mathfrak{W}_i; \mu, L) := \Psi_i^{\rm ss}(w_1, \mathfrak{W}_1; \mu, L) + \Psi_i^{\rm su}(w_1, \mathfrak{W}_1; \mu, L)$$

with

$$\begin{pmatrix} \Psi_1^{\rm ss}(w_1; \mathfrak{W}_1, \mu, L)(\xi) \\ \Psi_1^{\rm su}(w_1; \mathfrak{W}_1, \mu, L)(\xi) \end{pmatrix} := \begin{pmatrix} \Phi_1^{\rm ss}(\xi, 0)\mathfrak{s}_1 + \int_0^\xi \Phi_1^{\rm ss}(\xi,\zeta) g_1(\zeta, w_1(\zeta); \mu) d\zeta \\ \Phi_1^{\rm su}(\xi, L)\mathfrak{u}_1 + \int_L^\xi \Phi_1^{\rm su}(\xi,\zeta) g_1(\zeta, w_1(\zeta); \mu) d\zeta \end{pmatrix},$$

$$\begin{pmatrix} \Psi_2^{\rm ss}(w_2; \mathfrak{W}_2, \mu, L)(\xi) \\ \Psi_2^{\rm su}(w_2; \mathfrak{W}_2, \mu, L)(\xi) \end{pmatrix} := \begin{pmatrix} \Phi_2^{\rm ss}(\xi, -L)\mathfrak{s}_2 + \int_{-L}^\xi \Phi_2^{\rm ss}(\xi,\zeta) g_2(\zeta, w_2(\zeta); \mu) d\zeta \\ \Phi_2^{\rm su}(\xi, 0)\mathfrak{u}_2 + \int_0^\xi \Phi_2^{\rm su}(\xi,\zeta) g_2(\zeta, w_2(\zeta); \mu) d\zeta \end{pmatrix}.$$

Finally, for some small $\delta > 0$ we denote

$$\Lambda^{\delta}_L = \{\mu \in \mathbb{R}^2 \,:\, \mathrm{e}^{(2\Delta\eta - \rho)L}|\mu| < \delta\}, \quad X^{\delta}_{\eta,L} = \{u \in X \,:\, \mathrm{e}^{\eta L}|u| < \delta\}. \tag{3.4.15}$$

Here, the weight in the parameter space Λ^{δ}_L was chosen to capture the $\mathcal{O}(\mathrm{e}^{2\Delta\nu L})$ leading-order dynamics of the bifurcation equation for μ. It is readily seen that if w_i is a fixed point of Ψ_i then it must also solve (3.4.5) or (3.4.1) for $i = 1, 2$. We then have the following proposition,

Proposition 3.4.3. *There exists an $\epsilon_0 > 0$ such that the following holds. For all $0 < \epsilon < \epsilon_0$, and L sufficiently large, there exists a $\delta > 0$ such that for all $\mu \in \Lambda^{\delta}_L$ and $\mathfrak{W}_1 = (\mathfrak{s}_1, \mathfrak{u}_1)$ which satisfy*

$$\mathfrak{s}_1 \in X^{\epsilon/6}_{\gamma_{\rm ss},L}, \qquad \mathfrak{u}_1 \in X^{\epsilon/6}_{\eta_{\rm su}+\gamma_{\rm su},L}, \tag{3.4.16}$$

the variational equation (3.4.5) *has a unique solution $w_1^*(\mathfrak{W}_1, \mu, L) \in \Gamma^{\epsilon}_{1,L}$ which is C^k in $(\xi, \mathfrak{W}_1, \mu)$ and satisfies the boundary conditions* (3.4.11).

Proof. We prove this result by showing that the operator,

$$\Psi_1(\mathfrak{W}_1) : \Gamma^{\epsilon}_{1,L} \times \Lambda^{\delta}_{L} \to \Gamma^{\epsilon}_{1,L},$$

which can readily be shown to be C^k in both arguments, is well-defined and a uniform contraction. The resulting unique fixed point will then be the desired solution.

We shall need the following pointwise estimates on the the nonlinearity g_1. For any $\xi \in [0, L]$ with $w \in X$ and $\mu \in \mathbb{R}^2$ sufficiently small, Hypothesis 3.3.7 and Lemma 3.4.1 give a constant $C_1 > 0$ such that

$$\begin{aligned}
|g_1(\xi, w; \mu)| &\leq C_1(|w(\xi)|^2 + |w(\xi)||\mu|) \\
&\leq C_1\Big(|w^{\mathrm{ss}}(\xi)|^2 + |w^{\mathrm{su}}(\xi)|^2 + |\mu|\left(|w^{\mathrm{ss}}(\xi)| + |w^{\mathrm{su}}(\xi)|\right)\Big) \\
&\leq C_1\Big(\mathrm{e}^{-2\eta_{\mathrm{ss}}\xi - 2\gamma_{\mathrm{ss}}L}||w^{\mathrm{ss}}||^2_{1,L} + \mathrm{e}^{-2\eta_{\mathrm{su}}\xi - 2\gamma_{\mathrm{su}}L}||w^{\mathrm{su}}||^2_{1,L} \\
&+ |\mu|\left(\mathrm{e}^{-\eta_{\mathrm{ss}}\xi - \gamma_{\mathrm{ss}}L}||w^{\mathrm{ss}}||_{1,L} + \mathrm{e}^{-\eta_{\mathrm{su}}\xi - \gamma_{\mathrm{su}}L}||w^{\mathrm{su}}||_{1,L}\right)\Big).
\end{aligned} \tag{3.4.17}$$

Note that $w^j(\xi) = P^j_1(\xi)w(\xi)$. Similarly, for $w, v \in X$ we have the quadratic estimate

$$\begin{aligned}
|g_1(\xi, w; \mu) - g_1(\xi, v; \mu)| &\leq C_1'\Big(|w(\xi)| + |v(\xi)| \cdot |w(\xi) - v(\xi)| + |\mu||w(\xi) - v(\xi)|\Big) \\
&\leq C_1'\mathrm{e}^{-2\eta_{\mathrm{ss}}\xi - 2\gamma_{\mathrm{ss}}L}\left(||w^{\mathrm{ss}}||_{1,L} + ||v^{\mathrm{ss}}||_{1,L}\right) \cdot ||w^{\mathrm{ss}} - v^{\mathrm{ss}}||_{1,L} \\
&\quad + C_1'\mathrm{e}^{-2\eta_{\mathrm{su}}\xi - 2\gamma_{\mathrm{su}}L}\left(||w^{\mathrm{su}}||_{1,L} + ||v^{\mathrm{su}}||_{1,L}\right) \cdot ||w^{\mathrm{su}} - v^{\mathrm{su}}||_{1,L} \\
&+ C_1'|\mu|\left(\mathrm{e}^{-\eta_{\mathrm{ss}}\xi - \gamma_{\mathrm{ss}}L}||w^{\mathrm{ss}} - v^{\mathrm{ss}}||_{1,L} + \mathrm{e}^{-\eta_{\mathrm{su}}\xi - \gamma_{\mathrm{su}}L}||w^{\mathrm{su}} - v^{\mathrm{su}}||_{1,L}\right).
\end{aligned} \tag{3.4.18}$$

We then find

$$\begin{aligned}
&\sup_{\xi \in I_1} \mathrm{e}^{\eta_{\mathrm{ss}}\xi + \gamma_{\mathrm{ss}}L}|\Psi^{\mathrm{ss}}_1(w_1)(\xi)| \leq \\
&\quad \sup_{\xi \in I_1} \mathrm{e}^{(\eta_{\mathrm{ss}} - r_{\mathrm{ss}})\xi + \gamma_{\mathrm{ss}}L}|\mathfrak{s}_1| + \mathrm{e}^{\eta_{\mathrm{ss}}\xi + \gamma_{\mathrm{ss}}L}\int_0^{\xi} \mathrm{e}^{-r_{\mathrm{ss}}(\xi - \zeta)}C_1\left(|w_1(\zeta)|^2 + |w_1(\zeta)||\mu|\right) d\zeta.
\end{aligned} \tag{3.4.19}$$

The condition on $\mathfrak{s}_1$ gives

$$\sup_{\xi\in I_1} \mathrm{e}^{(\eta_{\rm ss}-r_{\rm ss})\xi+\gamma_{\rm ss}L}|\mathfrak{s}_1| \leq \frac{\epsilon}{6}. \tag{3.4.20}$$

Next we estimate the term involving $|w_1|^2$ in (3.4.19):

$$\begin{aligned}
&\sup_{\xi\in I_1} \mathrm{e}^{\eta_{\rm ss}\xi+\gamma_{\rm ss}L}\int_0^{\xi} \mathrm{e}^{-r_{\rm ss}(\xi-\zeta)}C_1|w_1(\zeta)|^2d\zeta \\
&\qquad \leq C_1\left(\mathrm{e}^{-(\gamma_{\rm ss}+\delta_{\rm ss})L}-\mathrm{e}^{-(\gamma_{\rm ss}+\eta_{\rm ss})L}\right)\frac{||w^{\rm ss}||^2_{1,L}}{2\eta_{\rm ss}-r_{\rm ss}} \\
&\qquad\qquad + C_1\left(\mathrm{e}^{(\gamma_{\rm ss}-2\gamma_{\rm su}+\eta_{\rm ss}-2\eta_{\rm su})L}-\mathrm{e}^{(\gamma_{\rm ss}-2\gamma_{\rm su}-\delta_{\rm ss})L}\right)\frac{||w^{\rm su}||^2_{1,L}}{|2\eta_{\rm su}-r_{\rm ss}|} \\
&\qquad \leq 2C_1C_1^*||w_1||^2_{1,L} < \epsilon/6.
\end{aligned} \tag{3.4.21}$$

where $C_* = \max\{\frac{1}{2\eta_{\rm ss}-r_{\rm ss}}, \frac{1}{|2\nu_{\rm su}-r_{\rm ss}|}\}$, and we require $\epsilon < \frac{1}{12C_1C_*}$. Also note that we have used the fact that $\gamma_{\rm ss}-2\gamma_{\rm su} = 2\eta_{\rm su}-\eta_{\rm ss}-|m|-2\rho$.

The term with $|w_1||\mu|$ in (3.4.19) can similarly be estimated by

$$\begin{aligned}
&C_1\sup_{\xi\in I_1} \mathrm{e}^{\eta_{\rm ss}\xi+\gamma_{\rm ss}L}\int_0^{L} \mathrm{e}^{-r_{\rm ss}(\xi-\zeta)}|\mu|\left(\mathrm{e}^{-\eta_{\rm ss}\zeta-\gamma_{\rm ss}L}||w^{\rm ss}||_{1,L}+\mathrm{e}^{-\eta_{\rm su}\zeta-\gamma_{\rm su}L}||w^{\rm su}||_{1,L}\right) \\
&\qquad \leq C_1|\mu|\left(\mathrm{e}^{-\delta_{\rm ss}L}||w^{\rm ss}||_{1,L}+\mathrm{e}^{(\gamma_{\rm ss}-\gamma_{\rm su}+\Delta\eta)L}||w^{\rm su}||_{1,L}\right) \\
&\qquad \leq C_1\delta||w||_{1,L} < \epsilon/6,
\end{aligned} \tag{3.4.22}$$

for any $0<\delta<\frac{1}{6C_1}$, since $\mu\in\Lambda_L^\delta$ and $\gamma_{\rm ss}-\gamma_{\rm su} = -2\rho$.

Combining (3.4.20), (3.4.21), and (3.4.22) we obtain

$$||\Psi_1^{\rm ss}(w_1)||_{1,L} < \epsilon/2. \tag{3.4.23}$$

Similar estimates may be applied to obtain

$$||\Psi_1^{\rm su}(w_1)||_{1,L} < \epsilon/2, \tag{3.4.24}$$

for any $\epsilon < (C_1\max\{\frac{1}{2\eta_{\rm ss}-r_{\rm su}}, \frac{1}{2\eta_{\rm su}-r_{\rm su}}\})^{-1}$. These can then be combined to obtain

$||\Psi_1(w)||_{1,L} < \epsilon$.

To prove the contraction, the pointwise estimate (3.4.18) can be used in a similar way to obtain

$$||\Psi_1(w;\mathfrak{W}_1,\mu,L) - \Psi_1(v;\mathfrak{W}_1,\mu,L)||_{1,0} \leq C_1C_*\left(4\epsilon + |\mu|\mathrm{e}^{\Delta\eta L}\right)||w-v||_{1,L} < \frac{1}{2}||w-v||_{1,L},$$
$$w, v \in \Gamma^{\epsilon}_{1,L}, \tag{3.4.25}$$

For ϵ_0 sufficiently small, and L sufficiently large. Since Ψ_1 is smooth in μ and $\mathfrak{W}_1$, the Uniform Contraction principle then gives the result. □

An analogous proof gives the existence of a solution for (3.4.1).

Proposition 3.4.4. *There exists an $\epsilon_0 > 0$ such that the following holds: For all $0 < \epsilon < \epsilon_0$ and L sufficiently large there exists a $\delta > 0$ such that for all $\mu \in \Lambda^{\delta}_L$ and $\mathfrak{W}_2 = (\mathfrak{s}_2, \mathfrak{u}_2)$ which satisfy*

$$\mathfrak{s}_2 \in X^{\epsilon/6}_{\kappa_{\mathrm{ss}},L}, \qquad \mathfrak{u}_2 \in X^{\epsilon/6}_{\eta_{\mathrm{su}}+\kappa_{\mathrm{su}},L}, \tag{3.4.26}$$

equation (3.4.1) *has a unique solution $w^*_2(\mathfrak{W}_2,\mu,L) \in \Gamma^{\epsilon}_{2,L}$ which is C^k in $(\xi,\mathfrak{W}_2,\mu)$.*

3.4.3 Gluing

We now wish to find boundary data $\mathfrak{W}_1 = (\mathfrak{s}_1,\mathfrak{u}_1)$ and $\mathfrak{W}_2 = (\mathfrak{s}_2,\mathfrak{u}_2)$ for which the solutions w^*_1, w^*_2 satisfy the gluing equation (3.4.6). We use the projections $P^{\mathrm{ss}}_2(-L)$ and $P^{\mathrm{su}}_1(L)$ to decompose the gluing equation (3.4.6) into the system

$$\begin{aligned} P^{\mathrm{ss}}_2(-L)w^*_1(L) - \mathfrak{s}_2 &= P^{\mathrm{ss}}_2(-L)\Delta q(L) \\ \mathfrak{u}_1 - P^{\mathrm{su}}_1(L)w^*_2(-L) &= P^{\mathrm{su}}_1(L)\Delta q(L) \end{aligned} \tag{3.4.27}$$

where $\Delta q(L) = q_2(-L) - q_1(L)$.

To simplify this system, we use the following estimates on the ξ-dependent projections.

Lemma 3.4.5. *For L sufficiently large there exists a constant $K > 0$ such that*

$$|P_1^j(L)u - P_{1,\infty}^j u| \leq K\mathrm{e}^{-\Delta\eta L}|u|, \tag{3.4.28}$$
$$|P_2^j(-L)u - P_{1,\infty}^j u| \leq K\mathrm{e}^{-\Delta\eta L}|u|, \tag{3.4.29}$$

for $j = \mathrm{ss}, \mathrm{su}$, $u \in X$.

Proof. Using the asymptotic decay of $A_i(\xi)$ as $\xi \to \pm\infty$ for $i = 1, 2$ respectively, this result follows from [114, Cor. 2]. □

From this lemma, the heteroclinic asymptotics in Hypothesis 3.3.7 then give that (3.4.27) has the leading order form

$$\begin{aligned}\mathfrak{s}_2 &= \left[w_1^{*,\mathrm{ss}}(L) - q_1(L)\right]\left(1 + \mathcal{O}(\mathrm{e}^{-\Delta\eta L})\right)\\ \mathfrak{u}_1 &= \left[w_2^{*,\mathrm{su}}(-L) + q_2(-L)\right]\left(1 + \mathcal{O}(\mathrm{e}^{-\Delta\eta L})\right).\end{aligned}$$

Hence, it suffices to prove the existence of solutions to the truncated system

$$\begin{aligned}\mathfrak{s}_2 &= w_1^{*,\mathrm{ss}}(L) - q_1(L)\\ \mathfrak{u}_1 &= w_2^{*,\mathrm{su}}(-L) + q_2(-L).\end{aligned}$$

Such solutions can be found as fixed points of the following operator,

$$\begin{aligned}&H_{\mathrm{gl}} : \mathfrak{X}_L^\epsilon \times \mathfrak{X}_0^\epsilon \times \Lambda_L^\delta \to \mathfrak{X}_L^\epsilon\\ &\quad(\mathfrak{W}^L; \mathfrak{W}^0, \mu) \mapsto \begin{pmatrix} \Psi_1^{\mathrm{ss}}(w_1^*(\mathfrak{s}_1, \mathfrak{u}_1, \mu, L), \mu, L)(L) \\ \Psi_2^{\mathrm{su}}(w_2^*(\mathfrak{s}_2, \mathfrak{u}_2, \mu, L); \mu, L)(-L) \end{pmatrix} + \begin{pmatrix} -q_1(L;\mu) \\ q_2(L;\mu) \end{pmatrix},\end{aligned} \tag{3.4.30}$$

where we solve for the inner boundary values near the equilibrium U_*,

$$\mathfrak{W}^L := (\mathfrak{s}_2, \mathfrak{u}_1) \in \mathfrak{X}_L^\epsilon := X_{\kappa_{\mathrm{ss}},L}^\epsilon \times X_{\eta_{\mathrm{su}}+\gamma_{\mathrm{su}},L}^\epsilon,$$

in terms of the outer boundary values near $q_1(0)$ and $q_2(0)$,

$$\mathfrak{W}^0 := (\mathfrak{s}_1, \mathfrak{u}_2) \in \mathfrak{X}_0^\epsilon := X_{\gamma_{\mathrm{ss}},L}^\epsilon \times X_{\eta_{\mathrm{su}}+\kappa_{\mathrm{su}},L}^\epsilon.$$

The exponential weights on these values are chosen to be consistent with the contraction arguments in Propositions 3.4.3 and 3.4.4. We then obtain the following existence result,

Proposition 3.4.6. *There exists an $\epsilon_1 > 0$ such that the following holds. For all $\epsilon < \epsilon_1$, L sufficiently large, there exists a $\delta > 0$ such that the mapping $H_{\mathrm{gl}} : \mathfrak{X}_L^\epsilon \times \mathfrak{X}_0^\epsilon \times \Lambda_L^\delta \to \mathfrak{X}_L^\epsilon$ has a unique fixed point $\mathfrak{W}_\dagger^L(\mathfrak{W}^0, \mu, L) := \left(\mathfrak{s}_2^\dagger(\mathfrak{W}^0, \mu, L), \mathfrak{u}_1^\dagger(\mathfrak{W}^0, \mu, L)\right)$ which is C^k smooth in all its variables.*

Proof. First note that since w_i^* is smooth in $\mathfrak{W}_i$ and μ, and $w_i^*(0; 0, L) = 0$, we have that

$$\begin{aligned} ||w_1^*(\mathfrak{W}_1; \mu, L)||_{1,L} &\leq C_3 \left(\mathrm{e}^{\gamma_{\mathrm{ss}} L} |\mathfrak{s}_1| + \mathrm{e}^{(\eta_{\mathrm{su}} + \gamma_{\mathrm{su}})L} |\mathfrak{u}_1| + \mathrm{e}^{\Delta\eta L} |\mu| \right), \\ ||w_2^*(\mathfrak{W}_2; \mu, L)||_{2,L} &\leq C_3 \left(\mathrm{e}^{\kappa_{\mathrm{ss}} L} |\mathfrak{s}_2| + \mathrm{e}^{(\eta_{\mathrm{su}} + \kappa_{\mathrm{su}})L} |\mathfrak{u}_2| + \mathrm{e}^{\Delta\eta L} |\mu| \right). \end{aligned} \tag{3.4.31}$$

Similar to the proofs in the previous section, the pointwise estimates (3.4.17) and (3.4.18) then give the estimates

$$\mathrm{e}^{\kappa_{\mathrm{ss}} L} |\Phi_1^{\mathrm{ss}}(L, 0)\mathfrak{s}_1| \leq K_1 \mathrm{e}^{(\kappa_{\mathrm{ss}} - r_{\mathrm{ss}})L} |\mathfrak{s}_1|,$$

$$\begin{aligned} \mathrm{e}^{\kappa_{\mathrm{ss}} L} \Big| \int_0^L \Phi_1^{\mathrm{ss}}(L, \zeta) g_1(\zeta, w_1^*; \mu) d\zeta \Big| \leq & \\ C_2 \mathrm{e}^{\kappa_{\mathrm{ss}} L} \left(\mathrm{e}^{-2(\eta_{\mathrm{ss}} + \gamma_{\mathrm{ss}})L} ||w_1^{\mathrm{ss}}||_{1,L}^2 + \mathrm{e}^{-2(\eta_{\mathrm{su}} + \gamma_{\mathrm{su}})L} ||w_1^{\mathrm{su}}||_{1,L}^2 \right) & \\ + |\mu| \left(\mathrm{e}^{-(\eta_{\mathrm{ss}} + \gamma_{\mathrm{ss}})L} ||w_1^{\mathrm{ss}}||_{1,L} + \mathrm{e}^{-(\eta_{\mathrm{su}} + \gamma_{\mathrm{su}})L} ||w_1^{\mathrm{su}}||_{1,L} \right), & \end{aligned}$$

for the first component of H_{gl}.

For the second component we obtain for some constants $K_2, K_2' > 0$,

$$\begin{aligned}
&\mathrm{e}^{(\eta_{\mathrm{su}}+\gamma_{\mathrm{su}})L}|\Phi_2^{\mathrm{su}}(-L,0)\mathfrak{u}_2| \leq K_2\mathrm{e}^{(2\eta_{\mathrm{su}}+\gamma_{\mathrm{su}})L}|\mathfrak{u}_2| \leq K_2\mathrm{e}^{(\eta_{\mathrm{su}}+\gamma_{\mathrm{su}}-\kappa_{\mathrm{su}})L}\epsilon, \qquad (3.4.32)\\
&\mathrm{e}^{(\eta_{\mathrm{su}}+\gamma_{\mathrm{su}})L}\Big|\int_0^{-L}\Phi_2^{\mathrm{su}}(-L,\zeta)g_2(\zeta,w_2^*;\mu)d\zeta\Big| \leq\\
&\qquad K_2\mathrm{e}^{(2\eta_{\mathrm{su}}+\gamma_{\mathrm{su}}-\delta_{\mathrm{su}})L}\Bigg(\mathrm{e}^{-2(\eta_{\mathrm{ss}}+\kappa_{\mathrm{ss}})L}||w_2^{\mathrm{ss}}||_{2,L}^2+\mathrm{e}^{-2(\eta_{\mathrm{su}}+\kappa_{\mathrm{su}})L}||w_2^{\mathrm{su}}||_{2,L}^2\\
&\qquad\quad+|\mu|\left(\mathrm{e}^{-(\eta_{\mathrm{ss}}+\kappa_{\mathrm{ss}})L}||w_2^{\mathrm{ss}}||_{2,L}+\mathrm{e}^{-(\eta_{\mathrm{su}}+\kappa_{\mathrm{su}})L}||w_2^{\mathrm{su}}||_{2,L}\right)\Bigg)\\
&\qquad\leq K_2\Bigg(\mathrm{e}^{(-3\Delta\eta-|m|-\eta_{\mathrm{su}})L}||w_2^{\mathrm{ss}}||_{2,L}^2+\mathrm{e}^{(-\eta_{\mathrm{su}}-\Delta\eta-|m|)L}||w_2^{\mathrm{su}}||_{2,L}^2\\
&\qquad\quad+|\mu|\left(\mathrm{e}^{-\Delta\eta L}||w_2^{\mathrm{ss}}||_{2,L}+\mathrm{e}^{-(\delta_{\mathrm{su}}+\rho)L}||w_2^{\mathrm{su}}||_{2,L}\right)\Bigg),\\
&\mathrm{e}^{\eta_{\mathrm{su}}+\gamma_{\mathrm{su}}L}|q_2(L)| \leq K_2'\mathrm{e}^{(\Delta\eta+|m|-r_{\mathrm{u}})L}.
\end{aligned}$$

Pairing these estimates with those in (3.4.31) and using Hypothesis 3.3.4, we can then obtain the desired invariance of H_{gl} for sufficiently small ϵ.

Uniform Contraction then follows in a similar manner, using the fact that $||w_i^*(\mathfrak{W}_i) - w_i^*(\mathfrak{V}_i)||_{i,L} \leq C_2|\mathfrak{W}_i - \mathfrak{V}_i|$ for small enough $\mathfrak{W}_i, \mathfrak{V}_i$. □

This proposition implies the existence of boundary data

$$\mathfrak{W}_{\mathrm{gl}}^L(\mathfrak{W}^0,\mu,L) := \left(\mathfrak{s}_2^{\mathrm{gl}}(\mathfrak{W}^0,\mu,L),\mathfrak{u}_1^{\mathrm{gl}}(\mathfrak{W}^0,\mu,L)\right),$$

smooth in all dependent variables, which give glued solutions

$$w_1^{\mathrm{gl}}(\mathfrak{W}^0,\mu,L)(\xi) := w_1^*(\mathfrak{s}_1,\mathfrak{u}_1^{\mathrm{gl}}(\mathfrak{W}^0),\mu,L)(\xi), \quad w_2^{\mathrm{gl}}(\mathfrak{W}^0,\mu,L)(\xi) := w_2^*(\mathfrak{s}_2^{\mathrm{gl}}(\mathfrak{W}^0),\mathfrak{u}_2,\mu,L)(\xi),$$

satisfying (3.4.27).

3.4.4 Transverse matching

Now we match the glued solution with the stable manifold $W^{\mathrm{s}}(\tilde{U}_*)$ inside Σ_2. Since this manifold is C^k-smooth and intersects $W^{\mathrm{su}}(U_*)$ transversely, we have that $W^{\mathrm{s}}(\tilde{U}_*) \cap \Sigma_2$ can be locally described near $q_2(0)$ as a graph $h_2 : E^{\mathrm{s}}_{+2}(0) \cap \Sigma_2 \to E^{\mathrm{su}}_2(0) \cap \Sigma_2$, where $E^{\mathrm{s}}_{+2}(0) := P^{\mathrm{s}}_{+2}(0)X$ and

$$|h_2(v_2;\mu)| \leq K_{\mathrm{s}}|v_2|(|\mu| + |v_2|),$$

for some $K_{\mathrm{s}} > 0$, and sufficiently small μ and $v_2 \in E^{\mathrm{s}}_{+2}(0) \cap \Sigma_2$. Here, $P^{\mathrm{s}}_{+2}(\xi)$ is the projection associated with the dichotomy used to construct the invariant manifold $W^{\mathrm{s}}(\tilde{U}_*)$. We thus obtain the matching equation

$$w^{\mathrm{gl}}_2(\mathfrak{W}^0;\mu,L)(0) = v_2 + h_{\mathrm{s}}(v_2;\mu), \tag{3.4.33}$$

which we use to solve for $(\mathfrak{u}_2, v_2)$ in terms of $(\mathfrak{s}_1, \mu)$. Defining

$$\tilde{g}_i(\xi,\mathfrak{W}^0;\mu) := g_i(\xi, w^{\mathrm{gl}}_i(\mathfrak{W}^0;\mu,L)(\xi);\mu), \quad i = 1,2,$$

we use the projected solution operators $\Psi^{\mathrm{ss/su}}_2$ to write (3.4.33) as

$$\mathfrak{u}_2 - v_2 = h_{\mathrm{s}}(v_2,\mu) - \Phi^{\mathrm{ss}}_2(0,-L)\mathfrak{s}^{\mathrm{gl}}_2(\mathfrak{W}^0) - \int_{-L}^{0} \Phi^{\mathrm{ss}}_2(0,\zeta)\tilde{g}_2(\zeta;\mathfrak{W}^0;\mu)d\zeta. \tag{3.4.34}$$

Proposition 3.4.7. *For some $\epsilon_2 > 0$ the following holds: For all $0 < \epsilon < \epsilon_2$ there exists a $\delta > 0$ such that (3.4.33) has a C^k-solution $(\mathfrak{u}^{\mathrm{tr}}_2, v^{\mathrm{tr}}_2)(\mathfrak{s}_1,\mu) \in X^{\epsilon}_{\eta_{\mathrm{su}}+\kappa_{\mathrm{su}},L} \times X^{\epsilon}_{\eta_{\mathrm{su}}+\kappa_{\mathrm{su}},L}$, for each $(\mathfrak{s}_1,\mu) \in X^{\epsilon/8}_{\gamma_{\mathrm{ss}},L} \times \Lambda^{\delta}_L$.*

Proof. First, Hypothesis 3.3.12 implies that the canonical mapping

$$\begin{aligned} S_2 :&(E^{\mathrm{su}}_2(0) \cap \Sigma_2) \times (E^{\mathrm{s}}_{+2}(0) \cap \Sigma_2) \to \Sigma_2 \\ &(\mathfrak{u}_2, v_2) \mapsto \mathfrak{u}_2 - v_2, \end{aligned}$$

is invertible with uniformly bounded inverse. Thus (3.4.33) can be rewritten as the fixed

point problem

$$(\mathfrak{u}_2, v_2) = S_2^{-1}\Big(h_{\mathrm{s}}(v_2,\mu) - \Phi_2^{\mathrm{ss}}(0,-L)\mathfrak{s}_2^{\mathrm{gl}}(\mathfrak{W}^0) - \int_{-L}^{0}\Phi_2^{\mathrm{ss}}(0,\zeta)\tilde{g}_2(\zeta,\mathfrak{W}^0;\mu)d\zeta\Big)$$
$$= \left(h_{\mathrm{s}}(v_2;\mu)\,,\, -P_{+2}^{\mathrm{s}}(0)\left(\Phi_2^{\mathrm{ss}}(0,-L)\mathfrak{s}_2^{\mathrm{gl}}(\mathfrak{W}^0) + \int_{-L}^{0}\Phi_2^{\mathrm{ss}}(0,\zeta)\tilde{g}_2(\zeta,\mathfrak{W}^0;\mu)d\zeta\right)\right). \tag{3.4.35}$$

since $S_2^{-1}(x) = (P_{2,+}^{\mathrm{su}}(0)x, -P_{+2}^{\mathrm{s}}(0)x)$, where $P_{2,+}^{\mathrm{su}}(\xi)$ was defined in Hypothesis 3.3.13 above.

We then obtain the following estimates on the different terms of the right-hand side of the above equation for some constant $K > 0$,

$$\mathrm{e}^{(\eta_{\mathrm{su}}+\kappa_{\mathrm{su}})L}\Big|h_{\mathrm{s}}(v_2,\mu)\Big| \leq K\mathrm{e}^{(\eta_{\mathrm{su}}+\kappa_{\mathrm{su}})L}\left(|v_2||\mu| + |v_2|^2\right)$$
$$\leq K\epsilon(\delta+\epsilon), \tag{3.4.36}$$
$$\mathrm{e}^{(\eta_{\mathrm{su}}+\kappa_{\mathrm{su}})L}|P_{+2}^{\mathrm{s}}(0)w_2^{\mathrm{ss}}(0)| \leq K\mathrm{e}^{(\eta_{\mathrm{su}}+\kappa_{\mathrm{su}}-\eta_{\mathrm{ss}}-\kappa_{\mathrm{ss}})L}||w_2^{\mathrm{ss}}||_{2,L} = K\mathrm{e}^{(\rho-\Delta\eta)L}||w_2^{\mathrm{ss}}||_{2,L}. \tag{3.4.37}$$

Applying the estimates in (3.4.31) we conclude that (3.4.35) is a uniform contraction and thus possesses a unique fixed point.

□

We denote the subsequent glued solutions which also solve the transverse matching problem as

$$w_1^{\mathrm{tr}}(\mathfrak{s}_1,\mu,L)(\xi) := w_1^{\mathrm{gl}}(\mathfrak{s}_1,\mathfrak{u}_2^{\mathrm{tr}},\mu,L)(\xi), \quad w_2^{\mathrm{tr}}(\mathfrak{s}_1,\mu,L)(\xi) := w_2^{\mathrm{gl}}(\mathfrak{s}_1,\mathfrak{u}_2^{\mathrm{tr}},\mu,L)(\xi),$$

where $\mathfrak{u}_2^{\mathrm{tr}} = \mathfrak{u}_2{}^{\mathrm{tr}}(\mathfrak{s}_1,\mu)$.

3.4.5 Non-Transverse matching

Now let us match the glued solution with $W^{\mathrm{cu}}(U_p)$ in Σ_1. In a neighborhood of $q_1(0;\mu)$, the intersection of the center-unstable manifold $W^{\mathrm{cu}}(U_p) \cap \Sigma_1$ can be described as a

graph $q_1^-(0;\mu) + v + h_p(v;\mu)$ with

$$h_p : E_{-1}^{\mathrm{cu}}(0) \cap \Sigma_2 \to \tilde{E}_1^{\mathrm{ss}}(0) \oplus E_1^{\perp}, \quad v \in E_{-1}^{\mathrm{cu}}(0) \cap \Sigma_2$$

where $E_{-1}^{\mathrm{cu}}(0) := P_{-1}^{\mathrm{cu}}(0)X$, $E_1 := E_{-1}^{\mathrm{cu}}(0) + E_1^{\mathrm{ss}}(0)$, and $\tilde{E}_1^{\mathrm{ss}}(0)$ is the orthogonal complement of $Z = E_{-1}^{\mathrm{cu}}(0) \cap E_1^{\mathrm{ss}}(0)$ in $E_1^{\mathrm{ss}}(0)$. Also define the orthogonal projection $Q_1 : E_{-1}^{\mathrm{cu}}(0) \to Z \cap \Sigma_2$ and let $\tilde{v}_1 = (I - Q_1)v$, $\mathfrak{v}_1 = Q_1 v$. We remark that since $\frac{d}{d\xi} q_1^0(0) \in Z$, the range of Q is a one-dimensional subspace.

We thus wish to solve the matching equation

$$w_1^{\mathrm{tr}}(\mathfrak{s}_1, \mu, L)(0) = q_1^-(0;\mu) - q_1(0;\mu) + \tilde{v}_1 + \mathfrak{v}_1 + h_p(\tilde{v}_1 + \mathfrak{v}_1;\mu). \tag{3.4.38}$$

In order to do this we shall first solve the projected equation on E_1 after which we can the solve on the complement $E_1^{\perp}$ using Melnikov integrals.

To achieve this first step, we apply the orthogonal projection $P_1 : X \to E_1$ to (3.4.38) and use (3.4.4) to obtain

$$\mathfrak{s}_1 - \tilde{v}_1 = \mathfrak{v}_1 + P_1 \left(h_p(\tilde{v}_1 + \mathfrak{v}_1;\mu) - \Phi_1^{\mathrm{su}}(0, L)\mathfrak{u}_1^{\mathrm{gl}}(\mathfrak{s}_1, \mathfrak{u}_2^{\mathrm{tr}}) - \int_L^0 \Phi_1^{\mathrm{su}}(0,\zeta)\tilde{g}_1(\zeta, \mathfrak{W}_{\mathrm{tr}}^0;\mu)d\zeta \right). \tag{3.4.39}$$

We then obtain the following result,

Proposition 3.4.8. *There exists $\epsilon_3 > 0$ such that the following holds. For all $\epsilon < \epsilon_3$ there exists a $\delta > 0$ such that there is a unique C^k-solution $(\mathfrak{s}_1^{\mathrm{m}}, \tilde{v}_1^{\mathrm{m}})(\mathfrak{v}_1, \mu, L) \in X_{\gamma_{\mathrm{ss}},L}^{\epsilon} \times X_{\gamma_{\mathrm{ss}},L}^{\epsilon}$ of (3.4.39) for each $\mathfrak{v}_1 \in X_{\gamma_{\mathrm{ss}},L}^{\epsilon}$, and $\mu \in \Lambda_L^{\delta}$.*

Proof. The proof follows in a similar manner as in Proposition 3.4.7 and we omit it. □

We denote the corresponding solutions as

$$w_i^{\mathrm{m}}(\mathfrak{v}_1, \mu, L)(\xi) = w_i^{\mathrm{tr}}(\mathfrak{s}_1^{\mathrm{m}}(\mathfrak{v}_1, \mu, L), \mu, L)(\xi).$$

Now we wish to solve the component of (3.4.38) in $E_1^{\perp}$ and thus complete the gluing

matching procedure. This can be done by solving the equations

$$\left\langle w_1^{\rm n}(\mathfrak{v}_1, L)(0), e_{j,0}^* \right\rangle = \left\langle q_1^-(0;\mu) - q_1(0;\mu), e_{j,0}^* \right\rangle + \langle h_p(\mathfrak{v}_1 + \tilde{v}_1^{\rm n};\mu), e_{j,0}^* \rangle, \qquad j = 1, 2,$$

where and $e_{1,0}^*, e_{2,0}^* \in X$ have unit norm and form a basis of $E_1^\perp$. Also, these basis elements correspond to bounded solutions $e_j^*(\xi)$ of the adjoint variational equation (3.3.14) which satisfy $e_j^*(0) = e_{j,0}^*$. Applying the variation of constants formula to $w_1^{\rm n}$ and noticing that $\left\langle P_1^{\rm ss} w_1^{\rm n}(0), e_{j,0}^* \right\rangle = 0$ we then obtain, for $j = 1, 2$,

$$\begin{aligned}\left\langle \Phi_1^{\rm su}(0, L)\mathfrak{u}_1^{\rm tr}, e_{j,0}^* \right\rangle = \left\langle q_1^-(0;\mu) - q_1(0;\mu), e_{j,0}^* \right\rangle + \langle h_p(\mathfrak{v}_1 + \tilde{v}_1^{\rm n};\mu), e_{j,0}^* \rangle \\ - \left\langle \int_L^0 \Phi_1^{\rm su}(0,\zeta)\tilde{g}_1(\zeta, \mathfrak{W}_{\rm tr}^0;\mu)d\zeta, e_{j,0}^* \right\rangle. \qquad (3.4.40)\end{aligned}$$

The expressions from (3.4.2) and (3.4.3) give that

$$\begin{aligned}&\left\langle q_1^-(0;\mu) - q_1(0;\mu), e_{j,0}^* \right\rangle = \\ &\qquad \left\langle \int_{-\infty}^0 \Phi_{-1}^{\rm s}(\xi,\zeta)G_1(\zeta, v^{\rm cu}(\zeta);\mu)d\zeta + \int_0^\infty \Phi_1^{\rm su}(\xi,\zeta)G_1(\zeta, v^{\rm ss}(\zeta);\mu)d\zeta, e_{j,0}^* \right\rangle \\ &\qquad\qquad = \left(\int_{-\infty}^\infty \left\langle\, D_\mu F(q_1^0(\zeta);0), e_j^*(\zeta) \,\right\rangle d\zeta \right) \mu + \mathcal{O}(|\mu|^2).\end{aligned}$$

Now, since there exists constants $C > 0$ such that

$$\begin{aligned}|h_p(\mathfrak{v}_1 + \tilde{v}_1^{\rm n}(\mathfrak{v}_1;\mu);\mu)| \le C(|\mathfrak{v}_1| + |\mu|)^2, \\ \left| \left\langle \int_L^0 \Phi_1^{\rm su}(0,\zeta)\tilde{g}_1(\zeta, \mathfrak{W}_{\rm tr}^0;\mu)d\zeta, e_{j,0}^* \right\rangle \right| \le {\rm e}^{-\gamma_{\rm ss} L} C\left(|\mathfrak{v}_1| + |\mu|\right)^2 \qquad (3.4.41)\end{aligned}$$

for μ sufficiently small and L sufficiently large, we can use the quadratic estimates on $\tilde{g}_1$ to obtain that (3.4.40) has the form

$$\left\langle \Phi_1^{\rm su}(0, L)\mathfrak{u}_1^{\rm tr}, e_{j,0}^* \right\rangle = \int_{-\infty}^\infty \left\langle\, D_\mu F(q_1^0(\zeta);0), e_j^*(\zeta) \,\right\rangle d\zeta \;\mu + \mathcal{O}\left((|\mu| + |\mathfrak{v}_1|)^2\right), \qquad (3.4.42)$$

or after rearranging,

$$\mathcal{M}\mu(\mathfrak{v}_1, L) = \Big(\sum_{j=1,2} \left\langle \Phi_1^{\mathrm{su}}(0, L)\mathfrak{u}_1^{\mathrm{tr}}, e_{j,0}^* \right\rangle e_{j,0}^* \Big) + \mathcal{O}\left((|\mu| + |\mathfrak{v}_1|)^2 \right). \tag{3.4.43}$$

Since the Melnikov mapping is invertible by assumption, the implicit function theorem then gives, for L sufficiently large, that there exists a family of solutions $\mu_{\mathrm{m}}(\mathfrak{v}_1, L)$ with the following leading order expansion

$$\mu_{\mathrm{tf}}(\mathfrak{v}_1, L) = \mathcal{M}^{-1}\Big(\sum_{j=1,2} \left\langle \Phi_1^{\mathrm{su}}(0, L)\mathfrak{u}_1^{\mathrm{tr}}, e_{j,0}^* \right\rangle e_{j,0}^* \Big) + \mathcal{O}\left(|\mathfrak{v}_1| \right). \tag{3.4.44}$$

Let us denote the corresponding glued solution for these parameters as $w_i^{\mathrm{tf}}(\xi) := W_i^{\mathrm{tf}}(\mathfrak{v}_1, \mu_{\mathrm{tf}}(\mathfrak{v}_1, L), L)(\xi)$ and the projections as $w_i^{\mathrm{tf,ss/su}}(\xi) = P_i^{\mathrm{ss/su}}(\xi) w_i^{\mathrm{tf}}(\xi)$. From these we immediately obtain the desired heteroclinic solution U_{tf} as a concatenation of the solutions $U_i^{\mathrm{tf}} := q_i + w_i^{\mathrm{tf}}$. This gives the existence of a one-parameter family of solutions for each L as described in the statement of the theorem. By uniqueness, the parameter $\mathfrak{v}_1$ must parameterize the group orbit of a solution under the S^1-action.

3.4.6 Leading order bifurcation equation expansions

In this section, we complete the proof of the theorem by obtaining the desired expansion of the bifurcation equation (3.4.44) obtained in the previous section. Let us ease notation by denoting $w_i = w_i^{\mathrm{tf}}, w_i^{\mathrm{ss/su}} = w_i^{\mathrm{tf,ss/su}}$, and $\mu = \mu_{\mathrm{tf}}$. To obtain finer expansions we isolate the leading components of the ξ-dependent subspaces as described in (3.3.17) above,

$$E_i^{\mathrm{ss}}(\xi) = E_i^{\mathrm{ss,l}}(\xi) + E_i^{\mathrm{ss,s}}(\xi), \qquad E_i^{\mathrm{su}}(\xi) = E_i^{\mathrm{su,l}}(\xi) + E_i^{\mathrm{su,u}}(\xi), \quad i = 1, 2.$$

In the following we will study these real subspaces using the complexified flow. Here the complexification of the eigenspaces $E_{1,\infty}^{\mathrm{ss/su,l}}$ are spanned by the eigenvectors $e_{1,\infty}^{\mathrm{ss/su,l}}$, $\overline{e_{1,\infty}^{\mathrm{ss/su,l}}}$ of $D_U F(U_*)$ corresponding to the leading complex-conjugate eigenvalues $\nu_{\mathrm{ss/su}}$, $\overline{\nu_{\mathrm{ss/su}}}$. Before continuing, we prove the following three lemmata which are needed in our derivation of the leading order bifurcation equation.

Lemma 3.4.9. *For $L > 0$ sufficiently large there exist constants $c_1, c_2 \in \mathbb{C}$ and $\rho > 0$ such that the following asymptotic expansions hold*

$$\Phi_2^{\mathrm{su}}(-L,0)P_{2,+}^{\mathrm{su}}(0)\Phi_2^{\mathrm{ss}}(0,-L)e_{1,\infty}^{\mathrm{ss,l}} = c_1 e^{\Delta\nu L} e_{1,\infty}^{\mathrm{su,l}} + \mathcal{O}(\mathrm{e}^{-(\Delta r+\rho)L}),$$
$$\Phi_2^{\mathrm{su}}(-L,0)P_{2,+}^{\mathrm{su}}(0)\Phi_2^{\mathrm{ss}}(0,-L)\overline{e_{1,\infty}^{\mathrm{ss,l}}} = c_2 \mathrm{e}^{\overline{\Delta\nu}L}\overline{e_{1,\infty}^{\mathrm{su,l}}} + \mathcal{O}(\mathrm{e}^{-(\Delta r+\rho)L}).$$

Proof. First note that by its construction, the restricted dichotomy $\Phi_2^{\mathrm{ss,l}}(\xi,\zeta)$ is well-defined for both $\xi \geq \zeta$ and $\xi \leq \zeta$. Hence there exists vectors $v_1^{\mathrm{ss}}, v_2^{\mathrm{ss}}$ which span $E_2^{\mathrm{ss,l}}(0)$ such that

$$\Phi_2^{\mathrm{ss,l}}(-L,0)v_1^{\mathrm{ss}} = \mathrm{e}^{-\nu_{\mathrm{ss}}L}e_{1,\infty}^{\mathrm{ss,l}} + \mathcal{O}(\mathrm{e}^{(r_{\mathrm{ss}}-\rho)L}),$$
$$\Phi_2^{\mathrm{ss,l}}(-L,0)v_2^{\mathrm{ss}} = \mathrm{e}^{-\overline{\nu_{\mathrm{ss}}}L}\overline{e_{1,\infty}^{\mathrm{ss,l}}} + \mathcal{O}(\mathrm{e}^{(r_{\mathrm{ss}}-\rho)L}).$$

Applying $\Phi_2^{\mathrm{ss}}(0,-L)$ to both sides of these equations, we then obtain

$$\Phi_2^{\mathrm{ss}}(0,-L)e_{1,\infty}^{\mathrm{ss,l}} = \mathrm{e}^{\nu_{\mathrm{ss}}L}v_1^{\mathrm{ss}} + \mathcal{O}(\mathrm{e}^{-(r_{\mathrm{ss}}+\rho)L}),$$
$$\Phi_2^{\mathrm{ss}}(0,-L)\overline{e_{1,\infty}^{\mathrm{ss,l}}} = \mathrm{e}^{\overline{\nu_{\mathrm{ss}}}L}v_2^{\mathrm{ss}} + \mathcal{O}(\mathrm{e}^{-(r_{\mathrm{ss}}+\rho)L}).$$

In a similar manner, there exists vectors $v_1^{\mathrm{su}}, v_2^{\mathrm{su}}$ which span $E_2^{\mathrm{su,l}}(0)$ such that

$$\Phi_2^{\mathrm{su}}(-L,0)v_1^{\mathrm{su}} = \mathrm{e}^{-\nu_{\mathrm{su}}L}e_{1,\infty}^{\mathrm{su,l}} + \mathcal{O}(\mathrm{e}^{(r_{\mathrm{su}}-\rho)L}),$$
$$\Phi_2^{\mathrm{su}}(-L,0)v_2^{\mathrm{su}} = \mathrm{e}^{-\overline{\nu_{\mathrm{su}}}L}\overline{e_{1,\infty}^{\mathrm{su,l}}} + \mathcal{O}(\mathrm{e}^{(r_{\mathrm{su}}-\rho)L}). \tag{3.4.45}$$

Hypothesis 3.3.13 then gives that there exists constants $c_1, c_1' \in \mathbb{C}$ not both zero such that

$$P_{2,+}^{\mathrm{su}}v_1^{\mathrm{ss}} = \mathcal{P}^{\mathrm{l}}v_1^{\mathrm{ss}} = c_1 v_1^{\mathrm{su}} + c_1' v_2^{\mathrm{su}}.$$

Since $\mathcal{P}^{\mathrm{l}}$ is an isomorphism which commutes with the action $T_1(\theta)$, it can then be obtained that $\mathcal{P}^{\mathrm{l}}$ is complex-linear so that $c_1' = 0$. Combing this all together we obtain,

$$\Phi_2^{\mathrm{su}}(-L,0)P_{2,+}^{\mathrm{su}}(0)\Phi_2^{\mathrm{ss}}(0,-L)e_{1,\infty}^{\mathrm{ss,l}} = c_1 \mathrm{e}^{(\nu_{\mathrm{ss}}-\nu_{\mathrm{su}})L}e_{1,\infty}^{\mathrm{su,l}} + \mathcal{O}(\mathrm{e}^{-(\Delta r+\rho)L}). \tag{3.4.46}$$

The expansion for $\overline{e^{\mathrm{ss,l}}_{1,\infty}}$ follows in an analogous way for some constant $c_2 \in \mathbb{C}$.

□

In a similar manner, we can also obtain expansions for bounded solutions of the adjoint variational equation along q_1.

Lemma 3.4.10. *Let $q_1(0)$ be sufficiently close to U_*, L sufficiently large, and $E_1^\perp = \mathrm{span}\{e^*_{j,0}\}_{j=1,2}$. Then, for some $\rho > 0$, there exists a complex eigenvector $e^*_{j,\infty}$ of $(D_U F(U_*))^*$ with eigenvalue $-\overline{\nu_{\mathrm{su}}}$ and $|e^*_{j,\infty}| = 1$, such that the bounded solutions of the adjoint equation satisfy*

$$e^*_j(L) = \Phi_1^{*,\mathrm{us}}(L,0)e^*_{j,0} = \left(\tilde{c}_j \mathrm{e}^{-\overline{\nu_{\mathrm{su}}}L} e^*_{j,\infty} + \mathrm{c.c.}\right)(1 + \mathcal{O}(\mathrm{e}^{-\rho L})),$$

for some constants $\tilde{c}_j \in \mathbb{C}$, where $\Phi_1^{*,\mathrm{us}}$ denotes the dichotomy of the adjoint variational equation (3.3.14) *associated with the spectral set $\{\nu : \mathrm{Re}\{\nu\} \leq r_{\mathrm{su}}\}$.*

Before completing the analysis of the bifurcation equation, we need one more prepatory lemma which estimates the scalar product contained inside of (3.4.43).

Lemma 3.4.11. *There exists a $\rho > 0$ such that for all L sufficiently large, and $j = 1, 2$ we have the following expansion*

$$\left\langle \mathfrak{u}_1, e^*_j(L) \right\rangle = \left\langle w_2^{\mathrm{su}}(-L), e^*_j(L) \right\rangle + \mathcal{O}(\mathrm{e}^{-(2\Delta\eta+\rho)L}). \tag{3.4.47}$$

Proof. Applying $P_2^{\mathrm{ss}}(-L)$ to (3.4.6), we use the asymptotic expansion of Hypothesis 3.3.7, and the projection estimates in Lemma 3.4.5 to obtain

$$\begin{aligned} \mathfrak{s}_2 &= -P_2^{\mathrm{ss}}(-L)\Delta q(L) + P_2^{\mathrm{ss}}(-L)w_1(L) \\ &= a\mathrm{e}^{\nu_{\mathrm{ss}}L} e^{\mathrm{ss,l}}_{1,\infty} + c.c. + \mathcal{O}(\mathrm{e}^{-(r_{\mathrm{ss}}+\Delta\eta)L}). \end{aligned} \tag{3.4.48}$$

This, combined with the result of Lemma 3.4.10, and the fact that $\left\langle e^{\mathrm{ss,l}}_{1,\infty}, e^*_{j,\infty} \right\rangle = 0$, allows us to obtain the estimate

$$|\left\langle w_2^{\mathrm{ss}}(-L), e^*_j(L) \right\rangle| \leq K\mathrm{e}^{-(2\Delta\eta+\delta_{\mathrm{ss}})L},$$

for some constant $K > 0$. Also, once again using the projection estimates in Lemma 3.4.5, we obtain

$$\begin{aligned}\left\langle \Delta q(L), e_j^*(L)\right\rangle &= \left\langle q_2(L), e_j^*(L)\right\rangle (1+\mathcal{O}(\mathrm{e}^{-\Delta\eta L})),\\ &\leq K\mathrm{e}^{(r_{\mathrm{su}}-r_{\mathrm{u}})L},\\ &\leq K\mathrm{e}^{-(2\Delta\eta+\rho)L},\end{aligned}$$

where this last inequality comes from the eigenvalue requirements in Hypothesis 3.3.4(i). Finally, we use the gluing equation (3.4.6), and the fact that $e_j^*(\xi) \perp E_1^{\mathrm{ss}}(\xi)$, to find

$$\begin{aligned}\left\langle \mathfrak{u}_1, e_j^*(L)\right\rangle &= \left\langle w_1^{\mathrm{su}}(L), e_j^*(L)\right\rangle\\ &= \left\langle w_2^{\mathrm{su}}(-L) + w_2^{\mathrm{ss}}(-L) - w_1^{\mathrm{ss}}(L) - \Delta q(L), e_j^*(L)\right\rangle\\ &= \left\langle w_2^{\mathrm{su}}(-L) + w_2^{\mathrm{ss}}(-L) - \Delta q(L), e_j^*(L)\right\rangle,\end{aligned}$$

which, combined with the above estimates yields the result. □

We may now complete the proof of the main theorem with the following proposition which gives the leading order expansion of the right-hand side of (3.4.43).

Proposition 3.4.12. *The bifurcation equation* (3.4.44) *has the following leading order expansion in* μ*,*

$$\mathcal{M}\mu = -\sum_{j=1,2}\left(\mathrm{e}^{2\Delta\nu L}d_j + \text{c.c.}\right)e_{j,0}^* + \mathcal{O}(\mathrm{e}^{-(2\Delta r+\rho)L}) + \mathcal{O}\left(|\mu|\left(|\mathfrak{v}_1| + |\mu|\right)\right), \qquad (3.4.49)$$

where

$$d_j = ac_1\overline{\tilde{c}_j}\left\langle e_{1,\infty}^{\mathrm{su,l}}, e_{j,\infty}^*\right\rangle_{\mathbb{C}},$$

for $a, c_1, \tilde{c}_j \in \mathbb{C}$ *as defined in Hypothesis 3.3.7, Lemma 3.4.9, and Lemma 3.4.10 respectively, and where* $\langle\cdot,\cdot\rangle_{\mathbb{C}}$ *is the complexified inner product induced by the real inner product on* X*.*

Proof. To begin, by applying the projection $P_{2,+}^{\mathrm{su}}(0)$, and its complement $I - P_{2,+}^{\mathrm{su}}(0)$ to

the transverse matching equation (3.4.33), we obtain

$$\mathfrak{u}_2 = w_2^{\mathrm{su}}(0) = -P_{2,+}^{\mathrm{su}}(0) w_2^{\mathrm{ss}}(0) + \mathcal{O}(\mathrm{e}^{-(\eta_{\mathrm{ss}}+\Delta\eta)L}).$$

Then, using estimates similar to those in the proof of Proposition 3.4.3 we find

$$\begin{aligned} w_2^{\mathrm{su}}(-L) &= \Phi_2^{\mathrm{su}}(-L,0)\mathfrak{u}_2 + \mathcal{O}(\mathrm{e}^{-(2\Delta\eta+\rho)L}) \\ w_2^{\mathrm{ss}}(0) &= \Phi_2^{\mathrm{ss}}(0,-L)\mathfrak{s}_2 + \mathcal{O}(\mathrm{e}^{-(r_{\mathrm{ss}}L+2\Delta\eta L)}). \end{aligned}$$

We then combine these estimates to obtain,

$$\begin{aligned} w_2^{\mathrm{su}}(-L) =& \Phi_2^{\mathrm{su}}(-L,0)\mathfrak{u}_2 + \mathcal{O}(\mathrm{e}^{-(2\Delta\eta+\rho)L}) \\ =& -\Phi_2^{\mathrm{su}}(-L,0)P_{2,+}^{\mathrm{su}}(0)w_2^{\mathrm{ss}}(0) + \mathcal{O}(\mathrm{e}^{-(2\Delta\eta+\rho)L}) \\ =& -\Phi_2^{\mathrm{su}}(-L,0)P_{2,+}^{\mathrm{su}}(0)\left[\Phi_2^{\mathrm{ss}}(0,-L)\mathfrak{s}_2 + \mathcal{O}(\mathrm{e}^{-(r_{\mathrm{ss}}L+2\Delta\eta L)})\right] + \mathcal{O}(\mathrm{e}^{-(2\Delta\eta+\rho)L}) \\ =& -\Phi_2^{\mathrm{su}}(-L,0)P_{2,+}^{\mathrm{su}}(0)\Phi_2^{\mathrm{ss}}(0,-L)\mathfrak{s}_2 + \mathcal{O}(\mathrm{e}^{-(2\Delta\eta+\rho)L}) \\ =& -\Phi_2^{\mathrm{su}}(-L,0)P_{2,+}^{\mathrm{su}}(0)\Phi_2^{\mathrm{ss}}(0,-L)\left(a\mathrm{e}^{\nu_{\mathrm{ss}}L}e_{1,\infty}^{\mathrm{ss,l}} + c.c.\right) + \mathcal{O}(\mathrm{e}^{-(2\Delta\eta+\rho)L}) \\ =& ac_1\mathrm{e}^{(2\nu_{\mathrm{ss}}-\nu_{\mathrm{su}})L}e_{1,\infty}^{\mathrm{su,l}} + ac_2\mathrm{e}^{(2\overline{\nu_{\mathrm{ss}}}-\overline{\nu_{\mathrm{su}}})L}\,\overline{e_{1,\infty}^{\mathrm{su,l}}} + \mathcal{O}(\mathrm{e}^{-(2\Delta\eta+\rho)L}), \end{aligned}$$

where estimate (3.4.48) was used in the fifth line, and Lemma 3.4.9 used in the sixth. Since this last expression must be real (being the flow of a real initial condition), it can be found that $c_2 = \overline{c_1}$. Hence we obtain

$$w_2^{\mathrm{su}}(-L) = ac_1\mathrm{e}^{(2\nu_{\mathrm{ss}}-\nu_{\mathrm{su}})L}e_{1,\infty}^{\mathrm{su,l}} + c.c + \mathcal{O}(\mathrm{e}^{-(2\Delta\eta+\rho)L}). \tag{3.4.50}$$

Applying Lemma 3.4.10 to (3.4.43), we obtain

$$\left\langle \Phi_1^{\mathrm{su}}(0,L)\mathfrak{u}_1, e_{j,0}^* \right\rangle_{\mathbb{C}} = \left\langle \mathfrak{u}_1, e_j^*(L) \right\rangle_{\mathbb{C}} = \left\langle \mathfrak{u}_1, \mathrm{e}^{-\nu_{\mathrm{su}}L}\tilde{c}_j\, e_{j,\infty}^* + \mathrm{c.c.} \right\rangle_{\mathbb{C}} (1 + \mathcal{O}(\mathrm{e}^{-\rho L})). \tag{3.4.51}$$

Finally by substituting the expansion obtained for $\mathfrak{u}_1$ in Lemma 3.4.11, and taking into account the fact that

$$\left\langle e_{1,\infty}^{\mathrm{su,l}}, \overline{e_{1,\infty}^*} \right\rangle_{\mathbb{C}} = 0,$$

we obtain the result.

□

3.5 Discussion

3.5.1 Application of results

We now discuss the applicability of our result in the examples given in Section 3.2.

Cubic-quintic complex Ginzburg-Landau equation

In this example, all of the required hypotheses either have been proven in previous works, or can be proven using straightforward techniques. As we study real equations above, one must first write (3.2.4) in terms of the variables $\mathrm{Re}u, \mathrm{Im}u$ or $u, \overline{u}$, obtaining a four-dimensional real system. We also note that the well-posedness assumption of Hypothesis 3.3.8 is trivially satisfied.

Next it can readily be calculated for parameters as in the following proposition, that the eigenvalues of the asymptotic linearization of (3.2.4) as $\xi \to +\infty$ about the equilibrium $u_* \equiv 0$ are hyperbolic, with a complex conjugate pair of eigenvalues on each side of the imaginary axis. Furthermore, for $\xi = -\infty$, the spectrum of the linearization consists of complex conjugate pairs $\nu_{\mathrm{ss}}, \overline{\nu_{\mathrm{ss}}}$, and $\nu_{\mathrm{su}}, \overline{\nu_{\mathrm{su}}}$ which satisfy the desired hypotheses. The results of [157] then give the following proposition

Proposition 3.5.1. *For α, β, γ sufficiently small, and $\rho > 1$, there exists a pushed front solution u_{ff} of the form $u_{\mathrm{ff}}(\xi, t) = \mathrm{e}^{\mathrm{i}\omega_{\mathrm{p}} t} u_{\mathrm{f}}(\xi)$ which invades u_* with speed $c_{\mathrm{p}} > c_{\mathrm{lin}}$ and some angular frequency ω_{p}. Here, u_{f} solves* (3.2.3)*, approaches the periodic pattern $u_{\mathrm{p}} = r_{\mathrm{p}} \mathrm{e}^{\mathrm{i}k_{\mathrm{p}}\xi}$ as $\xi \to -\infty$, and approaches u_* as $\xi \to +\infty$, where $c_{\mathrm{p}}, \omega_{\mathrm{p}}, r_{\mathrm{p}}$, and k_{p} satisfy the nonlinear dispersion relation* (3.2.2)*. Furthermore, the periodic orbit, u_p, has two-dimensional center-unstable manifold in the flow defined by* (3.2.3)*.*

Remark 3.5.2. *Note that our parameter assumptions differ slightly from those of [157] where ρ is scaled to be equal to 1, and the coefficient of the linear term u is small. In order to go from our parameters to theirs, one should make the scalings*

$$u = \frac{\tilde{u}}{a}, \quad x = \frac{\tilde{x}}{a^2}, \quad t = \frac{\tilde{t}}{a^4}, \quad c = a^2\tilde{c}, \quad \chi_\epsilon = a^4\tilde{\chi}_\epsilon, \quad \gamma = a^2\tilde{\gamma}, \quad a^2 = \rho.$$

Next, for the trigger χ_0 given in (3.2.4) above, or for a step-function trigger satisfying $\chi_0 \equiv \pm 1$ for $\xi \lessgtr 0$, we have that the trivial solution u_* is a preparation front, and that, for the variables $U = (\operatorname{Re} u, \operatorname{Re} u_\xi, \operatorname{Im} u, \operatorname{Im} u_\xi, \chi_0)$, the spatial dynamics equilibria $U_* = (0,0,0,0,-1), \tilde{U}_* = (0,0,0,0,1)$ satisfy $W^{\mathrm{su}}(U_*) = 3$ and $W^{\mathrm{s}}(\tilde{U}_*) = 3$, where one dimension from each count is from the χ direction. Also, let U_{ff} denote the heteroclinic orbit in this formulation which corresponds to u_{ff}. For χ_0, the tangent spaces of these invariant manifolds are constant and can be explicitly calculated in terms of the spatial eigenvalues. The desired transversality of the intersection about u_0 can then be obtained by calculating that

$$\det \begin{pmatrix} 1 & 1 \\ \nu_2^+ & \nu_1^- \end{pmatrix} \neq 0,$$

where $\nu_j^\pm$ solve the dispersion relation, $d_\pm(\nu) = (1 + \mathrm{i}\alpha)\nu^2 + c\nu + (\pm 1 - \mathrm{i}\omega)$, and are ordered by increasing real part. A standard singular-perturbation argument then gives the transversality for χ_ϵ with $0 < \epsilon \ll 1$.

All that is left is to verify are the intersection properties along U_{ff}, and the invertibility of the associated Melnikov matrix. Note that since there is no non-leading strong-stable eigenspace, $E^{\mathrm{ss,s}}_{1,\infty}$, the inclination assumption in Hypothesis 3.3.13 is trivially satisfied.

Proposition 3.5.3. *For $\alpha, \beta, \gamma, \epsilon$ sufficiently small,*

$$\dim T_{U_{\mathrm{ff}}(\xi)} W^{\mathrm{ss}}(U_*) \cap T_{U_{\mathrm{ff}}(\xi)} W^{\mathrm{cu}}(U_{\mathrm{p}}) = \dim \left(T_{U_{\mathrm{ff}}(\xi)} W^{\mathrm{ss}}(U_*) + T_{U_{\mathrm{ff}}(\xi)} W^{\mathrm{cu}}(U_{\mathrm{p}}) \right)^\perp = 2,$$

and the Melnikov matrix

$$M = \begin{pmatrix} \int_{-\infty}^{\infty} \langle \psi_1(\xi), \partial_c F(U_{\mathrm{ff}}(\xi)) \rangle \, d\xi & \int_{-\infty}^{\infty} \langle \psi_1(\xi), \partial_\omega F(U_{\mathrm{ff}}(\xi)) \rangle \, d\xi \\ \int_{-\infty}^{\infty} \langle \psi_2(\xi), \partial_c F(U_{\mathrm{ff}}(\xi)) \rangle \, d\xi & \int_{-\infty}^{\infty} \langle \psi_2(\xi), \partial_\omega F(U_{\mathrm{ff}}(\xi)) \rangle \, d\xi \end{pmatrix},$$

is invertible, where $\psi_j(\xi)$ are solutions of the adjoint variational equation of the linearization of (3.2.4) *with initial conditions $\psi_j(0)$ satifying*

$$\operatorname{span}_{j=1,2} \{\psi_j(0)\} = \left(T_{U_{\mathrm{ff}}(\xi)} W^{\mathrm{ss}}(U_*) + T_{U_{\mathrm{ff}}(\xi)} W^{\mathrm{cu}}(U_{\mathrm{p}}) \right)^\perp.$$

Proof. First, after scaling $t = \omega\tau$, note that $\partial_\tau u_{\mathrm{ff}}$ and $\partial_\xi u_{\mathrm{ff}}$ are linearly independent

and lie in the kernel of the linear operator

$$\mathcal{T} : V \mapsto -\omega V_\tau + (1 + \mathrm{i}\alpha)V_{\xi\xi} + cV_\xi + V + g_{A,\overline{A}}(A_{\mathrm{ff}}, \overline{A_{\mathrm{ff}}})V. \tag{3.5.1}$$

Since ϵ is small, it can be readily obtained that χ_ϵ does not induce any eigenfunctions corresponding to resonance poles of the Evans function about u_* and hence that $\partial_\tau u_{\mathrm{ff}}$, and $\partial_\xi u_{\mathrm{ff}}$ span the kernel, so that 0 is an eigenvalue of $\mathcal{T}$ with geometric multiplicity 2. We claim its algebraic multiplicity is also equal to 2. Momentarily assuming this claim, the first statement of the proposition follows immediately, as the adjoint variational equation is found to have two linearly independent bounded solutions. The proofs of Theorem 8.4 and Lemma 8.7 in [130] can then be used to obtain that M is invertible.

To prove the claim, we first note that in the real-coefficient case $\alpha = \gamma = \beta = 0$ the linearized operator $\mathcal{T}$ is self-adjoint when defined on an exponentially weighted space $L^2_{c/2}(\mathbb{R} \times \mathbb{T})$ with weight $\mathrm{e}^{\frac{c}{2}\xi}$. This implies that $\mathcal{T}$ does not have a generalized kernel for $\alpha = \gamma = \beta = 0$. Since algebraic simplicity is an open property, we then have that for complex parameters α, γ, β sufficiently small, the eigenfunctions $\partial_t u_{\mathrm{ff}}, \partial_\xi u_{\mathrm{ff}}$ remain algebraically simple. □

With these propositions in hand we can then apply our results to obtain the existence of a family of pushed trigger fronts in the modified qcGL equation which bifurcate from the pushed free front solution obtained in Proposition 3.5.1.

Remark 3.5.4. *We also note that our results could be obtained for qcGL with the step function trigger χ_0 by first simplifying the phase-space with the blow-up coordinates used in [64]. One then obtains a phase space $\mathbb{R}_+ \times \mathcal{S}^2$, where $\mathcal{S}^2$ denotes the Riemann sphere. In these coordinates, the dynamics are smoothly foliated over $\mathcal{S}^2$ which is a normally hyperbolic invariant manifold. Furthermore, the dynamics on $\mathcal{S}^2$ are described by a Ricatti equation which can be explicitly integrated. Here, the periodic orbit u_p reduces to a point, with one-dimensional unstable manifold, while the target manifold $W^{\mathrm{s}}_+(0)$ is two dimensional. Lin's method could then be readily applied to obtain the desired result.*

Cahn-Hilliard

In the case of Cahn-Hilliard, more work needs to be done to apply our bifurcation result. While the existence of a preparation front u_{pr} can be obtained using a Conley index argument (see [**?**, App. A]), the existence of an oscillatory pushed front is, to the authors' knowledge, still an open problem. Furthermore, the spectrum of the linearized modulated traveling wave problem would have to be obtained by first using a Fourier decomposition in time,

$$\mathrm{i}\omega\ell\hat{u} = -\partial_{\xi\xi}\left(\partial_{\xi\xi}\hat{u} + f'(u_*)\hat{u}\right) = c\partial_\xi\hat{u}, \quad \ell \in \mathbb{Z},$$

writing each equation as a first order equation in ξ, and finding the four spatial eigenvalues ν_ℓ which satisfy

$$0 = \nu^4 + f'(u_*)\nu^2 - c_{\mathrm{p}}\nu + \mathrm{i}\omega_{\mathrm{p}}\ell, \quad \ell \in \mathbb{Z}.$$

Using a scaling argument, it is possible to show that such spatial eigenvalues are bounded far away from the imaginary axis for large ℓ and thus only a few values of ℓ need be studied. From this one should hopefully be able to establish (or assume) the intersection properties of Section 3.3.3, possibly after factoring out the S^1-equivariance, and obtain a leading order expansion for the bifurcation equation.

In practice, one may also proceed by verifying the hypotheses with numerical computations. As shown above, numerical continuation can be used to provide evidence for the existence of a pushed invasion front. Then, the spatial eigenvalues ν_ℓ could be found for each ℓ using the values for c_{p} and ω_{p} obtained from the AUTO calculation in Figure 3.2.3. Regarding the discussion in Remark 3.3.14, we note that for the numerically determined c_{p} and ω_{p}, the leading eigenspaces corresponding to $\nu_{\mathrm{ss/su}}$ lie in the $\ell = 1$ Fourier subspace.

One could then use a numerical eigenvalue solver to test the transversality hypotheses on u_{pr} and u_{ff}. For the former, one need only verify that the kernel of the discretized linearization about u_{pr} is empty. For the latter, since the free pushed front is time-periodic in a co-moving frame, one must look at the spectrum of the discretized linear period map and determine that the algebraic multiplicity of the Floquet exponent at

0 is two. Finally, since inclination-flip configurations are degenerate, the failure of the inclination hypothesis could be tested by perturbing the preparation or free pushed fronts.

In many experiments and models using the Cahn-Hilliard equation (see for example [54, **?**, 152]), the preparation front is controlled by a traveling source term, instead of a spatial inhomogeniety as in (3.2.8) above. Such systems usually take the form

$$u_t = -(u_{xx} + f(u))_{xx} + cu_x + ch(x), \tag{3.5.2}$$

where the source term $h : \mathbb{R} \to \mathbb{R}$ is positive, spatially localized, and deposits mass into the system to transform a stable homogeneous equilibrium into to an unstable state in its wake. For simplicity, let us also assume that h' is compactly supported. To apply our results in this case we must take into account that this equation preserves mass and hence has a linearization with additional neutral modes. This is manifested in the corresponding spatial dynamics formulation,

$$\begin{aligned} u_x &= v \\ v_x &= \theta - f(u) \\ \theta_x &= w \\ w_x &= -\omega\partial_\tau + cu_x + h(\xi), \end{aligned} \tag{3.5.3}$$

as the existence of a conserved quantity

$$I(u_1; c) = \frac{1}{2\pi}\int_0^{2\pi} w - cu \; d\tau, \qquad u_1 = (u, v, \theta, w),$$

which is constant under the flow for all $|\xi|$ sufficiently large (i.e. outside of the support of h'). The existence of such a quantity implies the existence of a family of periodic orbits and hence pushed free invasion fronts which are parameterized by fixed values $I(u_1; s) \equiv m$. Thus, pushed free invasion fronts, if shown to exist, will come in a 1-parameter family as well. One can obtain existence of pushed trigger fronts, by restricting the phase-space to the affine, co-dimension one subspaces $\{I \equiv m\}$ and then applying our results.

More generally, if the spatial dynamics formulation of a pattern-forming system possesses conserved quantities one must perform a dimension counting to check that our genericity and intersection hypotheses still hold. Namely, one must verify that the introduction of neutral modes about the equilibria and periodic orbit preserves the transversality and Fredholm properties we require. For more information and an example of such calculations see [63, Sec. 4].

3.5.2 Other spectral splittings

As mentioned in the introduction, the spectral splitting associated with the pushed front's strong-stable decay and the next weakly-stable eigenvalue comes in other varieties in addition to the case we studied. First we remark that a system where ν_{ss} has a complex conjugate while ν_{su} is real and simple should behave in the same way as discussed above, as the quantity $\Delta\nu$ would still be complex. One such example arises in the Extended Fisher-Kolmogorov equation,

$$u_t = -\gamma\partial_x^4 u + \partial_x^2 u + \frac{u}{b}(b+u)(1-u), \quad x,t \in \mathbb{R},\ u \in \mathbb{R}. \tag{3.5.4}$$

It has been observed in [155] that pushed fronts exist for b sufficiently small. For $\gamma < 1/12$, this front is asymptotically constant in the wake, while for $\gamma > 1/12$ it forms a spatially periodic pattern of "kinks" and "anti-kinks". In the former case, with $\gamma = 0.08$ for example, the pushed speed is found to be $c_{\text{p}} \approx 2.175$ while spatial eigenvalues $\nu_{\text{ss}}, \overline{\nu_{\text{ss}}} \approx -0.575971 \pm 1.21251\,\text{i}$ and $\nu_{\text{su}} \approx -0.365678$. Hence, the pushed front in this case has an oscillatory tail and we thus predict that a triggered version of this equation, with say $\chi(x-ct)$ multiplied by the linear term u, would exhibit non-monotone front locking with respect to the trigger interface.

Many examples arise where both ν_{ss} and ν_{su} are real, generically leading to monotone front selection and no front locking phenomena unless a more complicated spatial trigger is introduced. One such example is the cubic-quintic Nagumo equation,

$$u_t = \partial_x^2 u + u + du^3 - u^5, \quad x,t \in \mathbb{R},\ u \in \mathbb{R}. \tag{3.5.5}$$

Here, using a reduction of order method (see [155]), one finds that free pushed fronts

exist for all $d > \frac{2\sqrt{3}}{3}$ and travel with speed $c_{\mathrm{p}} = \frac{-d+2\sqrt{d^2+4}}{\sqrt{3}}$.

While such fronts will always be asymptotically constant (i.e. no periodic pattern in the wake), we hypothesize that certain spatial triggers could induce the front locking phenomena discussed above. To this end, one could explore triggering phenomena by moving into a co-moving frame of speed c and studying the equation on a semi-infinite domain $x \in (-\infty, 0]$ with various boundary conditions $B_1(u_x) + B_2(u) = 0$ at $x = 0$. In order for the problem to be well-posed, one would look at conditions of the form $u_x(0,t) = \phi(u(0,t))$, for some smooth function $\phi : \mathbb{R} \to \mathbb{R}$. Triggered fronts would then be obtained by finding connections between the strong-stable manifold, $W^{\mathrm{ss}}(0)$, and the boundary manifold $\mathcal{B}^{\phi}$ defined by the graph of ϕ. By selecting specific boundary conditions, one could then obtain multi-stability of fronts which lock to the boundary condition at different distances. See [106] for a general study of this subject in the case where the co-moving frame speed is zero. We also remark that it may be possible to observe interesting dynamics if a triggering mechanism could be used to perturb pushed fronts in the phase-field system studied in [63].

3.5.3 Stability of pushed trigger fronts

Though we did not study the stability of pushed trigger fronts, direct numerical simulations lead us to expect such solutions to be stable for parameters lying on branches of the bifurcation curve $\mu_*(L)$. Since the asymptotic states are in general stable, so that there is no unstable continuous spectrum, only localized instabilities could arise. If the trigger is sufficiently sharp ($\epsilon << 1$ in the examples above) we expect the corresponding point spectrum to also be bounded away from the imaginary axis in the left half-plane.

For more general types of triggers, such as those with bounded regions with $\chi > 1$ or a shallow interface, resonance poles or branch poles ahead of the front could induce faster speeds and different wave-numbers in the wake. The solutions we construct here would in such a case be unstable. These effects have been documented in a particular, prototypical case of coupled KPP equations in [79]. In particular, such localized strong triggers can create resonance poles in the linearization at the trigger, which in turn induce spatio-temporal growth. In [79], it was shown that the growth rate of such a *real* resonance pole determines the speed of the front in the wake of the trigger.

In a pattern-forming context, as considered here, one suspects that such resonance poles would be complex, and thus determine not only speeds but also frequencies, and therefore wave-numbers, of patterns in the wake. For example, in the context of the examples given in Section 3.2, if ϵ were not small, the interface of χ_ϵ would be shallow, taking a long time to ramp up from -1 to 1. This would cause resonance poles to arise in the linearization about u_* leading to instabilities in the interfacial region where χ_ϵ is not close to ± 1. Such an example could also be realized in (3.5.2) by making the source term h only weakly localized. Here, the resulting preparation front would possess localized instabilities as the interface slowly passes through the spinodal region. Finally, see [162] for interesting numerical results where spatially periodic forcing induces the selection of different patterns and locking behavior.

Chapter 4

Hopf-bifurcation from fronts in the Cahn-Hilliard equation in one spatial dimension

The contents of this chapter originally appeared in the work [65]; with permission of Springer.

4.1 Introduction and main results

In this last chapter, we consider the problem discussed in Section 1.5.1. Namely, we use a direct functional analytic method for bifurcation in the presence of essential spectrum to prove the existence of oscillatory solutions to the triggered Cahn-Hilliard equation discussed above

$$u_t = -\left(u_{yy} + f(y - ct, u)\right)_{yy} + c\chi(y - ct; c). \tag{4.1.1}$$

Recall u is a real-valued function of $y, t \in \mathbb{R}$ and χ is a source term traveling with speed c through the domain. After stating and proving our results in Sections 4.1.1-4.3, we then study an explicit example for which we can verify all of the required hypothesis, apply our results, and obtain information about the nature of the bifurcating solutions. In Section 4.6 we use Conley index theory to give an existence proof for preparation fronts

when the nonlinearity f satisfies additional coercivity properties. Finally, in Section 4.7 we use our approach to simplify the Hopf bifurcation result found in [135].

4.1.1 Hypotheses and main existence result

In order to perform our analysis, we pass to a co-moving frame $x = y - ct$ so that (4.1.1) becomes

$$u_t = -\left[u_{xx} + f(x,u)\right]_{xx} + cu_x + c\,\chi(x;c). \tag{4.1.2}$$

We now specify the assumptions needed for our main result.

Nonlinearity and trigger. We start with assumptions on f and χ.

Hypothesis 4.1.1. *The nonlinearity f is smooth in both x and u, and converges with an exponential rate to smooth functions $f_\pm := f_\pm(u)$ as $x \to \pm\infty$. This convergence is uniform for u in bounded sets.*

Hypothesis 4.1.2. *The trigger $\chi = \chi(x;c_*)$ is smooth and exponentially localized in x.*

Piecewise-smooth nonlinearity. Our explicit example, and several explicit models mentioned above are formulated in terms of discontinuous nonlinearities. We therefore include an alternate setup to cover such cases.

Hypothesis 4.1.3. *Let $l > 0$, $\chi \equiv 0$, $u_*(x;c) \equiv u_-$ and $f(x,u) = b(x)(u-u_-) + g(u)$, where b is piecewise smooth in x with jump discontinuities at $x = \pm\ell$, and g is smooth in u such that $g(u) = \mathcal{O}(|u-u_-|^2)$.*

Remark 4.1.4. *Similar results will follow in the same manner if $b(x)$ has any finite number of jump discontinuities in x. For more general forms of f which possess x-discontinuities that depend nonlinearly on u, our results should still hold but more complicated modifications to the smooth case are required.*

Existence and robustness of trigger front. We assume existence of a "generic" propagating front.

Hypothesis 4.1.5. *There exists a front solution $u_*(y - c_*t; c_*)$ of (4.1.1) for some $c_* > 0$, with*

$$\lim_{x\to\pm\infty} u_*(x; c_*) = u_\pm, \quad u_+ - u_- = \int_{\mathbb{R}} \chi(\xi; c_*)\mathrm{d}\xi.$$

Moreover, $u_* \in C^4(\mathbb{R})$ and

$$|u_*(x) - u_\pm| + \sum_{j=1}^{3} |\partial_x^i u_*(x)| \leq C' \mathrm{e}^{-\gamma|x|},$$

for some $C, \gamma > 0$. We refer to this front solution as the primary trigger front

One can show, under appropriate assumptions on the nonlinearity f and $u_\pm$, that such trigger fronts necessarily exist. One can indeed find those as solutions to a non-autonomous, three-dimensional ODE with a gradient-like structure, using Conley's index; see Appendix 4.6 for a outline of the proof.

We are interested in Hopf bifurcations from u_*. In the following, we state our spectral assumptions and their immediate consequences.

The following hypothesis implies that $\ker L = \varnothing$ when considered on the spaces $L^2(\mathbb{R})$, $L^2_\eta(\mathbb{R}) := \{u : \mathrm{e}^{\eta\sqrt{1+x^2}}u(x) \in L^2(\mathbb{R})\}$, and $L^2_{+\eta}(\mathbb{R}) := \{u : \mathrm{e}^{\eta x}u(x) \in L^2(\mathbb{R})\}$ for any $\eta > 0$ small. It also follows that, when considered on the last of the spaces just listed, L is invertible. For background on the notion of extended point spectrum, see for example [49, Pg. 75].

Hypothesis 4.1.6. *The point $0 \in \mathbb{C}$ is not contained in the extended point spectrum of the linearization $L : H^4(\mathbb{R}) \subset L^2(\mathbb{R}) \to L^2(\mathbb{R})$ defined as*

$$Lv := -\partial_x^2 \left(\partial_x^2 v + \partial_u f(x, u_*(x))v\right) + c_*\partial_x v. \tag{4.1.3}$$

The following lemma guarantees that our assumptions so far are open in the class of problems considered here.

Lemma 4.1.7 (Robustness of Front Solution)**.** *Assuming the above hypotheses, for $\tilde{u}_\pm$ in a small neighborhood of $u_\pm$, with $\tilde{u}_+ - \tilde{u}_- = u_+ - u_-$, and c close to c_*, there exists a family of smooth front solutions $u_*(x; c)$ asymptotic to $\tilde{u}_\pm$, satisfying Hypothesis 4.1.5.*

Proof. Hypothesis 4.1.6 implies that the steady-state equation associated with (4.1.2) (known as the traveling-wave equation) has a transverse intersection of the respective stable and unstable manifolds emanating from the hyperbolic equilibria $u \equiv u_{\pm}$. Indeed if this intersection were not transverse, the intersection would give rise to an exponentially localized solution of the linearized equation, hence contributing to the extended point spectrum. ■

Hopf crossing and non-resonance. We formulate our main spectral hypotheses on Hopf bifurcation.

Hypothesis 4.1.8. *(simple Hopf-Crossing) The operator L, defined on $L^2(\mathbb{R})$ as in* (4.1.3) *above, has an isolated pair of algebraically simple eigenvalues $\lambda(c) = \mu(c) \pm \mathrm{i}\kappa(c)$ and corresponding $L^2(\mathbb{R})$-eigenfunctions $p(x), \overline{p}(x)$ such that for some $\omega_* \neq 0$, and $c_* > 0$ as above*

$$\mu(c_*) = 0, \quad \mu'(c_*) > 0, \quad \textit{and} \quad \kappa(c_*) = \omega_*.$$

Note that the hypothesis implicitly assumes that $\mathrm{i}\omega_*$ does not belong to the essential spectrum, that is, $L - \mathrm{i}\omega$ is Fredholm with index 0. Let ψ be the corresponding adjoint $L^2(\mathbb{R})$-eigenfunction which is normalized so that

$$\langle \psi, p \rangle_{L^2(\mathbb{R})} = 1.$$

Also, it can be readily obtained that

$$\langle \psi, \overline{p} \rangle_{L^2(\mathbb{R})} = 0.$$

Finally, we assume that there are no point or essential resonances:

Hypothesis 4.1.9. *(Absence of resonances) For all $\lambda \in \mathrm{i}\omega_*\mathbb{Z} \setminus \{0, \pm 1\}$, the operator $L - \lambda$ is invertible when considered on the unweighted space $L^2(\mathbb{R})$.*

Remark 4.1.10. *The Fredholm boundaries of $L - \lambda$ on the unweighted space $L^2(\mathbb{R})$ are equal to the continuous curves*

$$\sigma_{\pm} := \{\lambda \in \mathbb{C} : \lambda = -k^4 - f'_{\pm}(u_{\pm})k^2 + \mathrm{i}ck,\ k \in \mathbb{R}\},$$

Each of the curves $\sigma_\pm$ intersect the imaginary axis at $\lambda = 0$ and possibly two other points $\pm i\omega_e$. These last two intersections exist when $f'(u_\pm) > 0$, respectively. When considered on the doubly weighted space $L^2_\eta(\mathbb{R})$ mentioned above, the curves $\sigma_\pm$ are shifted

$$\sigma^\eta_\pm := \{\lambda \in \mathbb{C} : \lambda = -(ik \mp \eta)^4 - f'_\pm(u_\pm)(ik \mp \eta)^2 + c(ik \mp \eta),\, k \in \mathbb{R}\}.$$

Using the information in Remark 4.1.10, Figure 4.1.1 depicts examples of Fredholm boundaries, for $\eta = 0$, which do and do not satisfy Hypothesis 4.1.9. The second figure from the left portrays the intriguing case where both $f'_\pm(u_\pm) > 0$ and the Hopf eigenvalues are on the "wrong" side of the Fredholm borders $\sigma_\pm$. In other words, they lie inside of the essential spectrum of both of the constant coefficient operators $L_\pm := -\partial_{xx}\left(\partial_{xx} + f'_\pm(u_\pm)\right) + c_*\partial_x$, but, since the Fredholm index is determined by the difference in Morse indices between $L_\pm$, $L - \lambda_*$ has index 0 and our spectral hypothesis are still satisfied. Though our results give existence of time periodic solutions in this case, we believe that such solutions are not physically relevant: since the exponential weight selects the wrong spatial decay rates, the Hopf eigenvalues do not correspond to poles of the point-wise Green's function. Thus, any compactly supported initial data will be at most convectively unstable, leading to point-wise decay as $t \to \infty$. In other words, in this case the primary trigger front is linearly point-wise stable, even after the pair of Hopf eigenvalues has crossed the imaginary axis. Only perturbations with *weak* exponential decay ahead of the trigger front will induce linear exponential growth associated with this pair of Hopf eigenfunctions. One would expect that such weakly decaying perturbations eventually saturate at the time periodic profile constructed in our theorem. Although we do not prove this here, we suspect this time-periodic profile itself is stable against point-wise perturbations. If, on the other hand, the primary trigger front is perturbed by compactly supported initial conditions, such as the Hopf eigenfunctions multiplied by a bump function, one would expect the solution to converge back to the primary trigger front.

Large domain length. We may characterize the spectrum of L more explicitly if we further restrict our hypotheses by assuming that $f(x, u)$ is piecewise constant in x with $\partial_u f(x, u_0) \equiv C > 0$ for all $x \in [-\ell, \ell]$. The results of [127] imply that for $\ell >> 1$ all but

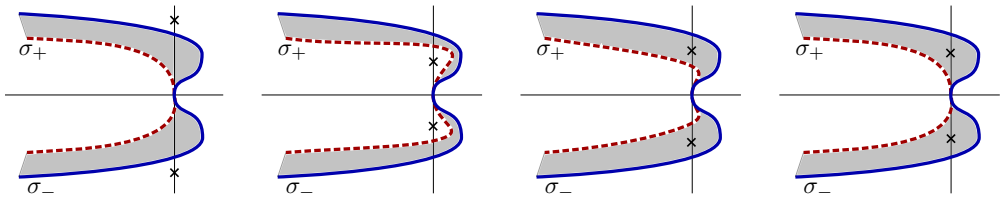

Figure 4.1.1: Examples of allowed (first two figures) and disallowed (last two figures) spectrum of $\mathcal{L}$ in $\mathbb{C}$ under our hypothesis with $\eta = 0$. The crosses denote the eigenvalues $\lambda_*(c_*), \overline{\lambda_*(c_*)}$, solid (blue) and dotted (red) lines denote the Fredholm borders $\sigma_\pm$ while the shaded region denotes the essential spectrum of L. (Color figure online)

a finite set of the point spectrum of L is well approximated by the absolute spectrum, $\Sigma_{\text{abs}} \subset \mathbb{C}$, of the linearization about the homogeneous state u_0. Hence, eigenvalue crossings as described in Hypothesis 4.1.8 occur when Σ_{abs}, typically through one or more branch points, crosses into the right half of the complex plane. The front speed for which these crossings occur has come to be known as the linear spreading speed, which we denote as c_{lin}; see [80] and [156] for a more in depth discussion of these topics. Thus, as $\ell \to \infty$, the Hopf-crossing speed c_* will approach c_{lin}.

In Section 4, our assumptions on f allow us to use such an argument to prove the existence of a Hopf eigenvalue crossing and subsequently obtain explicit expansions for the corresponding eigenfunctions. This then allows us to apply Theorem 4.1.3 to prove the existence of a Hopf bifurcation for an explicit example of this form.

4.1.2 Main Result

We are now ready to state our main result.

Theorem 4.1.3. *Given Hypotheses 4.1.5, 4.1.6, 4.1.8, 4.1.9 and either the pair 4.1.1 and 4.1.2, or 4.1.3, there exists a one-parameter family of time-periodic solutions of* (4.1.2) *which bifurcate from the front solutions $u_*(x, c)$ as the speed c decreases through c_*. This solution branch $(u, c, \omega) \in (u_* + H^4(\mathbb{R})) \times \mathbb{R}^2$ can be parameterized by $r \geq 0$, the amplitude of oscillations. More precisely, there exist $r_* > 0$ and smooth functions Υ_j, $j \in \{c, \omega, u\}$, defined for $|r| < r_*$, $\Upsilon_j(0) = 0$, so that*

$$c = c_* + \Upsilon_c(r^2), \quad \omega = \omega_* + \Upsilon_\omega(r^2), \quad u = u_* + \Upsilon_u(r),$$

with expansions

$$\Upsilon_c(r^2) = \frac{\mathrm{Re}\{\theta_+\}}{\mu'(c_*)} r^2 + \mathcal{O}(r^4), \quad \Upsilon_\omega(r^2) = \mathrm{Im}\{\theta_+\}|r|^2 + \mathcal{O}(|r|^4),$$
$$\Upsilon_u(r) = rp\cos(\omega t) + \mathcal{O}(r^2).$$

Here, $\mu'(c_*)$ is the crossing speed from Hypothesis 4.1.8, and

$$\theta_+ = \left\langle \left(3\,\partial_u^3 f(x,u_*)\,p^2\overline{p} \;+\; \partial_u^2 f(x,u_*)\,[p\varphi_0 + \overline{p}\varphi_+]\right)_{xx}, \psi \right\rangle_{L^2_\eta(\mathbb{R})},$$

with p, ψ eigenfunctions and adjoint eigenfunctions, and φ_i, defined in (4.3.5) *below, encode quadratic interactions. In particular, if $\mathrm{Re}\{\theta_+\} > 0$, the bifurcation is supercritical; if $\mathrm{Re}\{\theta_+\} < 0$ then the bifurcation is subcritical.*

A numerical example of this bifurcation is given in Figure 4.1.2 where equation (4.1.2) is simulated with $f(x,u) = u - u^3$ and χ equal to a sum of two Gaussian source terms. The corresponding trigger front u_* connects two stable homogeneous equilibria at $x = \mp\infty$ with a spinodally unstable plateau state in-between. For speed $c > c_*$, oscillatory instabilities of this front are convected away, while for $c < c_*$ they are self-sustaining. This setting, for which our results give a rigorous characterization, is closely related to models used by [40] and [152], where χ is composed of only a single Gaussian and produces a front u_* which connects a stable equilibrium at $x = +\infty$ to a spinodally unstable equilibrium at $x = -\infty$. Here, a similar bifurcation occurs as the trigger speed is reduced. Numerical simulations of such a situation are depicted in Figure 4.1.3.

The remainder of the paper is organized as follows. In Section 4.2, we establish Fredholm properties of the linearization. This is done in Propositions 4.2.1 and 4.2.10, for f smooth and piecewise-smooth in x respectively, using the methods of [44] and [123]. In Section 4.3 we give the proof of Theorem 4.1.3. In Section 4.4 we study a prototypical example, showing the existence of a first crossing of Hopf eigenvalues. By finding leading order estimates for such a crossing and its corresponding eigenfunctions, we then apply Theorem 4.1.3 to obtain existence of a Hopf bifurcation and compute the direction of branching. In Section 4.5 we discuss possible extensions and applications of our results.

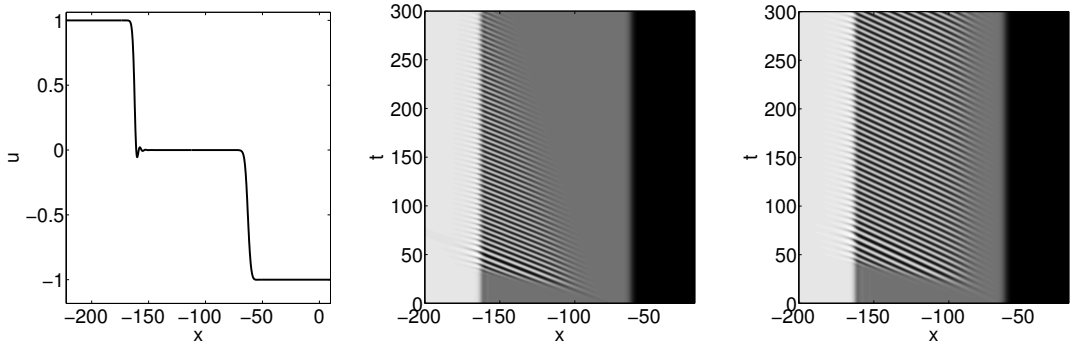

Figure 4.1.2: (Left): Front profile u_* in co-moving frame for two Gaussian source terms. (Middle), (Right): Spacetime plots in co-moving frame with speed $c > c_*$ and $c < c_*$ respectively. The initial condition for both is u_* plus a small localized perturbation near $x = -75$.

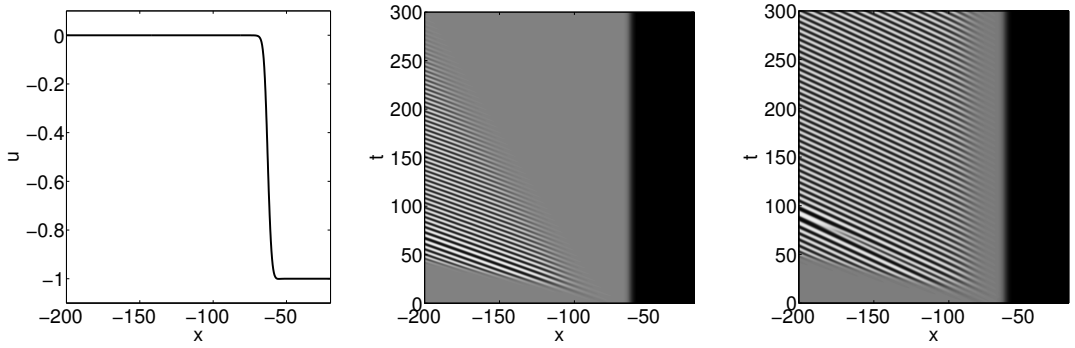

Figure 4.1.3: (Left): Front profile u_* in co-moving frame. (Middle), (Right): Spacetime plots in co-moving frame for speeds above and below a bifurcation point. The initial condition for both is u_* plus a small Gaussian perturbation near $x = -75$.

4.2 Preliminaries and Fredholm properties

After introducing some notation and function spaces, we establish Fredholm properties in weighted spaces in Section 4.2.1. We list necessary changes for the piecewise smooth case in Section 4.2.2.

For $\eta > 0$ we define the exponentially weighted norm

$$\|w\|_{2,\eta}^2 := \int_{\mathbb{R}} |e^{\eta\langle x\rangle} w(x)|^2 dx, \tag{4.2.1}$$

where $\langle x\rangle = \sqrt{1+x^2}$. We say that $w \in L^2_\eta(\mathbb{R})$ if w is Lebesgue-measureable and $\|w\|_{2,\eta} < \infty$. Similarly, we define Sobolev spaces H^k_η, with $\partial^j u \in L^2_\eta$ for $j \le k$. We use the following space-time norms,

$$\begin{aligned} &X = L^2(\mathbb{T}), \qquad Y = H^1(\mathbb{T}), \\ &\mathcal{X} = L^2_\eta(\mathbb{R}, X), \qquad \mathcal{Y} = L^2_\eta(\mathbb{R}, Y) \cap H^4_\eta(\mathbb{R}, X), \end{aligned} \tag{4.2.2}$$

where $x \in \mathbb{R}$ and $\tau \in \mathbb{T} = [0, 2\pi)$, the one-dimensional torus. Note that Y is dense and compactly embedded in X. Also note that $\mathcal{X}$ is a Hilbert space with the inner product

$$\langle u, v\rangle_{\mathcal{X}} := \frac{1}{2\pi} \int_0^{2\pi} \int_{-\infty}^{\infty} u(x,\tau)\overline{v(x,\tau)}\; e^{2\eta\langle x\rangle}\, dx\, d\tau.$$

Furthermore, the following norm makes $\mathcal{Y}$ a Hilbert space

$$\|u\|_{\mathcal{Y}}^2 := \int_{-\infty}^{\infty} \|u(x,\cdot)\|_Y^2 + \sum_{j=1}^{4} \|\partial_x^j u(x,\cdot)\|_X^2 dx. \tag{4.2.3}$$

We define $\mathcal{F} : \mathcal{Y} \times \mathbb{R}^2 \to \mathcal{X}$ as

$$\mathcal{F} : (v; \omega, c) \longmapsto \omega v_\tau + (v_{xx} + g(x, v; c))_{xx} - c\, v_x, \qquad g(x, v; c) := f(x, u_* + v) - f(x, u_*),$$

so that time-periodic solutions $u = u_* + v$ of (4.1.2) satisfy $F(v; \omega, c) \equiv 0$.

4.2.1 Smooth nonlinearity

We are interested in Fredholm properties of the linearization $\mathcal{L} : \mathcal{Y} \subset \mathcal{X} \to \mathcal{X}$ of $\mathcal{F}$ at the homogeneous solution $(v; \omega, c) = (0; \omega_*, c_*)$, which has the form

$$\mathcal{L} : v \longmapsto \omega_* \partial_\tau v - Lv = \omega_* \partial_\tau v - \partial_x \tilde{L} v, \qquad \tilde{L} : v \longmapsto -\partial_x \left(\partial_x^2 v + \partial_u f(x, u_*) v\right) + c_* v. \tag{4.2.4}$$

These properties will be necessary to implement the Lyapunov-Schmidt reduction used in the proof of Theorem 4.1.3. We prove that $\mathcal{L}$ is Fredholm in Proposition 4.2.1 and we compute its Fredholm index in Proposition 4.2.7.

Proposition 4.2.1. *Assuming Hypotheses 4.1.1, 4.1.2, 4.1.6, 4.1.8, and 4.1.9, the operator $\mathcal{L} : \mathcal{Y} \subset \mathcal{X} \to \mathcal{X}$ is Fredholm.*

To prove this proposition we shall need a few lemmata. First of all, we shall need a standard abstract closed range lemma.

Lemma 4.2.2. *(Abstract closed range lemma) Let V, W, Z be Banach spaces, $T : V \to W$ a bounded linear operator, and $K : V \to Z$ a compact linear operator such that*

$$||u||_V \leq C \left(||Ku||_Z + ||Tu||_W \right),$$

for all $u \in V$ and some $C > 0$. Then T has closed range and finite dimensional kernel.

Proof. The proof can be found in [147, Prop. 6.7, Pg. 583]. □

Next, we prove the following lemma which adapts the methods of [123]; see also [44]. For $J > 0$, let $\mathcal{Y}(J)$ and $\mathcal{X}(J)$ denote the spaces of functions, in $\mathcal{Y}$ and $\mathcal{X}$ respectively, which have x-support in the interval $[-J, J]$. Since the embedding $\mathcal{Y}(J) \hookrightarrow \mathcal{X}(J)$ is compact, the following lemma allows us to apply Lemma 4.2.2 to $\mathcal{L}$.

Lemma 4.2.3. *There exist constants $C > 0$ and $J > 0$ such that the operator $\mathcal{L}$ defined above satisfies*

$$\|\xi\|_{\mathcal{Y}} \leq C \left(\|\xi\|_{\mathcal{X}(J)} + \|\mathcal{L}\xi\|_{\mathcal{X}} \right). \tag{4.2.5}$$

Proof. Throughout, $C > 0$ will be a changing constant, possibly dependent on $\eta, c_*, \omega_*, f, u_*$ and $u_\pm$ but not ξ. Following [123, Lem. 3.7], the proof is divided into three steps:

Step 1: Prove that the estimate holds for $J = \infty$.

For this step, momentarily assume that the exponential weight has $\eta = 0$. To begin, we notice

$$\|\mathcal{L}\xi\|_{\mathcal{X}} \geq \|(\partial_\tau + \partial_x^4)\xi\|_{\mathcal{X}} - \|\partial_x^2(\partial_u f(x, u_*)\xi) - c_* \partial_x \xi\|_{\mathcal{X}}. \tag{4.2.6}$$

Since f and u_* are smooth, for all $\epsilon > 0$ we have

$$\begin{aligned}\|\partial_x^2(\partial_u f(x,u_*)\xi) - c_*\partial_x\xi\|_{\mathcal{X}} &\leq C\|\xi\|_{H^2(\mathbb{R},X)} \\ &\leq C\|\xi\|_{\mathcal{X}}^{\frac{1}{2}} \cdot \|\xi\|_{H^4(\mathbb{R},X)}^{\frac{1}{2}} \\ &\leq C\left(\epsilon\|\xi\|_{H^4(\mathbb{R},X)} + \frac{1}{4\epsilon}\|\xi\|_{\mathcal{X}}\right). \end{aligned} \tag{4.2.7}$$

Combining (4.2.6) and (4.2.7), we have for sufficiently small $\epsilon > 0$

$$\begin{aligned}\|\mathcal{L}\xi\|_{\mathcal{X}} + \frac{C}{4\epsilon}\|\xi\|_{\mathcal{X}} &\geq \|(\partial_\tau + \partial_x^4)\xi\|_{\mathcal{X}} - C\epsilon\|\xi\|_{H^4(\mathbb{R},X)} \\ &\geq C\|u\|_{\mathcal{Y}}. \end{aligned} \tag{4.2.8}$$

This gives the desired estimate.

If $\eta > 0$ then this step works in essentially the same manner. The only difference is that one must work with the conjugated operator $\mathcal{L}_\eta := \mathrm{e}^{\eta\langle x\rangle}\mathcal{L}\,\mathrm{e}^{-\eta\langle x\rangle}$ and deal with third derivative terms which are small due to the fact that $\eta > 0$ is small.

Step 2: Prove the estimate for the constant coefficient operators $\mathcal{L}_\pm$ given above.

We must work with the conjugated operators $\mathcal{L}_{\pm,\eta} := \mathrm{e}^{\eta\langle x\rangle}\mathcal{L}_\pm\,\mathrm{e}^{-\eta\langle x\rangle}$. By taking the Fourier transform in both x and τ, if

$$\mathcal{L}_{\pm,\eta}\xi = g, \tag{4.2.9}$$

then

$$\widehat{g}(\mathrm{i}\zeta,\mathrm{i}k) = \left[(\zeta \mp \eta)^4 - f'_\pm(u_\pm)(\zeta \mp \eta)^2 - \mathrm{i}c_*(\zeta \mp \eta) + \mathrm{i}\omega k\right]\widehat{\xi}, \quad \xi \in \mathbb{R}, k \in \mathbb{Z}.$$

By Hypothesis 4.1.9 and Remark 4.1.10, for $\eta > 0$ the essential spectrum of the time-independent operator does not intersect the set $\mathrm{i}\omega_*\mathbb{Z}$. Hence both equations in (4.2.9) are invertible and

$$\widehat{\xi} = \left((\zeta \mp \eta)^4 - f'_\pm(u_\pm)(\zeta \mp \eta)^2 - \mathrm{i}c_*(\zeta \mp \eta) + \mathrm{i}\omega k\right)^{-1}\widehat{g}$$

such that the coefficient on the right is bounded. The estimate

$$\|\widehat{\xi}\|_{\mathcal{X}} \leq \sup_{\zeta\in\mathbb{R},k\in\mathbb{Z}} |\left((\zeta\mp\eta)^4 - f'_{\pm}(u_{\pm})(\zeta\mp\eta)^2 - \mathrm{i}c_*(\zeta\mp\eta) + \mathrm{i}\omega k\right)^{-1}| \cdot \|\widehat{g}\|_{\mathcal{X}},$$

implies by Fourier-Plancherel that

$$\|\xi\|_{\mathcal{Y}} \leq C\|\mathcal{L}_{\pm}\xi\|_{\mathcal{X}}.$$

Step 3: To complete the proof we use the estimates of Step 1 and Step 2 to perform a patching argument in the same way as in [123] and [44]. To begin, for $J > 1$ let $\xi^{\pm} \in \mathcal{Y}$ such that $\xi^{+}(x) = 0$ for all $x \leq J-1$ and $\xi^{-}(x) = 0$ for all $x \geq 1-J$. The exponential decay of $u_* - u_{\pm}$ and $f - f_{\pm}$ as $x \to \pm\infty$ from Hypotheses 4.1.2 and 4.1.5 gives the following estimate. For any $\epsilon > 0$, there exists $J > 0$ sufficiently large such that

$$||(\mathcal{L}_{\pm} - \mathcal{L})\xi^{\pm}||_{\mathcal{X}} \leq \epsilon||\xi^{\pm}||_{H^2_{\eta}(\mathbb{R},\mathbb{T})}. \tag{4.2.10}$$

This allows us to obtain

$$\begin{aligned} ||\xi^{\pm}||_{\mathcal{Y}} &\leq C||\mathcal{L}_{\pm}\xi^{\pm}||_{\mathcal{X}} \\ &\leq C\left(||(\mathcal{L}_{\pm} - \mathcal{L})\xi^{\pm}||_{\mathcal{X}} + ||\mathcal{L}\xi^{\pm}||_{\mathcal{X}}\right) \\ &\leq C\left(\epsilon||\xi^{\pm}||_{H^2_{\eta}(\mathbb{R},\mathbb{T})} + ||\mathcal{L}\xi^{\pm}||_{\mathcal{X}}.\right) \end{aligned}$$

where we have used the estimate from Step 2 in the first inequality. Chosing $\epsilon < \frac{1}{C}$ we obtain

$$||\xi^{\pm}||_{\mathcal{Y}} \leq C||\mathcal{L}\xi^{\pm}||_{\mathcal{X}}. \tag{4.2.11}$$

Next note that for $\xi \in \mathcal{Y}$ with $\xi \equiv 0$ for all $|x| \leq J-1$ we can decompose $\xi = \xi^{+} + \xi^{-}$ with

$$\xi^{+} = \begin{cases} \xi(x), & x \geq 0 \\ 0, & x < 0, \end{cases} \qquad \xi^{-} = \begin{cases} 0, & x \geq 0 \\ \xi(x), & x < 0. \end{cases}$$

Applying estimate (4.2.11) we then obtain

$$\begin{aligned} ||\xi||_{\mathcal{Y}}^2 &= ||\xi^+||_{\mathcal{Y}}^2 + ||\xi^-||_{\mathcal{Y}}^2 \\ &\leq C\left(||\mathcal{L}\xi^+||_{\mathcal{X}}^2 + ||\mathcal{L}\xi^-||_{\mathcal{X}}^2\right) = C||\mathcal{L}\xi||_{\mathcal{X}}^2. \end{aligned} \tag{4.2.12}$$

Finally, given any $\xi \in \mathcal{Y}$ choose a smooth bump function β such that $\beta \equiv 1$ for $|x| \leq J-1$ and $\beta \equiv 0$ for $|x| \geq J$. Applying, (4.2.12) and Step 1 we obtain

$$\begin{aligned} ||\xi||_{\mathcal{Y}} &\leq ||\beta\xi||_{\mathcal{Y}} + ||(1-\beta)\xi||_{\mathcal{Y}} \\ &\leq C\left(||\beta\xi||_{\mathcal{X}} + ||\mathcal{L}(\beta\xi)||_{\mathcal{X}} + ||\mathcal{L}\left((1-\beta)\xi\right)||_{\mathcal{X}}\right) \\ &\leq C\left(||\xi||_{\mathcal{X}(T)} + ||\mathcal{L}\xi||_{\mathcal{X}}\right), \end{aligned}$$

giving the desired result.

■

Proof. [Proof of Prop. 4.2.1]

Lemma 4.2.3 gives that $\mathcal{L}$ has closed range and finite dimensional kernel. To finish the proof we define a suitable adjoint $\mathcal{L}^*$ and show it also satisfies a closed range lemma as above. In unweighted spaces the formal adjoint is

$$\mathcal{L}^* := \partial_x^4 + \partial_u f(x, u_*)\partial_x^2 + c_*\partial_x - \omega\partial_\tau.$$

But as we wish to work with exponentially weighted spaces $\mathcal{Y}$ and $\mathcal{X}$, we define the adjoint using the conjugated operator

$$\mathcal{L}_\eta^* := \mathrm{e}^{\eta\langle x\rangle}\mathcal{L}^*\mathrm{e}^{-\eta\langle x\rangle} : H^4(\mathbb{R}, X) \cap L^2(\mathbb{R}, Y) \subset L^2(\mathbb{R}, X) \to L^2(\mathbb{R}, X),$$

Note, since $\mathcal{L}_\eta$ is closed and densely defined, $\mathcal{L}_\eta^*$ is well-defined.

This operator can then be run through the same estimates as in Lemma 4.2.3, and we once again obtain that $\mathcal{L}_\eta^*$ has closed range and finite kernel. Therefore $\mathcal{L}$ is Fredholm.

■

Next, in Lemma 4.2.4 and 4.2.5, we determine the index of $\mathcal{L}$. We decompose $\mathcal{X}$ and

$\mathcal{Y}$ into a direct sum of invariant subspaces so that $\mathcal{L}$ is diagonal and the index of each restriction can be readily calculated. Elementary results (see for example [147]) then give that $\mathcal{L}$ has index equal to the sum of the indices of the restrictions.

The work of [5, Thm. 1.5] gives that $\mathcal{X}$ has a Fourier decomposition in the time variable

$$\mathcal{X} = \bigoplus_{k\in\mathbb{Z}} \mathcal{X}^k, \qquad \mathcal{X}^k := \left\{ v \in \mathcal{X} : v(x,\tau) = \tilde{v}(x)\mathrm{e}^{\mathrm{i}k\tau},\ \tilde{v} \in L^2_\eta(\mathbb{R}) \right\}.$$

Next, let $\mathcal{X}_h = \bigoplus_{k\neq 0} \mathcal{X}^k$, and $\mathcal{Y}_h = \bigoplus_{k\neq 0} \mathcal{Y}^k$, where $\mathcal{Y}^k = \mathcal{X}^k \cap \mathcal{Y}$, so the following decompositions hold

$$\mathcal{X} = \mathcal{X}^0 \oplus \mathcal{X}_h, \qquad \mathcal{Y} = \mathcal{Y}^0 \oplus \mathcal{Y}_h.$$

Note that $\mathcal{X}_0$ is the set of all time-independent functions in $\mathcal{X}$ while $\mathcal{X}_h$ is the set of all functions with time-average equal to zero.

Lemma 4.2.4. *The restriction $\mathcal{L}_0 := \mathcal{L} : \mathcal{Y}^0 \to \mathcal{X}^0$ has Fredholm index -1.*

Proof. On $\mathcal{Y}_0$ we have $\mathcal{L} = -L = -\partial_x \circ \tilde{L}$. Recall from (4.2.4) that $\tilde{L} : H^3_\eta(\mathbb{R}) \subset L^2_\eta(\mathbb{R}) \to L^2_\eta(\mathbb{R})$ is defined as $\tilde{L}v = -\partial_x(\partial_x^2 v + \partial_u f(x,u_*)v) + c_* v$. Hypothesis 4.1.2 implies that $\tilde{L}$ is an asymptotically constant operator:

$$\tilde{L} \to \tilde{L}_\pm \quad \text{as } x \to \pm\infty, \qquad \tilde{L}_\pm v := -\partial_x^3 v - f'_\pm(u_\pm)\partial_x v + c_* v.$$

Moreover, the constant coefficient first order systems associated with $\tilde{L}_\pm$ are hyperbolic with the same Morse index. Indeed, since $c > 0$, each of the polynomials $\nu^3 + f'_\pm(u_\pm)\nu - c = 0$ has two positive roots and one negative root. Thus, the piecewise constant operators $\tilde{L}_+$ and $\tilde{L}_-$ have relative Morse index equal to zero as well. This implies that the operator $\tilde{L}$ has Fredholm index equal to zero. (See for example [85, Sec. 3.1.10 - 11])).

To finish the proof it suffices to notice that $\partial_x : H^1_\eta(\mathbb{R}) \to L^2_\eta(\mathbb{R})$ is Fredholm with index -1. The result then follows using standard results on the composition of Fredholm operators (see for example [147, Sec. A.7]) ■

Lemma 4.2.5. *The restriction $\mathcal{L}_h := \mathcal{L} : \mathcal{Y}_h \to X_h$ has Fredholm index 0.*

Proof. First note that since $\mathcal{L}$ is Fredholm, $\mathcal{L}_h$ and $\mathcal{L}_h^*$ must have finite dimensional kernel. Next, it is straightforward to notice that each restriction $\mathcal{L}_k := \mathcal{L} : \mathcal{Y}^k \subset \mathcal{X}^k \to \mathcal{X}^k$ is well defined and takes the form

$$\mathcal{L}_k(\mathrm{e}^{\mathrm{i}k\tau}\tilde{v}(x)) = \partial_x^2\left(\partial_x^2\tilde{v} + \partial_u f(x, u_*(x))\tilde{v}\right) - c_*\partial_x\tilde{v} + \mathrm{i}\omega k\tilde{v}.$$

Hypothesis 4.1.6 and 4.1.9 imply that for $\mathcal{L}_k$ and its adjoint $\mathcal{L}_k^*$

$$\dim\ker\mathcal{L}_k = \begin{cases} 0 & k \neq \pm 1 \\ 1 & k = \pm 1, \end{cases} \qquad \dim\ker\mathcal{L}_k^* = \begin{cases} 0 & k \neq \pm 1 \\ 1 & k = \pm 1. \end{cases}$$

Comparing the dimensions of $\ker\mathcal{L}_h$ and $\ker\mathcal{L}_h^*$ then implies that $\mathcal{L}_h$ has Fredholm index 0. ∎

Remark 4.2.6. *For simplicity, we have included direct proofs to determine the Fredholm index of $\mathcal{L}$ in the preceding lemmas. We note that one could also calculate these using a spectral flow as in [123]. Namely, the index could be found by tracking spatial eigenvalue crossings as x moves from $-\infty$ to $+\infty$.*

The previous lemmas then give the following proposition.

Proposition 4.2.7. *Given the hypotheses in Proposition 4.2.1, the operator $\mathcal{L}$ has Fredholm index -1.*

Proof. Since $\mathcal{L}$ can be decomposed as

$$\mathcal{L} := \begin{pmatrix} \mathcal{L}_0 & 0 \\ 0 & \mathcal{L}_h \end{pmatrix} : \mathcal{Y}_0 \oplus \mathcal{Y}_h \longrightarrow \mathcal{X}_0 \oplus \mathcal{X}_h,$$

a standard result in Fredholm theory (see [147, Sec. A.7]) gives that the Fredholm index of $\mathcal{L}$ is equal to the sum of the indices of $\mathcal{L}_0$ and $\mathcal{L}_h$. This fact, in combination with Lemmas 4.2.4 and 4.2.5, proves the proposition. ∎

4.2.2 Piecewise smooth f

If Hypothesis 4.1.3 is assumed instead of Hypotheses 4.1.1 and 4.1.2 the setting must be slightly altered in order to obtain the Fredholm properties required in the proof of Theorem 4.1.3. In particular, since $\partial_u f$ has discontinuities in x, $\mathcal{L}$ is not well-defined on $\mathcal{Y}$ and hence jump-conditions are needed. Let us define the jump condition notation

$$\delta_{x_0} u = \lim_{x \to x_0^+} u(x,t) - \lim_{x \to x_0^-} u(x,t).$$

Also, for simplicity let us define the piecewise-smooth function

$$b(x) = \partial_u f(x, u_*(x)).$$

Next let us define the following set of conditions on a function $u(x,t)$,

$$(\#\#) := \begin{cases} t \in \mathbb{T},\ x_0 = \pm\ell, \\ \delta_{x_0} u = 0, \quad \delta_{x_0} u_x = 0, \quad \delta_{x_0} u_{xx} = -u(x_0,t)\,\delta_{x_0} b, \\ \delta_{x_0} u_{xxx} = -\left[u(x_0,t)\,\delta_{x_0} b_x + u_x(x_0,t)\,\delta_{x_0} b\right]. \end{cases}$$

A brief calculation then shows that $\mathcal{L}$ is well defined on the space

$$\mathcal{Y}^{\#\#} := \Big(H^4_\eta\big([\ell,\infty),X\big) \oplus H^4_\eta\big([-\ell,\ell]),X\big) \oplus H^4_\eta\big((-\infty,-\ell],X\big)\Big) \cap L^2\big(\mathbb{R},Y\big) \cap (\#\#) \subset \mathcal{X}.$$

Furthermore, it is easily seen that $\mathcal{L}$ is a closed, densely defined operator on $\mathcal{X}$. Indeed, the latter fact follows from the density of $\mathcal{Y}$ in $\mathcal{X}$, and the fact that for any $u \in \mathcal{Y}$ there exists a function v, which is smooth away from the points $x = \pm\ell$, has arbitrarily small L^2-norm, and yet satisfies the jump conditions $(\#\#)$ so that $u + v \in \mathcal{Y}^{\#\#}$.

For ease of notation, we restrict for the remainder of the section to f with one jump discontinuity located at $x = 0$. The result for a nonlinearity with multiple discontinuities will follow in the same manner. Hence we work with the operator

$$\mathcal{L} : \mathcal{Y}^{\#} := \big(H^4_\eta(\mathbb{R}^-,X) \oplus H^4_\eta(\mathbb{R}^+,X)\big) \cap L^2_\eta(\mathbb{R},Y) \cap (\#) \subset \mathcal{X} \to \mathcal{X}, \tag{4.2.13}$$

defined as in (4.1.3) above with

$$(\#) := \begin{cases} t \in \mathbb{T},\, x_0 = 0 \\ \delta_{x_0} u = 0, \quad \delta_{x_0} u_x = 0, \quad \delta_{x_0} u_{xx} = -u(x_0,t)\,\delta_{x_0} b, \\ \delta_{x_0} u_{xxx} = -\left[u(x_0,t)\,\delta_{x_0} b_x + u_x(x_0,t)\,\delta_{x_0} b\right]. \end{cases}$$

Our approach is to conjugate from $\mathcal{Y}$ to $\mathcal{Y}^{\#}$ through a change of variables $\tilde{u} = u + \Phi$ where $\Phi = \Phi(x,\tau)$ has jump discontinuities on $(0,\tau) \in \mathbb{R} \times \mathbb{T}$ which compensate for the discontinuities created by $b(x)$. We construct Φ using solutions of fractional order, $L^2(\mathbb{T})$-valued, evolution equations which have the jump conditions on $\{0\} \times \mathbb{T}$ as initial conditions.

For any $\mu, \tau \in [0,\infty)$, and open $U \subset \mathbb{R}$ let

$$W_\eta^{\sigma,\mu}(U \times \mathbb{T}) := H_\eta^\mu(U, X) \cap L_\eta^2(\mathbb{R}, H^\sigma(\mathbb{T})),$$

denote the anisotropic Sobolev space of order μ in space and order σ in time defined in the usual way via Fourier Transform. As they will repeatedly arise in the following, denote $V = \mathbb{R} \times \mathbb{T}$ and $V^\pm = \mathbb{R}^\pm \times \mathbb{T}$. Note also that $W_\eta^{0,0}(V) = \mathcal{X}$, $W_\eta^{1,0}(V) = L_\eta^2(\mathbb{R}, Y)$, $W_\eta^{0,4}(V) = H_\eta^4(\mathbb{R}, X)$, and $W_\eta^{1,4}(V) = \mathcal{Y}$.

To setup the evolution equations, for $i = 0, 1$ and $\alpha_i \in \mathbb{R}^+$, let $A_i : H^{\alpha_i}(\mathbb{T}) \to L^2(\mathbb{T})$ be the linear operators defined via Fourier series as

$$\widehat{(A_i v)}_k := (-|k|^{\alpha_i} - 1)\,\widehat{v}_k, \qquad k \in \mathbb{Z}. \tag{4.2.14}$$

Next, for $\beta_i \in \mathbb{R}^+$, define the trace operators $T_i : W_\eta^{1,4}(V^+) \to H^{\beta_i}(\mathbb{T})$ as

$$T_0[u] := -\delta_0(b) u(0,\tau), \qquad T_1[u] := -(\delta_0(b_x) u(0,\tau) + \delta_0(b) u_x(0,\tau)).$$

Anisotropic trace estimates give that $u(0,\tau) \in H^{7/8}(\mathbb{T})$ and $u_x(0,\tau) \in H^{5/8}(\mathbb{T})$ if $u \in W_\eta^{1,4}(V^+)$; see [35, Lem 3.5]. This means that T_0 and T_1 are well defined for $\beta_0 \le 7/8$ and $\beta_1 \le 5/8$ respectively. Also, note that if these inequalities are strict then each T_i is compact.

In order to obtain the desired regularity properties we set

$$\alpha_0 = \frac{5}{16}, \quad \alpha_1 = 1, \quad \beta_0 = \frac{7}{8} - \epsilon, \quad \beta_1 = \frac{5}{8} - \epsilon, \tag{4.2.15}$$

for some $\epsilon > 0$ sufficiently small. Then, define the X-valued initial value problems

$$\partial_x v_0 = A_0 v_0, \quad v_0(0) = T_0[u], \tag{4.2.16}$$

$$\partial_x v_1 = A_1 v_1, \quad v_1(0) = T_1[u] - A_0 T_0[u]. \tag{4.2.17}$$

where $v_i = v_i(x)$ take values in $X = L^2(\mathbb{T})$. We then obtain the following result characterizing solutions of these equations.

Proposition 4.2.8. *Given $u \in W^{1,4}_\eta(V^+)$, there exist unique solutions v_0^* and v_1^* of the initial value problems* (4.2.16) *and* (4.2.17) *which satisfy*

$$v_0^* \in W^{\beta_0-\alpha_0/2,1}_\eta(V^+) \cap W^{\beta_0+\alpha_0/2,0}_\eta(V^+) \cap W^{\beta_0-3\alpha_0/2,2}_\eta(V^+), \tag{4.2.18}$$

$$v_1^* \in W^{\beta_1-\alpha_1/2,1}_\eta(V^+) \cap W^{\beta_1+\alpha_1/2,0}_\eta(V^+). \tag{4.2.19}$$

Proof. This result can be proved using Fourier analysis. For a more general reference see [1] ∎

Note that for the specific values of α_i, β_i listed in (4.2.16) and (4.2.17), we have $v_0^* \in W^{1,2}_\eta(V^+)$ and $v_1^* \in W^{1,1}_\eta(V^+)$. We may then define functions $\Phi_i = \Phi_i(x,\tau)$ as

$$\Phi_0(x,\tau) := \int_0^x \int_0^y v_0^*(s,\tau) ds\, dy, \quad \Phi_1(x,\tau) := \int_0^x \int_0^y \int_0^z v_1^*(s,\tau) ds\, dz\, dy, \tag{4.2.20}$$

so that $\Phi_0, \Phi_1 \in W^{1,4}_\eta(V^+)$. By extending Φ_i by zero for $(x,\tau) \in V^-$ and using the fact that

$$(\Phi_0)_x \Big|_{x=0} = (v_0^*)_x \Big|_{x=0} = A_0 v_0^* \Big|_{x=0} = A_0 T_0[u],$$

our construction gives that $(\Phi_0 + \Phi_1)$ satisfies the jump conditions (#) defined above. Hence the following mapping is well defined

$$\Phi : W^{1,4}_\eta(V) \to \mathcal{Y}^\#, \tag{4.2.21}$$

$$u \longmapsto \Phi[u] = \Phi[u](x,\tau) := \rho(x)(\Phi_0(x,\tau) + \Phi_1(x,\tau)), \tag{4.2.22}$$

where $\rho = \rho(x)$ is a smooth bump function compactly supported and identically equal to 1 in a neighborhood of the origin. We then have the following lemma

Lemma 4.2.9. *The mapping* $\mathrm{id} + \Phi : \mathcal{Y} \to \mathcal{Y}^{\#}$ *is a linear isomorphism.*

Proof. It is readily found that this mapping is linear. Furthermore, since we have not used the full trace regularity of u, the mapping Φ is compact. Hence, it suffices to show that $\mathrm{id} + \Phi$ is one-to-one, since it then immediately follows that the mapping is onto. If $(u + \Phi[u]) = 0$, then for all $\tau \in \mathbb{T}$

$$\tilde{u}(0,\tau) = \Phi[u](0,\tau) = 0 = \Phi[u]_x(0,\tau) = u_x(0,\tau).$$

This implies

$$\delta_0(\Phi[u]_{xx}) = \delta_0(\Phi[u]_{xxx}) = 0,$$

so that the initial value problems (4.2.16) and (4.2.17) have zero initial conditions and hence that $u = 0$. ∎

We are now ready to prove the desired result.

Proposition 4.2.10. *Assuming the Hypotheses 4.1.6, 4.1.8, 4.1.9, and 4.1.3, the operator* $\mathcal{L} : \mathcal{Y}^{\#} \subset \mathcal{X} \to \mathcal{X}$ *is Fredholm with index -1.*

Proof.

First note that because $\mathcal{L}$ is closed and densely defined, its $\mathcal{X}$-adjoint is

$$\begin{aligned} &\mathcal{L}^* : \mathcal{Y} \subset \mathcal{X} \to \mathcal{X} \\ &\mathcal{L}^* v := -\partial_t u - \partial_x^4 u - b(x)\partial_x^2 u - c_* \partial_x u. \end{aligned} \tag{4.2.23}$$

This definition can be easily calculated using the jump conditions in (##) and integration by parts. The methods used to prove Proposition 4.2.1 can immediately be applied to obtain that $\mathcal{L}^*$ has closed range and finite dimensional kernel.

Since $\mathrm{id} + \Phi$ is an isomorphism, it suffices to prove that $\tilde{\mathcal{L}} := \mathcal{L} \circ (\mathrm{id} + \Phi) : \mathcal{Y} \to \mathcal{X}$ has closed range and finite dimensional kernel. We thus proceed as in Lemma 4.2.3. We only give the proof of Step 1, obtaining a Gårding type inequality as in (4.2.8).

The subsequent steps will then follow in an analogous way to those in Lemma 4.2.3. In particular, since $\tilde{\mathcal{L}}$ is equal to constant coefficient operators $\mathcal{L}_\pm$ for x outside the support of $\Phi[u]$, an even simpler patching argument than that of [44] and [123] can be implemented. Also, since we have conjugated to the space $\mathcal{Y}$, we still have the compact embedding of the truncated spaces $\mathcal{Y}(J) \hookrightarrow \mathcal{X}(J)$ and may apply the abstract closed range lemma. Therefore $\tilde{\mathcal{L}}$ and, by Lemma 4.2.9, $\mathcal{L}$ have closed range and finite dimensional kernel. Since $\mathcal{L}^*$ has the same properties, we find that $\mathcal{L}$ is Fredholm. The index can be found in the exact same manner as in Section 4.2.1.

Let $\lesssim$ and $\gtrsim$ denote inequality up to a constant independent of the variables being used. We first estimate

$$\begin{aligned}
\|\mathcal{L}\Phi[u]\|_{\mathcal{X}} &= \|\mathcal{L}\Phi[u]\|_{W^{0,0}_\eta(V^+)} \\
&\lesssim \|\Phi[u]\|_{W^{1,4}_\eta(V^+)} \lesssim \|\Phi[u]\|_{W^{1,0}_\eta(V^+)} + \|\Phi[u]\|_{W^{0,4}_\eta(V^+)} \\
&\lesssim \|u\|_{W^{1-\epsilon,0}_\eta(V)} + \|u\|_{W^{0,2}_\eta(V)} \\
&\leq c_1(\epsilon)\|u\|_{\mathcal{X}} + c_2(\epsilon)\|u\|_{\mathcal{Y}}. \qquad (4.2.24)
\end{aligned}$$

where $c_1(\epsilon) \to \infty$ and $c_2(\epsilon) \to 0$ as $\epsilon \to 0^+$. In the first two lines we restricted to V^+ because $\mathrm{supp}(\Phi) \subset V^+$. In the third line, the first term is obtained by exploiting the fact that less than maximal regularity of the trace, $u|_{x=0}$, is used. The second term in the third line is obtained using trace and inverse-trace estimates from [35, Lem. 3.5],

$$\begin{aligned}
\|\Phi[u]\|_{W^{0,4}_\eta(V^+)} \lesssim \|\Phi[u]_{xx}\|_{W^{0,2}_\eta(V^+)} &\lesssim \|u(0,\cdot)\|_{W^{3/4,3/2}_\eta(\{0\}\times\mathbb{T})} \\
&\lesssim \|u\|_{W^{0,2}_\eta(V^+)} + \|u\|_{W^{0,2}_\eta(V^-)} \\
&\lesssim \|u\|_{W^{0,2}(V)}. \qquad (4.2.25)
\end{aligned}$$

To obtain the last line in (4.2.24), we use the estimates

$$\|u\|_{W^{0,2}_\eta(V)} \lesssim \frac{1}{\epsilon}\|u\|_{\mathcal{X}} + \epsilon\|u\|_{\mathcal{Y}}, \qquad (4.2.26)$$

$$\|u\|_{W^{1-\epsilon,0}_\eta(V^+)} \leq \|u\|^{\epsilon}_{W^{0,0}_\eta(V)}\|u\|^{1-\epsilon}_{W^{1,0}_\eta(V)} \leq \tilde{c}_1(\epsilon)\|u\|_{W^{0,0}_\eta(V))} + \tilde{c}_2(\epsilon)\|u\|_{W^{1,0}_\eta(V)}, \qquad (4.2.27)$$

where $\tilde{c}_1(\epsilon) \to +\infty$ and $\tilde{c}_2(\epsilon) \to 0$ as $\epsilon \to 0$. The estimate (4.2.27) uses standard Sobolev

interpolation results (see [98]) and Young's inequality.

This finally allows us to obtain

$$\begin{aligned}
\|\tilde{\mathcal{L}}u\|_{\mathcal{X}} = \|\mathcal{L}\circ(\mathrm{id}+\Phi)u\|_{L^2_\eta(V)} &\gtrsim \sum_{i=\pm}\|\mathcal{L}\circ(\mathrm{id}+\Phi)u\|_{L^2_\eta(V^i)}\\
&\geq \sum_{i=\pm}\|\mathcal{L}u\|_{L^2_\eta(V^i)} - \|\mathcal{L}\Phi[u]\|_{L^2_\eta(V^i)}\\
&\gtrsim \sum_{i=\pm}\Big(\|u\|_{W^{1,4}_\eta(V^i)} - \|u\|_{L^2_\eta(V^i)}\Big) - \|\mathcal{L}\Phi[u]\|_{\mathcal{X}}\\
&\gtrsim \sum_{i=\pm}\Big(\|u\|_{W^{1,4}_\eta(V^i)} - \|u\|_{L^2_\eta(V^i)}\Big) - (c_1(\epsilon)\|u\|_{\mathcal{X}} + c_2(\epsilon)\|u\|_{\mathcal{Y}})\\
&\geq C_\epsilon\|u\|_{\mathcal{Y}} - C'_\epsilon\|u\|_{\mathcal{X}}, \qquad (4.2.28)
\end{aligned}$$

with $C_\epsilon, C'_\epsilon > 0$ for $\epsilon > 0$ sufficiently small. Since $\mathcal{L}\circ(\mathrm{id}+\Phi)u \in L^2_\eta(V)$, the first and last inequality follow from the equivalence of the Euclidean and box norms on $\mathbb{R}^2$. The third inequality is obtained by proceeding as in Step 1 of Lemma 4.2.3 on each V^i. The estimate (4.2.24) gives the fourth inequality. ■

In the more general case where $b(x)$ has more than one discontinuity, one must first construct jump functions Φ_i as above for each of the domain decompositions $\mathbb{R} = (-\infty,-\ell)\cup(-\ell,\infty), (-\infty,\ell)\cup(\ell,\infty)$. Then Φ may be obtained as a sum of the $\rho_i(x)\cdot\Phi_i(x,\tau)$, where each ρ_i is a sufficiently localized smooth bump function which is identically one in a neighborhood of a discontinuity of b.

4.3 Proof of main theorem

4.3.1 Smooth front profile u_*

In this section, we give the proof where Hypothesis 4.1.1 and 4.1.2 hold. The proof for Hypothesis 4.1.3 will follow in the same way with a few alterations and is lined out in Section 4.3.2.

Using Lyapunov-Schmidt reduction, we wish to solve $\mathcal{F}(w,\omega,c) = 0$ for (ω,c) close to (ω_*,c_*). Since $\mathcal{L}$ has Fredholm index -1, one must alter the setting before the Implicit

Function theorem may be applied in the reduction. In our setting, this alteration is simple. Let

$$\mathring{\mathcal{X}} := \{u \in \mathcal{X} : \left\langle u, \mathrm{e}^{-2\eta\langle x\rangle} \right\rangle_{\mathcal{X}} = 0\},$$

so that $\mathring{\mathcal{X}}$ is a closed subset of $\mathcal{X}$. Using the fact that, for any exponential weight with $\eta > 0$, the constant function $\mathrm{e}^{-2\eta\langle x\rangle}$ lies in the cokernel of $\mathcal{L}$, it is readily found that $\mathcal{L}$ maps $\mathcal{Y}$ into $\mathring{\mathcal{X}}$. Thus, we may restrict the codomain of our problem.

Furthermore, the linearization $\mathcal{L}$ has Fredholm index zero when considered as an operator $\mathcal{L} : \mathcal{Y} \to \mathring{\mathcal{X}}$. This follows from Proposition 4.2.1 and Fredholm algebra. Indeed $\mathcal{L} : \mathcal{Y} \to \mathcal{X}$ can be viewed as the composition $\mathcal{S} \circ \mathcal{L}$ where $\mathcal{S} : \mathcal{X} \to \mathring{\mathcal{X}}$ is the orthogonal projection onto $\mathring{\mathcal{X}}$ possessing fredholm index 1.

Let us define

$$\tilde{\omega} = \omega - \omega_*, \qquad \tilde{c} = c - c_*, \quad \Omega = (\tilde{\omega}, \tilde{c}), \tag{4.3.1}$$

so that $\mathcal{F}$ is now a function of $(u; \Omega) \in \mathcal{Y} \times \mathbb{R}^2$. For the following we suppress the dependence on parameters $(\tilde{\omega}, \tilde{c})$ unless it is needed.

By Hypothesis 4.1.8, for the functions $P_+(x,\tau) := \mathrm{e}^{\mathrm{i}\tau} p(x)$, $P_-(x,\tau) := \overline{P_+(x,\tau)}$,

$$\ker \mathcal{L} = \operatorname{span}\Big\{P_+, P_-\Big\}.$$

Furthermore, let us give $u_0 \in \ker \mathcal{L}$ the coordinates

$$u_0 = a\, P_+ + \overline{a}\, P_-,$$

with $a, \overline{a} \in \mathbb{C}$. Next, with the adjoint eigenfunctions $\psi(x)$ and $\overline{\psi(x)}$ as defined in Section 4.1.1, we define $\Psi_+(x,\tau) := \mathrm{e}^{\mathrm{i}\tau}\psi(x)$, $\Psi_- := \overline{\Psi_+}$. The algebraic simplicity assumed in Hypothesis 4.1.8 implies

$$\langle P_i, \Psi_j \rangle_{\mathcal{X}} = \delta_{ij},$$

where δ_{ij} is the Kronecker delta. Then since $\mathcal{L}$ is Fredholm by Proposition 4.2.1, we have the following decomposition

$$\mathring{\mathcal{X}} = \ker \mathcal{L}^* \oplus \mathcal{M}, \qquad \mathcal{M} = \left(\operatorname{span}\{\Psi_-, \Psi_+\}\right)^{\perp}.$$

This decomposition has the associated projections

$$\mathcal{Q} : \mathring{\mathcal{X}} \to \ker \mathcal{L}^*, \qquad \mathcal{P} := I - \mathcal{Q} : \mathring{\mathcal{X}} \to \mathcal{M}.$$

The projection onto $\ker \mathcal{L}^*$ can be explicitly defined as

$$\mathcal{Q}u = \sum_{i=\pm} \langle u, \Psi_i \rangle_{\mathcal{X}} \cdot \Psi_i. \tag{4.3.2}$$

Thus, solving $\mathcal{F} \equiv 0$ is equivalent to solving the following system of equations

$$0 = \mathcal{P}\mathcal{F}(u_0 + u_h, \Omega), \tag{4.3.3}$$

$$0 = \mathcal{Q}\mathcal{F}(u_0 + u_h; \Omega), \tag{4.3.4}$$

where $u_h \in \mathcal{N} := (\ker \mathcal{L})^{\perp}$.

Since the linearization $\mathcal{L}$ of $\mathcal{F}$ about the trivial state $(0; 0, 0)$ has Fredholm index zero, the linearization of the first equation with respect to u_h is invertible on $\mathcal{N}$. Since $\mathcal{F}$ is a smooth function of (v, ω, c), the Implicit Function theorem guarantees that there exists a smooth function $\varphi : \ker \mathcal{L} \times \mathbb{R}^2 \to \mathcal{N}$ such that $u_0 + \varphi(u_0; \Omega)$ solves the "auxiliary" equation (4.3.3) and $\varphi(0; \Omega) = D_{u_0}\varphi|_{(0,\Omega)} = 0$ for Ω sufficiently small.

Substituting the coordinatization for u_0 given above into the perturbation equations and matching terms, we obtain the expansion

$$\varphi(u_0; \Omega) = a^2 \mathrm{e}^{2\mathrm{i}t}\varphi_+(x; \Omega) + a\overline{a}\,\varphi_0(x; \Omega) + \overline{a}^2 \mathrm{e}^{-2\mathrm{i}t}\,\varphi_-(x; \Omega) + \mathcal{O}(|a|^3).$$

Inserting this into (4.3.3), it is readily found that the functions φ_i for $i = 0, -, +$ must solve the differential equations

$$\begin{aligned} \mathcal{L}(\mathrm{e}^{2\mathrm{i}t}\varphi_+) &= \mathrm{e}^{2\mathrm{i}t}(\partial_u^2 f(x, u_*(x))p^2)_{xx}, \\ \mathcal{L}(\varphi_0) &= (\partial_u^2 f(x, u_*(x))p\overline{p})_{xx}, \\ \mathcal{L}(\mathrm{e}^{-2\mathrm{i}t}\varphi_-) &= \mathrm{e}^{-2\mathrm{i}t}(\partial_u^2 f(x, u_*(x))\overline{p}^2)_{xx}. \end{aligned} \tag{4.3.5}$$

Note that each solution φ_i exists because the right hand side of each equation in (4.3.5)

is exponentially localized in x so that it is an element of $\mathring{\mathcal{X}}$ and, by the Fredholm alternative, lies in the range of $\mathcal{L}$.

Inserting these solutions into the bifurcation equation (4.3.4), we obtain the equivalent reduced system of equations

$$0 = \Phi_i(u_0;\Omega) := \langle \Psi_i, \mathcal{F}(u_0+\varphi(u_0,\Omega);\Omega)\rangle\,, \quad i=+,-. \tag{4.3.6}$$

Then, after calculations similar to [68, §VIII.3], the expansion of each Φ_i about $(a,\overline{a};\tilde{\omega},\tilde{c}) = (0,0,0,0)$ is found to be

$$\Phi_+(a,\overline{a};\Omega) = (\lambda_{\tilde{c}}(0)\tilde{c} + \mathrm{i}\,\tilde{\omega})\,a + \ \theta_+(0,0)\,a|a|^2 + \mathcal{O}\left((|\Omega|+|a|^2)|a||\Omega| + |a|^4\right), \tag{4.3.7}$$

$$\Phi_-(a,\overline{a};\Omega) = \left(\overline{\lambda_{\tilde{c}}}(0)\,\tilde{c} - \mathrm{i}\tilde{\omega}\right)\overline{a} + \ \theta_-(0,0)\ \overline{a}|a|^2 + \mathcal{O}\left((|\Omega|+|a|^2)|a||\Omega| + |a|^4\right), \tag{4.3.8}$$

where $\lambda_{\tilde{c}}(0) = \frac{d\lambda}{d\tilde{c}}(\tilde{c}=0) \neq 0$ by assumption and

$$\theta_+(\tilde{\omega},\tilde{c}) = \left\langle \left(3\partial_u^3 f(x,u_*)p^2\overline{p} + \partial_u^2 f(x,u_*)\left[p\varphi_0 + \overline{p}\varphi_+\right]\right)_{xx}, \psi\right\rangle_{L^2_\eta(\mathbb{R})}, \tag{4.3.9}$$

$$\theta_-(\tilde{\omega},\tilde{c}) = \left\langle \left(3\partial_u^3 f(x,u_*)p\overline{p}^2 + \partial_u^2 f(x,u_*)\left[p\varphi_- + \overline{p}\varphi_0\right]\right)_{xx}, \overline{\psi}\right\rangle_{L^2_\eta(\mathbb{R})}. \tag{4.3.10}$$

As common in Hopf bifurcation, the time-shift symmetry induces complex rotation equivariance of the bifurcation equation, so that we can factor a and obtain an equation that only depends on $|a|^2$.

Since $\operatorname{Re}\lambda_{\tilde{c}}(0)$ is non-zero by assumption, the Implicit Function theorem gives that there exists a bifurcating branch of solutions $(\tilde{\omega},\tilde{c})(|a|^2)$ parameterized by the amplitude $r^2 := |a|^2$ of the coordinate in $\ker\mathcal{L}^*$. Whenever $\operatorname{Re}\{\theta_+(0,0)\} \neq 0$, one can solve for $\tilde{c}$ as a function of r and readily confirm the statement on the direction of branching in the theorem.

Remark 4.3.1. *For the standard Cahn-Hilliard nonlinearity $f(u) = u - u^3$ linearized about $u_* \equiv 0$, we have $f''(u_*) = 0$ so that the expressions for $\theta_\pm$ simplify and, in practice, the inhomogeneous problems in* (4.3.5) *need not be solved.*

Remark 4.3.2. *We note that instead of restricting the codomain so that $\mathcal{L}$ is Fredholm index 0, one could also follow the work of [116] and [136] by adding an extra parameter*

via the ansatz

$$u(x) = b\chi(x) + w(x),$$

where $b \in \mathbb{R}$, $\chi(x) = (1 - \tanh(x))/2$ *and* $w \in \mathcal{X}$. *When considered in these coordinates,* $\mathcal{F} : \mathcal{Y} \times \mathbb{R}^3 \to \mathcal{X}$ *will then have a linearization which has Fredholm index 0 so that we may then perform a Lyapunov-Schmidt reduction as above. Such an approach would also be necessary when mass conservation only determines the asymptotic mass difference implicitly, say, when mass deposition through the trigger depends on concentrations* $\chi = \chi(x, u)$.

4.3.2 Alterations for Hypothesis 4.1.3

The proof under Hypothesis 4.1.3 follows in a similar manner and we only note the few differences. By taking into account the jump conditions at the discontinuities, it is readily found that $\mathcal{F}$ and hence $\mathcal{L}$ maps $\mathcal{Y}^{\#\#}$ into $\mathring{\mathcal{X}}$. A routine calculation then shows that the weak derivatives in the right sides of the three equations in (4.3.5) are well defined and in $\mathcal{X}$. The solvability of these equations then follows from the Fredholm Alternative, the fact that the eigenfunction p is exponentially localized, and $\ker(L - \mathrm{i}k\omega) = \{0\}$ for $k \neq \pm 1$.

4.4 Instability plateaus — an explicit example

In this section, we study an example where we can establish existence of modulated traveling waves. That is, we are able to verify the assumptions of Theorem 4.1.3. We first motivate our specific choice of nonlinearity in Section 4.4.1, and then introduce general concepts on absolute and convective instability in bounded domains in Section 4.4.2. Sections 4.4.3 to 4.4.5 then establish precise asymptotics for the first Hopf instability for long plateaus. Finally, Section 4.4.6 concludes by determining the cubic Hopf coefficient and the direction of branching.

4.4.1 Motivation

Establishing the existence of a Hopf bifurcation can generally be cumbersome. While the Hopf bifurcation that we analyzed here is ubiquitous in numerical simulations and experimental observations, it is generally difficult to rigorously prove that the assumptions of our theorem are satisfied. Intuitively, one expects a Hopf instability since for slow speed, mass deposition is slow so that the system develops a long, slowly varying plateau-like state in the intermediate spinodal regime. On this state, one expects a spinodal decomposition instability, with a typical selected spatial wavenumber. Since this instability is stationary in the steady frame, one would expect oscillations in the comoving frame of the trigger front. The absence of an explicit expression for the trigger front and the lack of tools to detect Hopf eigenvalues makes this problem in general quite intractable. We therefore set up a toy system, where the front is trivial, the "plateau" is an actual constant state, and nonlinearities are piecewise constant. As a benefit, we show how to make the above intuition rigorous in terms of branch points and absolute spectra, in particular obtaining corrections to the simple wavenumber prediction from fastest growing modes.

For the remainder of the section we let $u_*(x) \equiv 0$ and study (4.1.2) with nonlinearities of the form $f(x,u) = \chi(x)u + \gamma u^3 - \beta u^5$ where β and γ are real constants with $\beta > 0$ and

$$\chi(x) = \begin{cases} \chi_+ = 1 & x \in [-\ell, \ell] \\ \chi_- = -1 & x \in (-\infty, -\ell) \cap (\ell, \infty), \end{cases} \tag{4.4.1}$$

is a triggering mechanism which makes the homogeneous state $u \equiv 0$ linearly unstable inside the interval $[-\ell, \ell]$ and linearly stable everywhere else. Such triggers have been used to numerically study directional quenching (see [54] and [93]) and are a caricature of many others used in different situations; see Section 1.1 above. Also, by scaling we may assume that $\beta = 1$. This nonlinearity obviously satisfies Hypothesis 4.1.3 as noted above. Denote

$$Lu = -\left(u_{xx} + \chi u\right)_{xx} + cu_x,$$

and, as they will be of use in the following propositions, define the constant coefficient

operators

$$L_{\pm}u := -\left(u_{xx} + (\chi_{\pm})u\right)_{xx} + cu_x. \tag{4.4.2}$$

4.4.2 Absolute and convective instabilities in bounded domains

One can think of the linear problem with piecewise constant trigger χ as in (4.4.1) as a problem on $x \in (-l, l)$ with "effective" boundary conditions at $\pm l$, induced by the stable system on either side of the plateau. On the plateau, we see an instability which is advected by the drift term $c\partial_x$ induced by the co-moving frame. Only for sufficiently strong instabilities will the exponential growth outpace the linear advection. The eigenvalue problem on a finite domain is of course "explicitly solvable", in principle. On the other hand, calculations very quickly become quite impenetrable and we pursue a more conceptual approach.

In fact, the results in [126] and [127] show how to generally compute asymptotic behavior of spectra in finite bounded domains. For large domain length and separated boundary conditions which satisfy a certain non-degeneracy condition, all but finitely many eigenvalues are approximated by a set of curves called the *absolute spectrum*. This set is determined via the dispersion relation $d(\lambda, \nu)$ obtained by inserting $\mathrm{e}^{\lambda t + \nu x}$ into the asymptotic linearized equation. By viewing the *temporal* eigenvalue λ as a parameter and solving for the *spatial* eigenvalues $\nu = \nu(\lambda)$ ordered by real part $\operatorname{Re}\nu_j \geq \operatorname{Re}\nu_{j+1}$, one finds for well-posed operators that the system has fixed Morse index i_∞ so that $\operatorname{Re}\nu_{i_\infty}(\lambda) > 0 > \operatorname{Re}\nu_{i_\infty+1}(\lambda)$ for all λ with large real part. The absolute spectrum is then defined as

$$\Sigma_{\mathrm{abs}} = \{\lambda \in \mathbb{C} : \operatorname{Re}\nu_{i_\infty}(\lambda) = \operatorname{Re}\nu_{i_\infty+1}(\lambda)\}.$$

Though Σ_{abs} is not part of the spectrum of the linearized operator on an infinite domain, it dictates whether instabilities saturate the domain or are convected away. For typical problems, Σ_{abs} has an element λ_{br} with largest real part which determines when such instabilities arise. It is often the case that λ_{br} is a branch point of the dispersion relation and hence is an endpoint of a curve in Σ_{abs} which satisfies $\nu_{i_\infty}(\lambda_{\mathrm{br}}) = \nu_{i_\infty+1}(\lambda_{\mathrm{br}})$; see [121] or [126]). Additionally, the results of [126] give that eigenvalues of the finite domain problem of length ℓ accumulate on λ_{br} with rate $\mathcal{O}(\ell^{-2})$.

The work of [127] uses these concepts to study the spectrum of a pulse $p(x)$ connecting a stable rest state p_0 at $x \to \pm\infty$ to a plateau state which is close to an unstable rest state p_1 for $x \in [-\ell, \ell]$. By viewing such a pulse as the gluing of "front" and "back" solutions between p_0 and p_1, the limiting spectral set (as $\ell \to \infty$) of the linearization about this pulse can be decomposed into three parts: the absolute spectrum of the linearization about the unstable state p_1, the essential spectrum of the linearization about the state p_0, and a finite number of isolated eigenvalues determined by the spectrum of the front and back solutions. Using arguments as in [126], it is also shown that an infinite number of eigenvalues converge to the absolute spectrum with $\mathcal{O}(\ell^{-2})$ rate.

In our setting, the solution $u_*(x)$ can be viewed as a pulse whose asymptotic operator, defined above as L_-, has marginally stable spectrum. We will show for large ℓ that eigenvalue crossings are approximated by intersections of the absolute spectrum of L_+ with the imaginary axis. The absolute spectrum, which we denote as Σ^+_{abs}, is determined by the dispersion relation d_+ in (4.4.6) below. Furthermore, the first crossing is approximated by where the right-most part of Σ^+_{abs}, which consists of two complex conjugate branch points, intersects $\mathrm{i}\mathbb{R}$. As the front speed c is decreased, Σ^+_{abs} moves to the right towards the right half of the complex plane $\mathbb{C}^+$. As discussed above, when $\Sigma^+_{\text{abs}} \cap \mathbb{C}^+ \neq \varnothing$ instabilities which are stronger than the convective motion arise in the domain $[-\ell, \ell]$. This heuristically indicates that unstable eigenvalues will lie close to $\Sigma^+_{\text{abs}} \cap \mathbb{C}^+$. In the following, proof of these facts in our specific context is done by hand as the aforementioned results are not directly applicable and do not give explicit expansions of eigenvalues near the branch point.

4.4.3 Extended point spectrum

We now begin to verify the spectral hypotheses for our explicit example. In this section, we show that no eigenvalues arise from the front or back solutions. The genericity of the absolute spectrum, discussed in Section 4.4.4, will then allow us to show that eigenvalues which accumulate onto the absolute spectrum are the first to bifurcate.

In our case, the front and back solutions are $u_*(x) \equiv 0$ which solve the toy problem

with $\chi(x)$ defined respectively as

$$\chi_f(x) = \begin{cases} \chi_+ & x \in (-\infty, 0] \\ \chi_- & x \in (0, \infty) \end{cases}, \qquad \chi_b(x) = \begin{cases} \chi_- & x \in (-\infty, 0] \\ \chi_+ & x \in (0, \infty) \end{cases}. \tag{4.4.3}$$

These solutions then give the following piecewise-constant coefficient linearizations composed of $L_\pm$

$$L_{\mathrm{f/b}} u := -\big(u_{xx} + (\chi_{\mathrm{f/b}})u\big)_{xx} + cu_x, \tag{4.4.4}$$

which have domain $\mathcal{Y}^\# \subset \mathcal{X}$ where $x_0 = 0$ and $b = \chi_{\mathrm{f/b}}$.

We analyze the corresponding Evans functions $D_{\mathrm{f/b}}(\lambda)$ whose zeros are the eigenvalues of $L_{\mathrm{f/b}}$; for more background see [85] and references therein. In this simple case, the Evans function can be expressed in terms of the stable and unstable eigenspaces $E^\pm_{\mathrm{s}}(\lambda)$ and $E^\pm_{\mathrm{u}}(\lambda)$ of the first order systems associated with the operators $L_\pm - \lambda$ as in (4.4.2) above. Namely, $D_{\mathrm{f/b}}(\lambda) := E^\pm_{\mathrm{s}}(\lambda) \wedge E^\mp_{\mathrm{u}}(\lambda)$. Instead of the usual formulation in terms of u and its derivatives, we use a different set of variables in which the jump conditions (##) at $x = \pm\ell$ become continuity conditions. Namely we let $v = u_x, \theta = u_{xx} + \chi_{\mathrm{f/b}} u$, and $w = \theta_x$ so that the first order systems take the form

$$\begin{aligned} u_x &= v \\ v_x &= \theta - \chi_\pm u \\ \theta_x &= w \\ w_x &= cv - \lambda u. \end{aligned} \tag{4.4.5}$$

The eigenvalues of this system, denoted as $\nu^\pm_i(\lambda)$, are roots of the dispersion relations

$$d_\pm(\lambda, \nu) = -\nu^4 - \chi_\pm \nu^2 + c\nu - \lambda. \tag{4.4.6}$$

We order these roots by decreasing real part

$$\mathrm{Re}\{\nu^\pm_j(\lambda)\} \geq \mathrm{Re}\{\nu^\pm_{j+1}(\lambda)\},$$

and let

$$e_i^{\pm}(\lambda) := \left(1,\, \nu_i^{\pm}(\lambda),\, \nu_i^{\pm}(\lambda)^2 + \chi_{\pm},\, \nu_i^{\pm}(\lambda)(\nu_i^{\pm}(\lambda)^2 + \chi_{\pm})\right)^T$$

be the corresponding eigenvectors. As mentioned above, for λ with large positive real part it can readily be found that

$$\mathrm{Re}\{\nu_1^{\pm}(\lambda)\} \geq \mathrm{Re}\{\nu_2^{\pm}(\lambda)\} > 0 > \mathrm{Re}\{\nu_3^{\pm}(\lambda)\} \geq \mathrm{Re}\{\nu_4^{\pm}(\lambda)\}. \tag{4.4.7}$$

In fact this splitting holds for all λ to the right of $\Sigma_{\mathrm{ess}}^{\pm}$, the essential spectrum of $L_{\pm}$. For either $j = 1, 3$, if $\nu_j^i \neq \nu_{j+1}^i$ then e_j^i and e_{j+1}^i span the unstable and stable eigenspaces of (4.4.5) respectively. We find up to a normalization factor, for all $\lambda \in \mathbb{C} \diagdown \Sigma_{\mathrm{abs}}$ with $e_1^{\pm} \neq e_2^{\pm}$ and $e_3^{\pm} \neq e_4^{\pm}$,

$$D_f(\lambda) = \det \left| e_1^+\, e_2^+\, e_3^-\, e_4^- \right|, \qquad D_b(\lambda) = \det \left| e_1^-\, e_2^-\, e_3^+\, e_4^+ \right|, \tag{4.4.8}$$

where we have suppressed the dependence on λ of $e_j^{\pm}$ inside the determinant.

If for example $\nu_1^- = \nu_2^-$ for some λ_0, then one must view the spatial eigenvalues as functions of a variable ζ on a Riemann surface, $\lambda = g(\zeta)$, with a branch point at λ_0; see [85, §9.1]. Since ν_1^- is analytic in ζ, the vectors e_1^- and $\frac{d}{d\zeta} e_1^-$ form a basis for the corresponding unstable eigenspace.

With these definitions, we readily obtain the following lemma.

Lemma 4.4.1. *For all speeds $c > 0$, the functions $D_f(\lambda)$ and $D_b(\lambda)$ have no zeros in the set $\mathbb{C} \diagdown \Sigma_{\mathrm{abs}}^+$. Furthermore, they have a non-vanishing limit as λ approaches Σ_{abs}^+.*

Proof. As the argument will be the same for the back, we only consider the front. By applying Sobolev embeddings to the numerical range of both $L_{\pm}$, taking care to mind the jump conditions (#), it is readily found that L_f is uniformly sectorial on $L^2(\mathbb{R})$ in the plateau length ℓ. This implies that both D_f, being analytic off of the absolute spectrum, does not vanish identically in any connected component of $\mathbb{C} \diagdown \Sigma_{\mathrm{abs}}$.

It can be readily found that $D_f(0) \neq 0$. Assuming that $\lambda \neq 0$, we split the proof of the first statement into two cases.

Case 1: Assume that λ is such that $\nu_1^+ \neq \nu_2^+$ and $\nu_3^- \neq \nu_4^-$.

In this case the Evans functions $D_{f/b}$ are given by (4.4.8) above,

$$D_f(\lambda) = \det \begin{pmatrix} 1 & 1 & 1 & 1 \\ \nu_1^- & \nu_2^- & \nu_3^+ & \nu_4^+ \\ (\nu_1^-)^2 + \chi_- & (\nu_2^-)^2 + \chi_- & (\nu_3^+)^2 + \chi_+ & (\nu_4^+)^2 + \chi_+ \\ \nu_1^-((\nu_1^-)^2 + \chi_-) & \nu_2^-((\nu_2^-)^2 + \chi_-) & \nu_3^+((\nu_3^+)^2 + \chi_+) & \nu_4^+((\nu_4^+)^2 + \chi_+) \end{pmatrix}$$

$$= \det \begin{pmatrix} 1 & 1 & 1 & 1 \\ \nu_1^- & \nu_2^- & \nu_3^+ & \nu_4^+ \\ (\nu_1^-)^2 & (\nu_2^-)^2 & (\nu_3^+)^2 & (\nu_4^+)^2 \\ (\nu_1^-)^3 & (\nu_2^-)^3 & (\nu_3^+)^3 & (\nu_4^+)^3 \end{pmatrix}, \tag{4.4.9}$$

a Vandermonde determinant which we shall denote as $V(v_1^-, v_2^-, v_3^+, v_4^+)$. This equality can be obtained using the dispersion relation to find $(\nu_i^\pm)^2 + \chi_\pm = -\frac{\lambda - c\nu_i^\pm}{(\nu_i^\pm)^2}$ and then performing elementary row operations.

Hence, $D_f(\lambda) = 0$ if and only if $\nu_3^-(\lambda) = \nu_2^+(\lambda)$. This means that both dispersion relations $d_\pm$ are satisfied simultaneously and, since $\chi_+ \neq \chi_-$, that $\nu_3^- = \nu_2^+ = 0$. But we also have that $\nu_i^\pm(\lambda) = 0$ if and only if $\lambda = 0$. Therefore $D_f(\lambda) \neq 0$.

Case 2: Assume either $\nu_1^- = \nu_2^-$ or $\nu_3^+ = \nu_4^+$.

Say only the latter holds. Then we have

$$D_f(\lambda) = \partial_\zeta \nu_3^+ \cdot \frac{d}{d\nu_4^+}\Big|_{\nu_4^+ = \nu_3^+} V \neq 0,$$

for all $\lambda \neq 0$ because once again $D_f(\lambda) = 0$ if and only if $\nu_3^+ = \nu_2^-$ which holds if and only if $\lambda = 0$. If $\nu_1^- = \nu_2^-$ then take the derivative of V with respect to ν_1^-. If both equalities hold then take the derivatives of V with respect to both ν_1^- and ν_3^+. Note, we have that $\partial_\zeta \nu_3^+ \neq 0$ because double roots are simple for all $c > 0$. This gives the proof of the first part of the lemma.

To prove the second statement we note that if $\lambda \to \lambda_0 \in \Sigma_{\text{abs}}^+$ then, by definition, $\operatorname{Re}\nu_2^+ - \operatorname{Re}\nu_3^+ \to 0$. If $D_f(\lambda)$ were to approach zero as well, then arguments used above give that λ_0 must be 0, which is readily found to lie in the complement of the absolute spectrum for all speeds $c > 0$. This gives the proof of the second statement

and completes the lemma.

■

4.4.4 Branch points, rescalings and asymptotics

We now analyze the dispersion relation near the rightmost point of the absolute spectrum, defined in Section 4.4.2, in more detail. We give explicit formulas describing how branch points cross the imaginary axis and how the spatial eigenvalues $\nu(\lambda)$ behave around them. Furthermore, we will study how Σ^+_{abs} behaves near $\lambda_{\text{br}}(c)$.

For $c = c_{\text{lin}}$, it is readily found that the essential spectrum, Σ^+_{ess}, lies in the closed left-half plane when considered in an exponentially weighted space with weight $\mathrm{e}^{\mu_{\text{lin}}x}$, for μ_{lin} defined in Lemma 4.4.2 below. Since Σ^+_{abs} generically lies to the left of Σ^+_{ess}, elementary calculation shows that, for c near c_{lin}, the right most part of the absolute spectrum consists of a pair of complex conjugate branch points of the dispersion relation d_+. Such branch points, which we denote as $\lambda_{\text{br}}(c), \overline{\lambda_{\text{br}}(c)}$, solve the algebraic system

$$d_+(\lambda, \nu) = 0, \tag{4.4.10}$$

$$\frac{\partial}{\partial \nu} d_+(\lambda, \nu) = 0, \tag{4.4.11}$$

for some double spatial eigenvalue which we denote as $\nu_{\text{br}}(c) := \nu(\lambda_{\text{br}}(c))$.

In the context of front invasion into an unstable state, if $\nu_{\text{br}}(c)$ satisfies what is known as a "pinching"condition, the speed $c = c_{\text{lin}}$ for which $\lambda_{\text{br}}(c) \in \mathrm{i}\mathbb{R}$ is called the *linear spreading speed*; see [17], and [80]. Such "pinched double root" solutions of the Cahn-Hilliard dispersion relations have been studied previously and explicit expressions for $\lambda_{\text{lin}} := \lambda_{\text{br}}(c_{\text{lin}})$ and $\nu_{\text{lin}} := \nu_{\text{br}}(c_{\text{lin}})$ have been obtained. As they will be of use in the following, we sum them up in the following lemma.

Lemma 4.4.2. *Given f and u_* as above, for $\alpha = \partial_u f'(0, u_*(0))$, we have the following*

$$\begin{aligned}
\lambda_{\text{lin}} &= \mathrm{i}(3+\sqrt{7})\sqrt{\frac{2+\sqrt{7}}{96}}\cdot\alpha^2 \\
c_{\text{lin}} &= \frac{2}{3\sqrt{6}}(2+\sqrt{7})\sqrt{\sqrt{7}-1}\cdot\alpha^{3/2} \\
\mu_{\text{lin}} &:= \mathrm{Re}\{\nu_{\text{lin}}\} = -\sqrt{\frac{\sqrt{7}-1}{24}}\cdot\alpha^{1/2} \\
\kappa_{\text{lin}} &:= \mathrm{Im}\{\nu_{\text{lin}}\} = \sqrt{\frac{\sqrt{7}+3}{8}}\cdot\alpha^{1/2}.
\end{aligned} \tag{4.4.12}$$

Proof. These quantities can be found in [139, Lem 1.3] or [156]. ∎

In the next section, we will use spatial dynamics to obtain precise expansions for the first eigenvalue crossing and its corresponding eigenfunction. In order to do this we must obtain expansions for the spatial eigenvalues which solve the dispersion relation (4.4.6) for λ near λ_{lin}. Thus let $\hat{\lambda} = \lambda - \lambda_{\text{lin}}$, $\hat{\nu} = \nu - \nu_{\text{lin}}$, $\hat{c} = c - c_{\text{lin}}$ and $\Lambda = (\hat{\lambda}, \hat{c})$. In these variables the dispersion relation (4.4.27) takes the form

$$\hat{d}_+(\hat{\lambda}, \hat{\nu}) := \hat{\nu}^4 + 4\nu_{\text{lin}}\hat{\nu}^3 + (1+6\nu_{\text{lin}}^2)\hat{\nu}^2 - \hat{c}\hat{\nu} + \hat{\lambda} - \hat{c}\nu_{\text{lin}}. \tag{4.4.13}$$

We characterize the roots $\hat{\nu}(\hat{\lambda}, \hat{c})$ in the following lemma.

Lemma 4.4.3. *The dispersion relation* (4.4.13) *has four roots, $\hat{\nu}_{\text{s}}, \hat{\nu}_{\text{u}}, \hat{\nu}_{\text{cs}}, \hat{\nu}_{\text{cu}}$, which are functions of $\Lambda \in \mathbb{C}\times\mathbb{R}$ and, for all Λ close to $(0,0)$, satisfy the following properties*

(i) $\hat{\nu}_{\text{s/u}} = -2\nu_{\text{lin}} \pm \sqrt{-2\nu_{\text{lin}}^2 - 1} + \mathcal{O}(|\Lambda|)$.

(ii) The roots $\hat{\nu}_{\text{cs/cu}}$ solve

$$\hat{\nu}^2 + b_1(\Lambda)\hat{\nu} + b_0(\Lambda) = 0, \tag{4.4.14}$$

where, setting $\gamma_{\text{lin}} = (1+6\nu_{\text{lin}}^2)$, the coefficients b_0 and b_1 are analytic functions of Λ with leading order expansions

$$b_1(\Lambda) = \left(\frac{4\nu_{\text{lin}}}{\gamma_{\text{lin}}^2} - \frac{1}{\gamma_{\text{lin}}}\right)\hat{c} - \frac{4\nu_{\text{lin}}}{\gamma_{\text{lin}}^2}\hat{\lambda} + \mathcal{O}(|\Lambda|^2), \qquad b_0(\Lambda) = -\frac{\nu_{\text{lin}}}{\gamma_{\text{lin}}}\hat{c} + \frac{1}{\gamma_{\text{lin}}}\hat{\lambda} + \mathcal{O}(|\Lambda|^2). \tag{4.4.15}$$

(iii) For all Λ with $\hat{\lambda} + \lambda_{\rm lin} \notin \Sigma^+_{\rm abs}$ the roots $\hat{\nu}_{\rm cs/cu}$ split in the following way

$$\mathrm{Re}\{\hat{\nu}_{\rm cs}\} < -\frac{b_1(\Lambda)}{2} < \mathrm{Re}\{\hat{\nu}_{\rm cu}\}. \tag{4.4.16}$$

Proof. Property (i) is easily proved using standard perturbation techniques. Property (ii) is obtained using multi-parameter expansions and the Weierstrass Preparation Theorem; see for example [142, Ch. 4]. We note that (4.4.14) may be used to determine the branch point $(\hat{\lambda}_{\rm br}(\hat{c}), \hat{\nu}_{\rm br}(\hat{c}))$ in the shifted dispersion relation (4.4.13), for $\hat{c}$ near zero. Indeed, $\hat{\lambda}_{\rm br}(\hat{c})$ must satisfy

$$0 = b_0(\hat{\lambda}_{\rm br}(c), \hat{c}) - \frac{b_1(\hat{\lambda}_{\rm br}(\hat{c}), \hat{c})^2}{4}, \tag{4.4.17}$$

and hence has the form $\hat{\lambda}_{\rm br}(\hat{c}) = \nu_{\rm lin}\hat{c} + \mathcal{O}(\hat{c}^2)$, while $\hat{\nu}_{\rm br}(c) = -\frac{b_1(\lambda_{\rm br}(\hat{c}),\hat{c})}{2}$.

It now remains to prove property (iii). In order to find expansions for the roots of (4.4.14), we make the change of variables $\hat{\nu} = \tilde{\nu} - \frac{b_1(\Lambda)}{2}$ so that

$$0 = \tilde{\nu}^2 + \beta(\Lambda), \qquad \text{with} \quad \beta(\Lambda) = -b_0(\Lambda) + b_1(\Lambda)^2. \tag{4.4.18}$$

Fixing $\hat{c}$, setting $\tilde{\lambda} = \hat{\lambda} - \hat{\lambda}_{\rm br}(\hat{c})$, and expanding near $\hat{\lambda}_{\rm br}(\hat{c})$ we obtain

$$0 = \tilde{\nu}^2 + \tilde{\lambda}\,\tilde{b}_2(\tilde{\lambda}, \hat{c}), \tag{4.4.19}$$

for some function $\tilde{b}_2$ which is analytic in $\tilde{\lambda}$ with $\tilde{b}_2(0,0) = \frac{1}{\gamma_{\rm lin}}$. Finally, setting $\tilde{\lambda} = -\zeta^2$ and scaling $\tilde{\nu}_1 = \tilde{\nu}\zeta$ we find

$$\tilde{\nu}_1 = \pm\sqrt{\tilde{b}_2(-\zeta^2, \hat{c})} = \pm\gamma_{\rm lin}^{-1/2} + \mathcal{O}(|\zeta^2| + |\hat{c}|). \tag{4.4.20}$$

Unwinding all of these scalings gives two roots, $\hat{\nu}_{\rm cu}$ and $\hat{\nu}_{\rm cs}$, which are analytic on the Riemann surface defined by ζ, and satisfy

$$\mathrm{Re}\{\hat{\nu}_{\rm cs}\} < -\frac{b_1(-\zeta^2, \hat{c})}{2} < \mathrm{Re}\{\hat{\nu}_{\rm cu}\}, \quad \text{for all} \quad \zeta \notin S_{\rm abs} = \{\xi : \xi^2\,\tilde{b}_2(-\xi^2, \hat{c}) \in \mathbb{R}_-\},$$

where $\mathbb{R}_-$ is the non-positive part of the real line. This completes the proof of the lemma. ∎

We remark that the calculations of Lemma 4.4.2 imply that for all Λ small, the eigenvalues $\hat{\nu}_{\mathrm{s/u}}$ are bounded away from the imaginary axis, with real parts of opposite sign. The following lemma shows that $\Sigma^{+}_{\mathrm{abs}}$ is generic near the branch point $\lambda_{\mathrm{br}}(c)$ for all c near c_{lin}. The result of this lemma is the reducibility hypothesis in [127, §7]. Coupled with Lemma 4.4.1, this will imply that bifurcating spectra of L are only found near $\Sigma^{+}_{\mathrm{abs}}$.

Lemma 4.4.4. *Let $V \subset (\mathbb{C} - \Sigma_{\mathrm{ess}})$ be an open, bounded, and connected set containing the branch point $\lambda_{\mathrm{br}}(c)$ for all c close to c_{lin}. Given such a speed c, each $\lambda \in (\Sigma^{+}_{\mathrm{abs}} \cap V) \setminus \{\lambda_{\mathrm{br}}(c)\}$ satisfies the following:*

$$\nu_{\mathrm{i}_\infty}(\lambda) \neq \nu_{\mathrm{i}_\infty+1}(\lambda), \qquad \frac{d(\nu_{\mathrm{i}_\infty} - \nu_{\mathrm{i}_\infty+1})}{d\lambda} \neq 0. \tag{4.4.21}$$

Proof.

By definition, for any $\lambda \in \Sigma_{\mathrm{abs}} \cap V$ there exist $\nu \in \mathbb{C}$ and $\gamma \in \mathbb{R}$ such that

$$d_+(\lambda, \nu) = d_+(\lambda, \nu + \mathrm{i}\gamma) = 0.$$

Expanding from the branch point we find, after the change of variables $(\tilde{\lambda}, \tilde{\nu}) = (\lambda - \lambda_{\mathrm{br}}, \nu - \nu_{\mathrm{br}})$, that $\tilde{\lambda} + \lambda_{\mathrm{br}} \in \Sigma^{+}_{\mathrm{abs}}$ satisfies

$$\tilde{\lambda} = b\tilde{\nu}^2 + \mathcal{O}(\tilde{\lambda}\tilde{\nu}, \tilde{\lambda}^2, \tilde{\nu}^2), \tag{4.4.22}$$

$$\tilde{\lambda} = b(\tilde{\nu} + \mathrm{i}\gamma)^2 + \mathcal{O}(\tilde{\lambda}\tilde{\nu}, \tilde{\lambda}^2, \tilde{\nu}^2), \tag{4.4.23}$$

where $b \in \mathbb{C}$ is a non-zero constant. This implies that

$$\tilde{\nu} = -\frac{\gamma}{2}\mathrm{i} + \mathcal{O}(\gamma^2). \tag{4.4.24}$$

By substituting this into the first equation of (4.4.22) we then find

$$\tilde{\lambda} = -\frac{\gamma^2}{4} + \mathcal{O}(\gamma^3). \tag{4.4.25}$$

which implies for $0 < \tilde{\lambda} << 1$ that $\gamma \neq 0$ and

$$\frac{d(\tilde{\nu}_{\mathrm{i}_\infty} - \tilde{\nu}_{\mathrm{i}_\infty+1})}{d\tilde{\lambda}} \neq 0, \tag{4.4.26}$$

where i_∞ denotes the Morse index of the first order system corresponding to L_+, and counts the dimension of the unstable eigenspace as $\lambda \to \infty$. ■

4.4.5 Spatial dynamics near the branch point

Having collected spectral facts in Sections 4.4.2 - 4.4.4, we now are able to use spatial dynamics to characterize the first eigenvalue crossing and its corresponding eigenfunction. We construct eigenfunctions of L by conjugating with $\mathrm{e}^{\nu_{\mathrm{lin}} x}$ and solving the finite domain eigenvalue problem for $x \in [-\ell, \ell]$ subject to boundary conditions induced by the dynamics for $x \in \mathbb{R} \setminus [-\ell, \ell]$.

Inserting $u = \mathrm{e}^{\nu_{\mathrm{lin}} x}\tilde{u}$ into the eigenvalue equation $Lu = \lambda u$, dividing by $\mathrm{e}^{\nu_{\mathrm{lin}} x}$, and using the fact that $d_+(\lambda_{\mathrm{lin}}, \nu_{\mathrm{lin}}) = \frac{d}{d\nu} d_+(\lambda_{\mathrm{lin}}, \nu_{\mathrm{lin}}) = 0$, we obtain an equivalent eigenvalue equation which, when expressed in scaled variables, takes the form

$$\partial_x^4\tilde{u} + 4\nu_{\mathrm{lin}}\partial_x^3\tilde{u} + (\chi_+ + 6\nu_{\mathrm{lin}}^2)\partial_x^2\tilde{u} - \hat{c}\partial_x\tilde{u} + (\hat{\lambda} - \hat{c}\nu_{\mathrm{lin}})\tilde{u} = 0, \quad x \in [-\ell, \ell], \tag{4.4.27}$$

$$\partial_x^4\tilde{u} + 4\nu_{\mathrm{lin}}\partial_x^3\tilde{u} + (\chi_- + 6\nu_{\mathrm{lin}}^2)\partial_x^2\tilde{u} - (\hat{c} + 2(\delta\chi)\nu_{\mathrm{lin}})\partial_x\tilde{u} + (\hat{\lambda} - \hat{c}\nu_{\mathrm{lin}} - (\delta\chi)\nu_{\mathrm{lin}}^2)\tilde{u} = 0,$$
$$x \in \mathbb{R} \setminus [-\ell, \ell], \tag{4.4.28}$$

where $\delta\chi = \chi_- - \chi_+$. Using the coordinates of (4.4.5), these operators have the first order systems

$$\begin{aligned}
\tilde{u}_x &= \tilde{v} - \nu_{\mathrm{lin}}\tilde{u} \\
\tilde{v}_x &= \tilde{\theta} - \chi_\pm\tilde{u} - \nu_{\mathrm{lin}}\tilde{v} \\
\tilde{\theta}_x &= \tilde{w} - \nu_{\mathrm{lin}}\tilde{\theta} \\
\tilde{w}_x &= (c_{\mathrm{lin}} + \hat{c})\tilde{v} - (\lambda_{\mathrm{lin}} + \tilde{\lambda})\tilde{u} - \nu_{\mathrm{lin}}\tilde{w}.
\end{aligned} \tag{4.4.29}$$

If $\hat{\nu}_i^\pm$ are the eigenvalues for this system, ordered by decreasing real part, then the

corresponding eigenvectors take the form

$$\hat{e}_i^{\pm} = \left(1, \hat{\nu}_i^{\pm} + \nu_{\text{lin}}, (\hat{\nu}_i^{\pm} + \nu_{\text{lin}})^2 + \chi_{\pm}, (\hat{\nu}_i^{\pm} + \nu_{\text{lin}})\left((\hat{\nu}_i^{\pm} + \nu_{\text{lin}})^2 + \chi_{\pm}\right)\right)^T, \quad i = 1, 2, 3, 4.$$

Note, with χ_+ chosen, the eigenvalues of (4.4.29) are precisely the scaled spatial eigenvalues derived in Lemma 4.4.3 above. Also, for $\lambda + \hat{\lambda}_{\text{lin}} \in \mathbb{C} \setminus \Sigma_{\text{ess}}^-$, the subspaces $\hat{E}_-^{\text{s}} := \text{span}_{i=3,4}\{e_i^-\}$ and $\hat{E}_-^{\text{u}} := \text{span}_{i=1,2}\{e_i^-\}$ are the stable and unstable eigenspaces of (4.4.29) with χ_- chosen.

The boundary conditions at $x = \pm l$ for the eigenfunction are determined as follows. In order for $\tilde{u}$ to be an $L^2(\mathbb{R})$ eigenfunction, it is necessary and sufficient to require exponential decay as $|x| \to \infty$. Hence, for $\tilde{U} := (\tilde{u}, \tilde{v}, \tilde{\theta}, \tilde{w})^T$, we require

$$\tilde{U}(\ell) \in \tilde{E}_-^{\text{s}}, \qquad \tilde{U}(-\ell) \in \tilde{E}_-^{\text{u}}. \tag{4.4.30}$$

We note that the dimensions of the boundary spaces $\tilde{E}_-^{\text{s/u}}$ are the same as the corresponding subspaces for the unconjugated problem $L_- u = \lambda u$. This can be seen by homotoping the conjugation factor $\mathrm{e}^{\nu_{\text{lin}} s\, x}$ from $s = 0$ to $s = 1$ and noticing that the essential spectrum of L_- never intersects some sufficiently small neighborhood of λ_{lin}, implying that no spatial eigenvalue ν_i^- crosses the imaginary axis during this homotopy.

Finally, let $\tilde{E}_+^{\text{cs}}$ be the 2-dimensional eigenspace of (4.4.29) (with χ_+ chosen) spanned by the eigenvectors of $\hat{\nu}_{\text{cs}}$ and $\hat{\nu}_{\text{s}}$. Define $\tilde{E}_+^{\text{cu}}$ in the same way so that it is spanned by the eigenvectors associated with $\hat{\nu}_{\text{cu}}$ and $\hat{\nu}_{\text{u}}$. We remark that both of these subspaces are analytic in the Riemann surface variable ζ used in the proof of Lemma 4.4.3 and can be analytically continued as ζ approaches S_{abs}, also defined in the above proof.

With these definitions we obtain the following lemma which precludes embedded eigenvalues (see [126, §5.3]), and will be important in the construction of eigenfunctions.

Lemma 4.4.5. *(Non-Degenerate Boundary Conditions) For all Λ close to $(0, 0)$ with $\hat{\lambda} + \lambda_{\text{lin}} \notin \Sigma_{\text{abs}}$, the conjugated eigenspaces of $L_\pm$ satisfy*

$$\tilde{E}_-^{\text{u}} \pitchfork \tilde{E}_+^{\text{cs}} = \{0\}, \qquad \tilde{E}_-^{\text{s}} \pitchfork \tilde{E}_+^{\text{cu}} = \{0\}, \tag{4.4.31}$$

where $\pitchfork$ denotes the transverse intersection of linear subspaces.

Proof. This follows from Lemma 4.4.3 using similar arguments as in Lemma 4.4.1. ■

We are now able to state our existence result and give expansions for the first crossing eigenvalues and their eigenfunctions. This is done in the following proposition.

Proposition 4.4.6. *For $\ell > 0$ sufficiently large, there exists a speed $c_* > 0$ and simple eigenvalues $\lambda_*(c,\ell), \overline{\lambda_*(c,\ell)}$ of L with the following properties for $c \sim c_*$:*

(i) (First Crossing) *There exists some $\epsilon > 0$ so that for all $c > c_{\text{lin}} - \epsilon$, $\lambda_*(c_*,\ell)$ and $\overline{\lambda_*}(c_*,\ell)$ are the only eigenvalues lying in the closed right half-plane.*

(ii) (Bifurcation) *$\lambda_*(c,\ell)$ is an algebraically simple eigenvalue and satisfies*

$$\lambda_*(c_*,\ell) = \mathrm{i}\kappa_*(c_*,\ell), \quad \frac{d\mathrm{Re}\{\lambda_*\}}{dc}|_{c=c_*} < 0.$$

(iii) (Expansions) *For $\hat{c} \in \mathbb{R}$ and $\hat{\lambda} \in \mathrm{i}\mathbb{R}$, the crossing speed $c_*(\ell) = c_{\text{lin}} + \hat{c}$ and crossing location $\lambda_*(c_*,\ell) = \lambda_{\text{lin}} + \hat{\lambda}$ satisfy*

$$\hat{\lambda} = \mathrm{i}\frac{\pi^2}{4\mu_{\text{lin}}\ell^2}(-1+6(\mu_{\text{lin}}^2+\kappa_{\text{lin}}^2))+\mathcal{O}(\ell^{-3}), \qquad \hat{c} = -\frac{\pi^2}{4\mu_{\text{lin}}\ell^2}(1+6(\mu_{\text{lin}}^2-\kappa_{\text{lin}}^2))+\mathcal{O}(\ell^{-3}), \tag{4.4.32}$$

with $\kappa_{\text{lin}} := \mathrm{Im}\{\nu_{\text{lin}}\}$ and $\mu_{\text{lin}} := \mathrm{Re}\{\nu_{\text{lin}}\}$.

Associated with λ_*, L has an eigenfunction p and corresponding adjoint eigenfunction ψ, which satisfy the following properties:

(iv) For $x \in [-\ell,\ell]$,

$$p(x) = A\mathrm{e}^{(\nu_{\text{lin}}+\alpha(\ell))x}\left(\sin\left(\frac{\pi\,(x-\ell)}{2\ell}\right)+\mathcal{O}(\ell^{-1})\right), \tag{4.4.33}$$

$$\psi(x) = B\mathrm{e}^{-(\overline{\nu_{\text{lin}}+\alpha(\ell)})x}\left(\sin\left(\frac{\pi(x-\ell)}{2l}\right)+\mathcal{O}(\ell^{-1})\right). \tag{4.4.34}$$

Furthermore, for $j = 1,2,3$

$$\partial_x^j p(x) = (\nu_{\text{lin}}+\alpha(\ell))^j p(x) + \mathcal{O}(\ell^{-1}), \tag{4.4.35}$$

$$\partial_x^j \psi(x) = (\nu_{\text{lin}}+\alpha(\ell))^j \psi(x) + \mathcal{O}(\ell^{-1}). \tag{4.4.36}$$

Here the error terms are uniform in x, $\alpha(\ell) = \mathcal{O}(\ell^{-2})$, and $A, B > 0$ are undetermined normalization constants.

(v) Let $U_h := (h, h_x,\ h_{xx} + \chi_- h,\ h_{xxx} + (\chi_- h)_x)^T$ as in (4.4.5) above. Then for $h = p$ or $h = \psi$, there exists a constant $C > 0$, independent of ℓ such that,

$$|U_h(x)| \leq C\ell^{-1} \mathrm{e}^{-\mu_{\mathrm{lin}}\ell} \mathrm{e}^{\delta(x+\ell)}, \qquad x \leq -\ell, \tag{4.4.37}$$

$$|U_h(x)| \leq C\ell^{-1} \mathrm{e}^{\mu_{\mathrm{lin}}\ell} \mathrm{e}^{-\delta'(x-\ell)}, \qquad x \geq \ell, \tag{4.4.38}$$

with $\delta = |\mathrm{Re}\{\nu_2^-(\lambda_*)\}| > 0$, $\delta' = |\mathrm{Re}\{\nu_3^-(\lambda_*)\}| > 0$, and $\nu_i^-(\lambda)$ defined in (4.4.6) above.

Proof.

Existence of λ_* and properties (ii), (iii), and (iv) will all follow from our construction of a solution to the first order system associated with (4.4.27).

Property (i) follows using similar methods as in [127, §6] and the fact that $\lambda_{\mathrm{br}}(c)$ is the right-most part of Σ^+_{abs} for all c near c_*. In particular, for V as in Lemma 4.4.4, possibly enlarged to contain the positive real part of the sector which contains the spectrum of L, a construction similar to the following can be used to obtain that any $\lambda \in V$ not in a sufficiently small neighborhood of Σ^+_{abs} is not an eigenvalue.

Now let us begin our construction of the eigenfunctions on the interval $[-\ell, \ell]$. Since the construction of the adjoint eigenfunction ψ follows in the same way, we only describe how p is obtained. After an analytic change of variables, the first order system (4.4.29) can be split into hyperbolic and center dynamics as

$$\dot{W}_{\mathrm{h}} = \begin{pmatrix} \hat{\nu}_{\mathrm{s}} & 0 \\ 0 & \hat{\nu}_{\mathrm{u}} \end{pmatrix} W_{\mathrm{h}}, \tag{4.4.39}$$

$$\dot{W}_{\mathrm{c}} = \begin{pmatrix} \alpha & 1 \\ -\beta & \alpha \end{pmatrix} W_{\mathrm{c}}, \tag{4.4.40}$$

where $W := (W_{\mathrm{h}}, W_{\mathrm{c}})^T \in \mathbb{C}^2 \times \mathbb{C}^2$, and $\alpha = \alpha(\Lambda), \beta = \beta(\Lambda)$ are parameters, analytic in $(\hat{\lambda}, \hat{c})$, which unfold the two-dimensional Jordan block at $\Lambda = (0, 0)$; see [6], for instance. In fact, the leading order expansion of β is given in (4.4.18) and $\alpha = -b_1(\Lambda)/2$. This

can be seen by comparing the characteristic polynomial of the matrix on the right hand side of (4.4.40) to (4.4.14).

Next we study how the non-degeneracy conditions given by Lemma 4.4.5 affect the boundary conditions in (4.4.30). Since $\tilde{E}^+_{\mathrm{cs}} \oplus \tilde{E}^-_{\mathrm{cu}} = \mathbb{C}^4$, there exist linear transformations $T_\pm$ such that, for $W_{\mathrm{h}} = (w_{\mathrm{s}}, w_{\mathrm{u}})^T$ and $W_{\mathrm{c}} = (w_{\mathrm{c},0}, w_{\mathrm{c},1})^T$,

$$\begin{pmatrix} w_{\mathrm{s}}(-\ell) \\ w_{\mathrm{c},0}(-\ell) \end{pmatrix} = T_- \begin{pmatrix} w_{\mathrm{u}}(-\ell) \\ w_{\mathrm{c},1}(-\ell) \end{pmatrix}, \qquad \begin{pmatrix} w_{\mathrm{u}}(\ell) \\ w_{\mathrm{c},1}(\ell) \end{pmatrix} = T_+ \begin{pmatrix} w_{\mathrm{s}}(\ell) \\ w_{\mathrm{c},0}(\ell) \end{pmatrix}. \tag{4.4.41}$$

Then, given the flow $\Phi_{x,y}$ of the system (4.4.39) - (4.4.40), any solution must satisfy the matching condition $\Phi_{\ell,-\ell} W(-\ell) = W(\ell)$. Using a Lyapunov-Schmidt reduction (i.e. project onto the stable, unstable, and center subspaces) it can be obtained for some constants $c_1, c_2 \in \mathbb{C}$ that

$$w_{\mathrm{s}}(-\ell) = c_1 w_{\mathrm{c},0}(-\ell) + \mathcal{O}(\mathrm{e}^{-\delta\ell}), \quad w_{\mathrm{u}}(\ell) = c_2 w_{\mathrm{c},1}(\ell) + \mathcal{O}(\mathrm{e}^{-\delta\ell}), \tag{4.4.42}$$

from which boundary conditions on $w_{\mathrm{u}}(-\ell)$ and $w_{\mathrm{s}}(-\ell)$ can be determined via (4.4.41). The solvability of this reduction follows from Lemma 4.4.5.

Furthermore, we readily obtain

$$|W_{\mathrm{h}}(\pm\ell)| \leq C|W_{\mathrm{c}}(\pm\ell)| + \mathcal{O}(\mathrm{e}^{-\delta\ell}), \tag{4.4.43}$$

for some $\tilde{\delta} > 0$ dependent on $\hat{\nu}_{\mathrm{s}}$ and $\hat{\nu}_{\mathrm{u}}$. The boundary conditions for $W_{\mathrm{c}}(\pm\ell)$ can then be obtained from this reduction and can be found to be independent of $W_{\mathrm{h}}(\pm\ell)$ up to an $\mathcal{O}(\mathrm{e}^{-\tilde{\delta}\ell})$ correction.

We now construct solutions to the center system (4.4.40). We make the scalings $x = \tilde{x} - \ell$, $W_{\mathrm{c}} = \mathrm{e}^{\alpha\tilde{x}}\tilde{W}_{\mathrm{c}}$, and define $\mu^2 = -\beta$ so that (4.4.40) becomes

$$\tilde{W}_{\mathrm{c}}' = \begin{pmatrix} 0 & 1 \\ -\mu^2 & 0 \end{pmatrix} \tilde{W}_{\mathrm{c}}. \tag{4.4.44}$$

In order to ease the derivation, the boundary conditions on the center system may, up

to an $\mathcal{O}(\mathrm{e}^{-\delta\ell})$ correction, be written as

$$\begin{pmatrix} -1 \\ r_+ \end{pmatrix}^T \tilde{W}_{\mathrm{c}}(2\ell) = 0, \qquad \begin{pmatrix} -1 \\ r_- \end{pmatrix}^T \tilde{W}_{\mathrm{c}}(0) = 0,$$

for some $r_\pm \in \mathbb{C}$ which depend analytically on μ.

Under these conditions, the system (4.4.44) has the solution, $\tilde{W}_{\mathrm{c},*}$, with first component $w(\tilde{x}) = A(\sin(\mu x) + r_-\mu\cos(\mu x))$, where μ must satisfy the equation

$$\frac{\tan(2\mu\ell)}{2\mu\ell} = \frac{(r_+ - r_-)}{2\ell(1 + r_-\, r_+\mu^2)}. \tag{4.4.45}$$

For l large, this equation has the solutions $\mu = \frac{\pi k}{2\ell} + \mathcal{O}(\ell^{-2})$ for integers $k \neq 0$. To obtain the first eigenvalue crossing, we set $\mu = \frac{\pi}{2\ell}$ so that

$$\tilde{W}_{\mathrm{c},*}(\tilde{x}) = A \begin{pmatrix} \sin(\frac{\pi\tilde{x}}{2\ell}) \\ \frac{\pi}{2\ell}\cos(\frac{\pi\tilde{x}}{2\ell}) \end{pmatrix} + \mathcal{O}(\ell^{-1}),$$

with error term uniform in x.

Recalling that $\mu^2 = -\beta$, we have

$$\frac{\pi^2}{4\ell^2} = -\beta(\Lambda) = \frac{1}{\gamma_{\mathrm{lin}}}(\hat{\lambda} - \nu_{\mathrm{lin}}\hat{c}) + \mathcal{O}(|\Lambda|^2),$$

which can then be solved for $\hat{\lambda} \in \mathrm{i}\mathbb{R}$ and $\hat{c} \in \mathbb{R}$ to obtain the expressions in (4.4.32) as desired. Inserting these expressions into the conjugating exponent α, we find it has the asymptotics

$$\alpha(\ell) = -\frac{b_1(\Lambda)}{2} = \mathcal{O}(\ell^{-2}).$$

The eigenfunction p given in the statement of the proposition can then be obtained by unwinding all the scalings made above.

To obtain the decay conditions in (v), we notice that $|\tilde{W}_{\mathrm{c},*}(0)|, |\tilde{W}_{\mathrm{c},*}(2\ell)| \leq C' l^{-1}$ and thus, given the estimates (4.4.43), for $h = \psi, p$ and some constant $C' > 0$,

$$|U_h(\pm l)| \leq C'\ell^{-1}\mathrm{e}^{\pm\mu_{\mathrm{lin}}\ell}.$$

The boundary conditions (4.4.30) then give the estimates (4.4.37) and (4.4.38) above.

■

Remark 4.4.7. *The leading order term in the expansions for the Hopf crossing location* λ_* *and speed* c_* *in* (4.4.32) *were compared with numerical calculations of the spectrum of* L *and were found to be in excellent agreement. In particular, the operator* L *was discretized using fourth-order accurate centered finite differences with discretization size* $\Delta x = 0.05$ *on a domain of length* 400*. Hopf eigenvalues* $\lambda_{*,\text{num}}$ *and approximate crossing speed* $c_{*,\text{num}}$ *were found numerically using the built-in eigenvalue solver "*eigs*" in MATLAB. The errors between each of the leading order terms of* $\hat{\lambda}(\ell)$ *and* $\hat{c}(\ell)$*, and those of* $\lambda_{*,\text{num}} - \lambda_{\text{lin}}$ *and* $c_{*,\text{num}} - c_{\text{lin}}$ *were respectively found to converge with rate* $\mathcal{O}(\ell^{-3})$ *as* ℓ *was varied between* $\ell = 10$ *and* $\ell = 150$*.*

Remark 4.4.8. *We note that the above result could also be obtained via a similar, and in some sense equivalent, geometric singular perturbation method. If* $\hat{\lambda}$ *and* $\hat{c}$ *are scaled by* $\epsilon = \ell^{-2}$*, one obtains a slow equation which is equivalent to a heat equation. Furthermore for* $\epsilon = 0$ *the boundary conditions for a solution on the slow manifold reduce to Dirichlet conditions. By solving this system, the same leading order expansions for the eigenfunction, and eigenvalue-front speed pair* (λ_*, c_*) *may be obtained.*

4.4.6 Nonlinear Hopf bifurcation — direction of branching

We are now able to state our main result of this section which gives the existence of bifurcated solutions and determines the direction of bifurcation in terms of the the cubic nonlinearity parameter γ.

Theorem 4.4.4. *For* f *and* u_* *described above and* $\ell > 0$ *sufficiently large, the results of Theorem 4.1.3 hold and the direction of bifurcation is given by*

$$\operatorname{sign}[\theta_+] = -\operatorname{sign}\gamma. \tag{4.4.46}$$

Proof. Using Proposition 4.4.6, it is readily checked that Hypotheses 4.1.6, 4.1.8, and 4.1.9 are all satisfied. The existence of a Hopf bifurcation then follows by applying Theorem 4.1.3.

All that is left is to determine the sign of θ_+. In order to facilitate this determination, let p and ψ be as given in Proposition 4.4.6 with normalization constants A, B such that $A^3B = \mathrm{e}^{2\mu_{\mathrm{lin}}\ell}$. Since the first order system vector U_p decays exponentially fast outside the unstable interval, $(-\ell, \ell)$, the estimates (4.4.37), (4.4.38) in Proposition 4.4.6 give

$$\theta_+ = \int_{-\ell}^{\ell} \left(3\partial_u^3 f(x, u_*(x))p(x)^2\overline{p(x)}\right)_{xx} \overline{\psi(x)} + \mathcal{O}(\ell^{-4}). \tag{4.4.47}$$

The form of the solution $\tilde{W}_{\mathrm{c},*}$ found in the proof of Proposition 4.4.6 gives

$$\begin{aligned}\int_{-\ell}^{\ell} \left(3\partial_u^3 f(x, u_*(x))p(x)^2\overline{p(x)}\right)_{xx} \overline{\psi(x)}\, dx = \\ 18\gamma A^3 B \int_{-\ell}^{\ell} \mathrm{e}^{2\mu_{\mathrm{lin}}x} \left[(2\nu + \overline{\nu})^2 \sin^4\left(\frac{\pi(x-\ell)}{2\ell}\right) + \mathcal{O}(\ell^{-l})\right] dx \\ = -\frac{27\gamma(2\nu_{\mathrm{lin}} + \overline{\nu_{\mathrm{lin}}})^2}{8\mu_{\mathrm{lin}}} + \mathcal{O}(\ell^{-1}).\end{aligned} \tag{4.4.48}$$

Thus, for $\ell > 0$ sufficiently large,

$$\begin{aligned}\operatorname{sign}\left[\operatorname{Re}\theta_+\right] &= -\operatorname{sign}\left[\operatorname{Re}\frac{27\gamma(2\nu_{\mathrm{lin}} + \overline{\nu_{\mathrm{lin}}})^2}{8\mu_{\mathrm{lin}}}\right] \\ &= \operatorname{sign}\left[\operatorname{Re}\gamma\,(2\nu_{\mathrm{lin}} + \overline{\nu_{\mathrm{lin}}})^2\right] = \operatorname{sign}\left[\gamma\,(9\mu_{\mathrm{lin}}^2 - \kappa_{\mathrm{lin}}^2)\right] \\ &= -\operatorname{sign}\gamma\end{aligned} \tag{4.4.49}$$

where the expressions given in Lemma 4.4.2 are used in the last two lines.

■

Remark 4.4.9. *Since the argument of ν_{lin}, and hence the sign of $9\mu_{\mathrm{lin}}^2 - \kappa_{\mathrm{lin}}^2$, is invariant with respect to changes in the value of $f'(\alpha)$ for α near zero, the sign of $9\mu_{\mathrm{lin}}^2 - \kappa_{\mathrm{lin}}^2$ will remain constant when our equation is linearized about a front $u_* \equiv \alpha$.*

Remark 4.4.10. *We note that since λ_{lin} is an accumulation point of the eigenvalues of L as $l \to \infty$ successive Hopf bifurcations will rapidly occur as c is decreased below c_{lin}.*

Remark 4.4.11. *The findings of Theorem 4.4.4 are in agreement with numerical simulations, where supercritical behavior was found for $\gamma < 0$ and subcritical behavior was*

found for $\gamma > 0$. In the latter case, for c slightly larger than c_*, we also observed hysteretic behavior between the front u_* and a bifurcating periodic pattern. This region of bistable, hysteretic behavior should, in principle, be able to be determined by finding higher order coefficients in the bifurcation equation. We also note that the wavenumber of the periodic pattern was different than that predicted by the linearized equation, indicating that such solutions should be related to pushed fronts.

4.5 Discussion

Our methods should be applicable in many different settings. First of all, the existence result for viscous shocks in [135] can readily be obtained (and shortened significantly) with a nearly direct translation of our approach; see Appendix 4.7 for more detail. Also, problems with more general u-dependent source terms which are still exponentially localized in space could also be treated using our method. With such a source, the corresponding nonlinear solution operator $\mathcal{F}$ would lose its conservation form. Since the codomain cannot be restricted as above, the method described in Remark 4.3.2 must be employed to obtain a Fredholm index 0 operator. One such area where these source terms appear is in the equations governing the propagation of oscillatory detonation waves. Here an ignition function, dependent on the characteristics of the gas, controls the reaction terms in the equation which feed the combustion; see [150]. These sources also arise in certain forms of the chemotaxis equation where the aggregation of bacteria depends nonlinearly on the density of bacteria (in addition to the gradient of the chemoattractant); see [110].

Furthermore, our method could possibly be used to study problems with spatial dimension larger than one. In particular, for systems whose spatial domain is an infinite cylinder, one could imagine that Fredholm properties could be established using exponentially weighted spaces and a closed range lemma, while the index could be determined via a spectral flow. This would then allow one to perform a Lyapunov-Schmidt reduction to obtain a bifurcation equation for transverse modes. Such an abstract functional analytic method would hopefully be simpler than the spatial dynamics formulations developed in [114] and subsequent works, and the diffusive stability approach used by

[117].

4.6 Existence of trigger fronts

In this appendix we give the outline of a proof for the existence of trigger fronts in the case where the nonlinearity satisfies certain coercivity conditions. Such conditions are satisfied by many typical nonlinearities, including the polynomial cases such as $f(u) = u - u^3$ and $f(u) = u + u^3 - u^5$.

Theorem 4.6.5. *Let Hypotheses 4.1.1 and 4.1.2 from above hold, and assume the following coercivity conditions on the nonlinearity f and $p \geq 3$, odd,*

(i) For some $C > 0$, $-uf(x,u) \geq C(u^{p+1} - 1)$ uniformly in x.

(ii) For each $\delta > 0$, there exists a constant $C'(\delta) > 0$ such that $|f(x,u)| \leq C\delta|u|^{p+1} + C'(\delta)$ uniformly in x.

Then there exists a front solution u_* of the traveling-wave equation (4.1.1)*, satisfying Hypothesis 4.1.5.*

Proof. The construction is based on ideas from [139]. We integrate the traveling-wave equation

$$-(u_{xx} + f(x,u))_{xx} + cu_x + c\chi(x) = 0,$$

and find

$$-(u_{xx} + f(x,u))_x + c(u + H(\xi) - u_+) = 0,$$

where $H(x) = \int_\infty^x \chi(\zeta)\mathrm{d}\zeta$, so that $H(+\infty) = 0$ and $H(-\infty) = u_- - u_+$.
We then write the equation as a first-order system,

$$\begin{aligned} u_x &= v \\ v_x &= -f(x,u) + \theta \\ \theta_x &= c(u + H - u_+). \end{aligned} \tag{4.6.1}$$

We consider the set of bounded solutions $\mathcal{A}$ to this equation, and claim that $\mathcal{A}$ is bounded, uniformly with respect to $|H|_\infty$ and u_+, for fixed $c > 0$. Consider the functions

$$E_\pm(u, v, \theta) = \frac{1}{2}v^2 - F_\pm - \theta(u + H(\pm\infty) - u_+), \qquad F'_\pm(u) = f_\pm(u).$$

A direct calculation shows that

$$\frac{\mathrm{d}E_\pm}{\mathrm{d}x} = -c(u + H(\pm\infty) - u_+)^2,$$

so that $E_\pm$ is a strict Lyapunov function for the systems where $H \equiv H(\pm\infty)$ respectively. We compactify time in (4.6.1), using for instance $y_x = \gamma(1 - y^2)$ with solution $y(x) = \tanh(\gamma x)$ and $0 < \gamma \ll 1$. For γ sufficiently small we can extend

$$\tilde{H}(y) := H(\delta^{-1}\operatorname{arctanh}(y)), \qquad \tilde{f}(y, u) := f(\delta^{-1}\operatorname{arctanh}(y), u)$$

smoothly to $|y| \geq 1$, obtaining an extended, autonomous equation which possesses an isolated invariant set consisting of all bounded solutions.

Since $E_\pm$ is a Lyapunov function on the flow restricted to the subspaces $\{y = \pm 1\}$, the set of accumulation points of these restricted flows consists only of the equilibria $U_\pm = (u_\pm, 0, f_\pm(u_\pm), \pm 1)^T$ respectively. Then because the y-flow is monotone from $y = -1$ to $y = 1$, the chain-recurrent set of the extended flow is contained in the subspaces $\{y = \pm 1\}$. Using the fact that omega limit sets are contained in the chain-recurrent set, we obtain that all bounded solutions are heteroclinic orbits connecting $U_\pm$. A direct calculation then shows that both of these equilibria are saddles, with one-dimensional unstable and two-dimensional stable manifolds in the subspaces $\{y = \pm 1\}$, respectively. We will show below that the set of such heteroclinic orbits is a priori bounded in terms of $|H|_\infty$ and u_+, for fixed $c > 0$.

Given those a priori bounds, one can then readily conclude the existence of heteroclinics by studying the Conley index of $\mathcal{A}$. By employing a homotopy to a spatially independent nonlinearity $\tilde{f}(u) = -u - u^p$ and then to a monotone flow $y_x = -\delta(1 + y^2)$, it can readily be seen that the Conley index of $\mathcal{A}$ is trivial. Finally, if the set of heteroclinics were empty, the Conley index of $\mathcal{A}$ would be the direct sum of the Conley indices of the two hyperbolic equilibria at $y = \pm 1$, thus giving a contradiction.

To establish a priori estimates, we rewrite the first-order system (4.6.1) as an equation in θ,

$$\begin{aligned}\theta_x &= w\\ w_x &= \rho\\ \rho_x &= c\left(-f(\frac{w}{c} - H + u_+) + \theta\right) + cH''.\end{aligned} \tag{4.6.2}$$

Here, $w = c(u + H - u_+)$, and $\rho = c(v + H')$. The equivalent higher-order system is

$$\theta_{xxx} = c\left(-f(\frac{\theta_x}{c} - H + u_+) + \theta + H''\right).$$

Multiplying by θ_x and integrating in x now gives

$$-\int \theta_{xx}^2 \mathrm{d}x = -c\int \theta_x\left(f(\frac{\theta_x}{c} - H + u_+) + H''\right)\mathrm{d}x - \frac{c}{2}\,\theta^2\big|_{\pm\infty}.$$

Using the boundedness of the solutions and the assumptions on f with $\delta > 0$ sufficiently small, one readily concludes,

$$\int (\theta_{xx}^2 + \theta_x^{p+1})\mathrm{d}x \le C'(1 + \theta^2\big|_{\pm\infty}),$$

where C' possibly depends on $|H|_\infty$, c, and $u_\pm$. This gives bounds on u in L^∞, which one can easily use in the third-order equation for u to bootstrap to BC^k-uniform bounds for any finite k.

■

4.7 Hopf bifurcation in viscous shocks

In this section we show how our functional analytic method can significantly shorten the existence of bifurcation proof in [135]. We briefly recount the setup and hypotheses given there.

For smooth $f : \mathbb{R}^n \to \mathbb{R}^n$ and $n \in \mathbb{N}$, consider the viscous conservation law in a co-moving frame of speed of c,

$$u_t = \left[u_x + cu - f(u)\right]_x, \qquad x \in \mathbb{R},\, u \in \mathbb{R}^n. \tag{4.7.1}$$

and viscous-shock solutions $q^\epsilon(x)$ which satisfy

$$\lim_{x \to \pm\infty} q^\epsilon(x) = u^\epsilon_\pm,$$

for smooth curves $u^\epsilon_\pm$ in $\mathbb{R}^n$ which are defined for $\epsilon \in \mathbb{R}$ near zero. Such solutions must satisfy the integrated steady-state equation

$$u_x = \left[f(u) - f(u^\epsilon_-)\right] - c^\epsilon[u - u^\epsilon_-], \tag{4.7.2}$$

where c^ϵ is a family of speeds satisfying the Rankine-Hugoniot condition,

$$c^\epsilon = \frac{f_j(u^\epsilon_+) - f_j(u^\epsilon_-)}{u^\epsilon_{+,j} - u^\epsilon_{-,j}}, \quad j = 1, ..., n.$$

In other words, $q_\epsilon(x)$ lies in the intersection of the unstable manifold $W^{\mathrm{u}}_-(\epsilon)$ of u^ϵ_- and the stable manifold $W^{\mathrm{s}}_+(\epsilon)$ of u^ϵ_+.

Next, we assume that these solutions are Lax shocks:

Hypothesis 4.7.1. *For some $p = 0, ..., n-1$, let $u^\epsilon_\pm$ and q^ϵ satisfy the following,*

(i) $\dim W^{\mathrm{u}}_-(0) = p + 1, \quad \dim W^{\mathrm{s}}_+(0) = n - p.$

(ii) (transversality) The intersection $W^{\mathrm{u}}_-(0) \cap W^{\mathrm{s}}_+(0)$ is transverse along q^0.

(iii) (strict hyperbolicity) The Jacobian $f_u(u^0_\pm)$ has real and distinct eigenvalues.

From this it readily follows that q^ϵ and c^ϵ are smooth in ϵ. This remark and the above hypothesis also give exponential decay estimates analogous to those in Hypothesis 4.1.5 with decay rate $0 < \gamma < \min |\nu^\pm_j|$ where the $\nu^\pm_j$ correspond to the ingoing characteristics. In other words, ν^-_j ranges over the $p+1$ eigenvalues of (4.7.2) corresponding to $W^{\mathrm{u}}_-(0)$ and ν^+_j ranges over the $n-p$ eigenvalues corresponding to $W^{\mathrm{s}}_+(0)$. Next, the operator

$L^\epsilon := \partial_x \left[\partial_x + c^\epsilon - f_u(q^\epsilon(x))\right]$ is a closed, densely defined operator on $L^2(\mathbb{R}, \mathbb{R}^n)$. It is readily seen that the essential spectrum lies in the closed left-half plane only touching the imaginary axis at $0 \in \mathbb{C}$. Furthermore, since there is a spatial translation symmetry, an embedded eigenvalue lies at 0 which is simple due to the transversality assumption.

We also assume a simple Hopf-crossing in the same way as in Hypothesis 4.1.8 and 4.1.9 above:

Hypothesis 4.7.2. *The point spectrum of L^ϵ lies in the open left half-plane, bounded away from the imaginary axis, except for an isolated pair of algebraically simple eigenvalues $\lambda(\epsilon) = \mu(\epsilon) \pm \mathrm{i}\kappa(\epsilon)$ which satisfy*

$$\mu(0) = 0, \quad \kappa(0) = \mathrm{i}\omega_*, \quad \mu'(0) > 0,$$

and have $L^2(\mathbb{R}, \mathbb{R}^n)$-eigenfunctions $p(x), \overline{p}(x)$ for $\epsilon = 0$.

This hypothesis, along with the statement about the essential spectrum above gives the absence of resonances as in Hypothesis 4.1.9 above. Once again denote the corresponding adjoint eigenfunctions as $\psi(x), \overline{\psi}(x)$ normalized as before. We define our function spaces as

$$X = L^2(\mathbb{T}, \mathbb{R}^n),\ Y = H^1(\mathbb{T}, \mathbb{R}^n), \qquad \mathcal{X} = L^2_\eta(\mathbb{R}, X),\ \mathcal{Y} = L^2_\eta(\mathbb{R}, Y) \cap H^2_\eta(\mathbb{R}, X),$$

with $\eta > 0$ sufficiently small.

We can then define the nonlinear operator $\mathcal{F} : \mathcal{Y} \times \mathbb{R}^2 \to \mathcal{X}$ and its linearization $\mathcal{L} : \mathcal{Y} \subset \mathcal{X} \to \mathcal{X}$ about $(v; \omega, \epsilon) = (0; \omega_*, 0)$ as

$$\begin{aligned}
\mathcal{F} : (v; \omega, \epsilon) &\longmapsto \omega v_\tau - \left(v_x + c^\epsilon v + g(x, v; c)\right)_x, \\
g(x, v; \epsilon) &:= f(q^\epsilon(x) + v) - f(q^\epsilon(x)), \qquad \tau = \omega t, \qquad (4.7.3) \\
\mathcal{L} : v &\mapsto \omega_* \partial_\tau v - L^0 v = \omega_* \partial_\tau v - \partial_x \left[\partial_x v + c^0 v - f_u(q^0(x)) v\right]. \qquad (4.7.4)
\end{aligned}$$

We may then obtain the following proposition

Proposition 4.7.3. *Assuming Hypotheses 4.7.1 and 4.7.2, the operator $\mathcal{L} : \mathcal{Y} \subset \mathcal{X} \to \mathcal{X}$ is Fredholm.*

Proof. Given the exponential decay of q^0 and its derivatives as $x \to \pm\infty$, this follows by similar estimates as in Section 4.2.1 above. ■

Lemma 4.7.4. *The operator $\mathcal{L}$ has Fredholm index $1-n$.*

Proof. We once again decompose the space $\mathcal{X} = \mathcal{X}^0 \oplus \mathcal{X}_{\mathrm{h}}$ as in the discussion above Lemma 4.2.4 and 4.2.5.

On $\mathcal{X}^0$we have $\mathcal{L} = -L^0 = \partial_x \circ \tilde{L}$ with $\tilde{L}v := \partial_x v + c^0 v + f_u(q^0)v$. It then follows from Hypothesis 4.7.1 that $\tilde{L}$ restricted to $\mathcal{X}^0$ has Fredholm index 1. Furthermore, since we are working in exponentially weighted spaces, ∂_x has Fredholm index $-n$. Combining these two facts, we have that $\mathcal{L}$ has index $1-n$ on $\mathcal{X}^0$.

Then, by a similar argument as in the proof of Lemma 4.2.5, we find that $\mathcal{L}_k := \mathcal{L} : \mathcal{Y}^k \subset \mathcal{X}^k \to \mathcal{X}^k$ satisfies $\dim\ker\mathcal{L}_k = \dim\ker\mathcal{L}_k^* = 0$ for $k \neq \pm 0, 1$ and $\dim\ker\mathcal{L}_k = \dim\ker\mathcal{L}_k^* = 1$ for $k = \pm 1$. This once again implies that $\mathcal{L}_{\mathrm{h}}$ has index 0 and thus gives the result. ■

Next we define $\mathring{\mathcal{X}} = \{u \in \mathcal{X} : \left\langle u, \mathrm{e}^{-2\eta\langle x\rangle} r \right\rangle,\ \forall r \in \mathbb{R}^n\}$. Then, since $\mathrm{e}^{-2\eta\langle x\rangle} r$ lies in the cokernel of $\mathcal{L}$ for all $r \in \mathbb{R}^n$, we find that $\mathcal{L}$ maps $\mathcal{Y}$ into $\mathring{\mathcal{X}}$ and obtain the following corollary to Lemma 4.7.4

Corollary 4.7.5. *The operator $\mathcal{L} : \mathcal{Y} \to \mathring{\mathcal{X}}$ has Fredholm index 1.*

Proof. This follows from the fact that the orthogonal projection $\mathcal{S} : \mathcal{X} \to \mathring{\mathcal{X}}$ has Fredholm index n. ■

Combining this all together, we obtain the following result which is equivalent to Theorem 1 of [135].

Theorem 4.7.6. *Given Hypotheses 4.7.1 and 4.7.2, there exists a 1-parameter family of time-periodic solutions of* (4.7.1)*, unique up to spatial translates, which bifurcate from the shock solutions $q^\epsilon(x)$ as ϵ is varied through* 0*. The solution branch $(u, \omega, \epsilon) \in \left(q^\epsilon + H^2(\mathbb{R}, L^2(\mathbb{T}))\right) \times \mathbb{R}^2$ can be parameterized by $r \geq 0$, the amplitude of oscillations. More precisely, there exists $r_* > 0$ and smooth functions Υ_j, $j \in \{\omega, \epsilon, u\}$, defined for*

$|r| < r_*$, $\Upsilon_j(0) = 0$, *so that*

$$\epsilon = \Upsilon_\epsilon(r^2), \quad \omega = \omega_* + \Upsilon_\omega(r^2), \quad u = q^\epsilon + \Upsilon_u(r),$$

with expansions

$$\begin{aligned} \Upsilon_\epsilon(r^2) &= \frac{\operatorname{Re}\{\theta_+\}}{\mu'(0)} r^2 + \mathcal{O}(r^4), \qquad \Upsilon_\omega(r^2) = \operatorname{Im}\{\theta_+\}|r|^2 + \mathcal{O}(|r|^4), \\ \Upsilon_u(r) &= rp\cos(\omega t) + \mathcal{O}(r^2), \end{aligned} \tag{4.7.5}$$

where θ_+ *satisfies* (4.7.10) *below.*

Proof. First we see that the restricted operator $\mathcal{L} : \mathcal{Y} \to \mathring{\mathcal{X}}$ has 3-dimensional kernel spanned by

$$P_+ = \mathrm{e}^{\mathrm{i}\tau} p(x), \quad P_- = \overline{P_+}, \quad P_0 = \partial_x q^0(x),$$

where $\partial_x q^0$ is the exponentially localized translational mode and spans the eigenspace corresponding to the embedded eigenvalue 0 of L.

This implies that $\mathcal{L}$ has 2-dimensional cokernel and is thus spanned by

$$\Psi_+ = \mathrm{e}^{\mathrm{i}\tau}\psi, \quad \Psi_- = \overline{\Psi_+}.$$

We coordinatize elements $u_0 \in \ker \mathcal{L}$ using

$$u_0 = aP_+ + \overline{a}P_- + bP_0, \quad (a, b) \in \mathbb{C} \times \mathbb{R}.$$

The rest of the proof follows in a similar manner as in Section 4.3 where the only alteration is that the coordinate $b \in \mathbb{R}$ corresponding to the extra dimension in the kernel must be treated as a parameter which, as we shall see below, parameterizes the translational shifts of solutions.

Defining $\Omega := (\omega - \omega_*, \epsilon)$ and the projections $\mathcal{Q} : \mathring{X} \to \ker \mathcal{L}^*$, $\mathcal{P} := I - \mathcal{Q} : \mathring{X} \to (\operatorname{span}\{\Psi_i\})^\perp$ as before, we can then solve the "auxiliary" equation analogous to (4.3.3). We obtain a smooth solution $\varphi : \ker \mathcal{L} \times \mathbb{R}^2 \to (\ker \mathcal{L})^\perp$ which is a function of (a, b, Ω) and satisfies $\varphi(0; \Omega) = D_{u_0}\varphi|_{(0,\Omega)} = 0$ for Ω sufficiently small. Fixing $b = 0$, we then

obtain

$$\varphi(a,\overline{a},0;\Omega) = a^2\mathrm{e}^{2\mathrm{i}t}\varphi_+(x;\Omega) + a\overline{a}\varphi_0(x;\Omega) + \overline{a}^2\mathrm{e}^{-2\mathrm{i}t}\varphi_-(x;\Omega) + \mathcal{O}(|a|^3),$$

where φ_i satisfy

$$\begin{aligned}\mathcal{L}(\mathrm{e}^{2\mathrm{i}t}\varphi_+) &= \mathrm{e}^{2\mathrm{i}t}(f_{uu}(q^\epsilon(x))[p,p])_x,\\ \mathcal{L}(\varphi_0) &= (f_{uu}(q^\epsilon(x))[p,\overline{p}])_x,\\ \mathcal{L}(\mathrm{e}^{-2\mathrm{i}t}\varphi_-) &= \mathrm{e}^{-2\mathrm{i}t}(f_{uu}(q^\epsilon(x))[\overline{p},\overline{p}])_x. \end{aligned} \tag{4.7.6}$$

Next, we obtain the same expansion for φ and the expanded bifurcation equations

$$\Phi_+(a,\overline{a};\Omega) = (\lambda_\epsilon(0)\epsilon + \mathrm{i}\,\tilde{\omega})\,a + \,\theta_+(0,0)\,a|a|^2 + \mathcal{O}\left((|\Omega|+|a|^2)|a||\Omega| + |a|^4\right), \tag{4.7.7}$$

$$\Phi_-(a,\overline{a};\Omega) = \left(\overline{\lambda_\epsilon}(0)\,\epsilon - \mathrm{i}\tilde{\omega}\right)\overline{a} + \,\theta_-(0,0)\,\overline{a}|a|^2 + \mathcal{O}\left((|\Omega|+|a|^2)|a||\Omega| + |a|^4\right), \tag{4.7.8}$$

where

$$\theta_+(\tilde{\omega},\epsilon) = \left\langle \Big(3f_{uuu}(q^\epsilon(x))[p,p,\overline{p}] + f_{uu}(q^\epsilon(x))\left([p,\varphi_0] + [\overline{p},\varphi_+]\right)\Big)_x, \psi\right\rangle_{L^2_\eta(\mathbb{R})}, \tag{4.7.9}$$

$$\theta_-(\tilde{\omega},\epsilon) = \left\langle \Big(3f_{uuu}(q^\epsilon(x))[p,\overline{p},\overline{p}] + f_{uu}(q^\epsilon(x))\left([p,\varphi_-] + [\overline{p},\varphi_0]\right)\Big)_x, \overline{\psi}\right\rangle_{L^2_\eta(\mathbb{R})}. \tag{4.7.10}$$

After once again factoring out the dependence on a using the time-shift symmetry, we use the assumption that $\operatorname{Re}\lambda_\epsilon(0) = \mu'(0) \neq 0$ to obtain a unique 1-parameter family of solutions $(\tilde{\omega},\epsilon)(|a|^2)$.

Then since $\mathcal{F}$ is equivariant with respect to the spatial translation symmetry, the uniqueness of the implicit solution φ gives that the family of solution branches obtained when b varies near 0 are in fact the spatial translates.

■

Remark 4.7.6. *We note that one could also deal with the translational mode and the extra dimension it adds to* $\ker\mathcal{L}$ *by imposing a phase condition such as* $\langle u, q^0_x\rangle = 0$ *on the domain of* $\mathcal{L}$*. This would in effect pin fronts down, getting rid of spatial translates.*

Remark 4.7.7. *Along the lines of Remark 4.3.2, we could alternatively study the original linearization $\mathcal{L} : \mathcal{Y} \to \mathcal{X}$ with index $1-n$ and obtain an index-0 operator by inserting into $\mathcal{F}$ the ansatz*

$$u(x) = \sum b_j^{\pm} e_j^{\pm} \chi_{\pm}(x) + w(x),$$

where $\chi_{\pm}(x) = (1 \pm \tanh(x))/2$, $w \in \mathcal{X}$, $b_j^{\pm}$ are real parameters, and $e_j^{\pm}$ are the eigenvectors of $f_u(u_{\pm})$ corresponding to the $n-1$ outgoing characteristics $\nu_j^{\pm} \gtrless 0$ (this requires the $e_j^{\pm}$ to be linearly independent). This allows the outgoing characteristics to vary in the modulated front. We also remark that this technique should allow for the study of under- and overcompressive shocks. Denoting i as the number of incoming characteristics, $\mathcal{L}$ would then have Fredholm index $i - 2n$. By fixing ingoing characteristics and allowing outgoing characteristics to vary, one obtains a linearization about the shock with index 0. In a slightly different direction, one can also consider systems with reactive variables, in which case it may be more appropriate to include the wave speed c as a free parameter in order to compensate for a cokernel associated with translational invariance. Such scenarios are very intriguing and would provide an interesting avenue of research in the future.

References

[1] H. Amann, *Linear and Quasilinear Parabolic Problems: Volume I: Abstract Linear Theory*, vol. 1, Springer, 1995.

[2] A. Aotani, M. Mimura, and M. Mollee, *A model aided understanding of spot pattern formation in chemotactic e. coli colonies.*, Japan J. Ind. Appl. Math., 27 (2010), pp. 5–22.

[3] I. S. Aranson and L. Kramer, *The world of the complex ginzburg-landau equation*, Reviews of Modern Physics, 74 (2002), p. 99.

[4] A. J. Archer, M. Walters, U. Thiele, and E. Knobloch, *Solidification in soft-core fluids: Disordered solids from fast solidification fronts*, Physical Review E, 90 (2014), p. 042404.

[5] W. Arendt and S. Bu, *Fourier series in banach spaces and maximal regularity*, in Vector Measures, Integration and Related Topics, G. Curbera, G. Mockenhaupt, and W. Ricker, eds., vol. 201 of Operator Theory: Advances and Applications, Birkhuser Basel, 2010, pp. 21–39.

[6] V. I. Arnol′d, *Matrices depending on parameters*, Uspehi Mat. Nauk, 26 (1971), pp. 101–114.

[7] D. G. Aronson and H. F. Weinberger, *Nonlinear diffusion in population genetics, combustion, and nerve pulse propagation*, in Partial differential equations and related topics, Springer, 1975, pp. 5–49.

[8] D. Barkley, *Euclidean symmetry and the dynamics of rotating spiral waves*, Phys. Rev. Lett., 72 (1994), pp. 164–167.

[9] M. Barrandon and G. Iooss, *Water waves as a spatial dynamical system; infinite depth case*, Chaos: An Interdisciplinary Journal of Nonlinear Science, 15 (2005), pp. –.

[10] C. Beaume, E. Knobloch, G. Chini, and K. Julien, *Modulated patterns in a reduced model of a transitional shear flow*, Physica Scripta, (2015).

[11] E. Ben-Jacob, H. Brand, G. Dee, L. Kramer, and J. S. Langer, *Pattern propagation in nonlinear dissipative systems*, Phys. D, 14 (1985), pp. 348–364.

[12] H. Berestycki, G. Nadin, B. Perthame, and L. Ryzhik, *The non-local fisher–kpp equation: travelling waves and steady states*, Nonlinearity, 22 (2009), p. 2813.

[13] G. Berteloot, A. Hoang, A. Daerr, H. P. Kavehpour, F. Lequeux, and L. Limat, *Evaporation of a sessile droplet: Inside the coffee stain*, Journal of colloid and interface science, 370 (2012), pp. 155–161.

[14] R. M. Bradley and J. M. E. Harper, *Theory of ripple topography induced by ion bombardment*, Journal of Vacuum Science and Technology A: Vacuum, Surfaces, and Films, 6 (1988), pp. 2390–2395.

[15] R. M. Bradley and P. D. Shipman, *Spontaneous pattern formation induced by ion bombardment of binary compounds*, Phys. Rev. Lett., 105 (2010), p. 145501.

[16] T. Brand, M. Kunze, G. Schneider, and T. Seelbach, *Hopf bifurcation and exchange of stability in diffusive media*, Arch. Ration. Mech. Anal., 171 (2004), pp. 263–296.

[17] L. Brevdo and T. J. Bridges, *Absolute and convective instabilities of spatially periodic flows*, Philos. T. Roy. Soc. A, 354 (1996), pp. 1027–1064.

[18] R. Briggs, *Electron-stream interaction with plasmas, res. monogr., 29*, 1964.

[19] E. O. Budrene and H. C. Berg, *Dynamics of formation of symmetrical patterns by chemotactic bacteria*, Nature, 376 (1995), pp. 49–53.

[20] J. Cahn and J. Hilliard, *J. chem. phys.*, J. Chem. Phys., 28 (1958), pp. 258–267.

[21] X.-Y. Chen, *A strong unique continuation theorem for parabolic equations*, Mathematische Annalen, 311 (1998), pp. 603–630.

[22] J.-M. Chomaz, *Global instabilities in spatially developing flows: non-normality and nonlinearity*, Annu. Rev. Fluid Mech., 37 (2005), pp. 357–392.

[23] J.-M. Chomaz and A. Couairon, *Against the wind*, Physics of Fluids (1994-present), 11 (1999), pp. 2977–2983.

[24] P. Chossat and R. Lauterbach, *Methods in equivariant bifurcations and dynamical systems*, vol. 15 of Advanced Series in Nonlinear Dynamics, World Scientific Publishing Co. Inc., River Edge, NJ, 2000.

[25] A. Couairon and J.-M. Chomaz, *Absolute and convective instabilities, front velocities and global modes in nonlinear systems*, Physica D, 108 (1997), pp. 236–276.

[26] A. Couairon and J.-M. Chomaz, *Pattern selection in the presence of a cross flow*, Phys. Rev. Lett., 79 (1997), p. 2666.

[27] A. Couairon and J.-M. Chomaz, *Pushed global modes in weakly inhomogeneous subcritical flows*, Physica D, 158 (2001), pp. 129–150.

[28] S. M. Cox and P. C. Matthews, *Exponential time differencing for stiff systems*, J. Comput. Phys., 176 (2002), pp. 430–455.

[29] E. J. Crampin, E. A. Gaffney, and P. K. Maini, *Reaction and diffusion on growing domains: scenarios for robust pattern formation*, Bulletin of mathematical biology, 61 (1999), pp. 1093–1120.

[30] M. Cross and A. C. Newell, *Convection patterns in large aspect ratio systems*, Physica D: Nonlinear Phenomena, 10 (1984), pp. 299–328.

[31] M. C. Cross and P. C. Hohenberg, *Pattern formation outside of equilibrium*, Rev. Mod. Phys., 65 (1993), p. 851.

[32] G. Dangelmayr, K. Kirchgässner, B. Fiedler, and A. Mielke, *Dynamics of Nonlinear Waves in Dissipative Systems Reduction, Bifurcation and Stability*, vol. 352, CRC Press, 1996.

[33] G. Dee and J. S. Langer, *Propagating pattern selection*, Phys. Rev. Lett., 50 (1983), pp. 383–386.

[34] J. Deng and S. Nii, *An infinite-dimensional evans function theory for elliptic boundary value problems*, Journal of Differential Equations, 244 (2008), pp. 753–765.

[35] R. Denk, M. Hieber, and J. Prüss, *Optimal Lp-Lq-regularity for parabolic problems with inhomogeneous boundary data*, Fachbereich für Mathematik und Statistik, 2005.

[36] F. Dias and G. Iooss, *Water-waves as a spatial dynamical system*, Handbook of mathematical fluid dynamics, 2 (2003), pp. 443–499.

[37] A. Doelman, B. Sandstede, A. Scheel, and G. Schneider, *Propagation of hexagonal patterns near onset*, European Journal of Applied Mathematics, 14 (2003), pp. 85–110.

[38] ——, *The dynamics of modulated wave trains*, American Mathematical Soc., 2009.

[39] A. Doelman, P. van Heijster, and F. Xie, *A geometric approach to stationary defect solutions in one space dimension*, preprint.

[40] M. Droz, *Recent theoretical developments on the formation of liesegang patterns*, Journal of Statistical Physics, 101 (2000), pp. 509–519.

[41] F. Dumortier, *Techniques in the theory of local bifurcations: blow-up, normal forms, nilpotent bifurcations, singular perturbations*, in Bifurcations and periodic orbits of vector fields (Montreal, PQ, 1992), vol. 408 of NATO Adv. Sci. Inst. Ser. C Math. Phys. Sci., Kluwer Acad. Publ., Dordrecht, 1993, pp. 19–73.

[42] J.-P. Eckmann and C. E. Wayne, *The nonlinear stability of front solutions for parabolic partial differential equations*, Comm. Math. Phys., 161 (1994), pp. 323–334.

[43] G. Faye and M. Holzer, *Modulated traveling fronts for a nonlocal fisher-kpp equation: a dynamical systems approach*, Journal of Differential Equations, 258 (2015), pp. 2257–2289.

[44] G. Faye and A. Scheel, *Fredholm properties of nonlocal differential operators via spectral flow*, ArXiv e-prints, (2013).

[45] G. Faye and A. Scheel, *Existence of pulses in excitable media with nonlocal coupling*, Advances in Mathematics, 270 (2015), pp. 400–456.

[46] N. Fenichel, *Persistence and smoothness of invariant manifolds for flows*, Indian Univ. Math. J., 21 (1972), pp. 193–226.

[47] ——, *Asymptotic stability with rate conditions*, Indian Univ. Math. J., 23 (1974), pp. 1109–1137.

[48] ——, *Asymptotic stability with rate conditions ii*, Indian Univ. Math. J., 26 (1977), pp. 81–93.

[49] B. Fiedler and A. Scheel, *Spatio-temporal dynamics of reaction-diffusion patterns*, in Trends in nonlinear analysis, Springer, 2003, pp. 23–152.

[50] P. C. Fife, *Pattern formation in gradient systems*, Handbook of dynamical systems, 2 (2002), pp. 677–722.

[51] ——, *Pattern formation in gradient systems*, Handbook of Dynamical Systems, 2 (2002), pp. 677–722.

[52] D. Finkelshtein, Y. Kondratiev, and P. Tkachov, *Traveling waves and long-time behavior in a doubly nonlocal fisher-kpp equation*, arXiv preprint arXiv:1508.02215, (2015).

[53] R. A. Fisher, *The wave of advance of advantageous genes*, Annals of eugenics, 7 (1937), pp. 355–369.

[54] E. M. Foard and A. J. Wagner, *Survey of morphologies formed in the wake of an enslaved phase-separation front in two dimensions*, Phys. Rev. E, 85 (2012), p. 011501.

[55] F. Frost, B. Ziberi, A. Schindler, and B. Rauschenbach, *Surface engineering with ion beams: from self-organized nanostructures to ultra-smooth surfaces*, Applied Physics A, 91 (2008), pp. 551–559.

[56] T. Gallay, *Local stability of critical fronts in nonlinear parabolic partial differential equations*, Nonlinearity, 7 (1994), p. 741.

[57] P. Gandhi, C. Beaume, and E. Knobloch, *Time-periodic forcing of spatially localized structures*, in Nonlinear Dynamics: Materials, Theory and Experiments, Springer, 2016, pp. 303–316.

[58] P. Gandhi, E. Knobloch, and C. Beaume, *Dynamics of phase slips in systems with time-periodic modulation*, Physical Review E, 92 (2015), p. 062914.

[59] M. P. Gelfand and R. M. Bradley, *Highly ordered nanoscale patterns produced by masked ion bombardment of a moving solid surface*, Phys. Rev. B, 86 (2012), p. 121406.

[60] K. Glasner, *Traveling waves in rapid solidification*, Electron. J. Differential Equations, 2000 (2000), pp. 1–28.

[61] R. Goh, R. Beekie, D. Matthias, J. Nunley, and A. Scheel, *Universal wavenumber selection laws in apical growth*, ArXiv e-prints, (2016).

[62] R. Goh, S. Mesuro, and A. Scheel, *Coherent structures in reaction-diffusion models for precipitation*, Precipitation patterns in reaction-diffusion systems, Research Signpost, (2010), pp. 73–93.

[63] R. Goh, S. Mesuro, and A. Scheel, *Spatial wavenumber selection in recurrent precipitation*, SIAM J. Appl. Dyn. Syst., 10 (2011), pp. 360–402.

[64] R. Goh and A. Scheel, *Triggered fronts in the complex Ginzburg Landau equation*, J. Nonlinear Sci., 24 (2014), pp. 117–144.

[65] ——, *Hopf bifurcation from fronts in the cahn–hilliard equation*, Archive for Rational Mechanics and Analysis, 217 (2015), pp. 1219–1263.

[66] R. Goh and A. Scheel, *Pattern formation in the wake of triggered pushed fronts*, ArXiv e-prints, (2015).

[67] M. Golubitsky, V. G. LeBlanc, and I. Melbourne, *Meandering of the spiral tip: an alternative approach*, J. Nonlinear Sci., 7 (1997), pp. 557–586.

[68] M. Golubitsky, I. Stewart, and D. G. Schaeffer, *Singularities and groups in bifurcation theory*, Springer, 1988.

[69] M. Grinfeld and A. Novick-Cohen, *Counting stationary solutions of the cahn–hilliard equation by transversality arguments*, Proceedings of the Royal Society of Edinburgh: Section A Mathematics, 125 (1995), pp. 351–370.

[70] M. Grinfeld and A. Novick-Cohen, *The viscous cahn-hilliard equation: Morse decomposition and structure of the global attractor*, Transactions of the American Mathematical Society, 351 (1999), pp. 2375–2406.

[71] E. Haeckel, *Art forms in nature*, New York: Dover Publications, 1974.

[72] F. Hamel and L. Ryzhik, *On the nonlocal fisher–kpp equation: steady states, spreading speed and global bounds*, Nonlinearity, 27 (2014), p. 2735.

[73] W. Han and Z. Lin, *Learning from coffee rings: Ordered structures enabled by controlled evaporative self-assembly*, Angewandte Chemie International Edition, 51 (2012), pp. 1534–1546.

[74] M. Haragus and A. Scheel, *Corner defects in almost planar interface propagation*, in Annales de l'IHP Analyse non linéaire, vol. 23, 2006, pp. 283–329.

[75] B. Hashmi, P. D. Shipman, and R. M. Bradley, *Highly ordered square arrays of nanoscale pyramids produced by ion bombardment of a crystalline binary material*, Phys. Rev. E, 93 (2016), p. 032207.

[76] D. Henry, *Geometric theory of semilinear parabolic equations*, vol. 840, Berlin: Springer-Verlag, 1981.

[77] T. Hillen and K. J. Painter, *A users guide to pde models for chemotaxis*, Journal of mathematical biology, 58 (2009), pp. 183–217.

[78] M. Holzer and A. Scheel, *A slow pushed front in a Lotka–Volterra competition model*, Nonlinearity, 25 (2012), p. 2151.

[79] M. Holzer and A. Scheel, *Accelerated fronts in a two-stage invasion process*, SIAM J. Math. Anal., 46 (2014), pp. 397–427.

[80] M. Holzer and A. Scheel, *Criteria for pointwise growth and their role in invasion processes*, J. Nonlinear Sci., 24 (2014), pp. 661–709.

[81] A. J. Homburg and B. Sandstede, *Homoclinic and heteroclinic bifurcations in vector fields*, Handbook of Dynamical Systems, 3 (2010), pp. 379–524.

[82] S. W. Hong, J. Xia, and Z. Lin, *Spontaneous formation of mesoscale polymer patterns in an evaporating bound solution*, Advanced Materials, 19 (2007), pp. 1413–1417.

[83] G. Iooss and A. Mielke, *Bifurcating time-periodic solutions of Navier-Stokes equations in infinite cylinders*, J. Nonlinear Sci., 1 (1991), pp. 107–146.

[84] G. Iooss and A. Mielke, *Time-periodic Ginzburg-Landau equations for one-dimensional patterns with large wave length*, Z. Angew. Math. Phys., 43 (1992), pp. 125–138.

[85] T. Kapitula and K. Promislow, *Spectral and dynamical stability of nonlinear waves*, Springer, 2013.

[86] A. Katok and B. Hasselblatt, *Introduction to the modern theory of dynamical systems*, vol. 54 of Encyclopedia of Mathematics and its Applications, Cambridge University Press, Cambridge, 1995. With a supplementary chapter by Katok and Leonardo Mendoza.

[87] J. B. Keller and S. I. Rubinow, *Recurrent precipitation and liesegang rings*, The Journal of Chemical Physics, 74 (1981), pp. 5000–5007.

[88] K. Kirchgässner, *Wave-solutions of reversible systems and applications*, J. Differential Equations, 45 (1982), pp. 113–127.

[89] A. Kiselev and L. Ryzhik, *Enhancement of the traveling front speeds in reaction-diffusion equations with advection*, in Annales de l'IHP Analyse non linéaire, vol. 18, 2001, pp. 309–358.

[90] A. Kolmogorov, I. Petrovskii, and N. Piskunov, *A study of the equation of diffusion with increase in the quantity of matter, and its application to a biological problem*, Bjul. Moskovskogo Gos. Univ, 1 (1937), pp. 1–26.

[91] M. H. Köpf, S. V. Gurevich, R. Friedrich, and U. Thiele, *Substrate-mediated pattern formation in monolayer transfer: a reduced model*, New Journal of Physics, 14 (2012), p. 023016.

[92] M. H. Köpf and U. Thiele, *Emergence of the bifurcation structure of a Langmuir-Blodgett transfer model*, Nonlinearity, 27 (2014), p. 2711.

[93] A. Krekhov, *Formation of regular structures in the process of phase separation*, Phys. Rev. E, 79 (2009), p. 035302.

[94] M. Kunze and G. Schneider, *Exchange of stability and finite-dimensional dynamics in a bifurcation problem with marginally stable continuous spectrum*, Z. Angew. Math. Phys., 55 (2004), pp. 383–399.

[95] R. Liesegang, *Über einige Eigenschaften von Gallerten*, Naturwiss. Wochenschr., 11 (1896), pp. 353–362.

[96] X.-B. Lin, *Using Melnikov's method to solve Silnikov's problems*, Proc. Roy. Soc. Edinburgh Sec. A, 116 (1990), pp. 295–325.

[97] D. J. Lloyd, B. Sandstede, D. Avitabile, and A. R. Champneys, *Localized hexagon patterns of the planar swift-hohenberg equation*, SIAM Journal on Applied Dynamical Systems, 7 (2008), pp. 1049–1100.

[98] J. B.-J. Lofstrom and J. Bergh, *Interpolation spaces: An introduction*, Springer, 1976.

[99] N. Manz, V. Davydov, V. Zykov, and S. Müller, *Excitation fronts in a spatially modulated light-sensitive Belousov-Zhabotinsky system*, Phys. Rev. E, 66 (2002), p. 036207.

[100] M. Matsushita, F. Hiramatsu, N. Kobayashi, T. Ozawa, and T. Yamazaki, Y.and Matsuyama, *Colony formation in bacteria: experiments and modeling*, Biofilms, 1 (2004), pp. 305–317.

[101] K. McQuighan and B. Sandstede, *Oscillons in the planar ginzburg–landau equation with 2: 1 forcing*, Nonlinearity, 27 (2014), p. 3073.

[102] A. Mielke, *The ginzburg-landau equation in its role as a modulation equation*, Handbook of dynamical systems, 2 (2002), pp. 759–834.

[103] D. G. Míguez, M. Dolnik, A. P. Muñuzuri, and L. Kramer, *Effect of axial growth on turing pattern formation*, Physical review letters, 96 (2006), p. 048304.

[104] D. Mijatovic, J. C. T. Eijkel, and A. van den Berg, *Technologies for nanofluidic systems: top-down vs. bottom-up-a review*, Lab Chip, 5 (2005), pp. 492–500.

[105] R. A. Monteiro, *Transverse steady bifurcation of viscous shock solutions of a system of parabolic conservation laws in a strip*, Journal of Differential Equations, 257 (2014), pp. 2035–2077.

[106] D. Morrissey and A. Scheel, *Characterizing the effect of boundary conditions on striped phases*, SIAM J. on Appl. Dyn. Syst., 14 (2015), pp. 1387–1417.

[107] A. Novick-Cohen, *The cahn–hilliard equation*, Handbook of differential equations: evolutionary equations, 4 (2008), pp. 201–228.

[108] K. Nozaki and N. Bekki, *Pattern selection and spatiotemporal transition to chaos in the Ginzburg-Landau equation*, Phys. Rev. Lett., 51 (1983), pp. 2171–2174.

[109] T. Ohta and K. Kawasaki, *Equilibrium morphology of block copolymer melts*, Macromolecules, 19 (1986), pp. 2621–2632.

[110] K. J. Painter and T. Hillen, *Volume-filling and quorum-sensing in models for chemosensitive movement*, Can. Appl. Math. Quart, 10 (2002), pp. 501–543.

[111] D. A. Pearson, R. M. Bradley, F. C. Motta, and P. D. Shipman, *Producing nanodot arrays with improved hexagonal order by patterning surfaces before ion sputtering*, Physical Review E, 92 (2015), p. 062401.

[112] M. Pennybacker and A. C. Newell, *Phyllotaxis, pushed pattern-forming fronts, and optimal packing*, Physical review letters, 110 (2013), p. 248104.

[113] M. F. Pennybacker, P. D. Shipman, and A. C. Newell, *Phyllotaxis: Some progress, but a story far from over*, Physica D: Nonlinear Phenomena, 306 (2015), pp. 48–81.

[114] D. Peterhof, B. Sandstede, and A. Scheel, *Exponential dichotomies for solitary-wave solutions of semilinear elliptic equations on infinite cylinders*, J. Differential Equations, 140 (1997), pp. 266 – 308.

[115] B. Pier, P. Huerre, J.-M. Chomaz, and A. Couairon, *Steep nonlinear global modes in spatially developing media*, Physics of Fluids (1994-present), 10 (1998), pp. 2433–2435.

[116] A. Pogan and A. Scheel, *Instability of spikes in the presence of conservation laws*, Zeitschrift für Angewandte Mathematik und Physik (ZAMP), 61 (2010), pp. 979–998.

[117] A. Pogan, J. Yao, and K. Zumbrun, *O (2) hopf bifurcation of viscous shock waves in a channel*, arXiv preprint arXiv:1401.2197, (2014).

[118] K. Promislow and B. Wetton, *Pem fuel cells: a mathematical overview*, SIAM Journal on Applied Mathematics, 70 (2009), pp. 369–409.

[119] K. Promislow and Q. Wu, *Existence of pearled patterns in the planar functionalized cahn–hilliard equation*, Journal of Differential Equations, 259 (2015), pp. 3298–3343.

[120] J. D. Rademacher, *Homoclinic orbits near heteroclinic cycles with one equilibrium and one periodic orbit*, J. Differential Equations, 218 (2005), pp. 390 – 443.

[121] J. D. Rademacher, B. Sandstede, and A. Scheel, *Computing absolute and essential spectra using continuation*, Physica D: Nonlinear Phenomena, 229 (2007), pp. 166–183.

[122] J. D. Rademacher and A. Scheel, *Instabilities of wave trains and turing patterns in large domains*, International Journal of Bifurcation and Chaos, 17 (2007), pp. 2679–2691.

[123] J. Robbin and D. Salamon, *The spectral flow and the maslov index*, Bull. London Math. Soc., 27 (1995).

[124] B. Sandstede, *Absolute and essential spectra*, online lecture notes, 2016.

[125] B. Sandstede and A. Scheel, *Essential instability of pulses and bifurcations to modulated travelling waves*, Proc. Roy. Soc. Edinburgh Sec. A, 129 (1999), pp. 1263–1290.

[126] B. Sandstede and A. Scheel, *Absolute and convective instabilities of waves on unbounded and large bounded domains*, Physica D: Nonlinear Phenomena, 145 (2000), pp. 233 – 277.

[127] B. Sandstede and A. Scheel, *Gluing unstable fronts and backs together can produce stable pulses*, Nonlinearity, 13 (2000), pp. 1465–1482.

[128] B. Sandstede and A. Scheel, *Spectral stability of modulated travelling waves bifurcating near essential instabilities*, Proc. Roy. Soc. Edinburgh Sect. A, 130 (2000), pp. 419–448.

[129] B. Sandstede and A. Scheel, *Essential instabilities of fronts: bifurcation, and bifurcation failure*, Dyn. Syst., 16 (2001), pp. 1–28.

[130] ——, *On the structure of spectra of modulated travelling waves*, Mathematische Nachrichten, 232 (2001), pp. 39–93.

[131] B. Sandstede and A. Scheel, *Superspiral structures of meandering and drifting spiral waves*, Phys. Rev. Lett., 86 (2001), pp. 171–174.

[132] B. Sandstede and A. Scheel, *Defects in oscillatory media: Toward a classification*, SIAM Journal on Applied Dynamical Systems, 3 (2004), pp. 1–68.

[133] B. Sandstede and A. Scheel, *Absolute instabilities of standing pulses*, Nonlinearity, 18 (2005), pp. 331–378.

[134] ——, *Basin boundaries and bifurcations near convective instabilities: a case study*, J. Differential Equations, 208 (2005), pp. 176–193.

[135] B. Sandstede and A. Scheel, *Hopf bifurcation from viscous shock waves*, SIAM Journal on Mathematical Analysis, 39 (2008), pp. 2033–2052.

[136] B. Sandstede and A. Scheel, *Relative morse indices, fredholm indices, and group velocities*, Discrete and Continuous Dynamical Systems A, (2008), pp. 139–158.

[137] B. Sandstede, A. Scheel, and C. Wulff, *Dynamics of spiral waves on unbounded domains using center-manifold reductions*, J. Differential Equations, 141 (1997), pp. 122–149.

[138] B. Sandstede, A. Scheel, and C. Wulff, *Bifurcations and dynamics of spiral waves*, J. Nonlinear Sci., 9 (1999), pp. 439–478.

[139] A. Scheel, *Spinodal decomposition and coarsening fronts in the cahn–hilliard equation*, Journal of Dynamics and Differential Equations, pp. 1–34.

[140] ——, *Robustness of liesegang patterns*, Nonlinearity, 22 (2009), p. 457.

[141] G. Schneider, *Hopf bifurcation in spatially extended reactiondiffusion systems*, Journal of Nonlinear Science, 8 (1998), pp. 17–41.

[142] A. P. Seyranian and A. Mailybaev, *Multiparameter Stability Theory with Mechanical Applications*, vol. 13 of Series on Stability, Vibration and Control of Systems, Series A, World Scientific Inc., 2003.

[143] E. Siero, A. Doelman, M. Eppinga, J. Rademacher, M. Rietkerk, and K. Siteur, *Striped pattern selection by advective reaction-diffusion systems: Resilience of banded vegetation on slopes*, Chaos: An Interdisciplinary Journal of Nonlinear Science, 25 (2015), p. 036411.

[144] M. J. Smith, J. D. M. Rademacher, and J. A. Sherratt, *Absolute stability of wavetrains can explain spatiotemporal dynamics in reaction-diffusion systems of lambda-omega type*, SIAM J. Appl. Dyn. Syst., 8 (2009), pp. 1136–1159.

[145] T. M. Squires and S. R. Quake, *Microfluidics: Fluid physics at the nanoliter scale*, Rev. Mod. Phys., 77 (2005), pp. 977–1026.

[146] R. Suganthi, E. Girija, S. Narayana Kalkura, H. Varma, and A. Rajaram, *Self-assembled right handed helical ribbons of the bone mineral hydroxyapatite*, Journal of Materials Science: Materials in Medicine, 20 (2009), pp. 131–136.

[147] M. E. Taylor, *Partial differential equations I: Basic theory*, vol. 1, Springer, 1996.

[148] M. Teichmann, J. Lorbeer, B. Ziberi, F. Frost, and B. Rauschenbach, *Pattern formation on ge by low energy ion beam erosion*, New Journal of Physics, 15 (2013), p. 103029.

[149] B. Texier and K. Zumbrun, *Relative poincare-hopf bifurcation and galloping instabilities for traveling waves*, Meth. App. Analysis, 12 (2005), pp. 349–380.

[150] B. Texier and K. Zumbrun, *Galloping instability of viscous shock waves*, Physica D: Nonlinear Phenomena, 237 (2008), pp. 1553 – 1601. Perspectives in Fluid Dynamics.

[151] U. Thiele, *Patterned deposition at moving contact lines*, Advances in colloid and interface science, 206 (2014), pp. 399–413.

[152] S. Thomas, I. Lagzi, F. Molnár, and Z. Rácz, *Probability of the emergence of helical precipitation patterns in the wake of reaction-diffusion fronts*, Phys. Rev. Lett., 110 (2013), p. 078303.

[153] S. Tobias, M. Proctor, and E. Knobloch, *Convective and absolute instabilities of fluid flows in finite geometry*, Physica D: Nonlinear Phenomena, 113 (1998), pp. 43 – 72.

[154] A. M. Turing, *The chemical basis of morphogenesis*, Philosophical Transactions of the Royal Society of London B: Biological Sciences, 237 (1952), pp. 37–72.

[155] W. Van Saarloos, *Front propagation into unstable states. ii. linear versus nonlinear marginal stability and rate of convergence*, Phys. Rev. A, 39 (1989), p. 6367.

[156] W. van Saarloos, *Front propagation into unstable states*, Phys. Rep., 386 (2003), pp. 29 – 222.

[157] W. van Saarloos and P. Hohenberg, *Fronts, pulses, sources and sinks in generalized complex Ginzburg-Landau equations*, Physica D, 56 (1992), pp. 303 – 367.

[158] A. Vanderbauwhede and G. Iooss, *Center manifold theory in infinite dimensions*, in Dynamics Reported, C. Jones, U. Kirchgraber, and H. Walther, eds., vol. 1 of Dynamics Reported, Springer Berlin Heidelberg, 1992, pp. 125–163.

[159] A. Volkening and B. Sandstede, *Modelling stripe formation in zebrafish: an agent-based approach*, Journal of The Royal Society Interface, 12 (2015), p. 20150812.

[160] J. Vörös, T. Blättler, and M. Textor, *Bioactive patterns at the 100-nm scale produced using multifunctional physisorbed monolayers*, MRS Bulletin, 30 (2005), pp. 202–206.

[161] d. Wentworth Thompson, *On growth and form*, Cambridge: University Press, 1915.

[162] M. Wilczek and S. V. Gurevich, *Locking of periodic patterns in Cahn-Hilliard models for Langmuir-Blodgett transfer*, Phys. Rev. E, 90 (2014), p. 042926.

[163] M. Wilczek, W. B. Tewes, S. V. Gurevich, M. H. Köpf, L. Chi, and U. Thiele, *Modelling pattern formation in dip-coating experiments*, arXiv preprint arXiv:1502.03632, (2015).

[164] J. Xin, *Front propagation in heterogeneous media*, Siam Review, 42 (2000), pp. 161–230.

[165] B. Ziberi, M. Cornejo, F. Frost, and B. Rauschenbach, *Highly ordered nanopatterns on ge and si surfaces by ion beam sputtering*, Journal of Physics: Condensed Matter, 21 (2009), p. 224003.

[166] A. Zlatoš, *Generalized traveling waves in disordered media: existence, uniqueness, and stability*, Archive for Rational Mechanics and Analysis, 208 (2013), pp. 447–480.

[167] A. Zlatos, *Propagation of reactions in inhomogeneous media*, arXiv preprint arXiv:1401.1175, (2014).